1. Report No.	2. Government Accession No.	3. Recipient's Catalog No.
FHWA/TX-07/0-4863-2		

4. Title and Subtitle	5. Report Date
EVALUATION OF RIDE SPECIFICATION BASED ON DYNAMIC LOAD MEASUREMENTS FROM INSTRUMENTED TRUCK	March 2007 Published: May 2007
	6. Performing Organization Code

7. Author(s)	8. Performing Organization Report No.
Emmanuel G. Fernando, Gerry Harrison, and Stacy Hilbrich	Report 0-4863-2

9. Performing Organization Name and Address	10. Work Unit No. (TRAIS)
Texas Transportation Institute The Texas A&M University System College Station, Texas 77843-3135	11. Contract or Grant No. Project 0-4863

12. Sponsoring Agency Name and Address	13. Type of Report and Period Covered
Texas Department of Transportation Research and Technology Implementation Office P. O. Box 5080 Austin, Texas 78763-5080	Technical Report: September 2004 – August 2006
	14. Sponsoring Agency Code

15. Supplementary Notes

Project performed in cooperation with the Texas Department of Transportation and the Federal Highway Administration.

Project Title: Characterizing the Effects of Surface Roughness on Vehicle Dynamic Loads and Pavement Life

URL: http://tti.tamu.edu/documents/0-4863-2.pdf

16. Abstract

The Texas Department of Transportation is implementing a ride specification that uses profile data collected with inertial profilers for acceptance testing of the finished surface. This specification is based primarily on ride quality criteria. The objective of the present project is to establish whether the current specification permits frequency components of surface profile to pass that are potentially detrimental to pavement life based on the induced dynamic loading. To carry out this objective, researchers in this project conducted measurements of surface profiles and vehicle dynamic loads on recently completed TxDOT paving projects. For these tests, researchers instrumented a truck with sensors for measurement of dynamic loads and put together an inertial profiling system for measurement of surface profiles. This research report documents the instrumentation and test programs carried out by researchers as well as the analyses of the test data and the findings thereof.

17. Key Words	18. Distribution Statement
Surface Roughness, Vehicle Dynamic Loads, Truck Instrumentation, Profile Measurement, Strain Gages	No restrictions. This document is available to the public through NTIS: National Technical Information Service Springfield, VA 22161 http://www.ntis.gov

19. Security Classif.(of this report)	20. Security Classif.(of this page)	21. No. of Pages	22. Price
Unclassified	Unclassified	210	

EVALUATION OF RIDE SPECIFICATION BASED ON DYNAMIC LOAD MEASUREMENTS FROM INSTRUMENTED TRUCK

by

Emmanuel G. Fernando
Research Engineer
Texas Transportation Institute

Gerry Harrison
Research Technician
Texas Transportation Institute

and

Stacy Hilbrich
Assistant Research Engineer
Texas Transportation Institute

Report 0-4863-2
Project 0-4863
Project Title: Characterizing the Effects of Surface Roughness on Vehicle Dynamic Loads and Pavement Life

Performed in cooperation with the
Texas Department of Transportation
and the
Federal Highway Administration

March 2007 Published: May 2007

TEXAS TRANSPORTATION INSTITUTE
The Texas A&M University System
College Station, Texas 77843-3135

DISCLAIMER

The contents of this report reflect the views of the authors, who are responsible for the facts and the accuracy of the data presented. The contents do not necessarily reflect the official views or policies of the Texas Department of Transportation (TxDOT) or the Federal Highway Administration (FHWA). This report does not constitute a standard, specification, or regulation, nor is it intended for construction, bidding, or permit purposes. The United States Government and the State of Texas do not endorse products or manufacturers. Trade or manufacturers' names appear herein solely because they are considered essential to the object of this report. The engineer in charge of the project was Dr. Emmanuel G. Fernando, P.E. # 69614.

ACKNOWLEDGMENTS

The work reported herein was conducted as part of a research project sponsored by the Texas Department of Transportation and the Federal Highway Administration. The authors gratefully acknowledge the support and technical guidance of the project director, Mr. Brian Michalk, of the Materials and Pavements Section of TxDOT. In addition, the authors give special thanks to Dr. Roger Walker of the University of Texas at Arlington for his help in profile instrumentation and in the evaluation of transfer functions. His contributions are sincerely appreciated.

TABLE OF CONTENTS

TABLE OF CONTENTS (CONT.)

APPENDIX Page

LIST OF FIGURES

Figure Page

LIST OF FIGURES (CONT.)

LIST OF FIGURES (CONT.)

Figure Page

LIST OF FIGURES (CONT.)

Figure Page

LIST OF FIGURES (CONT.)

Figure Page

LIST OF FIGURES (CONT.)

Figure Page

LIST OF FIGURES (CONT.)

LIST OF FIGURES (CONT.)

Figure Page

LIST OF FIGURES (CONT.)

Figure Page

LIST OF TABLES

LIST OF TABLES (CONT.)

LIST OF TABLES (CONT.)

CHAPTER I. INTRODUCTION

The Texas Department of Transportation (TxDOT) is implementing a new ride specification that uses profile data collected with inertial profilers for acceptance testing of the finished surface. The new ride specification, Item 585, is applicable for either hot-mix asphalt or Portland cement concrete pavements and is included in TxDOT's 2004 standard specifications.

Item 585 incorporates criteria on section smoothness and localized roughness to evaluate the acceptability of the finished surface. Section smoothness is evaluated at 0.1-mile intervals using the international roughness index (IRI) computed from measured profiles. In this evaluation, the average of the left and right wheel path IRIs is computed and used in the appropriate schedule to determine the pay adjustment for a given 0.1-mile section. To evaluate localized roughness, the specification computes the point-to-point differences between the average profile and its 25-ft moving average and compares the differences to a 150-mil threshold to locate bumps and dips. The method currently implemented by TxDOT is an adaptation of the original methodology proposed by Fernando and Bertrand (2002).

The new standard smoothness specification (Item 585) includes pay adjustments that relate to the ride quality achieved from construction. The specification is based primarily on ride quality as determined from the measured surface profile on a given section. However, another factor to consider is whether the current specification permits frequency components of surface profile to pass that are potentially detrimental to pavement life based on the induced dynamic loading. The present research evaluated TxDOT's current ride specification based on dynamic load measurements from an instrumented truck. To carry out this objective, researchers in this project conducted measurements of surface profiles and vehicle dynamic loads on recently completed TxDOT paving projects. For these tests, researchers instrumented a truck with sensors for measurement of dynamic loads and put together an inertial profiling system for measurement of surface profiles. This research report documents the instrumentation and test programs carried out by researchers as well as the analyses of the test data and the findings thereof. It is organized into the following chapters:

- Chapter I (this chapter) provides a brief introduction on the rationale for this project.
- Chapter II documents the truck instrumentation for measurement of dynamic loads. It presents the methodology used for these measurements, preliminary tests conducted to verify and develop the methodology, sensor installation, and laboratory calibrations conducted to establish calibration curves relating sensor output to measured tire loads.
- Chapter III presents results from field tests conducted to verify the measurements from a test vehicle instrumented with an inertial profiling system at the Texas Transportation Institute (TTI). Researchers used this test vehicle to collect profile measurements for the purpose of analyzing dynamic load data from the instrumented truck. Prior to collecting profile data, researchers tested the profiler to verify its compliance with the certification requirements specified in TxDOT Test Method Tex-1001S.
- Chapter IV presents the field tests conducted by researchers to collect data for the purpose of evaluating TxDOT's Item 585 ride specification. The field test program covered profile measurements with TTI's inertial profiler and dynamic load measurements with the instrumented truck on recently completed TxDOT paving projects. It also included tests on a weigh-in-motion (WIM) site to verify the dynamic load measurements from the instrumented truck. Chapter IV presents results from the field test program and the evaluation of TxDOT's ride specification based on test data from the instrumented truck.
- Finally, Chapter V summarizes the findings and recommendations from this project.

The appendices provide supporting material for the tasks conducted in this project. Appendix A presents the findings from the literature review to gather existing information relevant to this project. Appendix B presents the profile measurements collected on TxDOT paving projects. Finally, Appendix C presents charts of transfer functions of vehicle dynamic tire loading from tests conducted with the instrumented truck in this project.

CHAPTER II. TRUCK INSTRUMENTATION FOR MEASUREMENT OF DYNAMIC TIRE LOADS

The literature review conducted in this project identified strain gages as a method for instrumenting vehicles to measure dynamic loads. To use strain gages for this application, researchers:

- reviewed principles of strain gage measurement;
- conducted laboratory tests to verify their application; and
- performed small-scale experiments with an instrumented trailer to verify procedures for strain gage calibration and to test a system for collecting dynamic load measurements.

This staged approach led to the instrumentation and calibration of a test vehicle that is presented in this chapter.

STRAIN GAGE PRINCIPLES

Engineering design requires information on the stresses and deformations that a structure or structural member are expected to sustain during service. For many design problems, mechanics of materials gives a basis for predicting the structural response to service loads. Indeed, solutions for stresses and deformations induced under typical design loadings for simple structural members are found in the literature, and for more complicated geometric and loading configurations, numerical techniques are available. Still, many engineering problems are encountered in practice where theoretical analysis may not be sufficient, and experimental measurements are required to verify theoretical predictions or to obtain actual measurements from laboratory or full-scale models. In most cases, force or stress cannot be measured directly, but the deformations they generate can. Thus, when an object is weighed on a scale, it is the extension of the spring that is measured, and the weight is calculated using Hooke's law with the measured spring displacement. In a similar manner, load cells have sensors that measure the deformations induced under loading that relate to the magnitude of the applied load. When the deformation is defined as the change in length per unit length of a given object, it is called strain. Of the strain-measuring systems that are available for practical applications, the most frequently used device for strain measurement is the electrical-resistance strain gage.

The term "strain gage" usually refers to a thin wire or foil, folded back and forth on itself to form a grid pattern, as illustrated in Figure 2.1. The grid pattern maximizes the amount of metallic wire or foil subject to strain in the parallel direction. The grid is bonded to a thin backing, called the carrier, which is attached directly to the test specimen. Therefore, the strain experienced by the test specimen is transferred directly to the strain gage, which responds with a linear change in electrical resistance.

The discovery of the principle upon which the electrical-resistance strain gage is based was made in 1856 by Lord William Thomson Kelvin who observed from an experiment that the resistance of a wire increases with increasing strain according to the relationship (Dally and Riley, 1978):

$$R = \rho \frac{L}{A} \tag{2.1}$$

where R is the measured resistance in the wire of length L and cross-sectional area A having a specific resistance ρ. From this relationship, it can be shown that the strain sensitivity of any conductor derives from the change in its dimensions during loading and the change in specific resistance according to the relation:

$$\frac{dR/R}{\varepsilon} = 1 + 2\nu + \frac{d\rho/\rho}{\varepsilon} \tag{2.2}$$

where ν is the Poisson's ratio of the conductor, ε is the strain, and the other terms are as previously defined. In practice, the strain sensitivity is also referred to as the gage factor S_g. Thus:

$$S_g = \frac{dR/R}{\varepsilon} \approx \frac{\Delta R/R}{\varepsilon} \tag{2.3}$$

For most alloys, the gage factor varies from about 2 to 4 (Dally and Riley, 1978). Most strain gages are fabricated from a 45 percent nickel – 55 percent copper alloy known as Constantan, which has a gage factor of approximately 2. This alloy exhibits several characteristics that are useful for engineering applications. Among these are:

- The strain sensitivity is linear over a wide range of strain.
- The strain sensitivity does not change as the material goes plastic permitting measurements of strain in both the elastic and plastic ranges of most materials.
- The alloy has a low temperature coefficient, which reduces the temperature sensitivity of the strain gage.

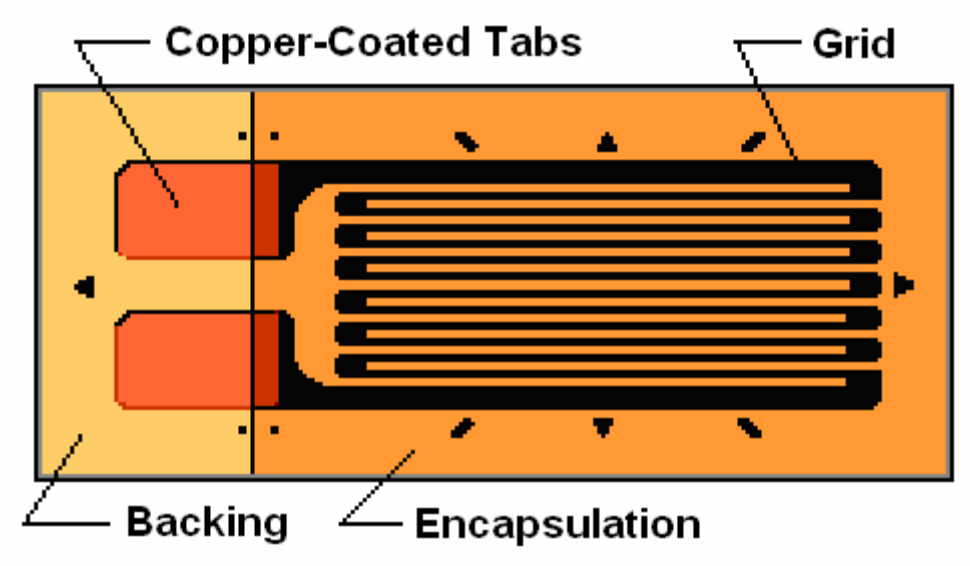

Figure 2.1. Diagram of an Electrical-Resistance Strain Gage.

- The temperature properties of selected melts of the alloy permit the production of temperature-compensated strain gages for a variety of materials on which the gages are commonly used.

In practice, the application of strain gages will require measurement of the resistance change and its conversion to strain using Eq. 2.3. This conversion is made with the gage factor that is supplied by the manufacturer of the particular sensor used in the experiment. Since the strains to be measured are typically within a few milli-strains, the resistance changes are usually too small to be measured with a simple ohmmeter. For example, at 1 percent strain, the resistance change would be only 2 percent for a sensor with a gage factor of 2. In practice, much smaller strains have to be measured. Thus, the application of strain gages will require accurate measurement of very small changes in resistance. To accomplish these measurements, a Wheatstone bridge is typically used. This method permits both static and dynamic strain gage measurements. It is interesting to note that this is the same method Lord Kelvin used to measure resistance changes in the classic experiment he conducted in the mid-19th century.

Figure 2.2 illustrates the Wheatstone bridge circuit. Up to four strain gages may be connected to the four arms of the bridge. When the gage resistance is changed by strain, the bridge becomes unbalanced resulting in a voltage change that is easily measured. For a Wheatstone bridge with a constant voltage excitation V and resistances R_1, R_2, R_3, and R_4, the

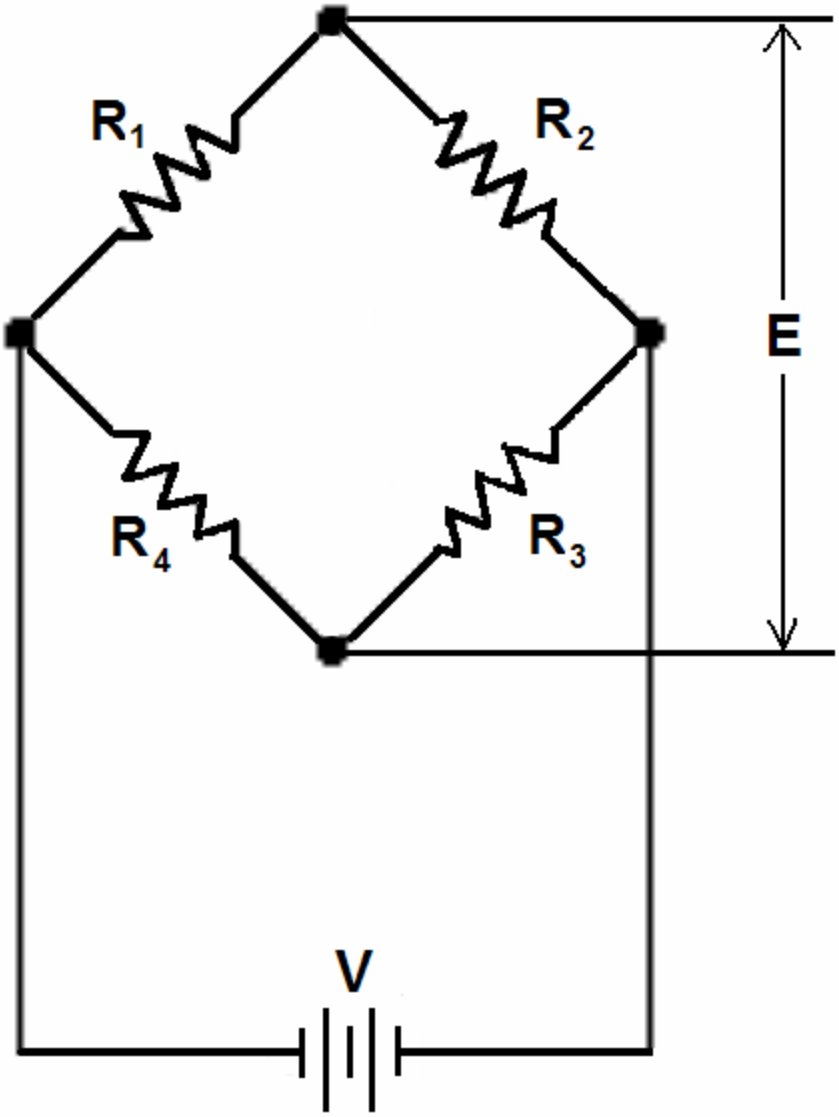

Figure 2.2. Wheatstone Bridge Circuit with Constant Voltage Excitation.

voltage change ΔE is related to the change in resistance ΔR_i in each bridge arm i by the relation (Dally and Riley, 1978):

$$\Delta E = V \frac{R_1 R_2}{(R_1 + R_2)^2} \left(\frac{\Delta R_1}{R_1} - \frac{\Delta R_2}{R_2} + \frac{\Delta R_3}{R_3} - \frac{\Delta R_4}{R_4} \right) \tag{2.4}$$

For a multiple gage circuit with n gages (n = 1, 2, 3, or 4) whose outputs sum when placed in the bridge circuit, Eq. 2.4 can be rewritten as:

$$\Delta E = V \frac{R_1 R_2}{(R_1 + R_2)^2} n \frac{\Delta R}{R} \tag{2.5}$$

where ΔR is the change in the bridge resistance and R is the nominal resistance of the bridge elements. The bridge circuit sensitivity S_c is defined as the change in voltage per unit strain. Setting $r = R_1/R_2$, this parameter is determined from Eqs. 2.3 and 2.5 as follows:

$$S_c = \frac{\Delta E}{\varepsilon} = V \frac{r}{(1+r)^2} n S_g \qquad (2.6)$$

It can be shown that the maximum circuit sensitivity is achieved when $r = 1$. With one strain gage connected to the Wheatstone bridge, Eq. 2.6 gives the sensitivity of this configuration as $S_g V/4$, compared to a sensitivity of $S_g V$ for a four-arm active configuration. The four-arm active bridge is of particular interest as it was the bridge configuration used for dynamic load measurements with the instrumented tractor-semitrailer in this project. In addition to providing the highest sensitivity, this bridge arrangement is also temperature-compensated and rejects both axial and bending strains for applications involving shear strain measurement. For this bridge configuration, the strain corresponding to the measured voltage change in the Wheatstone bridge is determined from the formula:

$$\varepsilon = \frac{\Delta E}{S_g V} \qquad (2.7)$$

Prior to instrumenting a tractor-semitrailer with strain gages for dynamic load measurements, researchers conducted laboratory and field tests to verify the application of the strain gage principles presented in this section. Specifically, the researchers verified the principles presented in the laboratory through an experiment that they conducted with a simple shear beam load cell. Following up on this experiment, researchers instrumented and conducted laboratory and field tests on a small trailer to verify the intended method of measuring dynamic loads using shear strain gages. Subsequent sections present the tests performed.

SHEAR BEAM LOAD CELL EXPERIMENT

For a prismatic cantilevered beam of solid rectangular cross section with a load W at its free end, the shear stress τ at any given cross section along its length is given by the formula:

$$\tau = \frac{W Q}{I b} \qquad (2.8)$$

where:

Q = area moment about the neutral axis,

I = moment of inertia about the neutral axis, and

b = width of the beam.

For a solid rectangular cross section of width b and height h, Q and I are given by the equations:

$$Q = \frac{bh^2}{8} \tag{2.9}$$

$$I = \frac{bh^3}{12} \tag{2.10}$$

Substituting Eqs. 2.9 and 2.10 in Eq. 2.8 and considering that the shear stress τ equals the shear modulus G multiplied by the shear strain γ, the following equation for computing the load W is obtained:

$$W = \frac{2bhG\gamma}{3} \tag{2.11}$$

To verify the application of shear strain gages for load measurement, researchers instrumented a steel bar of rectangular cross section with a pair of two-element 90-degree strain rosettes. Figure 2.3 illustrates the strain rosette used for this laboratory experiment. Two such gages were mounted on opposite faces of the rectangular steel bar in a four-arm active or full bridge configuration. The steel bar was then clamped to a workbench as shown in Figure 2.4 and used to measure a known weight suspended at the free end of the bar. The strain rosettes were wired to a signal conditioner, which measured the voltage change as the bar was loaded. From this measurement, a shear strain of about 8 με was computed. Researchers note that the bridge was zeroed prior to placing the circular disks of known weights at the free end of the bar (see Figure 2.4). This action removes the initial strain due to the weight of the bar and the weight of the disk holder.

Given the Young's modulus E_{mod} for the bar of 29,000 ksi, researchers computed the corresponding shear modulus from the equation:

$$G = \frac{E_{\text{mod}}}{2(1+\nu)} \tag{2.12}$$

This calculation gave a shear modulus of 11,284 ksi for a Poisson's ratio ν of 0.285 for the steel bar. Since the cross-sectional area ($b \times h$) of the bar is 1 inch^2, the total weight of the

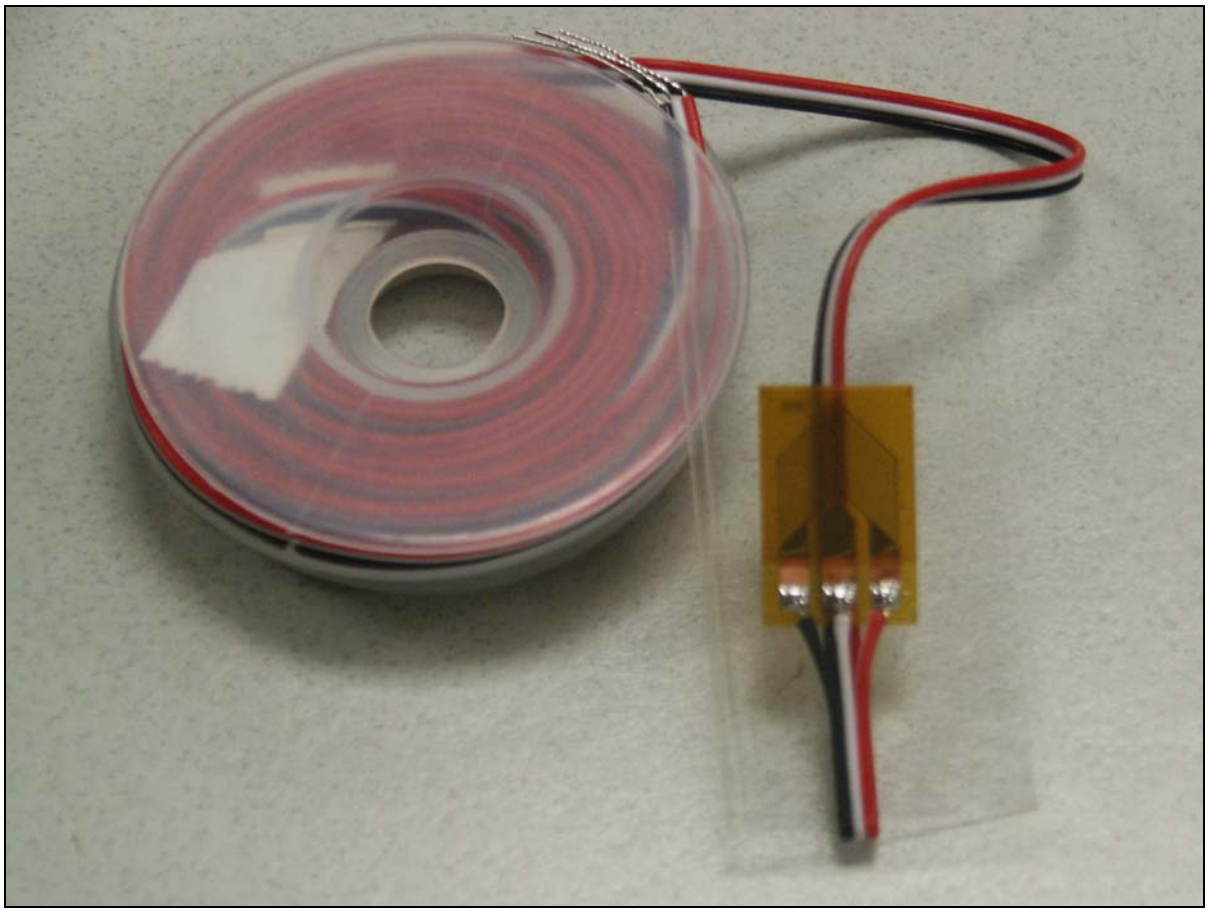

Figure 2.3. Shear Strain Gage Used for Tests.

Figure 2.4. Shear Beam Load Cell Experimental Setup.

circular disks at the free end was computed to be 60.2 lb from Eq. 2.11. This value compares very closely with the reference weight of 60 lb placed on the bar. The close agreement verifies the correct application of the strain gage principles in this laboratory experiment.

SMALL-SCALE TESTING WITH AN INSTRUMENTED TRAILER

Following up on the laboratory test with the shear beam load cell, researchers instrumented a small trailer with shear strain gages to verify the intended method of measuring dynamic loads. Considering the high cost of renting, instrumenting, and calibrating an 18-wheeler for the tests planned in this project, researchers believed that a small-scale experiment to verify the intended method of dynamic load measurement was a prudent step to take. For this experiment, researchers instrumented the single-axle trailer shown in Figure 2.5. For this instrumentation, researchers instrumented the left side of the

Figure 2.5. Small-Scale Trailer Used to Verify Strain Measurement Methodology.

trailer axle with a pair of two-element 90-degree strain rosettes (Figure 2.3) of the same make and model used in the shear beam load cell experiment. This gage is made of Constantan alloy that is self-temperature compensated for tests on cast iron and steel materials. As shown in Figure 2.3, the sensor has two grids arranged in a chevron pattern that sense normal strains in perpendicular directions. The grids have a common connection for use in half-bridge circuits, which yield the shear strain directly. Two such gages were mounted on the left side of the trailer axle on opposite faces and were connected to a signal conditioner in a full bridge configuration. The gages were mounted between the leaf-spring suspension and the inside of the left tire as shown in Figure 2.6. Researchers followed manufacturer's recommendations for mounting the gages on the material to be tested.

In addition, two other sensors were included in the data acquisition system for field testing. One was a distance encoder that researchers attached to the left wheel hub of the towing vehicle to tie the strain measurements to ground distance. The other was a start sensor to locate the start of the section to be tested with the instrumented trailer.

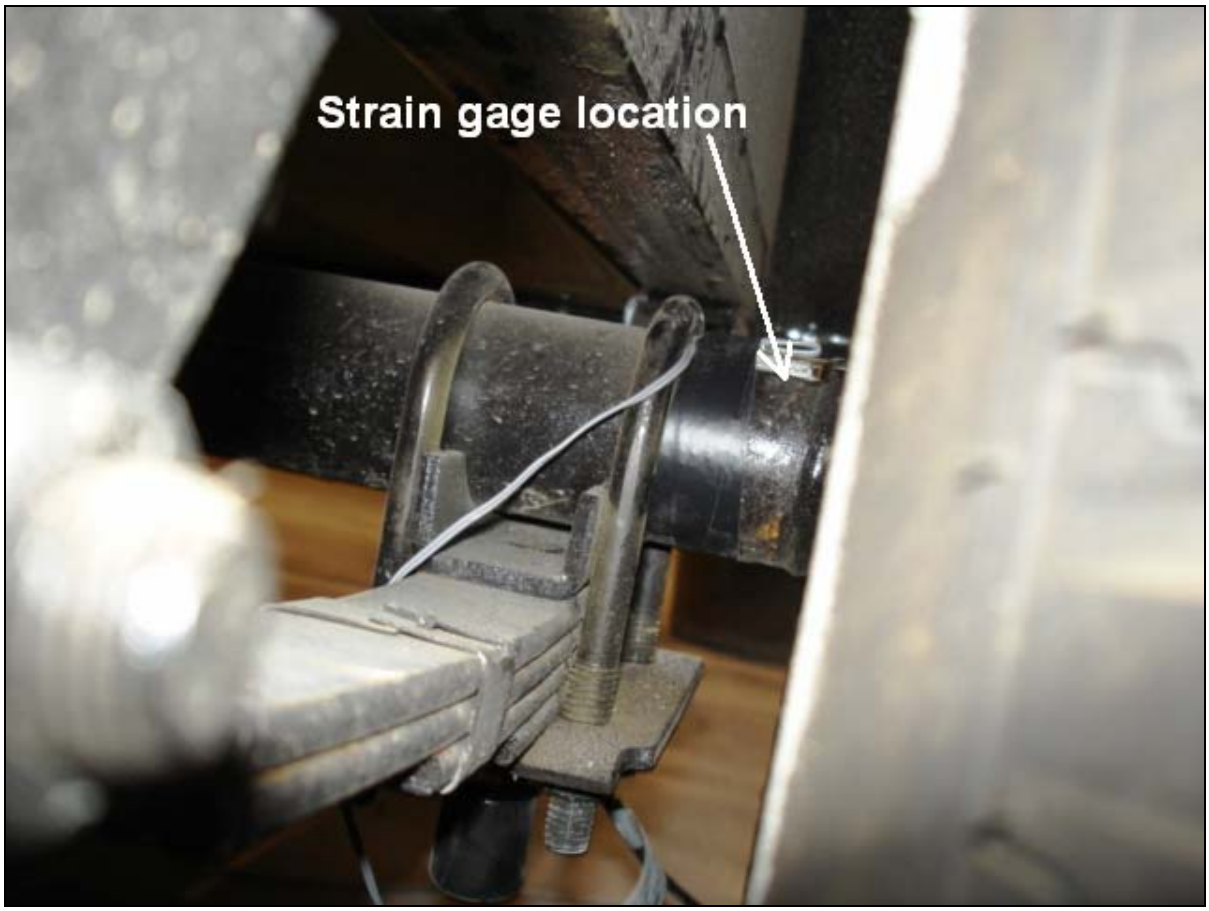

Figure 2.6. Strain Gages Positioned between Suspension and Tire of Small Trailer.

Researchers determined the load calibration curve for the strain gages mounted to the trailer using an MTS loading system. For this laboratory calibration, the loading ram of the MTS was used to apply load at the middle of the axle as illustrated in Figure 2.5. As loads were applied, corresponding strains were determined from the voltage readings measured with the signal conditioner and recorded with the data acquisition software. These voltage readings were converted to strains using Eq. 2.7 with S_g = 2.065 and V = 10 volts. In addition, the force underneath each tire was determined with a load cell positioned under the tire as illustrated in Figure 2.7. From these load and strain measurements, researchers determined the load calibration curve given in Figure 2.8. As observed, the load-strain relationship is linear over the range of loads at which the trailer was tested, and the regression line fits the data points quite well. This linear relationship is given by the equation:

$$\text{Left tire load (lb)} = -18.9 - 15.1 \times \text{shear strain } (\mu\varepsilon) \qquad (2.13)$$

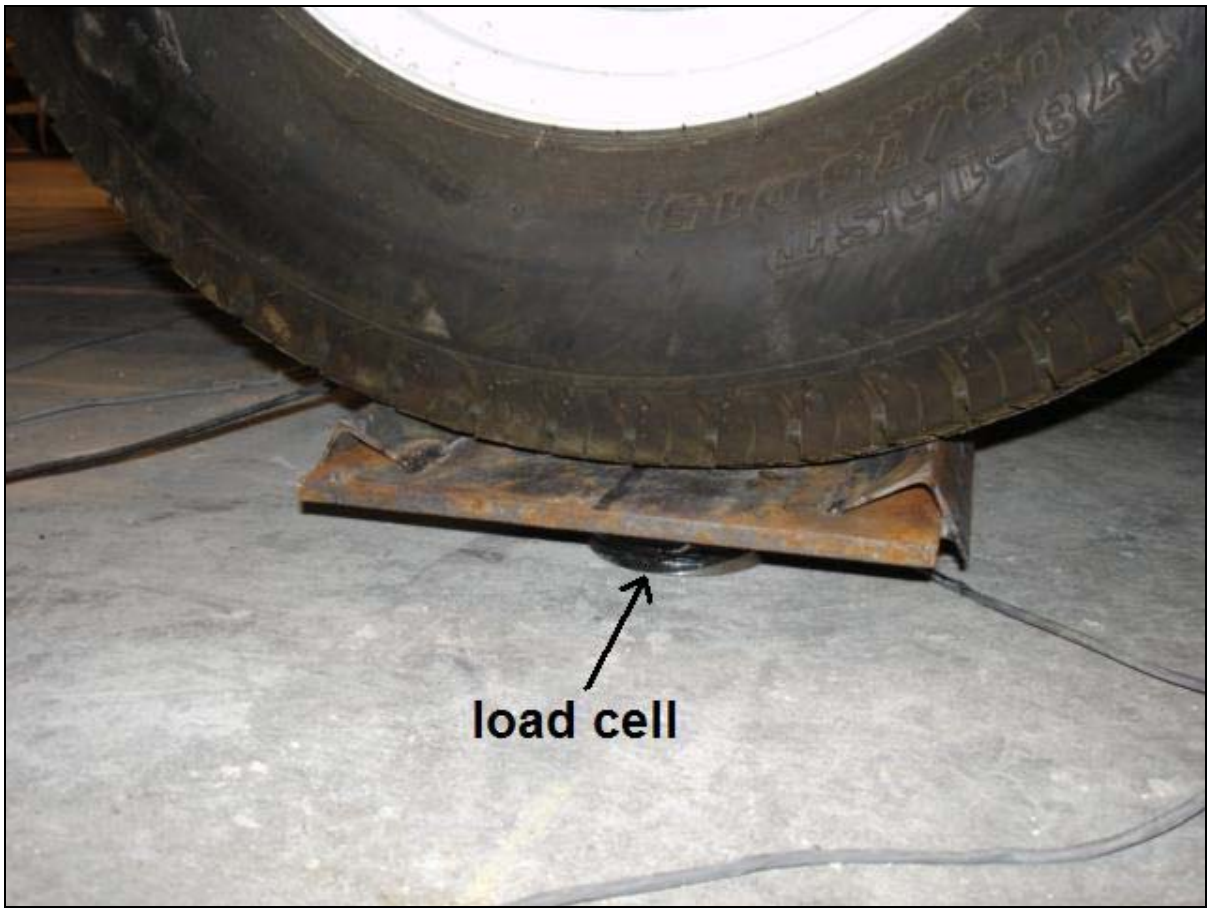

Figure 2.7. Load Cell Placed under Tire during Calibration of Small Trailer.

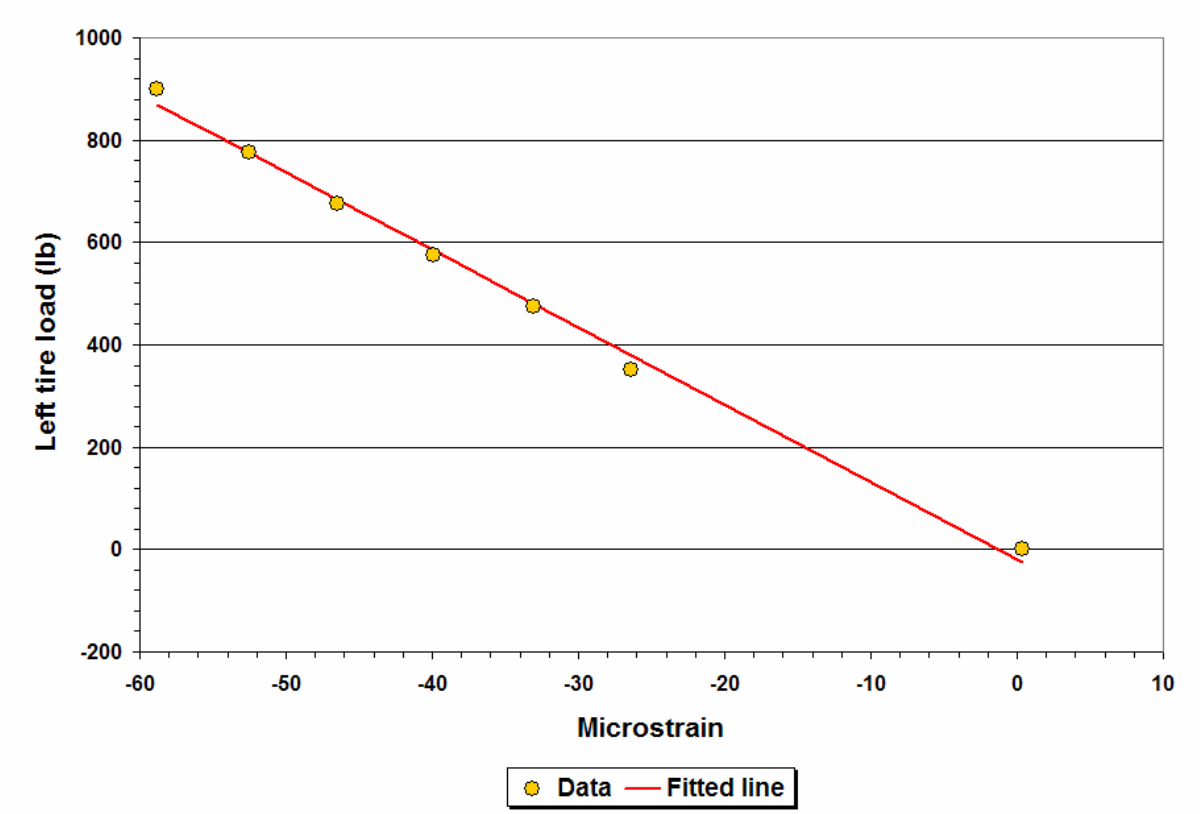

Figure 2.8. Data from Laboratory Calibration of Small Trailer.

The above equation has a coefficient of determination (R^2) of 99.5 percent and a standard error of the estimate (SEE) of 22.7 lb.

After the laboratory calibration, researchers collected data with the trailer on a WIM site located along SH6 close to the intersection with FM60 in College Station. Figures 2.9 to 2.13 plot the dynamic tire loads determined from the left strain gage readings collected from five runs made with the instrumented trailer. Also shown is the WIM measurement for each run. Researchers note the following observations from these charts:

- The dynamic tire loads vary closely about the static tire load of 700 lb.
- The dynamic tire loads determined around the vicinity of the WIM sensor are in reasonable agreement with the corresponding WIM measurement on each of the five runs.
- The load measurements show similar patterns between repeat runs.

In the authors' opinion, these observations provide verification of the methodology for using strain gages to measure dynamic tire loads. Consequently, researchers proceeded with

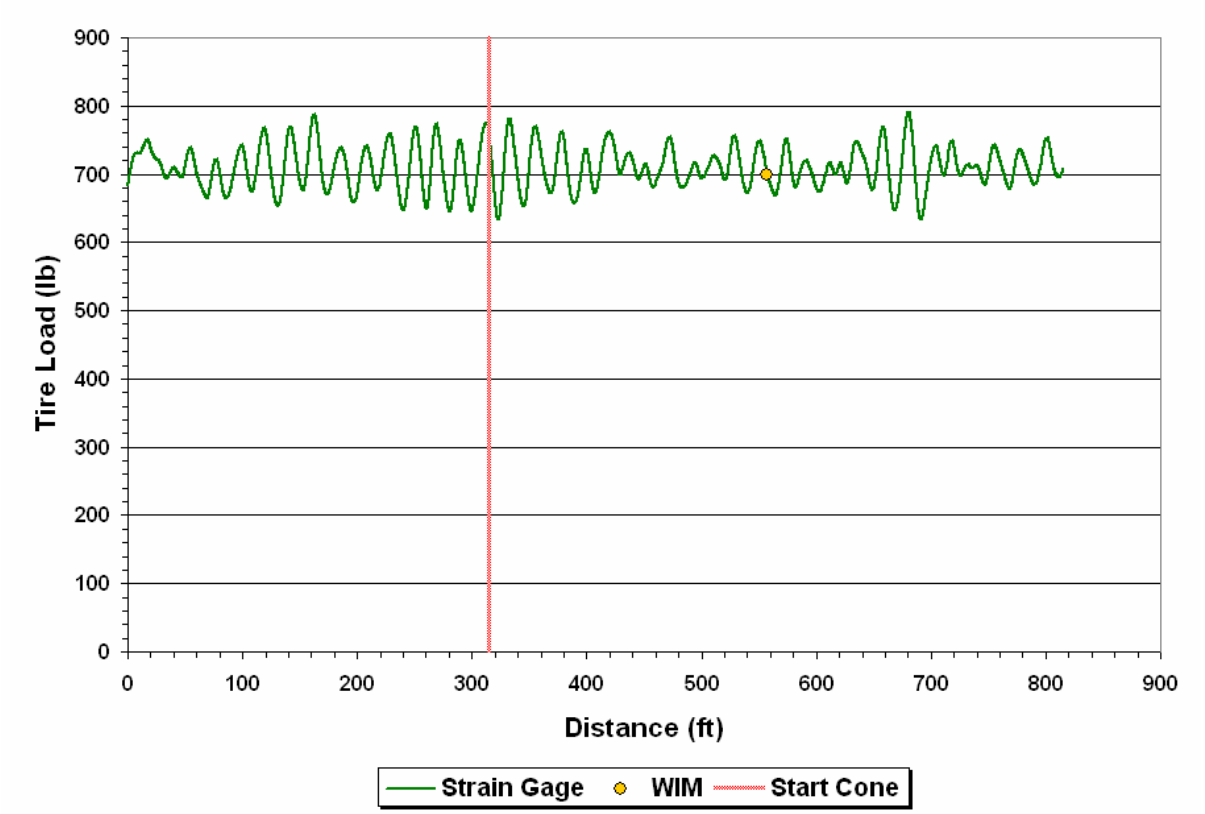

Figure 2.9. Dynamic Loads on Left Tire from Run 1 of Small Trailer on SH6 WIM Site.

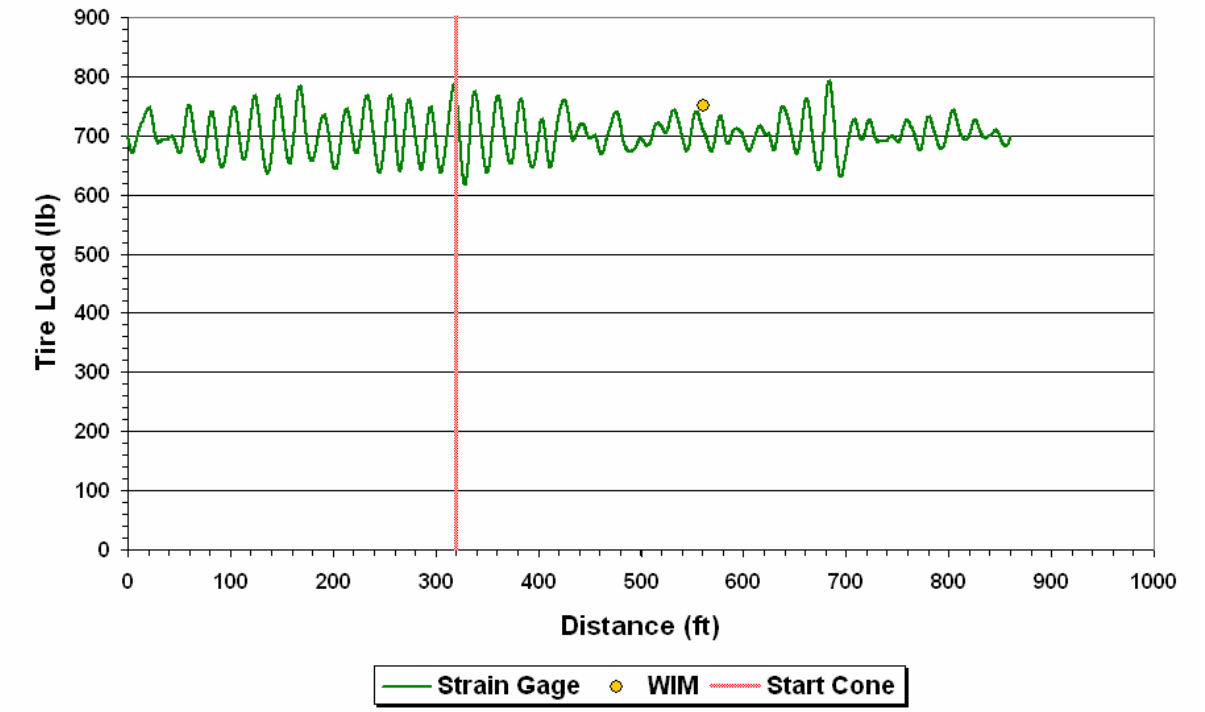

Figure 2.10. Dynamic Loads on Left Tire from Run 2 of Small Trailer on SH6 WIM Site.

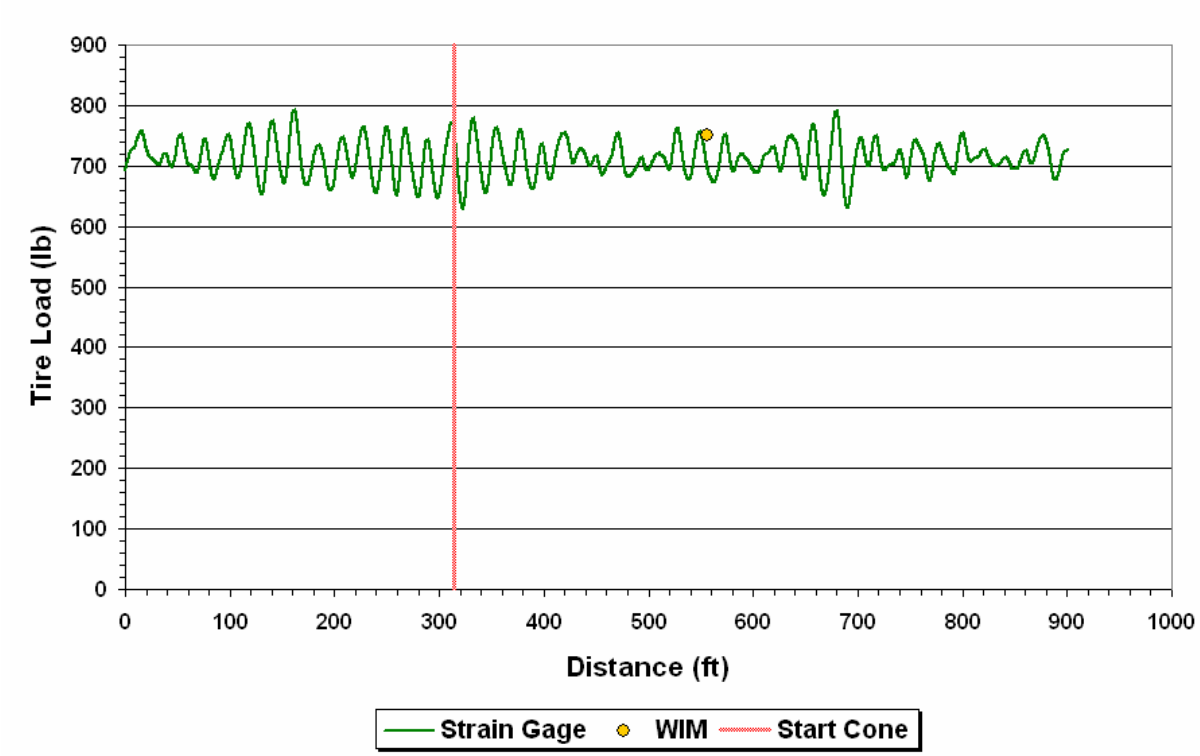

Figure 2.11. Dynamic Loads on Left Tire from Run 3 of Small Trailer on SH6 WIM Site.

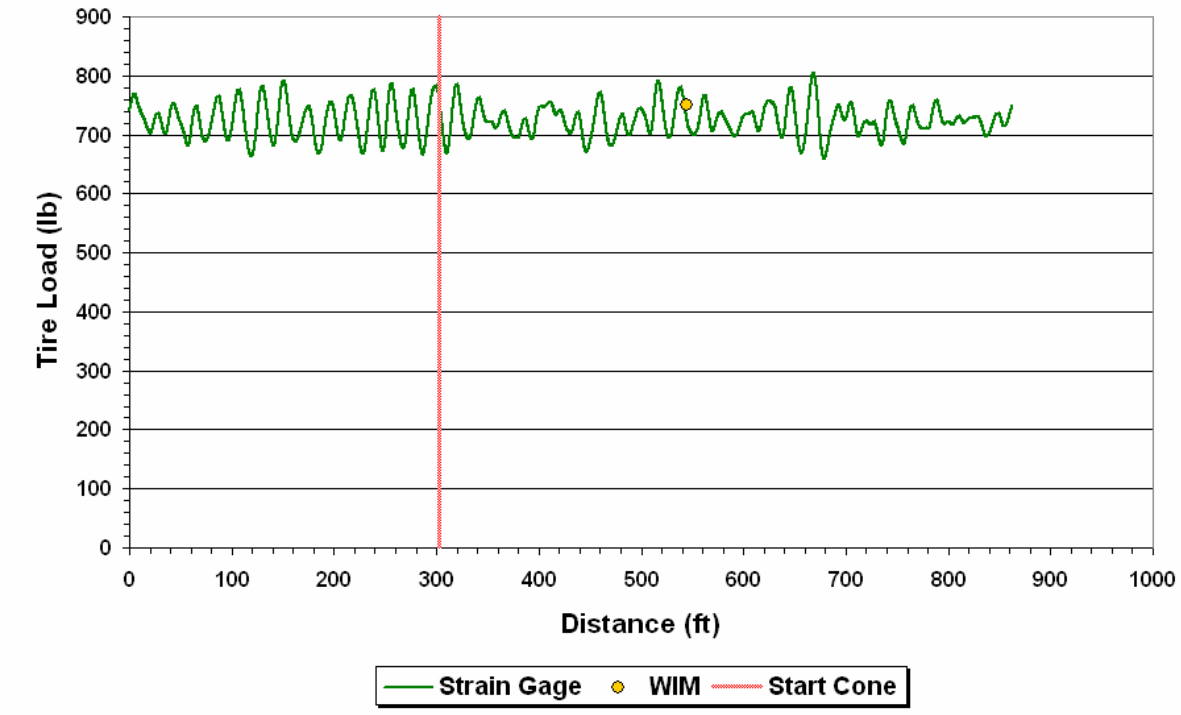

Figure 2.12. Dynamic Loads on Left Tire from Run 4 of Small Trailer on SH6 WIM Site.

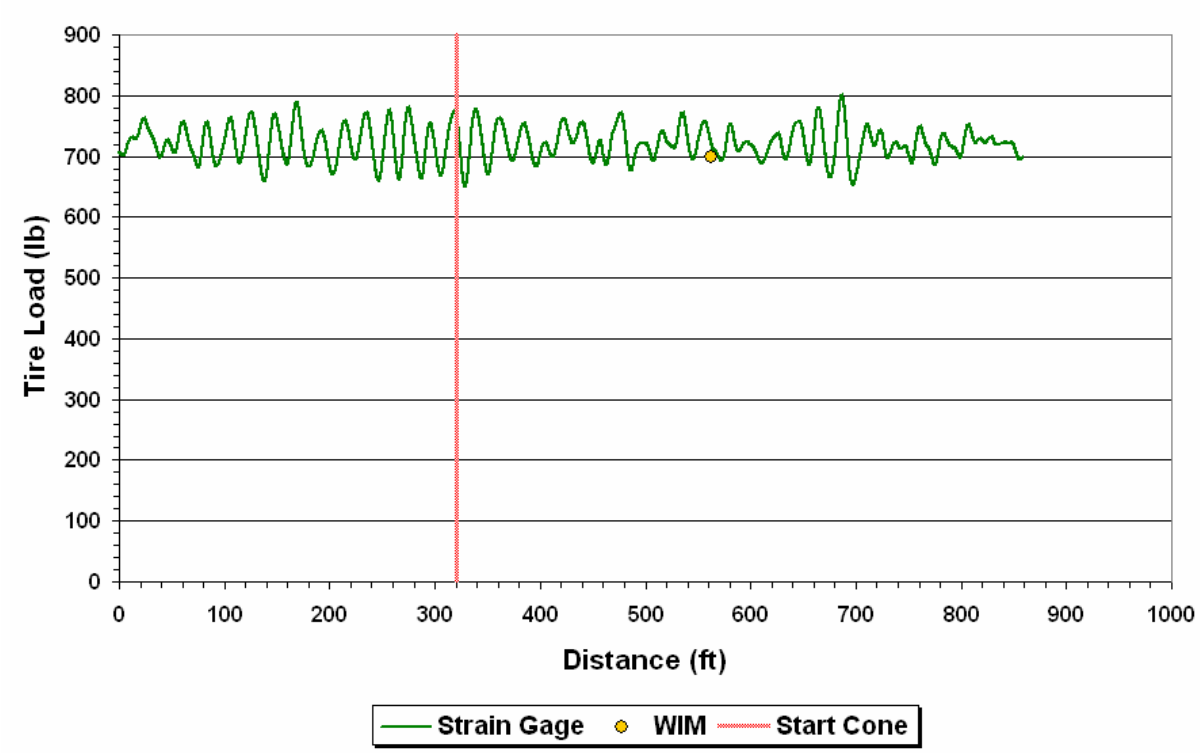

Figure 2.13. Dynamic Loads on Left Tire from Run 5 of Small Trailer on SH6 WIM Site.

instrumenting and calibrating a tractor-semitrailer following the same approach used with the small-scale trailer testing. The next section presents this task.

INSTRUMENTATION AND CALIBRATION OF TRACTOR-SEMITRAILER COMBINATION

Figure 2.14 shows a picture of the tractor-semitrailer combination that researchers tested in this project. To select a vehicle combination for instrumentation and testing, researchers considered the findings of a truck survey conducted by Wang et al. (2000) in an earlier TxDOT project. In that survey, researchers identified the tractor-semitrailer as the most common truck configuration used by truck carriers in Texas. The survey also identified radial tires as the most common truck tire used by truckers, and leaf and air springs as the most popular suspensions. These suspensions were never observed to be on the same axle for the trucks that were sampled, with air spring suspensions commonly found on the drive axles, and semi-elliptic leaf springs on the trailer axles. In view of these findings, researchers selected an 18-wheeler with air bag suspensions on the drive axles and leaf springs on the trailer axles for instrumentation and testing in this project. In terms of truck tire use,

Figure 2.14. Instrumentation and Calibration of Test Vehicle in the Laboratory.

Wang et al. found that the 11R24.5 tire was most frequently used on steering axles, while the 295/75R22.5 radial tire was most often seen on non-steering axles. These same tires were specified on the vehicle instrumented by researchers on this project.

As shown in Figure 2.14, the 18-wheeler was driven into the high-bay structural and materials testing laboratory of the civil engineering department at Texas A&M University. This facility provided ample space and test equipment for instrumenting and calibrating the tractor-semitrailer in an air-conditioned environment. The instrumentation work covered the installation of the same types of sensors (shear strain gages, distance encoder, and start sensor) used for the small-scale trailer testing, except that more strain gages were used to permit measurement of tire loads for all five axles of the tractor-semitrailer. Additionally, researchers added thermocouple sensors to monitor temperatures at the steering, drive, and trailer axle assemblies during testing. Researchers note that temperature sensitivity of the strain measurements is not considered to be an issue in view of the temperature-compensated strain gages and the full bridge configuration used in the truck instrumentation. Nevertheless,

researchers decided to add thermocouples for monitoring test temperatures, which might later prove useful for data analysis and interpretation.

Figure 2.15 shows the layout of the sensors, signal conditioning, and data acquisition devices on the test vehicle. All strain gages were wired to the same signal conditioner used in the small-scale trailer testing. This conditioner amplifies the gage readings and measures the voltage changes in all strain gage channels during testing. Data from all channels, including the distance measuring instrument (DMI), start sensor, and thermocouples, feed into a 16-bit Model 9834 Data Translation module with a 500 KHz maximum sampling rate. This module connects to a notebook computer for data collection via a universal serial bus (USB) cable. A general purpose data acquisition program is used to read and record data from all channels during testing.

Similar to the installation of strain gages for the small-scale trailer testing, the gages were mounted on the 18-wheeler between the suspension and inside tire of each axle as illustrated in Figures 2.16 and 2.17. Two shear strain gages were mounted on each side of the axle on opposite faces, one toward the front and the other toward the rear of the test vehicle. Each strain gage pair was wired in a full bridge configuration for dynamic load measurement on that side of the given axle.

After installation of the gages and set up of the data acquisition system, researchers conducted calibrations to determine the load-strain relationships for the different gages. This calibration was conducted in a similar manner as the small trailer calibration except that more axles were tested beginning with the trailer tandem axle, then the drive, and finally the steering axle. For these tests, a loading plate (Figure 2.18) was positioned on the trailer flatbed at the geometric center of the tandem axle assembly where gages were to be calibrated. In addition, technicians used the loading crane of the high-bay laboratory to lift the axle assembly and position load cells underneath each dual tire (Figure 2.19).

Prior to calibrating the strain gages, researchers calibrated the load cells by determining the relationship between the readings from each load cell and the corresponding loads measured with the reference load cell maintained by the high-bay structural and materials testing laboratory. The authors note that the calibration of the reference load cell is National Institute of Standards and Technology (NIST) traceable. During calibration, the voltage readings from the test load cells were recorded along with the corresponding load magnitudes measured with the reference load cell. Figures 2.20 to 2.23 show the calibration

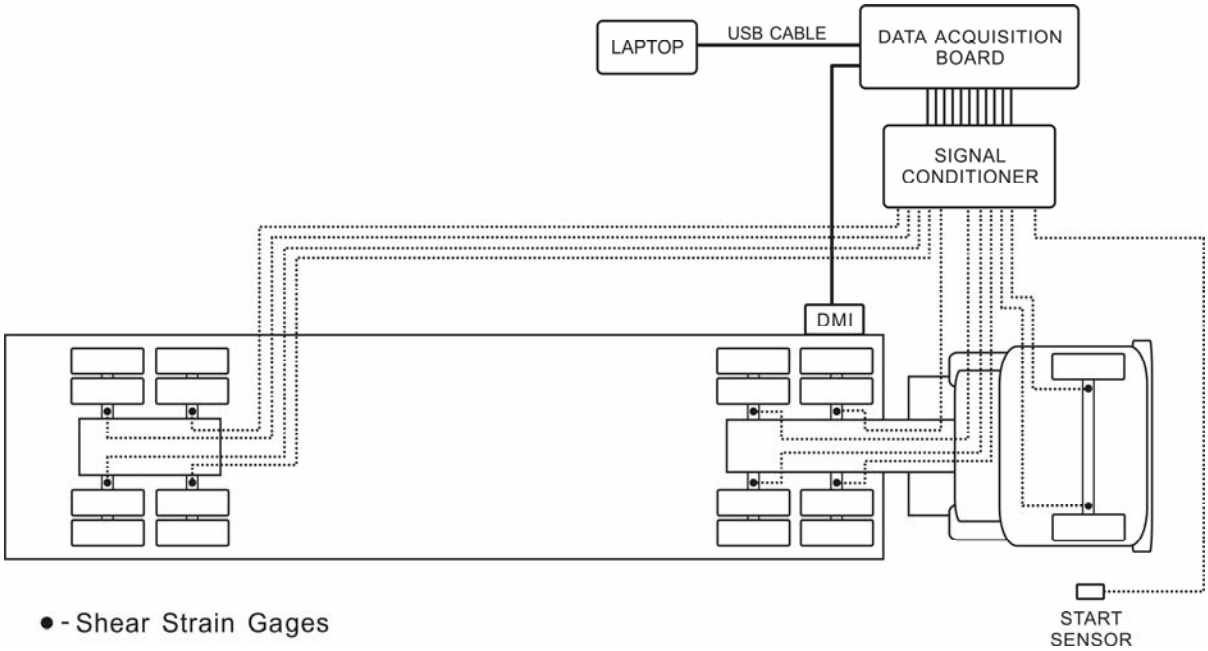

Figure 2.15. Layout of Sensors, Signal Conditioning, and Data Acquisition Devices on Instrumented Truck.

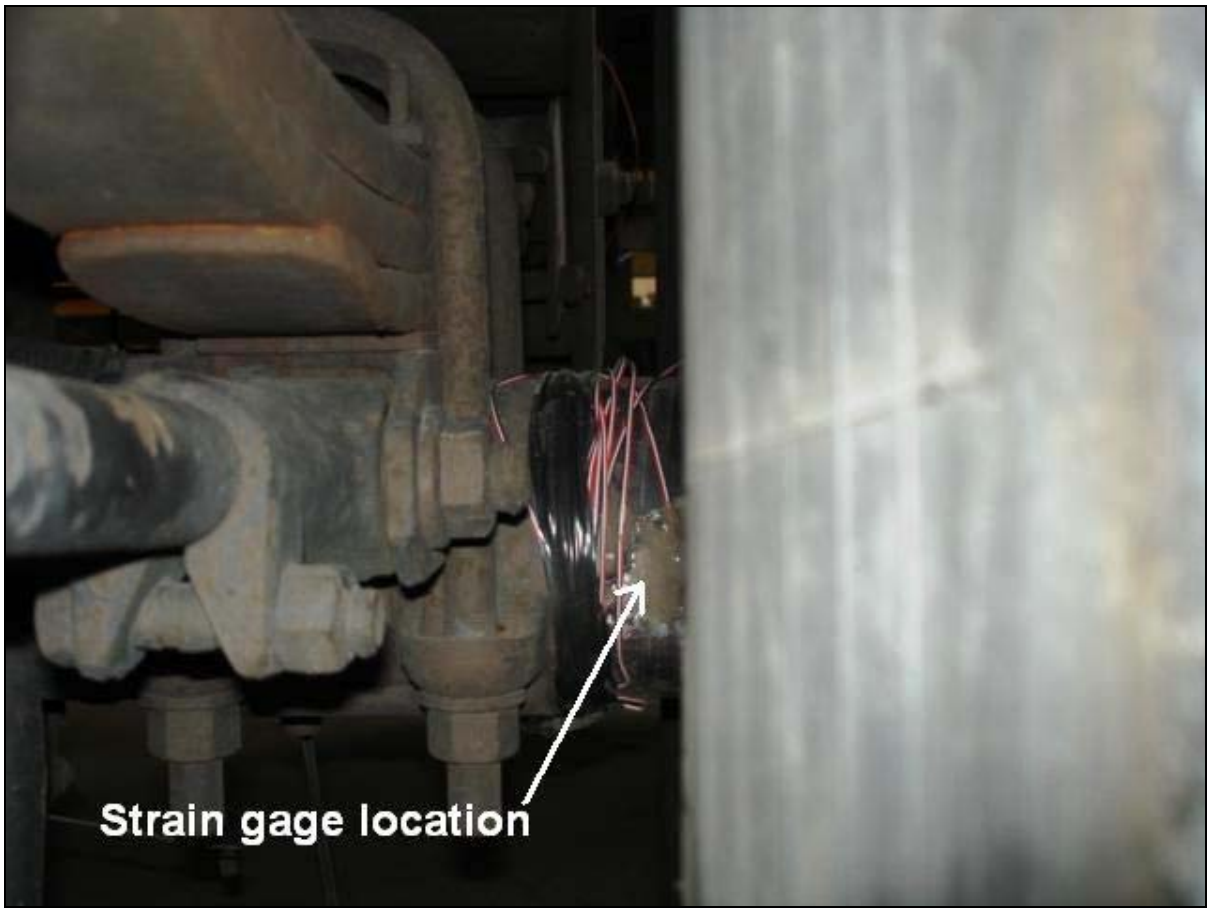

Figure 2.16. Strain Gage Mounted on Trailer Axle.

Figure 2.17. Strain Gage Mounted on Drive Axle.

Figure 2.18. Application of Load to Axle Assembly through Loading Plate. (axle assembly underneath the loading plate and load ram)

Figure 2.19. Load Cells Positioned under Dual Tires of Trailer Axle Assembly.

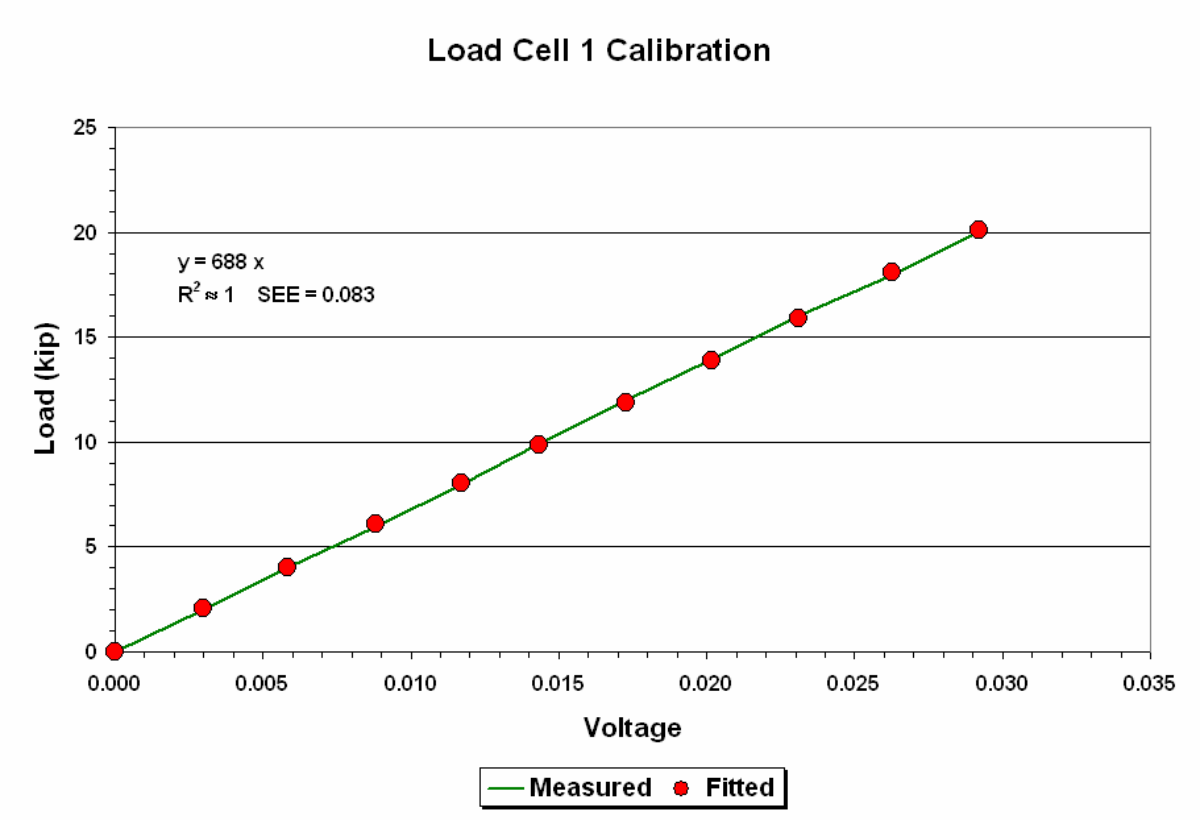

Figure 2.20. Calibration Results for Load Cell #1.

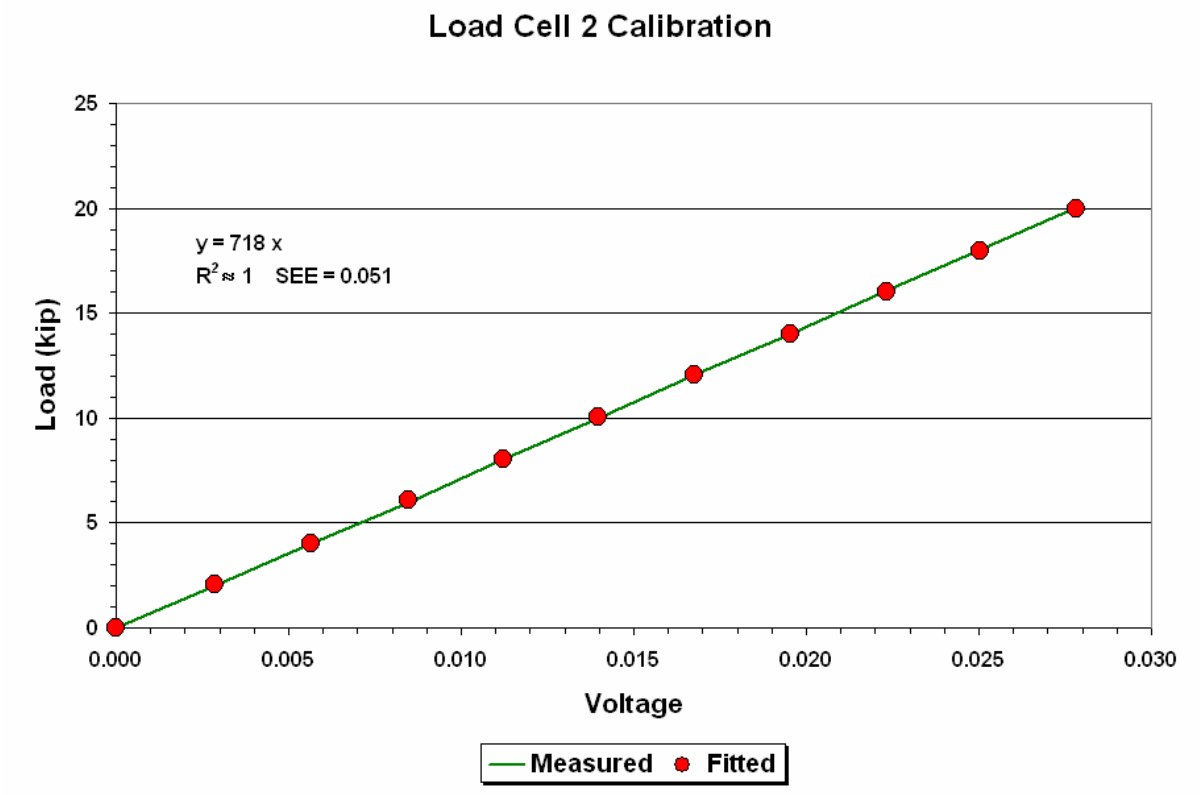

Figure 2.21. Calibration Results for Load Cell #2.

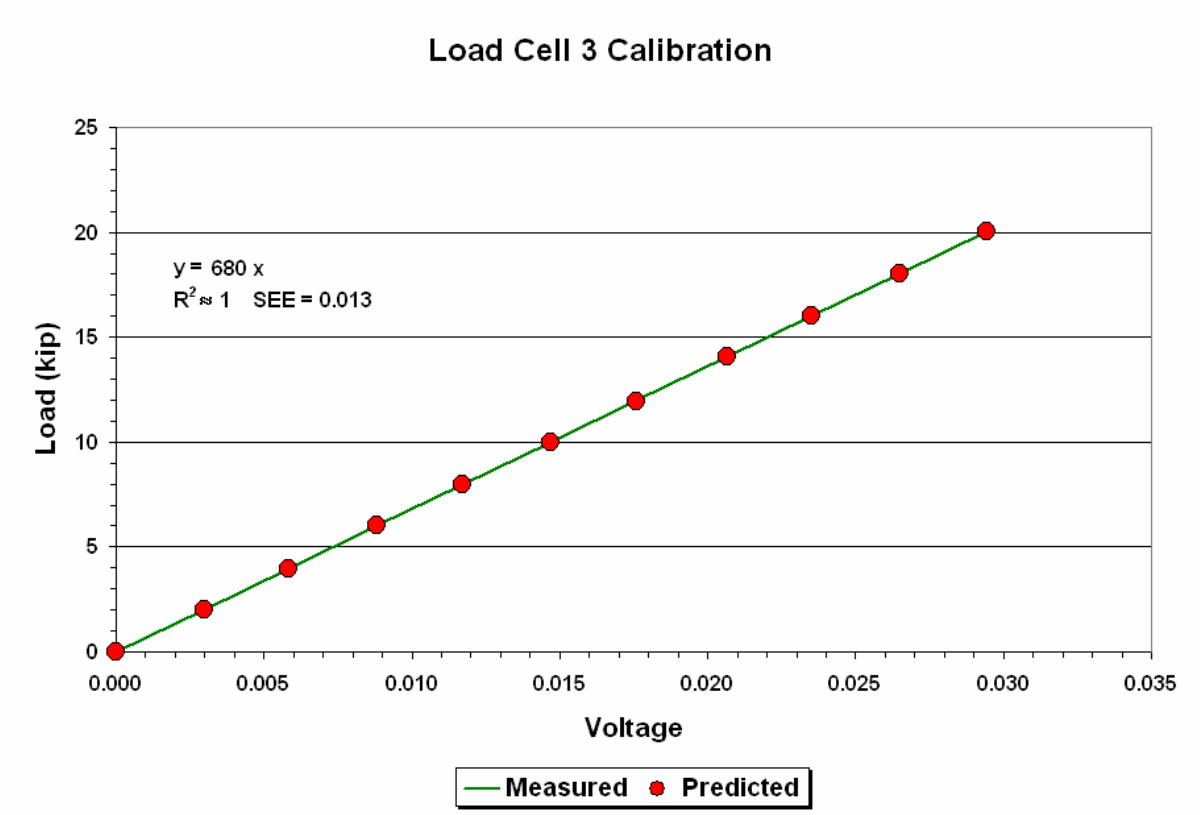

Figure 2.22. Calibration Results for Load Cell #3.

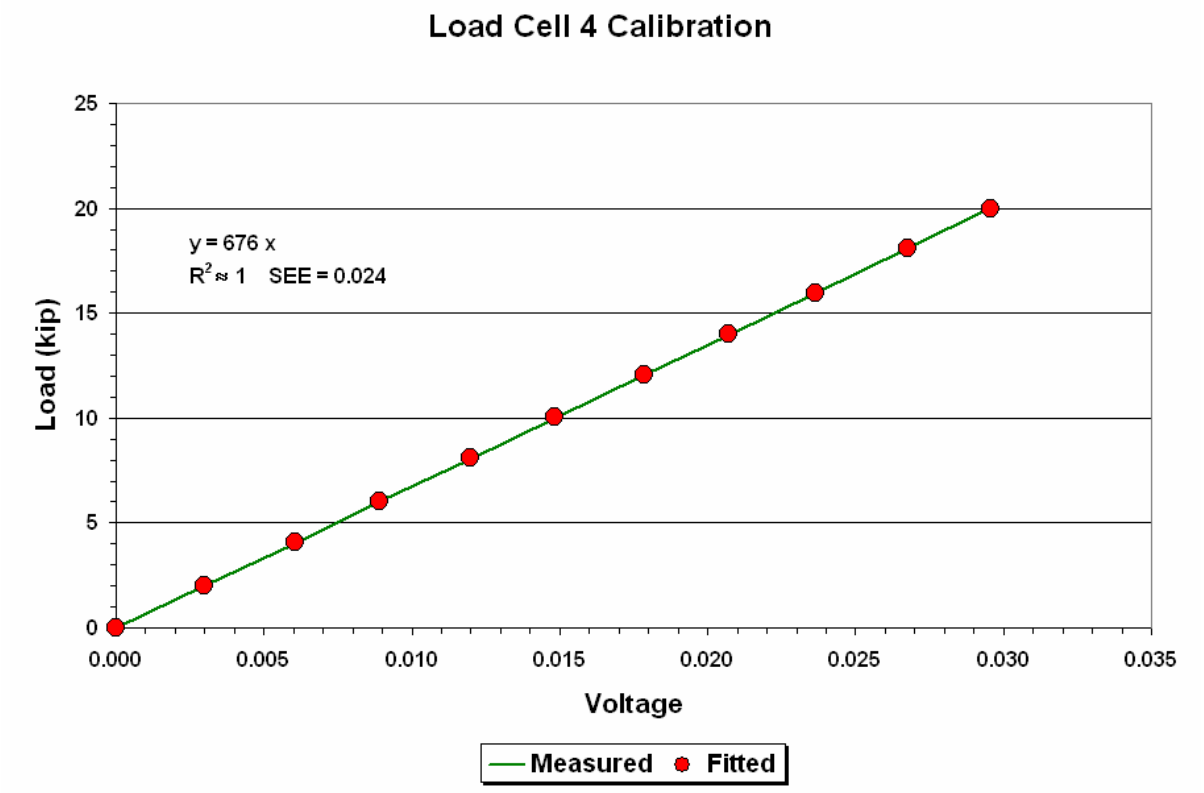

Figure 2.23. Calibration Results for Load Cell #4.

equations determined from these tests. The relationships show a high degree of linearity over the range of loads at which the calibrations were conducted. In addition, the regression line fits the test data for each load cell very well. Thus, researchers used the relationships shown to calibrate the strain gages mounted on the tractor-semitrailer for measurement of dynamic tire loads.

During calibration, researchers used a 100-kip MTS system to apply loads to the axle assembly through the plate located on the trailer flatbed. The first step in the calibration was to zero the strain gages and load cells. This step was accomplished with the axle assembly raised above ground using the loading crane. After zeroing the strain gages and load cells, technicians carefully lowered the axle assembly back onto the load cells. The initial strain and load cell readings were then recorded with no other loads applied to the trailer. Subsequently, researchers applied a series of loads to the axle using a 100-kip MTS system. At each load level, strain gage and load cell readings were recorded to collect data for determining the calibration curves of the different gages mounted on the axle assembly tested. This loading sequence was followed by an unloading sequence during which readings were taken as the loads were reduced.

Figures 2.24 to 2.27 illustrate the load-strain relationships determined from calibration of the strain gages mounted on the trailer axles. It is observed that the data exhibit a strong linear relationship between the strain gage readings and the tire load measurements for the range of loads applied. Note also the difference in signs of the shear strains between the left and right sides of each trailer axle. This difference is expected based on mechanics' principles.

Researchers used the same procedure for calibrating the trailer gages to calibrate the gages on the drive axles. Figures 2.28 to 2.31 show the calibration relationships determined for drive axle strain gages. Again, the test data exhibit a strong linear relationship between the strain gage readings and the measured tire loads. The regression line also fits the test data for each drive axle strain gage quite well, in the authors' opinion.

For the steering axle, there was no way of applying the load directly on top of the axle, either from the front of the tractor or from inside the engine compartment. Since the vehicle was rented, modifications were not possible. Consequently, the calibration data for the steering axle were collected with the loads applied through the drive axles. During this process, the loads transmitted to the steering axle were measured with load cells placed

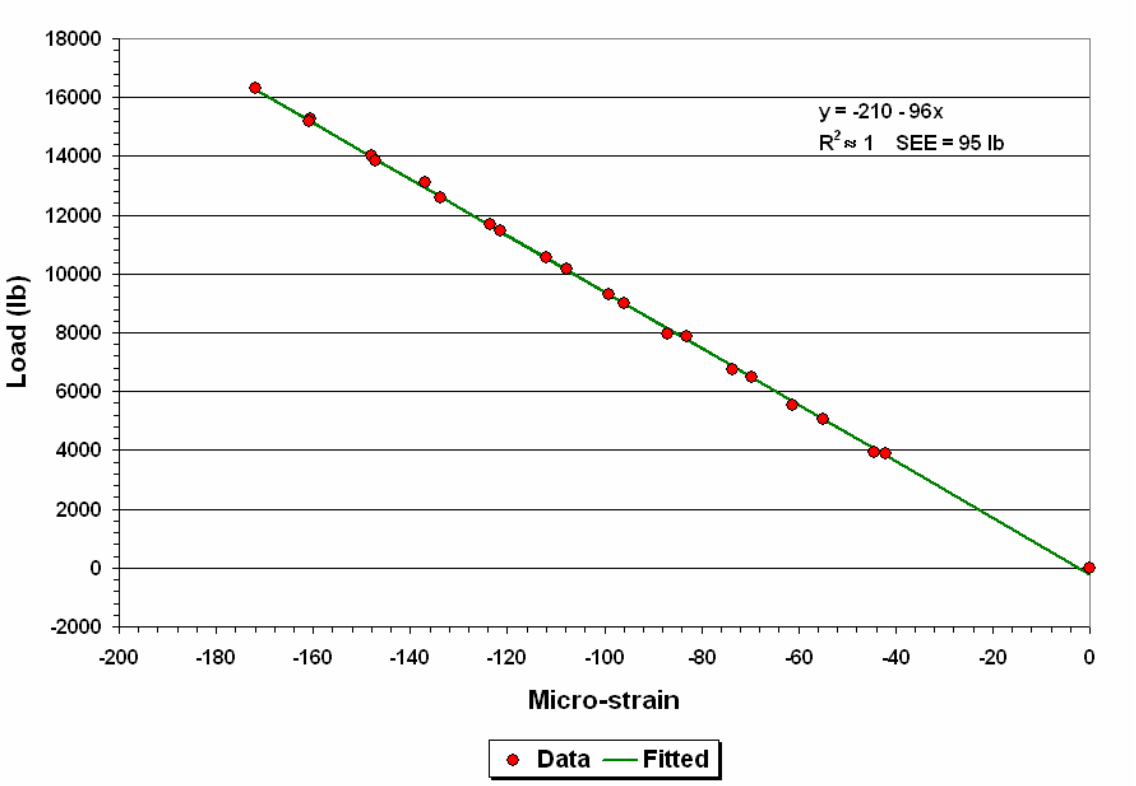

Figure 2.24. Strain Gage Calibration Curve for Left Side of Trailer Lead Axle.

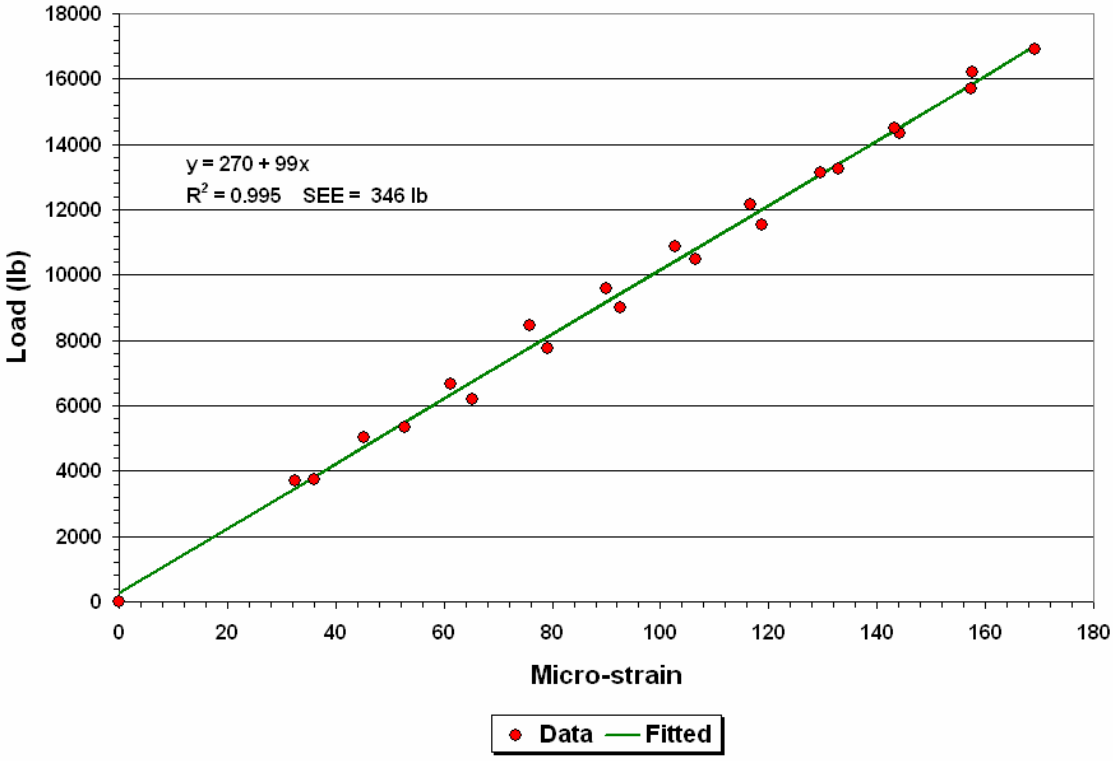

Figure 2.25. Strain Gage Calibration Curve for Right Side of Trailer Lead Axle.

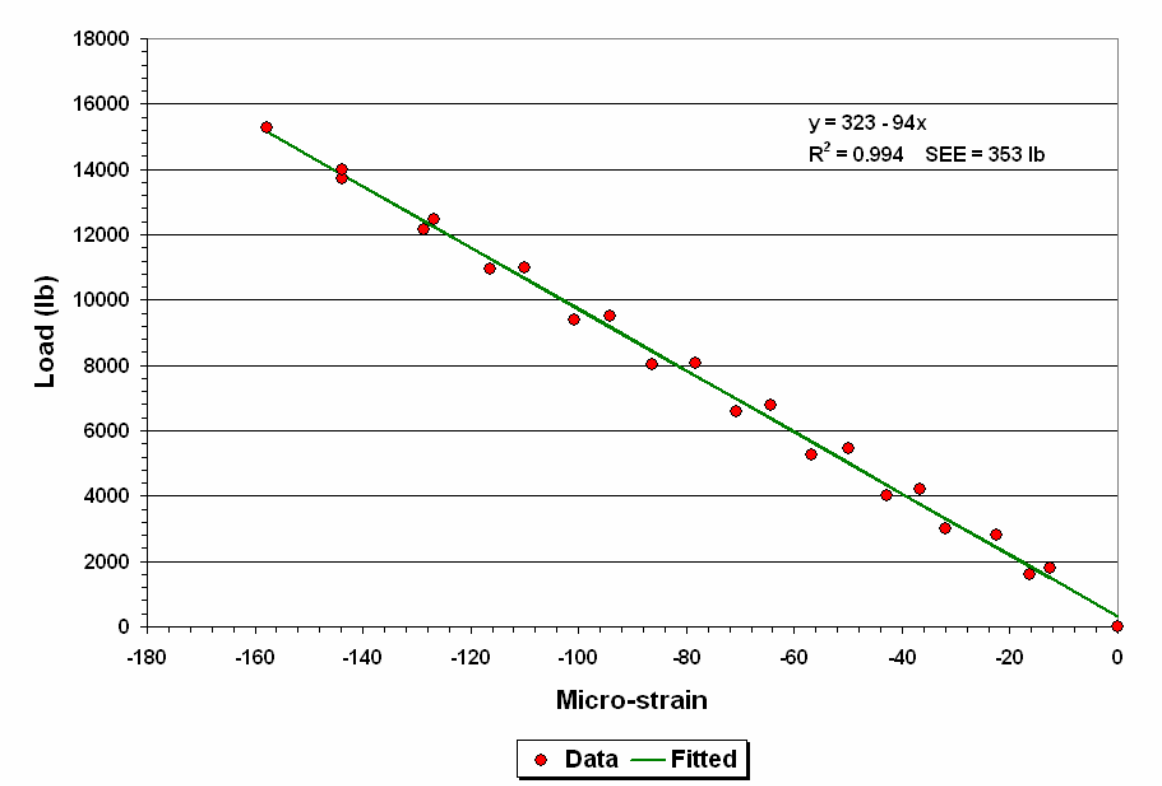

Figure 2.26. Strain Gage Calibration Curve for Left Side of Second Trailer Axle.

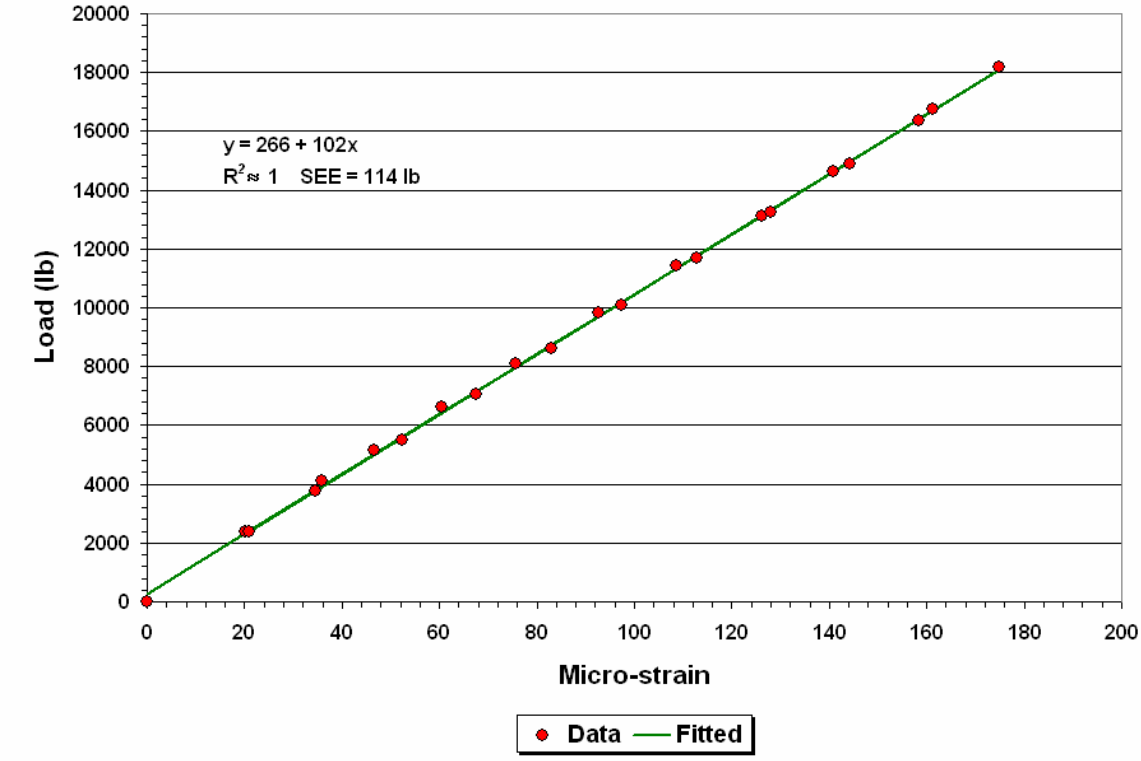

Figure 2.27. Strain Gage Calibration Curve for Right Side of Second Trailer Axle.

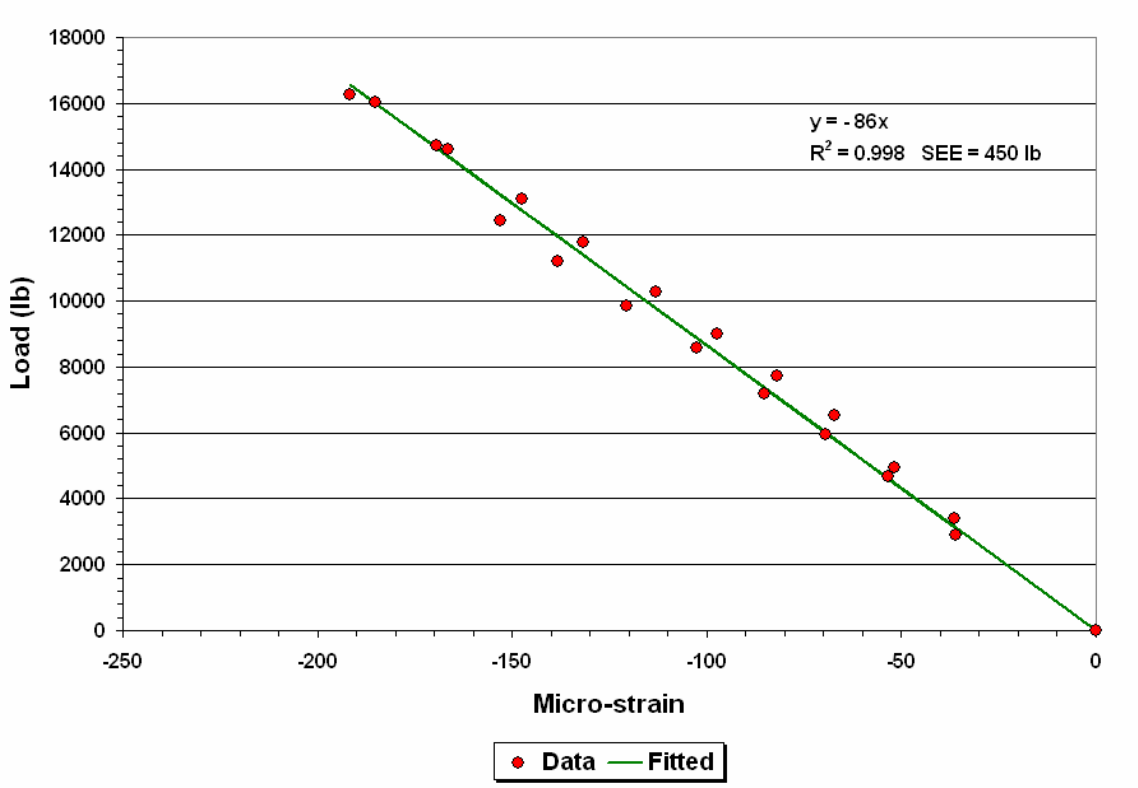

Figure 2.28. Strain Gage Calibration Curve for Left Side of Drive Lead Axle.

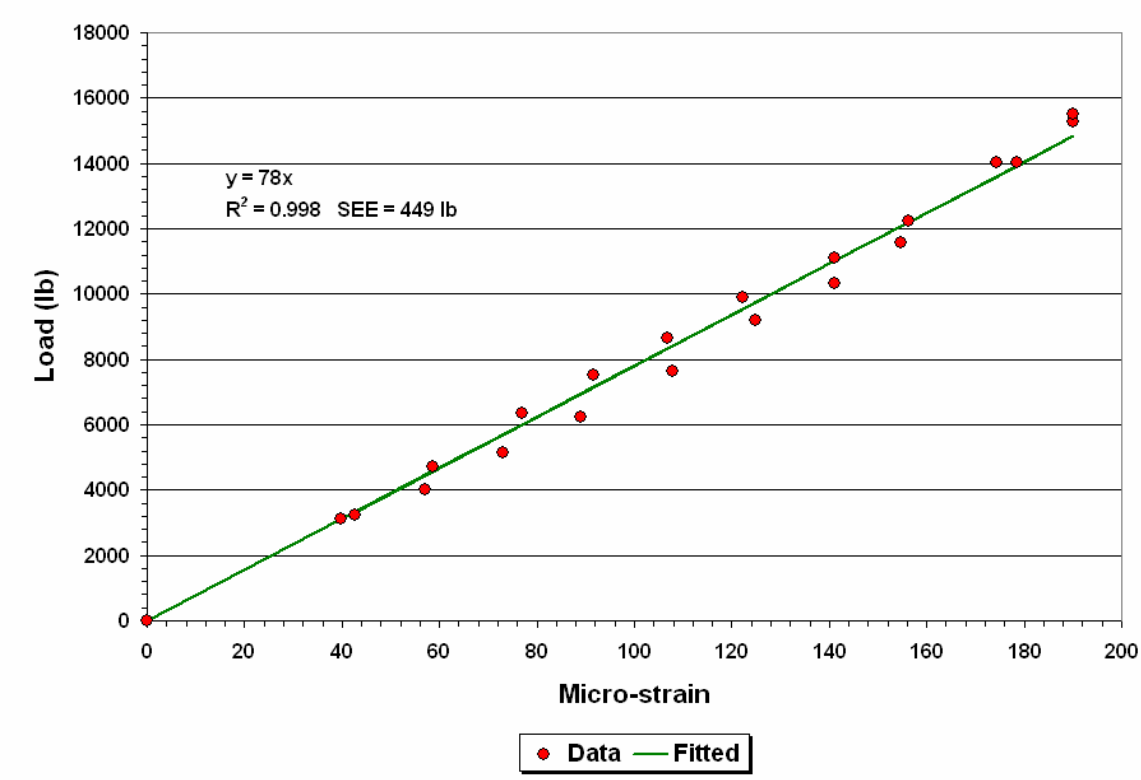

Figure 2.29. Strain Gage Calibration Curve for Right Side of Drive Lead Axle.

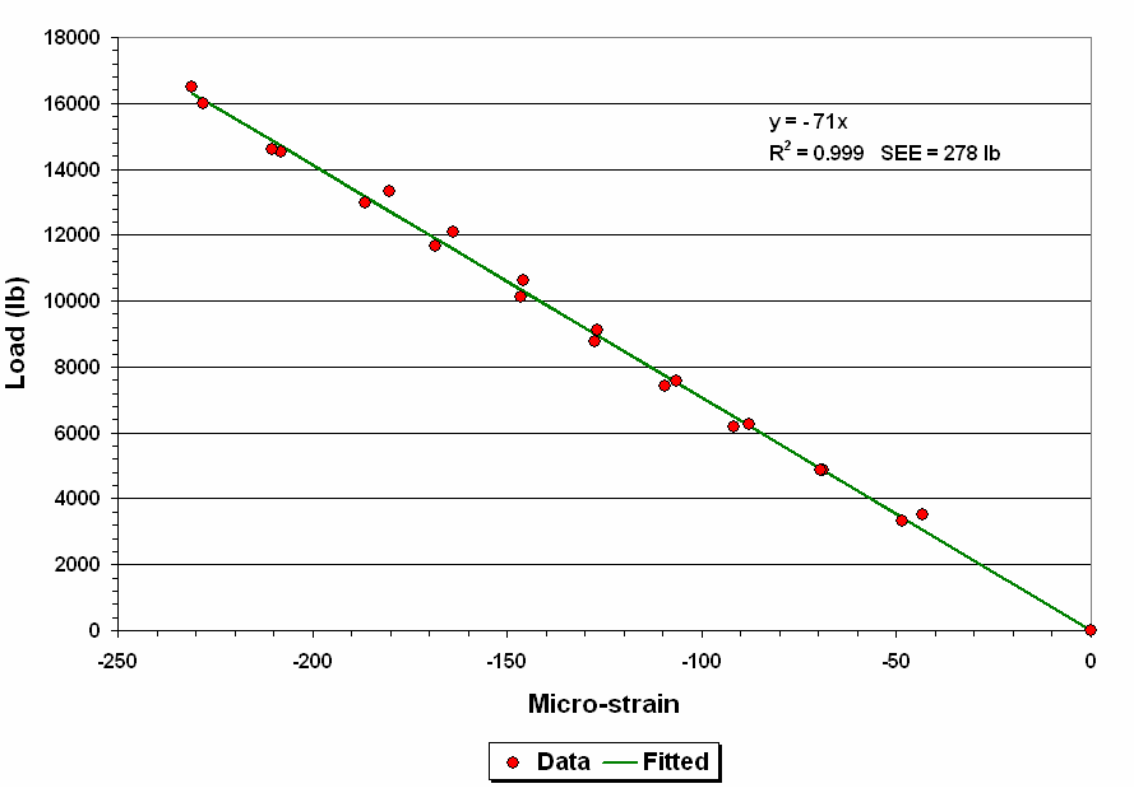

Figure 2.30. Strain Gage Calibration Curve for Left Side of Drive Trailing Axle.

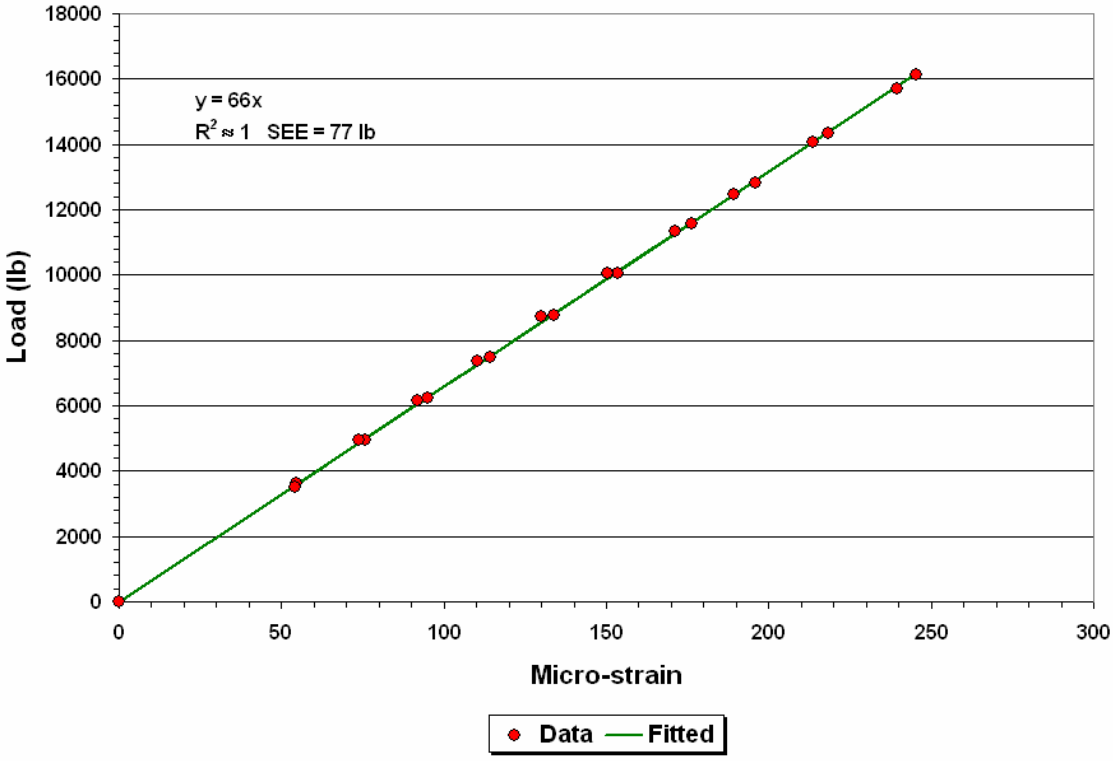

Figure 2.31. Strain Gage Calibration Curve for Right Side of Drive Trailing Axle.

underneath its left and right tires. To keep the tractor level, researchers placed spacers underneath the drive axles. While it was not possible to load the steering axle directly, researchers are of the opinion that the method used to calibrate the gages on the steering axle simulated more closely the way loads are transmitted or distributed to this axle in practice.

Figures 2.32 and 2.33 show the calibration relationships determined for the steering axle strain gages. During calibration, researchers observed that the tire loads on the steering axle did not vary appreciably with changes in the load applied through the drive axle assembly, as may be inferred from the range of tire loads plotted in Figures 2.32 and 2.33. This observation is consistent with weigh-in-motion data on five axle tractor-semitrailer combination trucks where the most consistent axle weight is from the steer axles, which remains reasonably constant under various loading scenarios.

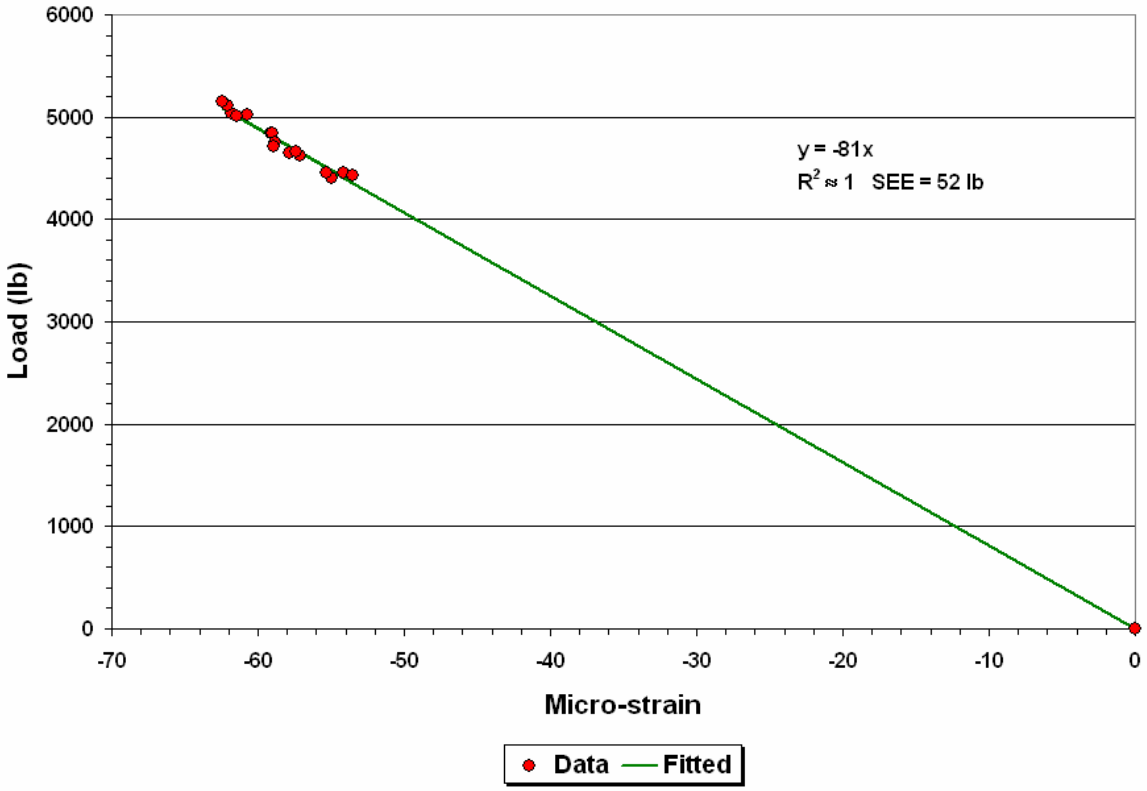

Figure 2.32. Strain Gage Calibration Curve for Left Side of Steering Axle.

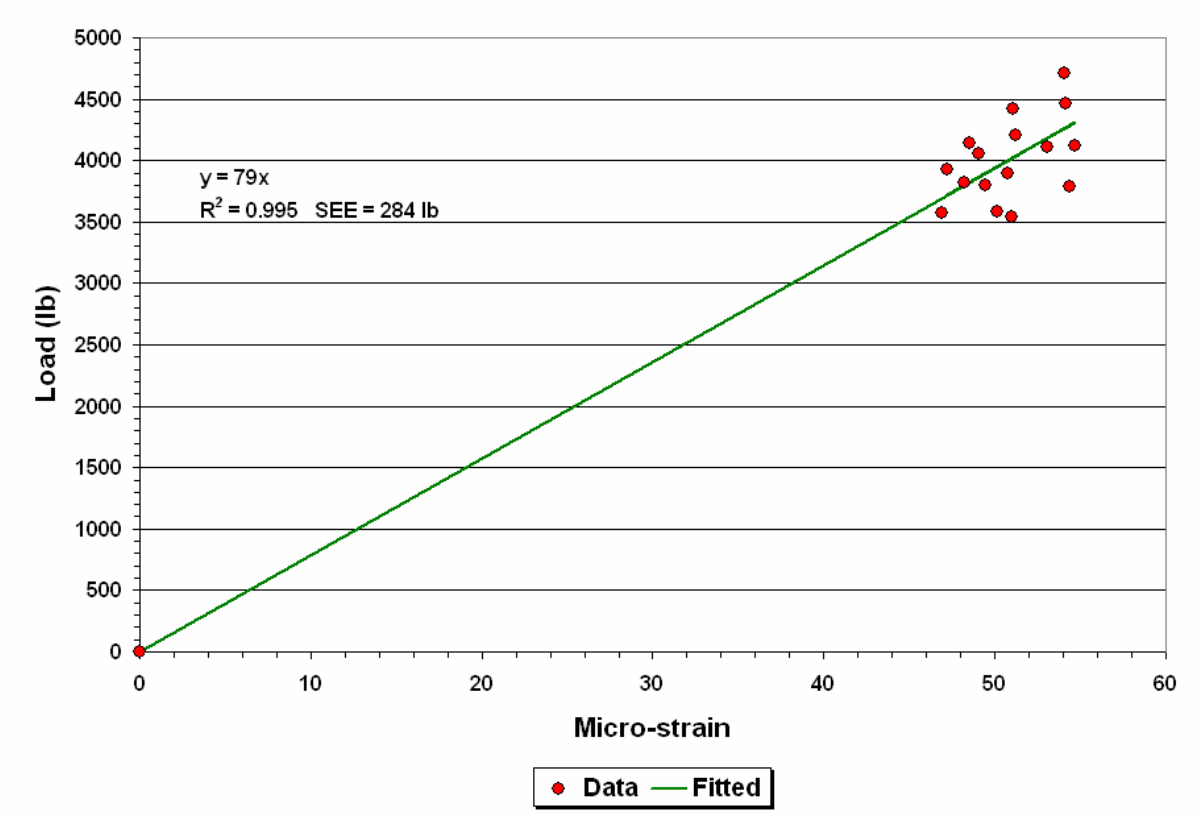

Figure 2.33. Strain Gage Calibration Curve for Right Side of Steering Axle.

CHAPTER III. FABRICATION AND VERIFICATION OF INERTIAL PROFILING SYSTEM

Profile measurements are needed to evaluate relationships between vehicle dynamic loads and surface roughness for the purpose of evaluating the current ride specification in this project. Initially, researchers instrumented a tractor-semitrailer with a portable inertial profiling system to permit synchronized collection of dynamic tire loads and surface profiles during testing. However, tests to verify profiler performance based on the certification requirements in TxDOT Test Method Tex-1001S were not successful. Compared to the vibrations from vans or light trucks on which profilers are commonly used, the vibrations from the test vehicle were considerably larger, resulting in failure of the dampeners used to isolate the accelerometers and lasers of the profiling system from vibrations of the test vehicle during testing. The dampeners sheared off after several repeat runs of the test truck on the pavement sections used to evaluate the on-board inertial profiling system.

Following the suggestion of the project monitoring committee, researchers dropped the idea of instrumenting a tractor-semitrailer with an inertial profiling system. Instead of this approach, profile data were to be collected using a high-speed inertial profiler separate from the instrumented vehicle combination. To minimize differences between wheel paths tracked, the sensors of the inertial profiler would be set to match the spacing between the dual wheels on the left and right sides of the instrumented tractor-semitrailer. In addition, the operator of the inertial profiler would try to take data as close as possible on the same wheel paths where dynamic load measurements were collected with the instrumented truck.

Ordinarily, this project would have used one of TxDOT's inertial profilers to collect profile measurements. However, problems with the availability of an inertial profiler led researchers to instrument a test vehicle with an inertial profiling system to conduct the required tests. This instrumentation was an in-house effort funded by TTI. The profiling system followed the same design developed by Walker (1997) and used existing software. The main components of the profiler are:

- a chassis unit containing the power supply and signal interface modules,
- two laser/accelerometer modules mounted on the front of the test vehicle,
- a Model 9803 Data Translation board for data acquisition,
- a distance encoder,

- a start sensor, and
- a notebook computer.

Figure 3.1 shows the laser/accelerometer modules mounted in front of the TTI truck that researchers instrumented for inertial profile measurements. As shown, the modules are positioned on a bar that goes into receiver hitches located on the front bumper of the truck. The groove along the middle of the bar permits the operator to position each module along the bar and vary the sensor spacing. The modules are tightened in place by set screws. In addition, the height of the bar can be changed to accommodate lasers with different standoffs.

Researchers evaluated the profiler shown in Figure 3.1 on the certification pad located at the Riverside Campus of Texas A&M University. For this evaluation, data were taken along the left and right wheel paths of two 530-ft sections (one smooth and the other medium-smooth) that researchers selected for testing the inertial profiler. Runs were made in the northbound direction of the pad, and profile elevations were recorded at 0.96-inch intervals in the data files. A total of 20 runs were made, 10 on each section. Researchers analyzed the test data to evaluate profile repeatability and accuracy, as well as IRI repeatability and accuracy.

Figures 3.2 to 3.5 illustrate the repeatability of the profiles measured on each section. Tables 3.1 to 3.4 summarize the statistics determined from the analysis of test data. The results presented show that the profiler (as configured) meets the requirements for inertial profiler certification stipulated in TxDOT Test Method Tex-1001S and that a suitable profiling system has been built for use on this project as well as on other research projects where this capability is needed. Having successfully fabricated an inertial profiler, researchers collected profile data on a number of TxDOT paving projects with this equipment. On these same projects, researchers also ran their instrumented tractor-semitrailer combination to measure dynamic tire loads. Researchers then analyzed these measurements in conjunction with the profile data collected on those projects to evaluate TxDOT's current ride specification, Item 585. The findings from this evaluation are presented in the next chapter of this report.

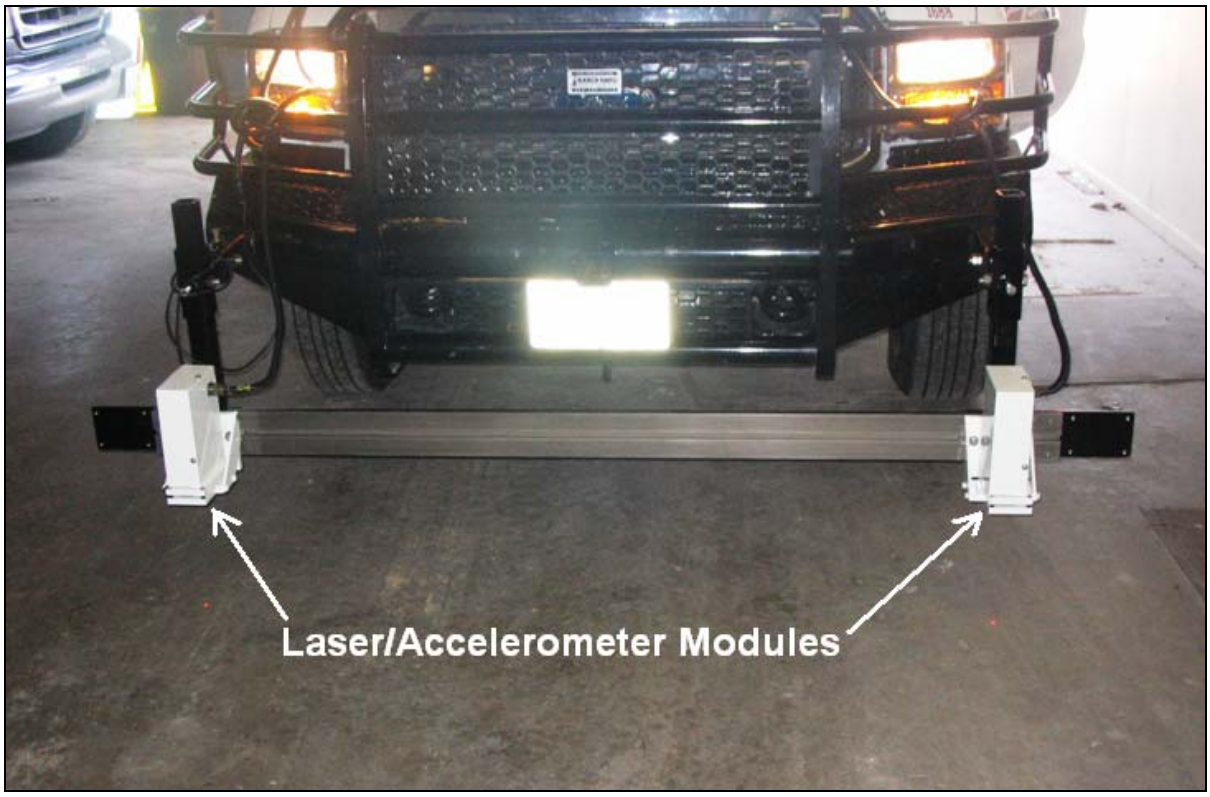

Figure 3.1. Laser/Accelerometer Modules Mounted in Front of Test Vehicle.

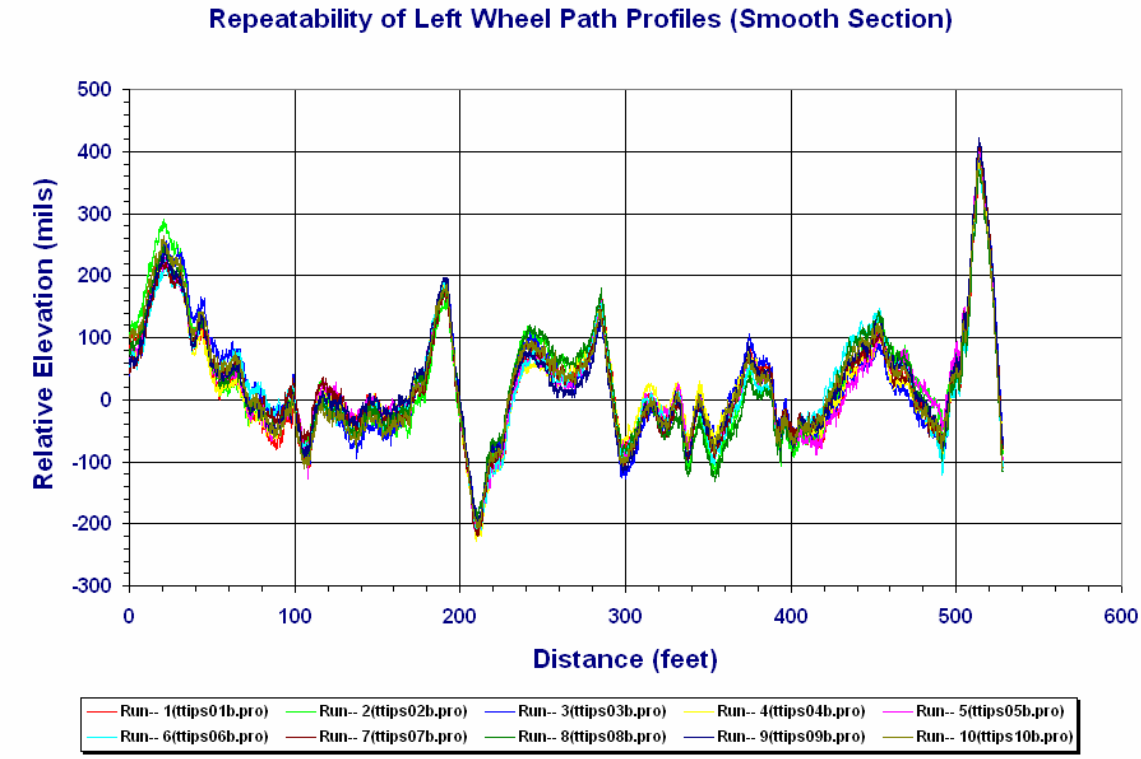

Figure 3.2. Repeatability of Profiles Measured on Left Wheel Path of Smooth Section.

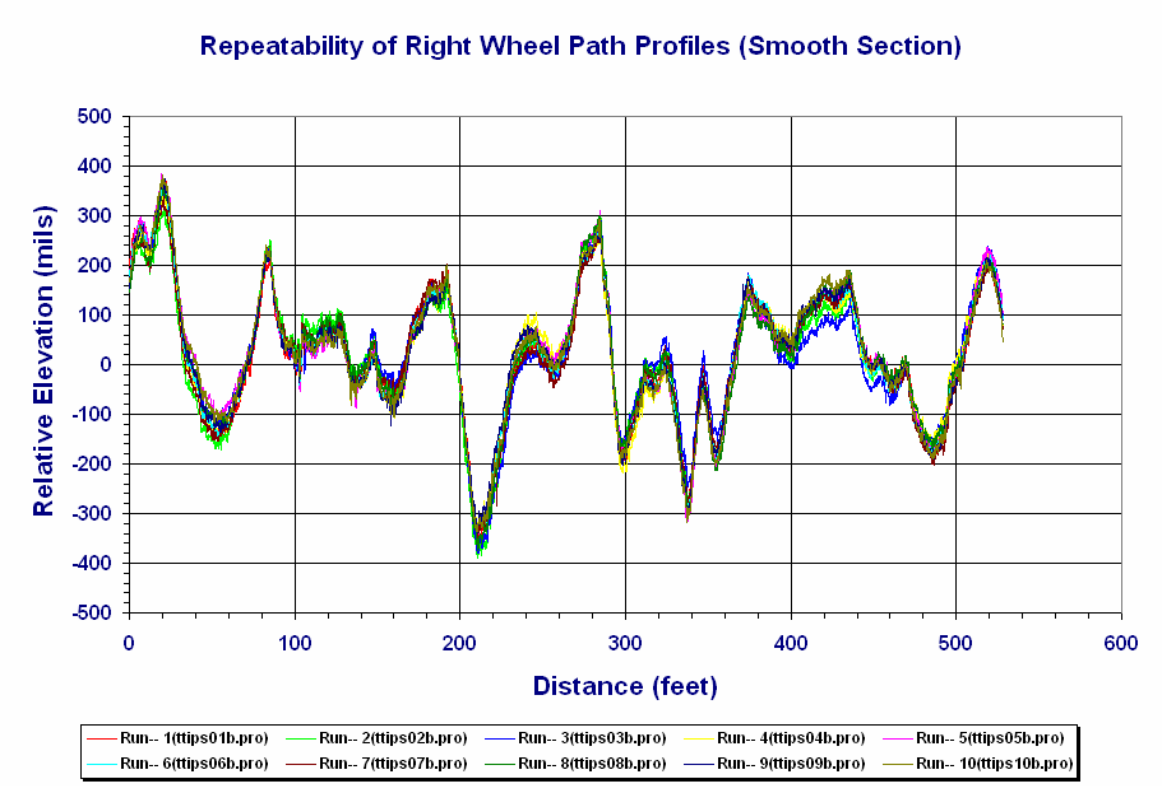

Figure 3.3. Repeatability of Profiles Measured on Right Wheel Path of Smooth Section.

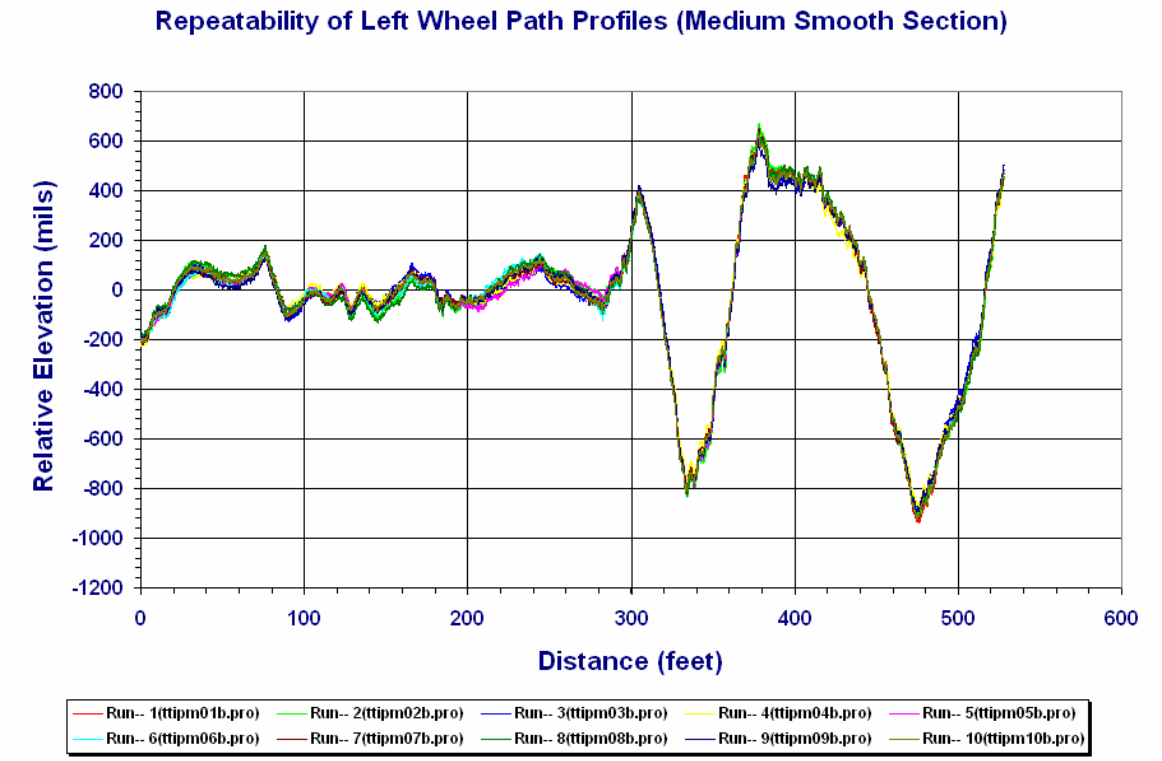

Figure 3.4. Repeatability of Profiles Measured on Left Wheel Path of Medium Smooth Section.

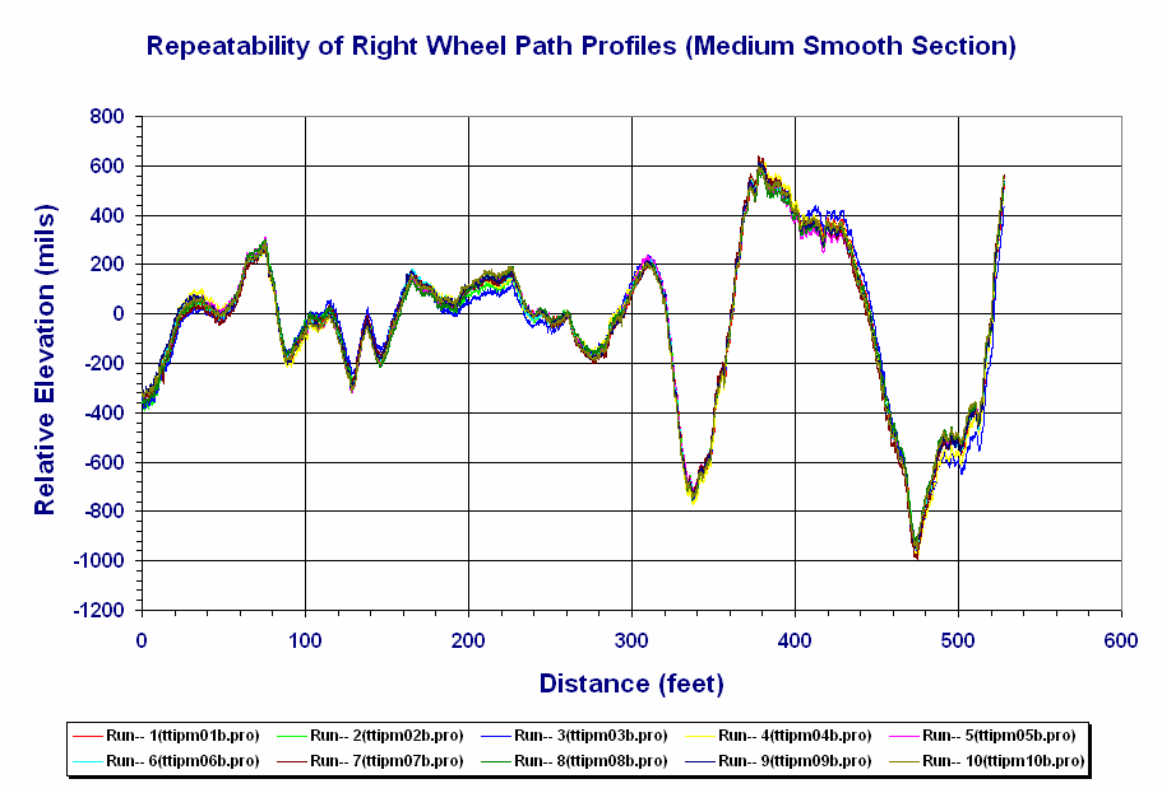

Figure 3.5. Repeatability of Profiles Measured on Right Wheel Path of Medium Smooth Section.

Table 3.1. Repeatability of Profile Measurements from TTI Profiler.

Test Section	Wheel Path	Average Standard Deviation (mils)[1]
Smooth	Left	16
	Right	17
Medium-Smooth	Left	18
	Right	21

[1] Not to exceed 35 mils per TxDOT Test Method Tex-1001S

Table 3.2. Repeatability of IRIs from Profile Measurements with TTI Profiler.

Test Section	Wheel Path	Standard Deviation (inches/mile)[1]
Smooth	Left	0.89
	Right	0.74
Medium-Smooth	Left	1.10
	Right	0.54

[1] Not to exceed 3.0 inches/mile per TxDOT Test Method Tex-1001S

Table 3.3. Accuracy of Profile Measurements from TTI Profiler.

Test Section	Wheel Path	Average Difference (mils)[1]	Average Absolute Difference (mils)[2]
Smooth	Left	-1	11
	Right	0	11
Medium-Smooth	Left	2	13
	Right	3	13

[1] Must be within ±20 mils per TxDOT Test Method Tex-1001S
[2] Not to exceed 60 mils per TxDOT Test Method Tex-1001S

Table 3.4. Accuracy of IRIs from Profile Measurements with TTI Profiler.

Test Section	Wheel Path	Difference (inches/mile)[1]
Smooth	Left	0.12
	Right	0.94
Medium-Smooth	Left	0.04
	Right	-1.19

[1] Absolute difference not to exceed 12 inches/mile per TxDOT Test Method Tex-1001S

CHAPTER IV. FIELD TESTING AND DATA ANALYSIS TO EVALUATE RIDE SPECIFICATION

This chapter presents the field tests conducted by researchers to collect data for the purpose of evaluating TxDOT's Item 585 ride specification. Field tests consisted of the following activities:

- profile measurements on completed TxDOT resurfacing projects,
- verification of instrumented tractor-semitrailer combination, and
- measurement of dynamic load profiles with instrumented truck.

Researchers analyzed the data collected to verify the current ride specification. This chapter presents the findings of this evaluation.

PROFILE DATA COLLECTION

Researchers collected profile data with TTI's inertial profiler on the projects identified in Table 4.1. All projects, with the exception of SH47 in Brazos County, were completed within 3 months of the profile surveys done in this research project. SH47 is an existing highway that is not a newly resurfaced project. Researchers included SH47 on the routes that were surveyed because of the smooth ride scores reported on this highway in TxDOT's pavement management information system database.

Appendix B shows plots of the profile data collected in this project while Tables 4.2 to 4.30 present the international roughness indices computed from the profiles collected during the surveys. The IRIs are the smoothness statistics used for quality assurance testing of pavement smoothness in Item 585. To provide an overall indication of the ride quality on each project tested, researchers prepared Table 4.31 that shows the overall average IRIs on each project as well as the total number of defects (bumps and dips) found. The data presented in this table are based on the results obtained from TxDOT's Ride Quality program using the measured profiles on the different projects as input. TxDOT engineers use this same program for quality assurance testing of pavement smoothness on hot-mix and Portland cement concrete paving projects.

The number of deficient 0.1-mile sections shown in Table 4.31 refers to sections where the average of the left and right wheel path IRIs is greater than 95 in/mile. For these sections, Item 585 requires corrective work to be performed by the contractor to reduce the

Table 4.1. Highways where Researchers Collected Profile and Dynamic Load Measurements.

Highway	County	Pavement Type	Limits		Number of Lanes	Length (miles)
			From	To		
SH21	Lee	Asphalt concrete	Jct. with US77	2.7 miles east of US77	4	2.4
SH21	Bastrop	Asphalt concrete	Jct. with US290	2.8 miles east of FM1441	4	3.6
SH47	Brazos	Asphalt concrete	RM412	RM418	2	6.0
SH47	Brazos	Asphalt concrete	RM418	5.7 miles from RM418	2	5.7
FM102 Group A	Wharton	Asphalt concrete	Wharton County Line	FM102 highway sign	2	5.0
FM102 Group B	Wharton	Asphalt concrete	RM504	RM510	2	6.0
SH36	Fort Bend	Asphalt concrete	Jct. with FM1994	Jct. with FM442	2	1.4
FM1462	Fort Bend	Asphalt concrete	Jct. with SH36	Jct. with FM361	2	3.6
FM1994	Fort Bend	Asphalt concrete	Jct. with SH36	Jct. with FM361	2	2.0
SH121 Group A	Denton	Portland cement concrete	Jct. with Hebron Parkway	Jct. with IH35	2	2.0
SH121 Group B	Denton	Portland cement concrete	Light pole at IH35 jct.	FM544 exit ¼ mile sign	2	2.3
SH121 Group C	Denton	Portland cement concrete	Sign post for IH35E N. Denton exit only	Jct. with IH35	2	1.18
SH121 Group D	Denton	Portland cement concrete	Jct. with IH35	Jct. with Denton Tap Road	1	2.26

Table 4.2. IRIs Computed from Profiles Collected on SH21 in Lee County (K1 Lane).

Interval (miles)	Left Wheel Path (LWP) IRI (in/mi)	Right Wheel Path (RWP) IRI (in/mi)	Average IRI (in/mi)
0.0000 to 0.1000	63.6	69.1	66.3
0.1000 to 0.2000	66.2	76.6	71.4
0.2000 to 0.3000	67.7	62.3	65.0
0.3000 to 0.4000	54.8	60.6	57.7
0.4000 to 0.5000	70.0	72.9	71.4
0.5000 to 0.6000	58.5	56.1	57.3
0.6000 to 0.7000	44.9	67.6	56.3
0.7000 to 0.8000	56.6	49.4	53.0
0.8000 to 0.9000	55.0	56.7	55.8
0.9000 to 1.0000	58.6	57.8	58.2
1.0000 to 1.1000	62.4	44.4	53.4
1.1000 to 1.2000	70.3	75.3	72.8
1.2000 to 1.3000	64.0	56.4	60.2
1.3000 to 1.4000	57.5	54.0	55.8
1.4000 to 1.5000	55.7	59.0	57.4
1.5000 to 1.6000	70.4	63.9	67.2
1.6000 to 1.7000	82.8	65.9	74.3
1.7000 to 1.8000	63.6	67.6	65.6
1.8000 to 1.9000	74.1	103.2	88.6
1.9000 to 2.0000	70.7	79.3	75.0
2.0000 to 2.1000	67.1	67.7	67.4
2.1000 to 2.2000	75.7	93.9	84.8
2.2000 to 2.3000	53.1	66.3	59.7
2.3000 to 2.4000	63.0	83.8	73.4

Table 4.3. IRIs Computed from Profiles Collected on SH21 in Lee County (K2 Lane).

Interval (miles)	LWP IRI (in/mi)	RWP IRI (in/mi)	Average IRI (in/mi)
0.0000 to 0.1000	52.5	54.7	53.6
0.1000 to 0.2000	52.9	48.0	50.5
0.2000 to 0.3000	50.4	50.1	50.3
0.3000 to 0.4000	46.5	58.6	52.6
0.4000 to 0.5000	37.3	40.2	38.8
0.5000 to 0.6000	46.0	52.9	49.4
0.6000 to 0.7000	42.7	36.6	39.6
0.7000 to 0.8000	50.0	43.0	46.5
0.8000 to 0.9000	41.3	31.8	36.5
0.9000 to 1.0000	58.0	52.0	55.0
1.0000 to 1.1000	54.4	52.8	53.6
1.1000 to 1.2000	47.4	40.8	44.1
1.2000 to 1.3000	31.0	32.1	31.6
1.3000 to 1.4000	38.5	38.1	38.3
1.4000 to 1.5000	39.7	37.4	38.6
1.5000 to 1.6000	54.4	70.7	62.5
1.6000 to 1.7000	56.4	51.8	54.1
1.7000 to 1.8000	49.4	47.4	48.4
1.8000 to 1.9000	44.5	47.7	46.1
1.9000 to 2.0000	43.3	50.1	46.7
2.0000 to 2.1000	38.6	43.5	41.0
2.1000 to 2.2000	48.7	40.6	44.7
2.2000 to 2.3000	39.4	34.4	36.9
2.3000 to 2.4000	51.9	56.7	54.3

Table 4.4. IRIs Computed from Profiles Collected on SH21 in Lee County (K6 Lane).

Interval (miles)	LWP IRI (in/mi)	RWP IRI (in/mi)	Average IRI (in/mi)
0.0000 to 0.1000	60.8	76.8	68.8
0.1000 to 0.2000	46.0	48.2	47.1
0.2000 to 0.3000	45.1	63.8	54.4
0.3000 to 0.4000	54.8	77.5	66.1
0.4000 to 0.5000	56.7	66.2	61.5
0.5000 to 0.6000	69.5	78.6	74.1
0.6000 to 0.7000	52.5	64.7	58.6
0.7000 to 0.8000	60.0	79.7	69.9
0.8000 to 0.9000	58.2	57.4	57.8
0.9000 to 1.0000	54.3	54.5	54.4
1.0000 to 1.1000	61.2	67.4	64.3
1.1000 to 1.2000	62.4	67.8	65.1
1.2000 to 1.3000	63.0	69.0	66.0
1.3000 to 1.4000	77.1	85.7	81.4
1.4000 to 1.5000	56.5	49.7	53.1
1.5000 to 1.6000	54.9	73.9	64.4
1.6000 to 1.7000	64.8	65.7	65.3
1.7000 to 1.8000	43.3	44.7	44.0
1.8000 to 1.9000	61.0	62.2	61.6
1.9000 to 2.0000	53.6	76.7	65.1
2.0000 to 2.1000	60.0	58.0	59.0
2.1000 to 2.2000	52.2	49.1	50.6
2.2000 to 2.3000	60.4	61.8	61.1
2.3000 to 2.4000	78.3	77.6	77.9

Table 4.5. IRIs Computed from Profiles Collected on SH21 in Lee County (K7 Lane).

Interval (miles)	LWP IRI (in/mi)	RWP IRI (in/mi)	Average IRI (in/mi)
0.0000 to 0.1000	57.3	47.4	52.3
0.1000 to 0.2000	40.2	36.9	38.5
0.2000 to 0.3000	48.6	46.6	47.6
0.3000 to 0.4000	47.5	48.6	48.1
0.4000 to 0.5000	41.0	36.3	38.6
0.5000 to 0.6000	42.0	42.8	42.4
0.6000 to 0.7000	40.1	39.9	40.0
0.7000 to 0.8000	42.9	45.2	44.1
0.8000 to 0.9000	43.7	32.8	38.3
0.9000 to 1.0000	44.0	37.7	40.9
1.0000 to 1.1000	42.8	41.6	42.2
1.1000 to 1.2000	32.8	35.1	34.0
1.2000 to 1.3000	43.4	41.5	42.4
1.3000 to 1.4000	47.7	48.5	48.1
1.4000 to 1.5000	58.0	48.9	53.5
1.5000 to 1.6000	39.5	32.1	35.8
1.6000 to 1.7000	56.1	51.7	53.9
1.7000 to 1.8000	39.2	35.6	37.4
1.8000 to 1.9000	48.5	49.4	48.9
1.9000 to 2.0000	44.8	47.8	46.3
2.0000 to 2.1000	44.3	51.5	47.9
2.1000 to 2.2000	54.9	48.5	51.7
2.2000 to 2.3000	57.0	54.7	55.8
2.3000 to 2.4000	58.5	57.4	58.0

Table 4.6. IRIs for K1 Lane Tested along SH21 Project in Bastrop County.

Interval (miles)	LWP IRI (in/mi)	RWP IRI (in/mi)	Average IRI (in/mi)
0.0000 to 0.1000	72.7	82.1	77.4
0.1000 to 0.2000	66.0	91.0	78.5
0.2000 to 0.3000	67.4	80.9	74.1
0.3000 to 0.4000	71.9	72.5	72.2
0.4000 to 0.5000	73.1	78.0	75.5
0.5000 to 0.6000	68.8	84.5	76.6
0.6000 to 0.7000	77.0	57.8	67.4
0.7000 to 0.8000	70.5	76.4	73.5
0.8000 to 0.9000	73.8	92.0	82.9
0.9000 to 1.0000	83.1	99.2	91.1
1.0000 to 1.1000	75.7	102.7	89.2
1.1000 to 1.2000	60.1	97.5	78.8
1.2000 to 1.3000	62.5	88.6	75.5
1.3000 to 1.4000	71.8	95.8	83.8
1.4000 to 1.5000	79.9	85.9	82.9
1.5000 to 1.6000	89.8	95.8	92.8
1.6000 to 1.7000	79.9	99.9	89.9
1.7000 to 1.8000	130.8	103.5	117.1
1.8000 to 1.9000	91.4	100.5	95.9
1.9000 to 2.0000	70.6	93.6	82.1
2.0000 to 2.1000	98.2	134.5	116.3
2.1000 to 2.2000	74.8	109.1	92.0
2.2000 to 2.3000	86.5	105.9	96.2
2.3000 to 2.4000	69.7	73.4	71.6
2.4000 to 2.5000	83.2	85.4	84.3
2.5000 to 2.6000	90.9	99.8	95.3
2.6000 to 2.7000	105.9	119.1	112.5
2.7000 to 2.8000	93.9	81.3	87.6
2.8000 to 2.9000	85.3	81.3	83.3
2.9000 to 3.0000	82.8	101.4	92.1
3.0000 to 3.1000	80.0	73.7	76.9
3.1000 to 3.2000	85.0	86.6	85.8
3.2000 to 3.3000	79.5	119.7	99.6
3.3000 to 3.4000	71.2	73.1	72.2
3.4000 to 3.5000	81.3	96.6	89.0
3.5000 to 3.6000	68.9	75.2	72.0

Table 4.7. IRIs for K2 Lane Tested along SH21 Project in Bastrop County.

Interval (miles)	LWP IRI (in/mi)	RWP IRI (in/mi)	Average IRI (in/mi)
0.0000 to 0.1000	68.6	82.0	75.3
0.1000 to 0.2000	76.2	55.3	65.8
0.2000 to 0.3000	65.3	48.0	56.7
0.3000 to 0.4000	72.1	55.7	63.9
0.4000 to 0.5000	69.8	54.0	61.9
0.5000 to 0.6000	51.3	58.3	54.8
0.6000 to 0.7000	67.5	51.5	59.5
0.7000 to 0.8000	72.9	49.4	61.2
0.8000 to 0.9000	69.6	55.8	62.7
0.9000 to 1.0000	63.2	55.8	59.5
1.0000 to 1.1000	60.0	45.1	52.6
1.1000 to 1.2000	43.6	38.5	41.0
1.2000 to 1.3000	49.8	38.9	44.3
1.3000 to 1.4000	51.2	40.3	45.7
1.4000 to 1.5000	51.9	40.7	46.3
1.5000 to 1.6000	59.1	47.4	53.3
1.6000 to 1.7000	80.3	91.1	85.7
1.7000 to 1.8000	90.6	143.3	117.0
1.8000 to 1.9000	66.9	75.6	71.2
1.9000 to 2.0000	53.6	57.3	55.4
2.0000 to 2.1000	53.1	55.4	54.3
2.1000 to 2.2000	64.4	79.7	72.1
2.2000 to 2.3000	74.3	68.5	71.4
2.3000 to 2.4000	66.9	44.7	55.8
2.4000 to 2.5000	79.9	86.6	83.2
2.5000 to 2.6000	60.6	69.4	65.0
2.6000 to 2.7000	63.6	73.0	68.3
2.7000 to 2.8000	53.1	70.7	61.9
2.8000 to 2.9000	58.6	61.1	59.8
2.9000 to 3.0000	51.6	56.2	53.9
3.0000 to 3.1000	52.2	47.6	49.9
3.1000 to 3.2000	41.9	49.9	45.9
3.2000 to 3.3000	55.6	51.2	53.4
3.3000 to 3.4000	44.8	46.8	45.8
3.4000 to 3.5000	40.2	40.6	40.4
3.5000 to 3.6000	62.2	46.8	54.5

Table 4.8. IRIs for K6 Lane Tested along SH21 Project in Bastrop County.

Interval (miles)	LWP IRI (in/mi)	RWP IRI (in/mi)	Average IRI (in/mi)
0.0000 to 0.1000	85.5	91.3	88.4
0.1000 to 0.2000	67.7	79.2	73.4
0.2000 to 0.3000	68.1	99.6	83.8
0.3000 to 0.4000	87.7	115.2	101.4
0.4000 to 0.5000	81.8	107.8	94.8
0.5000 to 0.6000	60.6	69.0	64.8
0.6000 to 0.7000	85.7	81.3	83.5
0.7000 to 0.8000	76.6	83.7	80.2
0.8000 to 0.9000	75.4	64.4	69.9
0.9000 to 1.0000	83.7	124.4	104.0
1.0000 to 1.1000	75.2	92.4	83.8
1.1000 to 1.2000	102.6	81.6	92.1
1.2000 to 1.3000	84.1	82.8	83.4
1.3000 to 1.4000	91.7	81.1	86.4
1.4000 to 1.5000	106.5	106.1	106.3
1.5000 to 1.6000	85.8	87.7	86.7
1.6000 to 1.7000	68.1	74.1	71.1
1.7000 to 1.8000	69.4	67.8	68.6
1.8000 to 1.9000	88.3	96.9	92.6
1.9000 to 2.0000	79.4	113.0	96.2
2.0000 to 2.1000	68.7	72.6	70.6
2.1000 to 2.2000	76.4	99.9	88.2
2.2000 to 2.3000	77.8	76.6	77.2
2.3000 to 2.4000	64.4	58.3	61.3
2.4000 to 2.5000	65.5	59.1	62.3
2.5000 to 2.6000	58.1	52.9	55.5
2.6000 to 2.7000	84.0	81.3	82.6
2.7000 to 2.8000	82.8	99.9	91.3
2.8000 to 2.9000	67.1	78.4	72.8
2.9000 to 3.0000	76.8	80.6	78.7
3.0000 to 3.1000	64.8	68.1	66.4
3.1000 to 3.2000	85.2	87.7	86.5
3.2000 to 3.3000	75.6	74.2	74.9
3.3000 to 3.4000	84.3	72.0	78.2
3.4000 to 3.5000	86.0	75.6	80.8
3.5000 to 3.6000	85.0	86.9	85.9

Table 4.9. IRIs for K7 Lane Tested along SH21 Project in Bastrop County.

Interval (miles)	LWP IRI (in/mi)	RWP IRI (in/mi)	Average IRI (in/mi)
0.0000 to 0.1000	81.9	58.2	70.1
0.1000 to 0.2000	59.3	43.4	51.4
0.2000 to 0.3000	52.2	38.5	45.4
0.3000 to 0.4000	67.6	61.0	64.3
0.4000 to 0.5000	54.5	37.6	46.1
0.5000 to 0.6000	55.9	45.3	50.6
0.6000 to 0.7000	81.2	59.7	70.5
0.7000 to 0.8000	73.6	46.5	60.0
0.8000 to 0.9000	70.1	53.8	61.9
0.9000 to 1.0000	63.9	63.3	63.6
1.0000 to 1.1000	87.6	65.1	76.3
1.1000 to 1.2000	98.1	74.4	86.3
1.2000 to 1.3000	78.1	52.6	65.3
1.3000 to 1.4000	84.0	68.3	76.2
1.4000 to 1.5000	78.3	75.0	76.6
1.5000 to 1.6000	77.5	55.8	66.6
1.6000 to 1.7000	58.7	45.8	52.2
1.7000 to 1.8000	53.9	46.6	50.3
1.8000 to 1.9000	69.0	62.5	65.8
1.9000 to 2.0000	56.2	47.1	51.6
2.0000 to 2.1000	49.0	45.1	47.1
2.1000 to 2.2000	52.4	38.9	45.7
2.2000 to 2.3000	62.4	58.0	60.2
2.3000 to 2.4000	53.1	44.6	48.9
2.4000 to 2.5000	46.5	38.0	42.3
2.5000 to 2.6000	48.0	40.3	44.1
2.6000 to 2.7000	58.1	42.3	50.2
2.7000 to 2.8000	57.5	53.5	55.5
2.8000 to 2.9000	56.2	44.3	50.3
2.9000 to 3.0000	60.0	58.0	59.0
3.0000 to 3.1000	58.7	40.3	49.5
3.1000 to 3.2000	53.5	45.5	49.5
3.2000 to 3.3000	67.9	60.7	64.3
3.3000 to 3.4000	58.8	71.8	65.3
3.4000 to 3.5000	55.4	78.4	66.9
3.5000 to 3.6000	53.3	62.2	57.7

Table 4.10. IRIs for R1 Lane Tested along SH47 in Brazos County.

Interval (miles)	LWP IRI (in/mi)	RWP IRI (in/mi)	Average IRI (in/mi)
0.0000 to 0.1000	52.2	39.7	45.9
0.1000 to 0.2000	57.0	42.0	49.5
0.2000 to 0.3000	49.7	41.3	45.5
0.3000 to 0.4000	32.8	31.2	32.0
0.4000 to 0.5000	36.2	32.6	34.4
0.5000 to 0.6000	46.5	42.3	44.4
0.6000 to 0.7000	41.7	39.1	40.4
0.7000 to 0.8000	33.3	43.9	38.6
0.8000 to 0.9000	38.7	47.4	43.1
0.9000 to 1.0000	32.6	44.0	38.3
1.0000 to 1.1000	38.5	38.2	38.4
1.1000 to 1.2000	190.9	162.4	176.6
1.2000 to 1.3000	35.7	33.0	34.3
1.3000 to 1.4000	50.8	56.6	53.7
1.4000 to 1.5000	41.6	33.4	37.5
1.5000 to 1.6000	37.2	32.3	34.8
1.6000 to 1.7000	55.9	47.7	51.8
1.7000 to 1.8000	35.4	31.5	33.4
1.8000 to 1.9000	63.7	49.6	56.7
1.9000 to 2.0000	41.6	38.5	40.0
2.0000 to 2.1000	103.7	88.4	96.1
2.1000 to 2.2000	52.4	42.6	47.5
2.2000 to 2.3000	59.0	36.2	47.6
2.3000 to 2.4000	42.4	36.2	39.3
2.4000 to 2.5000	84.3	79.9	82.1
2.5000 to 2.6000	66.5	72.2	69.3
2.6000 to 2.7000	53.1	50.6	51.9
2.7000 to 2.8000	43.5	40.4	42.0
2.8000 to 2.9000	39.2	35.8	37.5
2.9000 to 3.0000	34.1	28.4	31.2
3.0000 to 3.1000	41.9	40.9	41.4
3.1000 to 3.2000	31.4	25.0	28.2
3.2000 to 3.3000	45.2	41.1	43.1
3.3000 to 3.4000	44.2	40.6	42.4
3.4000 to 3.5000	50.2	55.9	53.0
3.5000 to 3.6000	45.4	47.6	46.5
3.6000 to 3.7000	52.3	47.5	49.9
3.7000 to 3.8000	68.6	60.2	64.4
3.8000 to 3.9000	46.3	43.5	44.9
3.9000 to 4.0000	39.6	38.9	39.2
4.0000 to 4.1000	59.1	55.7	57.4
4.1000 to 4.2000	50.3	39.2	44.8
4.2000 to 4.3000	52.2	42.8	47.5
4.3000 to 4.4000	34.3	36.1	35.2

Table 4.10. IRIs for R1 Lane Tested along SH47 in Brazos County (continued).

Interval (miles)	LWP IRI (in/mi)	RWP IRI (in/mi)	Average IRI (in/mi)
4.4000 to 4.5000	61.0	53.8	57.4
4.5000 to 4.6000	62.8	62.7	62.8
4.6000 to 4.7000	55.0	40.8	47.9
4.7000 to 4.8000	88.0	97.7	92.9
4.8000 to 4.9000	116.8	123.9	120.3
4.9000 to 5.0000	105.1	97.6	101.3
5.0000 to 5.1000	44.5	26.8	35.6
5.1000 to 5.2000	35.6	30.2	32.9
5.2000 to 5.3000	38.1	23.9	31.0
5.3000 to 5.4000	42.6	32.4	37.5
5.4000 to 5.5000	47.4	44.7	46.0
5.5000 to 5.6000	40.0	40.6	40.3
5.6000 to 5.7000	35.2	28.2	31.7
5.7000 to 5.8000	35.0	29.3	32.2
5.8000 to 5.9000	61.0	47.2	54.1
5.9000 to 6.0000	65.6	46.3	56.0

Table 4.11. IRIs for R2 Lane Tested along SH47 in Brazos County.

Interval (miles)	LWP IRI (in/mi)	RWP IRI (in/mi)	Average IRI (in/mi)
0.0000 to 0.1000	59.7	42.3	51.0
0.1000 to 0.2000	58.5	47.6	53.1
0.2000 to 0.3000	52.7	46.2	49.5
0.3000 to 0.4000	44.7	38.4	41.5
0.4000 to 0.5000	50.2	34.9	42.5
0.5000 to 0.6000	58.9	62.1	60.5
0.6000 to 0.7000	50.1	50.1	50.1
0.7000 to 0.8000	56.9	48.4	52.6
0.8000 to 0.9000	54.7	51.0	52.9
0.9000 to 1.0000	38.2	48.7	43.5
1.0000 to 1.1000	49.0	47.5	48.3
1.1000 to 1.2000	178.4	179.1	178.7
1.2000 to 1.3000	54.7	47.5	51.1
1.3000 to 1.4000	40.4	60.5	50.5
1.4000 to 1.5000	64.9	55.3	60.1
1.5000 to 1.6000	46.3	45.9	46.1
1.6000 to 1.7000	74.7	62.6	68.7
1.7000 to 1.8000	52.7	49.6	51.2
1.8000 to 1.9000	66.6	75.4	71.0
1.9000 to 2.0000	53.9	50.0	51.9
2.0000 to 2.1000	123.2	119.6	121.4
2.1000 to 2.2000	60.3	50.1	55.2
2.2000 to 2.3000	60.5	60.2	60.3
2.3000 to 2.4000	52.4	41.7	47.0
2.4000 to 2.5000	67.3	74.0	70.6
2.5000 to 2.6000	65.7	59.9	62.8
2.6000 to 2.7000	60.6	70.7	65.6
2.7000 to 2.8000	50.7	52.6	51.6
2.8000 to 2.9000	54.1	46.7	50.4
2.9000 to 3.0000	49.3	47.2	48.2
3.0000 to 3.1000	59.2	51.8	55.5
3.1000 to 3.2000	38.8	37.2	38.0
3.2000 to 3.3000	52.0	46.9	49.4
3.3000 to 3.4000	79.2	76.9	78.0
3.4000 to 3.5000	45.4	50.3	47.9
3.5000 to 3.6000	56.3	51.8	54.1
3.6000 to 3.7000	63.4	60.5	61.9
3.7000 to 3.8000	100.5	83.1	91.8
3.8000 to 3.9000	61.3	56.8	59.0
3.9000 to 4.0000	59.1	52.2	55.6
4.0000 to 4.1000	84.0	83.0	83.5
4.1000 to 4.2000	73.6	49.5	61.6
4.2000 to 4.3000	65.2	48.6	56.9
4.3000 to 4.4000	44.4	38.1	41.3

Table 4.11. IRIs for R2 Lane Tested along SH47 in Brazos County (continued).

Interval (miles)	LWP IRI (in/mi)	RWP IRI (in/mi)	Average IRI (in/mi)
4.4000 to 4.5000	89.6	75.6	82.6
4.5000 to 4.6000	81.1	74.8	77.9
4.6000 to 4.7000	67.2	54.8	61.0
4.7000 to 4.8000	68.2	88.5	78.3
4.8000 to 4.9000	100.8	104.4	102.6
4.9000 to 5.0000	106.3	99.8	103.1
5.0000 to 5.1000	46.0	48.8	47.4
5.1000 to 5.2000	36.0	34.2	35.1
5.2000 to 5.3000	61.5	44.2	52.8
5.3000 to 5.4000	65.0	56.7	60.9
5.4000 to 5.5000	57.1	65.7	61.4
5.5000 to 5.6000	49.0	57.5	53.2
5.6000 to 5.7000	45.7	43.6	44.7
5.7000 to 5.8000	50.9	43.4	47.2
5.8000 to 5.9000	69.8	64.0	66.9
5.9000 to 6.0000	87.7	78.1	82.9

Table 4.12. IRIs for L1 Lane Tested along SH47 in Brazos County.

Interval (miles)	LWP IRI (in/mi)	RWP IRI (in/mi)	Average IRI (in/mi)
0.0000 to 0.1000	73.3	60.9	67.1
0.1000 to 0.2000	56.2	45.1	50.7
0.2000 to 0.3000	50.4	41.2	45.8
0.3000 to 0.4000	54.7	39.9	47.3
0.4000 to 0.5000	66.7	45.8	56.2
0.5000 to 0.6000	92.2	68.7	80.4
0.6000 to 0.7000	105.6	102.1	103.9
0.7000 to 0.8000	63.0	44.5	53.8
0.8000 to 0.9000	60.9	54.8	57.9
0.9000 to 1.0000	62.2	56.7	59.4
1.0000 to 1.1000	146.7	114.7	130.7
1.1000 to 1.2000	128.7	111.5	120.1
1.2000 to 1.3000	49.4	39.8	44.6
1.3000 to 1.4000	62.1	62.0	62.1
1.4000 to 1.5000	54.4	45.0	49.7
1.5000 to 1.6000	62.1	49.1	55.6
1.6000 to 1.7000	49.9	46.0	48.0
1.7000 to 1.8000	51.8	42.5	47.1
1.8000 to 1.9000	66.1	48.7	57.4
1.9000 to 2.0000	58.4	58.4	58.4
2.0000 to 2.1000	58.0	46.9	52.5
2.1000 to 2.2000	43.0	40.4	41.7
2.2000 to 2.3000	106.4	105.3	105.9
2.3000 to 2.4000	50.2	44.0	47.1
2.4000 to 2.5000	75.6	63.1	69.3
2.5000 to 2.6000	50.8	45.6	48.2
2.6000 to 2.7000	63.2	73.6	68.4
2.7000 to 2.8000	48.7	31.3	40.0
2.8000 to 2.9000	52.9	50.2	51.5
2.9000 to 3.0000	50.6	49.1	49.9
3.0000 to 3.1000	55.2	54.8	55.0
3.1000 to 3.2000	52.9	46.2	49.6
3.2000 to 3.3000	50.1	54.3	52.2
3.3000 to 3.4000	50.3	51.8	51.1
3.4000 to 3.5000	78.4	67.2	72.8
3.5000 to 3.6000	58.8	53.8	56.3
3.6000 to 3.7000	46.1	57.4	51.7
3.7000 to 3.8000	76.8	73.3	75.0
3.8000 to 3.9000	101.8	106.0	103.9
3.9000 to 4.0000	73.7	64.5	69.1
4.0000 to 4.1000	71.4	58.8	65.1
4.1000 to 4.2000	74.8	68.3	71.6
4.2000 to 4.3000	48.3	43.5	45.9

Table 4.12. IRIs for L1 Lane Tested along SH47 in Brazos County (continued).

Interval (miles)	LWP IRI (in/mi)	RWP IRI (in/mi)	Average IRI (in/mi)
4.3000 to 4.4000	50.5	46.0	48.3
4.4000 to 4.5000	53.1	48.9	51.0
4.5000 to 4.6000	43.1	37.4	40.3
4.6000 to 4.7000	46.9	37.0	41.9
4.7000 to 4.8000	78.8	83.7	81.3
4.8000 to 4.9000	141.6	136.4	139.0
4.9000 to 5.0000	64.1	60.3	62.2
5.0000 to 5.1000	42.6	41.3	41.9
5.1000 to 5.2000	59.6	57.1	58.3
5.2000 to 5.3000	44.5	41.5	43.0
5.3000 to 5.4000	50.8	44.7	47.8
5.4000 to 5.5000	45.7	37.9	41.8
5.5000 to 5.6000	36.5	39.5	38.0
5.6000 to 5.7000	56.4	54.1	55.3

Table 4.13. IRIs for L2 Lane Tested along SH47 in Brazos County.

Interval (miles)	LWP IRI (in/mi)	RWP IRI (in/mi)	Average IRI (in/mi)
0.0000 to 0.1000	59.5	63.1	61.3
0.1000 to 0.2000	71.5	66.3	68.9
0.2000 to 0.3000	57.2	67.6	62.4
0.3000 to 0.4000	59.8	56.4	58.1
0.4000 to 0.5000	66.8	70.0	68.4
0.5000 to 0.6000	157.4	135.5	146.4
0.6000 to 0.7000	134.2	116.3	125.3
0.7000 to 0.8000	70.2	67.3	68.7
0.8000 to 0.9000	63.0	64.1	63.6
0.9000 to 1.0000	68.6	70.9	69.8
1.0000 to 1.1000	135.9	127.3	131.6
1.1000 to 1.2000	130.7	137.3	134.0
1.2000 to 1.3000	74.6	65.8	70.2
1.3000 to 1.4000	90.9	76.0	83.5
1.4000 to 1.5000	78.0	72.8	75.4
1.5000 to 1.6000	106.3	83.1	94.7
1.6000 to 1.7000	63.3	52.8	58.0
1.7000 to 1.8000	74.6	72.5	73.6
1.8000 to 1.9000	94.9	87.3	91.1
1.9000 to 2.0000	75.6	67.5	71.5
2.0000 to 2.1000	63.1	50.7	56.9
2.1000 to 2.2000	60.8	53.4	57.1
2.2000 to 2.3000	83.9	100.8	92.4
2.3000 to 2.4000	60.9	64.9	62.9
2.4000 to 2.5000	58.5	66.5	62.5
2.5000 to 2.6000	55.6	60.2	57.9
2.6000 to 2.7000	59.6	82.3	71.0
2.7000 to 2.8000	39.3	38.9	39.1
2.8000 to 2.9000	56.7	66.2	61.5
2.9000 to 3.0000	58.1	56.9	57.5
3.0000 to 3.1000	58.4	55.6	57.0
3.1000 to 3.2000	56.6	52.5	54.6
3.2000 to 3.3000	57.6	53.6	55.6
3.3000 to 3.4000	83.2	71.4	77.3
3.4000 to 3.5000	86.4	78.4	82.4
3.5000 to 3.6000	66.0	67.0	66.5
3.6000 to 3.7000	54.7	58.2	56.4
3.7000 to 3.8000	62.2	62.5	62.4
3.8000 to 3.9000	83.1	82.1	82.6
3.9000 to 4.0000	101.4	89.4	95.4
4.0000 to 4.1000	96.5	95.5	96.0
4.1000 to 4.2000	103.8	103.2	103.5
4.2000 to 4.3000	72.3	72.5	72.4

Table 4.13. IRIs for L2 Lane Tested along SH47 in Brazos County (continued).

Interval (miles)	LWP IRI (in/mi)	RWP IRI (in/mi)	Average IRI (in/mi)
4.3000 to 4.4000	61.9	50.5	56.2
4.4000 to 4.5000	65.8	63.3	64.6
4.5000 to 4.6000	56.6	43.1	49.9
4.6000 to 4.7000	71.2	55.2	63.2
4.7000 to 4.8000	89.9	82.1	86.0
4.8000 to 4.9000	141.3	144.9	143.1
4.9000 to 5.0000	62.2	56.9	59.5
5.0000 to 5.1000	49.8	45.8	47.8
5.1000 to 5.2000	66.3	62.9	64.6
5.2000 to 5.3000	54.8	49.6	52.2
5.3000 to 5.4000	51.4	45.4	48.4
5.4000 to 5.5000	57.5	52.6	55.1
5.5000 to 5.6000	55.6	54.6	55.1
5.6000 to 5.7000	67.5	56.9	62.2

Table 4.14. IRIs for K1 Lane (Group A) along FM102 in Wharton County.

Interval (miles)	LWP IRI (in/mi)	RWP IRI (in/mi)	Average IRI (in/mi)
0.0000 to 0.1000	86.7	100.2	93.5
0.1000 to 0.2000	78.6	64.4	71.5
0.2000 to 0.3000	114.5	51.0	82.7
0.3000 to 0.4000	62.8	60.4	61.6
0.4000 to 0.5000	113.3	78.5	95.9
0.5000 to 0.6000	114.0	71.4	92.7
0.6000 to 0.7000	103.5	80.8	92.1
0.7000 to 0.8000	73.1	83.6	78.4
0.8000 to 0.9000	61.2	60.9	61.1
0.9000 to 1.0000	47.0	51.3	49.2
1.0000 to 1.1000	51.9	42.1	47.0
1.1000 to 1.2000	58.2	55.3	56.8
1.2000 to 1.3000	76.3	53.5	64.9
1.3000 to 1.4000	54.1	49.9	52.0
1.4000 to 1.5000	65.5	47.7	56.6
1.5000 to 1.6000	62.3	47.1	54.7
1.6000 to 1.7000	47.1	43.8	45.4
1.7000 to 1.8000	59.5	53.0	56.3
1.8000 to 1.9000	59.6	62.3	61.0
1.9000 to 2.0000	79.2	50.5	64.8
2.0000 to 2.1000	76.1	50.3	63.2
2.1000 to 2.2000	109.1	91.5	100.3
2.2000 to 2.3000	67.1	79.6	73.4
2.3000 to 2.4000	74.1	63.7	68.9
2.4000 to 2.5000	94.2	83.8	89.0
2.5000 to 2.6000	102.3	65.2	83.8
2.6000 to 2.7000	76.9	85.9	81.4
2.7000 to 2.8000	51.0	76.4	63.7
2.8000 to 2.9000	51.2	71.2	61.2
2.9000 to 3.0000	56.8	74.6	65.7
3.0000 to 3.1000	44.0	59.1	51.6
3.1000 to 3.2000	49.9	64.1	57.0
3.2000 to 3.3000	64.7	81.5	73.1
3.3000 to 3.4000	53.6	97.3	75.4
3.4000 to 3.5000	51.7	76.1	63.9
3.5000 to 3.6000	45.7	68.7	57.2
3.6000 to 3.7000	59.5	77.2	68.3
3.7000 to 3.8000	60.1	81.7	70.9
3.8000 to 3.9000	44.0	68.5	56.2
3.9000 to 4.0000	53.9	98.6	76.2

Table 4.14. IRIs for K1 Lane (Group A) along FM102 in Wharton County (continued).

Interval (miles)	LWP IRI (in/mi)	RWP IRI (in/mi)	Average IRI (in/mi)
4.0000 to 4.1000	70.9	99.7	85.3
4.1000 to 4.2000	56.1	82.9	69.5
4.2000 to 4.3000	60.3	79.6	69.9
4.3000 to 4.4000	81.0	96.6	88.8
4.4000 to 4.5000	69.1	101.1	85.1
4.5000 to 4.6000	47.4	62.6	55.0
4.6000 to 4.7000	46.9	51.3	49.1
4.7000 to 4.8000	48.2	48.6	48.4
4.8000 to 4.9000	44.0	59.8	51.9
4.9000 to 5.0000	41.6	60.3	51.0

Table 4.15. IRIs for K6 Lane (Group A) along FM102 in Wharton County.

Interval (miles)	LWP IRI (in/mi)	RWP IRI (in/mi)	Average IRI (in/mi)
0.0000 to 0.1000	29.4	42.2	35.8
0.1000 to 0.2000	32.5	40.8	36.6
0.2000 to 0.3000	32.9	44.1	38.5
0.3000 to 0.4000	37.5	39.6	38.6
0.4000 to 0.5000	42.6	46.2	44.4
0.5000 to 0.6000	47.6	55.1	51.4
0.6000 to 0.7000	50.6	61.5	56.0
0.7000 to 0.8000	56.3	66.2	61.2
0.8000 to 0.9000	49.0	52.2	50.6
0.9000 to 1.0000	54.1	63.2	58.7
1.0000 to 1.1000	58.9	48.5	53.7
1.1000 to 1.2000	54.3	50.1	52.2
1.2000 to 1.3000	54.5	50.7	52.6
1.3000 to 1.4000	59.3	51.8	55.5
1.4000 to 1.5000	42.0	53.8	47.9
1.5000 to 1.6000	53.7	62.4	58.1
1.6000 to 1.7000	50.2	63.9	57.1
1.7000 to 1.8000	56.8	60.4	58.6
1.8000 to 1.9000	62.0	70.3	66.1
1.9000 to 2.0000	93.1	68.2	80.6
2.0000 to 2.1000	74.3	109.7	92.0
2.1000 to 2.2000	78.7	115.0	96.9
2.2000 to 2.3000	63.5	108.2	85.8
2.3000 to 2.4000	65.1	128.4	96.8
2.4000 to 2.5000	83.4	102.4	92.9
2.5000 to 2.6000	71.7	83.6	77.7
2.6000 to 2.7000	58.2	85.0	71.6
2.7000 to 2.8000	63.9	117.8	90.9
2.8000 to 2.9000	64.4	80.8	72.6
2.9000 to 3.0000	48.1	54.8	51.4
3.0000 to 3.1000	48.9	61.4	55.2
3.1000 to 3.2000	51.5	55.9	53.7
3.2000 to 3.3000	56.0	62.4	59.2
3.3000 to 3.4000	50.9	59.9	55.4
3.4000 to 3.5000	41.5	49.4	45.5
3.5000 to 3.6000	63.7	87.3	75.5
3.6000 to 3.7000	62.9	74.0	68.5
3.7000 to 3.8000	45.4	56.7	51.1
3.8000 to 3.9000	89.2	51.3	70.2
3.9000 to 4.0000	122.9	67.1	95.0

Table 4.15. IRIs for K6 Lane (Group A) along FM102 in Wharton County (continued).

Interval (miles)	LWP IRI (in/mi)	RWP IRI (in/mi)	Average IRI (in/mi)
4.0000 to 4.1000	48.9	39.7	44.3
4.1000 to 4.2000	58.0	54.5	56.3
4.2000 to 4.3000	60.8	50.8	55.8
4.3000 to 4.4000	55.7	40.0	47.8
4.4000 to 4.5000	51.6	48.1	49.9
4.5000 to 4.6000	77.8	64.2	71.0
4.6000 to 4.7000	98.2	60.3	79.3
4.7000 to 4.8000	103.7	82.5	93.1
4.8000 to 4.9000	74.6	63.3	69.0
4.9000 to 5.0000	82.0	91.9	86.9

Table 4.16. IRIs for K1 Lane (Group B) along FM102 in Wharton County.

Interval (miles)	LWP IRI (in/mi)	RWP IRI (in/mi)	Average IRI (in/mi)
0.0000 to 0.1000	41.4	48.3	44.8
0.1000 to 0.2000	39.2	46.7	42.9
0.2000 to 0.3000	41.6	57.0	49.3
0.3000 to 0.4000	49.7	66.2	58.0
0.4000 to 0.5000	51.2	81.2	66.2
0.5000 to 0.6000	43.3	67.5	55.4
0.6000 to 0.7000	44.9	58.1	51.5
0.7000 to 0.8000	42.1	68.2	55.2
0.8000 to 0.9000	55.9	65.8	60.9
0.9000 to 1.0000	53.2	66.6	59.9
1.0000 to 1.1000	39.7	47.9	43.8
1.1000 to 1.2000	42.0	44.2	43.1
1.2000 to 1.3000	48.1	48.2	48.1
1.3000 to 1.4000	51.3	43.7	47.5
1.4000 to 1.5000	45.1	57.9	51.5
1.5000 to 1.6000	41.7	56.2	48.9
1.6000 to 1.7000	37.9	46.5	42.2
1.7000 to 1.8000	50.7	61.1	55.9
1.8000 to 1.9000	71.7	130.3	101.0
1.9000 to 2.0000	59.7	80.6	70.1
2.0000 to 2.1000	58.9	52.6	55.8
2.1000 to 2.2000	39.7	48.7	44.2
2.2000 to 2.3000	41.9	50.8	46.3
2.3000 to 2.4000	40.5	51.0	45.7
2.4000 to 2.5000	34.9	60.2	47.6
2.5000 to 2.6000	33.8	53.8	43.8
2.6000 to 2.7000	36.4	55.2	45.8
2.7000 to 2.8000	38.6	44.8	41.7
2.8000 to 2.9000	37.3	51.6	44.4
2.9000 to 3.0000	34.0	61.0	47.5
3.0000 to 3.1000	35.0	53.9	44.4
3.1000 to 3.2000	35.7	47.4	41.5
3.2000 to 3.3000	32.1	39.5	35.8
3.3000 to 3.4000	34.9	36.3	35.6
3.4000 to 3.5000	37.6	37.9	37.8
3.5000 to 3.6000	37.2	48.5	42.8
3.6000 to 3.7000	35.8	44.4	40.1
3.7000 to 3.8000	34.1	38.2	36.2
3.8000 to 3.9000	33.5	42.3	37.9
3.9000 to 4.0000	31.4	42.9	37.2

Table 4.16. IRIs for K1 Lane (Group B) along FM102 in Wharton County (continued).

Interval (miles)	LWP IRI (in/mi)	RWP IRI (in/mi)	Average IRI (in/mi)
4.0000 to 4.1000	44.5	47.3	45.9
4.1000 to 4.2000	42.6	43.4	43.0
4.2000 to 4.3000	42.6	41.5	42.1
4.3000 to 4.4000	35.9	42.1	39.0
4.4000 to 4.5000	37.2	39.3	38.3
4.5000 to 4.6000	43.1	43.0	43.0
4.6000 to 4.7000	34.8	42.8	38.8
4.7000 to 4.8000	36.7	43.6	40.1
4.8000 to 4.9000	44.8	53.1	48.9
4.9000 to 5.0000	37.6	44.4	41.0
5.0000 to 5.1000	39.0	44.0	41.5
5.1000 to 5.2000	41.4	50.4	45.9
5.2000 to 5.3000	39.5	47.9	43.7
5.3000 to 5.4000	41.1	35.1	38.1
5.4000 to 5.5000	36.5	46.6	41.6
5.5000 to 5.6000	32.9	36.2	34.6
5.6000 to 5.7000	36.8	37.9	37.4
5.7000 to 5.8000	32.6	38.8	35.7
5.8000 to 5.9000	39.0	40.3	39.7
5.9000 to 6.0000	38.3	40.4	39.4

Table 4.17. IRIs for K6 Lane (Group B) along FM102 in Wharton County.

Interval (miles)	LWP IRI (in/mi)	RWP IRI (in/mi)	Average IRI (in/mi)
0.0000 to 0.1000	46.8	46.9	46.8
0.1000 to 0.2000	56.9	57.7	57.3
0.2000 to 0.3000	60.2	68.4	64.3
0.3000 to 0.4000	60.5	68.6	64.5
0.4000 to 0.5000	67.2	81.5	74.3
0.5000 to 0.6000	50.4	38.8	44.6
0.6000 to 0.7000	62.7	67.1	64.9
0.7000 to 0.8000	65.8	73.4	69.6
0.8000 to 0.9000	80.3	56.2	68.3
0.9000 to 1.0000	61.4	55.6	58.5
1.0000 to 1.1000	53.7	49.7	51.7
1.1000 to 1.2000	63.2	56.7	60.0
1.2000 to 1.3000	49.4	65.6	57.5
1.3000 to 1.4000	54.3	66.0	60.2
1.4000 to 1.5000	59.3	50.4	54.9
1.5000 to 1.6000	49.4	49.0	49.2
1.6000 to 1.7000	50.3	70.5	60.4
1.7000 to 1.8000	53.7	53.0	53.3
1.8000 to 1.9000	55.3	64.6	59.9
1.9000 to 2.0000	54.1	57.7	55.9
2.0000 to 2.1000	62.9	63.1	63.0
2.1000 to 2.2000	58.9	48.6	53.7
2.2000 to 2.3000	57.7	52.0	54.9
2.3000 to 2.4000	53.9	42.4	48.2
2.4000 to 2.5000	67.9	48.8	58.4
2.5000 to 2.6000	57.3	50.1	53.7
2.6000 to 2.7000	66.9	59.5	63.2
2.7000 to 2.8000	63.7	47.5	55.6
2.8000 to 2.9000	55.9	40.5	48.2
2.9000 to 3.0000	58.4	62.1	60.3
3.0000 to 3.1000	68.3	51.3	59.8
3.1000 to 3.2000	59.3	51.1	55.2
3.2000 to 3.3000	55.0	51.0	53.0
3.3000 to 3.4000	59.9	57.3	58.6
3.4000 to 3.5000	49.3	47.8	48.6
3.5000 to 3.6000	56.6	68.1	62.4
3.6000 to 3.7000	57.9	57.4	57.6
3.7000 to 3.8000	46.3	81.3	63.8
3.8000 to 3.9000	49.3	67.4	58.4
3.9000 to 4.0000	59.5	75.0	67.2

Table 4.17. IRIs for K6 Lane (Group B) along FM102 in Wharton County (continued).

Interval (miles)	LWP IRI (in/mi)	RWP IRI (in/mi)	Average IRI (in/mi)
4.0000 to 4.1000	86.4	64.5	75.5
4.1000 to 4.2000	70.0	58.4	64.2
4.2000 to 4.3000	89.7	71.2	80.4
4.3000 to 4.4000	57.9	108.0	83.0
4.4000 to 4.5000	59.1	116.2	87.7
4.5000 to 4.6000	58.5	83.7	71.1
4.6000 to 4.7000	59.4	75.9	67.6
4.7000 to 4.8000	55.4	73.1	64.2
4.8000 to 4.9000	49.4	57.8	53.6
4.9000 to 5.0000	50.0	60.1	55.1
5.0000 to 5.1000	52.0	57.2	54.6
5.1000 to 5.2000	52.6	58.5	55.6
5.2000 to 5.3000	48.6	44.8	46.7
5.3000 to 5.4000	39.9	46.1	43.0
5.4000 to 5.5000	43.4	65.6	54.5
5.5000 to 5.6000	49.8	63.9	56.8
5.6000 to 5.7000	51.5	72.8	62.1
5.7000 to 5.8000	41.4	65.0	53.2
5.8000 to 5.9000	46.7	58.2	52.5
5.9000 to 6.0000	51.8	59.6	55.7

Table 4.18. IRIs for K1 Lane Tested along SH36 in Fort Bend County.

Interval (miles)	LWP IRI (in/mi)	RWP IRI (in/mi)	Average IRI (in/mi)
0.0000 to 0.1000	66.1	70.0	68.1
0.1000 to 0.2000	64.5	75.6	70.1
0.2000 to 0.3000	76.7	81.7	79.2
0.3000 to 0.4000	76.4	63.2	69.8
0.4000 to 0.5000	64.3	64.8	64.6
0.5000 to 0.6000	66.1	69.5	67.8
0.6000 to 0.7000	67.7	59.8	63.8
0.7000 to 0.8000	55.1	71.0	63.1
0.8000 to 0.9000	69.5	75.6	72.5
0.9000 to 1.0000	65.7	56.8	61.2
1.0000 to 1.1000	66.5	57.7	62.1
1.1000 to 1.2000	82.4	73.3	77.9
1.2000 to 1.3000	93.3	80.2	86.8
1.3000 to 1.4000	66.2	56.2	61.2

Table 4.19. IRIs for K6 Lane Tested along SH36 in Fort Bend County.

Interval (miles)	LWP IRI (in/mi)	RWP IRI (in/mi)	Average IRI (in/mi)
0.0000 to 0.1000	65.9	62.6	64.2
0.1000 to 0.2000	73.7	54.5	64.1
0.2000 to 0.3000	79.3	81.3	80.3
0.3000 to 0.4000	78.3	75.9	77.1
0.4000 to 0.5000	91.5	96.1	93.8
0.5000 to 0.6000	105.5	79.1	92.3
0.6000 to 0.7000	74.7	69.6	72.1
0.7000 to 0.8000	71.2	52.5	61.9
0.8000 to 0.9000	74.1	62.6	68.3
0.9000 to 1.0000	74.9	62.0	68.4
1.0000 to 1.1000	95.0	67.8	81.4
1.1000 to 1.2000	72.7	60.5	66.6
1.2000 to 1.3000	45.7	47.6	46.6
1.3000 to 1.4000	43.9	39.2	41.5

Table 4.20. IRIs for K1 Lane Tested along FM1462 in Fort Bend County.

Interval (miles)	LWP IRI (in/mi)	RWP IRI (in/mi)	Average IRI (in/mi)
0.0000 to 0.1000	44.2	37.7	40.9
0.1000 to 0.2000	46.7	39.4	43.1
0.2000 to 0.3000	45.3	42.1	43.7
0.3000 to 0.4000	52.5	50.2	51.4
0.4000 to 0.5000	43.4	47.8	45.6
0.5000 to 0.6000	45.1	44.2	44.6
0.6000 to 0.7000	50.0	47.9	49.0
0.7000 to 0.8000	43.6	38.4	41.0
0.8000 to 0.9000	47.1	47.4	47.2
0.9000 to 1.0000	49.1	41.6	45.3
1.0000 to 1.1000	50.3	63.5	56.9
1.1000 to 1.2000	47.7	105.8	76.8
1.2000 to 1.3000	48.2	41.5	44.9
1.3000 to 1.4000	59.3	50.8	55.1
1.4000 to 1.5000	46.1	53.7	49.9
1.5000 to 1.6000	35.6	33.3	34.5
1.6000 to 1.7000	40.5	41.9	41.2
1.7000 to 1.8000	41.2	56.2	48.7
1.8000 to 1.9000	43.1	90.0	66.6
1.9000 to 2.0000	39.4	44.7	42.0
2.0000 to 2.1000	46.6	76.7	61.6
2.1000 to 2.2000	38.9	38.0	38.4
2.2000 to 2.3000	38.0	33.8	35.9
2.3000 to 2.4000	45.6	64.3	54.9
2.4000 to 2.5000	48.0	63.7	55.9
2.5000 to 2.6000	32.5	36.7	34.6
2.6000 to 2.7000	48.1	81.3	64.7
2.7000 to 2.8000	49.0	99.4	74.2
2.8000 to 2.9000	52.9	101.4	77.2
2.9000 to 3.0000	39.4	110.1	74.7
3.0000 to 3.1000	50.8	65.6	58.2
3.1000 to 3.2000	40.3	68.6	54.5
3.2000 to 3.3000	44.8	84.8	64.8
3.3000 to 3.4000	44.9	47.0	45.9
3.4000 to 3.5000	51.2	51.1	51.2
3.5000 to 3.6000	45.3	51.2	48.2

Table 4.21. IRIs for K6 Lane Tested along FM1462 in Fort Bend County.

Interval (miles)	LWP IRI (in/mi)	RWP IRI (in/mi)	Average IRI (in/mi)
0.0000 to 0.1000	51.2	44.4	47.8
0.1000 to 0.2000	48.4	42.9	45.6
0.2000 to 0.3000	55.0	45.7	50.3
0.3000 to 0.4000	54.0	49.4	51.7
0.4000 to 0.5000	40.3	35.9	38.1
0.5000 to 0.6000	49.8	54.9	52.3
0.6000 to 0.7000	44.6	41.6	43.1
0.7000 to 0.8000	38.8	42.4	40.6
0.8000 to 0.9000	42.5	49.1	45.8
0.9000 to 1.0000	57.1	52.5	54.8
1.0000 to 1.1000	46.4	45.6	46.0
1.1000 to 1.2000	36.8	40.4	38.6
1.2000 to 1.3000	44.0	46.4	45.2
1.3000 to 1.4000	42.0	39.2	40.6
1.4000 to 1.5000	40.6	38.1	39.4
1.5000 to 1.6000	49.4	73.6	61.5
1.6000 to 1.7000	59.2	100.4	79.8
1.7000 to 1.8000	45.7	105.4	75.5
1.8000 to 1.9000	47.7	107.1	77.4
1.9000 to 2.0000	50.3	105.5	77.9
2.0000 to 2.1000	70.8	51.2	61.0
2.1000 to 2.2000	40.2	35.8	38.0
2.2000 to 2.3000	37.1	34.9	36.0
2.3000 to 2.4000	45.8	39.8	42.8
2.4000 to 2.5000	39.2	39.9	39.5
2.5000 to 2.6000	41.0	36.3	38.7
2.6000 to 2.7000	40.0	39.5	39.8
2.7000 to 2.8000	39.1	36.3	37.7
2.8000 to 2.9000	41.1	37.5	39.3
2.9000 to 3.0000	50.6	48.0	49.3
3.0000 to 3.1000	38.8	37.5	38.2
3.1000 to 3.2000	37.4	33.3	35.4
3.2000 to 3.3000	40.2	45.5	42.9
3.3000 to 3.4000	39.6	34.6	37.1
3.4000 to 3.5000	40.3	45.0	42.6
3.5000 to 3.6000	42.7	46.6	44.6

Table 4.22. IRIs for K1 Lane Tested along FM1994 in Fort Bend County.

Interval (miles)	LWP IRI (in/mi)	RWP IRI (in/mi)	Average IRI (in/mi)
0.0000 to 0.1000	36.8	51.4	44.1
0.1000 to 0.2000	43.1	53.9	48.5
0.2000 to 0.3000	44.1	59.6	51.9
0.3000 to 0.4000	36.6	56.8	46.7
0.4000 to 0.5000	47.2	58.1	52.7
0.5000 to 0.6000	50.2	58.6	54.4
0.6000 to 0.7000	81.5	52.3	66.9
0.7000 to 0.8000	48.9	47.2	48.1
0.8000 to 0.9000	50.4	50.3	50.4
0.9000 to 1.0000	95.0	104.0	99.5
1.0000 to 1.1000	80.8	64.1	72.5
1.1000 to 1.2000	77.1	67.7	72.4
1.2000 to 1.3000	84.1	79.5	81.8
1.3000 to 1.4000	58.1	51.8	55.0
1.4000 to 1.5000	46.5	45.4	46.0
1.5000 to 1.6000	45.4	41.9	43.6
1.6000 to 1.7000	44.2	51.4	47.8
1.7000 to 1.8000	40.9	62.1	51.5
1.8000 to 1.9000	42.1	64.0	53.1
1.9000 to 2.0000	50.4	49.3	49.9

Table 4.23. IRIs for K6 Lane Tested along FM1994 in Fort Bend County.

Interval (miles)	LWP IRI (in/mi)	RWP IRI (in/mi)	Average IRI (in/mi)
0.0000 to 0.1000	49.2	48.7	49.0
0.1000 to 0.2000	47.2	44.1	45.7
0.2000 to 0.3000	45.3	59.0	52.1
0.3000 to 0.4000	46.2	57.8	52.0
0.4000 to 0.5000	50.0	50.1	50.0
0.5000 to 0.6000	55.3	45.2	50.2
0.6000 to 0.7000	46.2	42.0	44.1
0.7000 to 0.8000	49.3	49.5	49.4
0.8000 to 0.9000	49.1	43.2	46.1
0.9000 to 1.0000	53.7	51.0	52.4
1.0000 to 1.1000	49.8	50.1	49.9
1.1000 to 1.2000	45.6	43.0	44.3
1.2000 to 1.3000	40.6	41.7	41.1
1.3000 to 1.4000	51.2	43.5	47.3
1.4000 to 1.5000	50.3	47.8	49.1
1.5000 to 1.6000	39.0	43.6	41.3
1.6000 to 1.7000	40.5	39.5	40.0
1.7000 to 1.8000	40.3	44.3	42.3
1.8000 to 1.9000	43.0	46.3	44.6
1.9000 to 2.0000	38.6	65.6	52.1

Table 4.24. IRIs for R1 Lane (Group A) along SH121 in Denton County.

Interval (miles)	LWP IRI (in/mi)	RWP IRI (in/mi)	Average IRI (in/mi)
0.0000 to 0.1000	88.9	95.7	92.3
0.1000 to 0.2000	81.5	75.5	78.5
0.2000 to 0.3000	81.4	93.9	87.7
0.3000 to 0.4000	69.4	75.8	72.6
0.4000 to 0.5000	112.7	129.2	120.9
0.5000 to 0.6000	97.0	108.3	102.7
0.6000 to 0.7000	95.9	107.6	101.8
0.7000 to 0.8000	94.8	91.0	92.9
0.8000 to 0.9000	99.8	107.5	103.7
0.9000 to 1.0000	109.7	110.7	110.2
1.0000 to 1.1000	91.6	82.4	87.0
1.1000 to 1.2000	94.4	88.7	91.6
1.2000 to 1.3000	88.2	81.9	85.0
1.3000 to 1.4000	131.6	141.6	136.6
1.4000 to 1.5000	113.3	115.9	114.6
1.5000 to 1.6000	115.6	116.2	115.9
1.6000 to 1.7000	209.5	224.0	216.8
1.7000 to 1.8000	167.5	204.1	185.8
1.8000 to 1.9000	215.5	221.8	218.6
1.9000 to 2.0000	180.5	184.0	182.2

Table 4.25. IRIs for R2 Lane (Group A) along SH121 in Denton County.

Interval (miles)	LWP IRI (in/mi)	RWP IRI (in/mi)	Average IRI (in/mi)
0.0000 to 0.1000	83.3	76.3	79.8
0.1000 to 0.2000	83.1	63.6	73.4
0.2000 to 0.3000	108.2	58.6	83.4
0.3000 to 0.4000	88.8	61.7	75.3
0.4000 to 0.5000	114.2	103.6	108.9
0.5000 to 0.6000	129.6	92.2	110.9
0.6000 to 0.7000	90.5	89.1	89.8
0.7000 to 0.8000	78.9	87.6	83.2
0.8000 to 0.9000	80.2	84.1	82.1
0.9000 to 1.0000	90.7	98.8	94.8
1.0000 to 1.1000	66.5	67.5	67.0
1.1000 to 1.2000	58.3	53.9	56.1
1.2000 to 1.3000	66.4	60.8	63.6
1.3000 to 1.4000	128.3	122.9	125.6
1.4000 to 1.5000	64.1	78.4	71.3
1.5000 to 1.6000	68.6	75.9	72.2
1.6000 to 1.7000	196.6	206.0	201.3
1.7000 to 1.8000	163.6	167.5	165.6
1.8000 to 1.9000	216.6	213.9	215.3
1.9000 to 2.0000	184.6	186.9	185.7

Table 4.26. IRIs for L1 Lane (Group B) along SH121 in Denton County.

Interval (miles)	LWP IRI (in/mi)	RWP IRI (in/mi)	Average IRI (in/mi)
0.0000 to 0.1000	261.7	283.7	272.7
0.1000 to 0.2000	184.8	178.8	181.8
0.2000 to 0.3000	245.3	237.4	241.3
0.3000 to 0.4000	218.7	215.7	217.2
0.4000 to 0.5000	116.3	114.4	115.4
0.5000 to 0.6000	90.9	86.0	88.4
0.6000 to 0.7000	137.0	145.4	141.2
0.7000 to 0.8000	94.4	108.1	101.3
0.8000 to 0.9000	86.7	86.6	86.6
0.9000 to 1.0000	103.4	88.3	95.9
1.0000 to 1.1000	99.4	87.3	93.4
1.1000 to 1.2000	116.4	101.3	108.8
1.2000 to 1.3000	77.7	82.2	80.0
1.3000 to 1.4000	71.0	89.2	80.1
1.4000 to 1.5000	66.9	78.9	72.9
1.5000 to 1.6000	116.4	129.1	122.8
1.6000 to 1.7000	70.2	87.7	79.0
1.7000 to 1.8000	55.3	94.5	74.9
1.8000 to 1.9000	61.2	109.9	85.5
1.9000 to 2.0000	65.6	99.1	82.4
2.0000 to 2.1000	63.7	85.9	74.8
2.1000 to 2.2000	71.8	86.8	79.3
2.2000 to 2.3000	77.1	85.4	81.2

Table 4.27. IRIs for L2 Lane (Group B) along SH121 in Denton County.

Interval (miles)	LWP IRI (in/mi)	RWP IRI (in/mi)	Average IRI (in/mi)
0.0000 to 0.1000	235.2	253.5	244.4
0.1000 to 0.2000	175.3	177.6	176.5
0.2000 to 0.3000	219.0	234.5	226.8
0.3000 to 0.4000	211.1	216.6	213.9
0.4000 to 0.5000	139.0	160.4	149.7
0.5000 to 0.6000	138.6	139.8	139.2
0.6000 to 0.7000	152.7	149.7	151.2
0.7000 to 0.8000	73.2	93.7	83.5
0.8000 to 0.9000	81.5	96.2	88.8
0.9000 to 1.0000	89.6	86.6	88.1
1.0000 to 1.1000	85.5	84.9	85.2
1.1000 to 1.2000	92.3	88.9	90.6
1.2000 to 1.3000	102.7	113.8	108.3
1.3000 to 1.4000	98.7	70.9	84.8
1.4000 to 1.5000	69.7	59.7	64.7
1.5000 to 1.6000	118.3	119.5	118.9
1.6000 to 1.7000	67.7	65.5	66.6
1.7000 to 1.8000	63.8	75.5	69.6
1.8000 to 1.9000	56.9	78.8	67.9
1.9000 to 2.0000	59.3	64.7	62.0
2.0000 to 2.1000	60.5	64.5	62.5
2.1000 to 2.2000	67.1	74.1	70.6
2.2000 to 2.3000	72.7	71.5	72.1

Table 4.28. IRIs for L1 Lane (Group C) along SH121 in Denton County.

Interval (miles)	LWP IRI (in/mi)	RWP IRI (in/mi)	Average IRI (in/mi)
0.0000 to 0.1000	98.5	85.8	92.2
0.1000 to 0.2000	109.4	106.2	107.8
0.2000 to 0.3000	98.9	88.9	93.9
0.3000 to 0.4000	106.2	123.1	114.6
0.4000 to 0.5000	93.3	86.9	90.1
0.5000 to 0.6000	87.9	75.8	81.8
0.6000 to 0.7000	76.4	78.2	77.3
0.7000 to 0.8000	120.0	137.9	129.0
0.8000 to 0.9000	77.8	87.3	82.6
0.9000 to 1.0000	105.9	114.8	110.4
1.0000 to 1.1000	153.6	161.8	157.7
1.1000 to 1.1883	146.3	156.6	151.4

Table 4.29. IRIs for L2 Lane (Group C) along SH121 in Denton County.

Interval (miles)	LWP IRI (in/mi)	RWP IRI (in/mi)	Average IRI (in/mi)
0.0000 to 0.1000	105.1	83.4	94.3
0.1000 to 0.2000	128.5	93.8	111.1
0.2000 to 0.3000	130.6	76.4	103.5
0.3000 to 0.4000	107.9	106.9	107.4
0.4000 to 0.5000	138.0	89.8	113.9
0.5000 to 0.6000	102.2	78.6	90.4
0.6000 to 0.7000	105.0	78.9	92.0
0.7000 to 0.8000	154.5	116.0	135.2
0.8000 to 0.9000	112.0	75.4	93.7
0.9000 to 1.0000	158.7	128.2	143.4
1.0000 to 1.1000	159.2	167.7	163.5
1.1000 to 1.1874	148.5	144.1	146.3

Table 4.30. IRIs for R2 Lane (Group D) along SH121 in Denton County.

Interval (miles)	LWP IRI (in/mi)	RWP IRI (in/mi)	Average IRI (in/mi)
0.0000 to 0.1000	140.7	146.3	143.5
0.1000 to 0.2000	154.5	148.6	151.5
0.2000 to 0.3000	120.5	125.1	122.8
0.3000 to 0.4000	161.0	167.2	164.1
0.4000 to 0.5000	116.7	111.0	113.9
0.5000 to 0.6000	73.7	90.0	81.8
0.6000 to 0.7000	133.5	145.0	139.3
0.7000 to 0.8000	71.7	75.0	73.4
0.8000 to 0.9000	81.8	79.9	80.8
0.9000 to 1.0000	98.5	105.9	102.2
1.0000 to 1.1000	154.2	151.1	152.6
1.1000 to 1.2000	76.7	82.2	79.4
1.2000 to 1.3000	94.1	98.5	96.3
1.3000 to 1.4000	96.4	83.1	89.7
1.4000 to 1.5000	78.5	85.7	82.1
1.5000 to 1.6000	89.5	92.1	90.8
1.6000 to 1.7000	86.8	92.5	89.7
1.7000 to 1.8000	135.0	143.0	139.0
1.8000 to 1.9000	87.6	91.2	89.4
1.9000 to 2.0000	99.5	109.5	104.5
2.0000 to 2.1000	110.8	120.2	115.5
2.1000 to 2.2000	110.0	113.8	111.9
2.2000 to 2.2593	120.1	135.7	127.9

Table 4.31. Summary Indicators of Overall Ride Quality on Projects Tested.

Highway	County	Length (miles)	Lane	Overall Average IRI (in/mile)			Number of 0-1 Mile Sections		Number of defects
				LWP	RWP	Average	with average IRI < 60 in/mile	Deficient[1]	
SH21	Lee	2.4	K1	63.3	67.2	65.3	10	0	3
			K2	46.6	46.4	46.5	23	0	4
			K6	58.6	65.5	62.1	9	0	7
			K7	46.5	44.4	45.5	24	0	1
SH21	Bastrop	3.6	K1	79.6	90.9	85.3	0	5	15
			K2	61.2	59.3	60.3	21	1	15
			K6	78.6	83.9	81.3	1	4	15
			K7	63.5	53.8	58.7	19	0	7
SH47[2]	Brazos	6.0	R1	52.9	47.7	50.3	51	3	58
			R2	63.0	59.2	61.1	38	4	62
SH47[2]	Brazos	5.7	L1	63.4	56.9	60.2	39	6	66
			L2	74.0	70.3	72.2	18	6	104
FM102 Group A	Wharton	5.0	K1	65.8	68.6	67.2	17	2	7
			K6	60.4	65.5	63.0	29	2	9
FM102 Group B	Wharton	6.0	K1	40.9	50.4	45.7	56	1	5
			K6	56.8	61.0	58.9	34	0	1
SH36	Fort Bend	1.4	K1	69.7	67.8	68.8	0	0	0
			K6	73.9	64.3	69.1	2	0	2
FM1462	Fort Bend	3.6	K1	45.3	57.7	51.5	28	0	0
			K6	44.9	49.7	47.3	30	0	0
FM1994	Fort Bend	2.0	K1	54.9	58.1	56.5	15	1	4
			K6	46.2	47.4	46.8	20	0	0
SH121 Group A	Denton	2.0	R1	117.6	123.3	120.5	0	12	144
			R2	110.4	104.8	107.6	1	7	138
SH121 Group B	Denton	2.3	L1	109.9	118.9	114.4	0	9	150
			L2	108.9	113.7	111.3	0	9	157
SH121 Group C	Denton	1.18	L1	105.3	107.6	106.5	0	6	45
			L2	128.3	102.2	115.3	0	8	46
SH121 Group D	Denton	2.26	R2	107.5	111.6	109.6	0	13	98

[1] Average IRI on section greater than 95 in/mile.
[2] Existing highway, not a newly resurfaced project.

average IRI to specified levels based on the pay adjustment schedule implemented in the project plans. The number of defects shown in the table includes all bumps and defects reported by TxDOT's Ride Quality program. This program determines the defects based on the average of the left and right wheel path profiles. In this determination, the program applies a 25-ft moving average filter to the average profile. It then computes the difference between the average profile and its moving average to locate defects based on a 150-mil threshold. To determine pay adjustments, the program applies a 5-ft bump penalty gap such that multiple occurrences of defects within 5 ft are assessed only one penalty. Researchers looked at all defects reported by TxDOT's Ride Quality program to examine the relationship between ride quality and dynamic tire loading in this project.

TESTING OF INSTRUMENTED TRACTOR-SEMITRAILER AT WIM SITE

Prior to running the instrumented tractor-semitrailer to measure dynamic tire loads on the highway projects identified in Table 4.1, researchers tested the vehicle at the SH6 WIM site to check the dynamic load measurements based on the strain gages with the tire loads obtained from the WIM sensors installed at the site. For these tests, researchers collected data at test speeds of 50 and 60 mph. To locate the WIM sensors in the test data from the instrumented truck, researchers placed reflective tape at a known distance from one of the WIM sensors. When this tape is detected by the vehicle's start sensor, it causes a marker to be inserted in the data. Researchers used this marker to locate the position of each axle at any given time, knowing the distances between the start sensor and the five axles of the test vehicle.

Figures 4.1 to 4.5 plot the dynamic load profiles with the WIM tire loads measured under the five axles of the instrumented truck running at a test speed of 60 mph. Figures 4.6 to 4.10 show the same comparisons at the slower test speed of 50 mph. For both speeds, there is reasonable agreement between the WIM readings and the dynamic tire loads from the instrumented truck, particularly for the ECM™ and BL™ piezo-electric WIM sensors. With this verification of the test setup for collecting dynamic load measurements, researchers proceeded with testing the projects identified in Table 4.1 using the tractor-semitrailer combination instrumented in this research project. The next section discusses the findings from these tests.

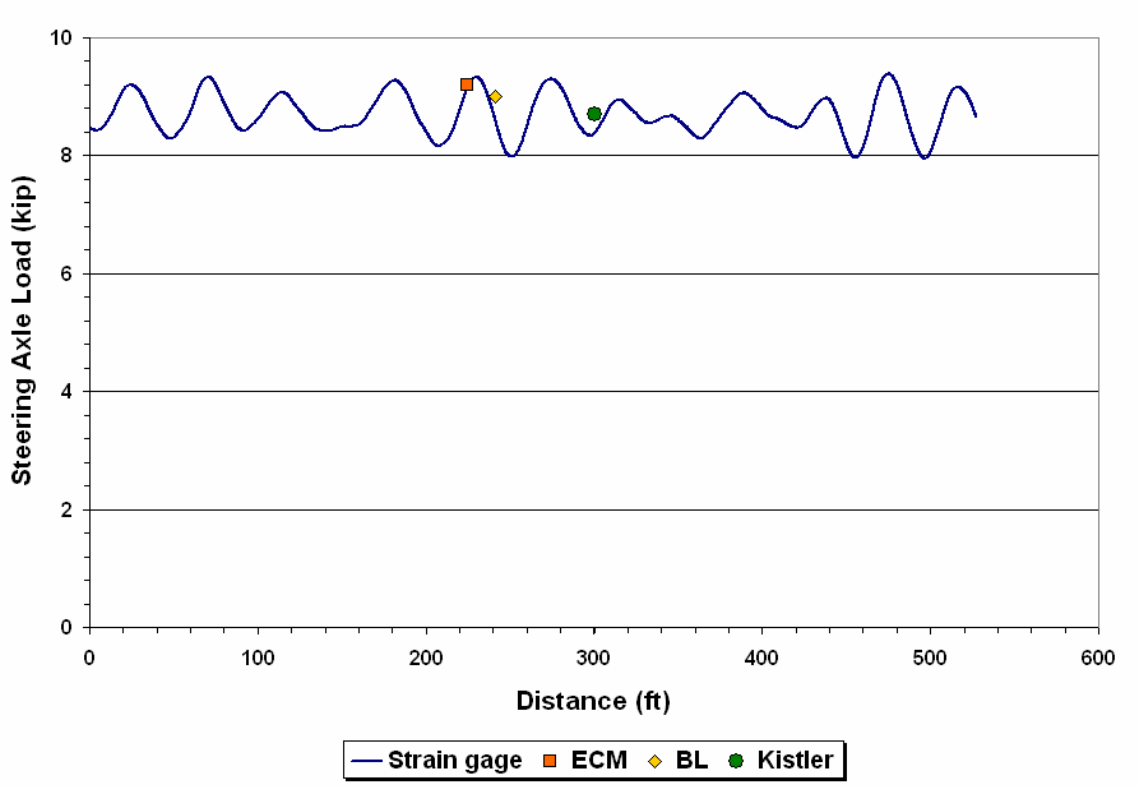

Figure 4.1. Comparison of Dynamic Load Measurements for Steering Axle with WIM Data at a Test Speed of 60 mph.

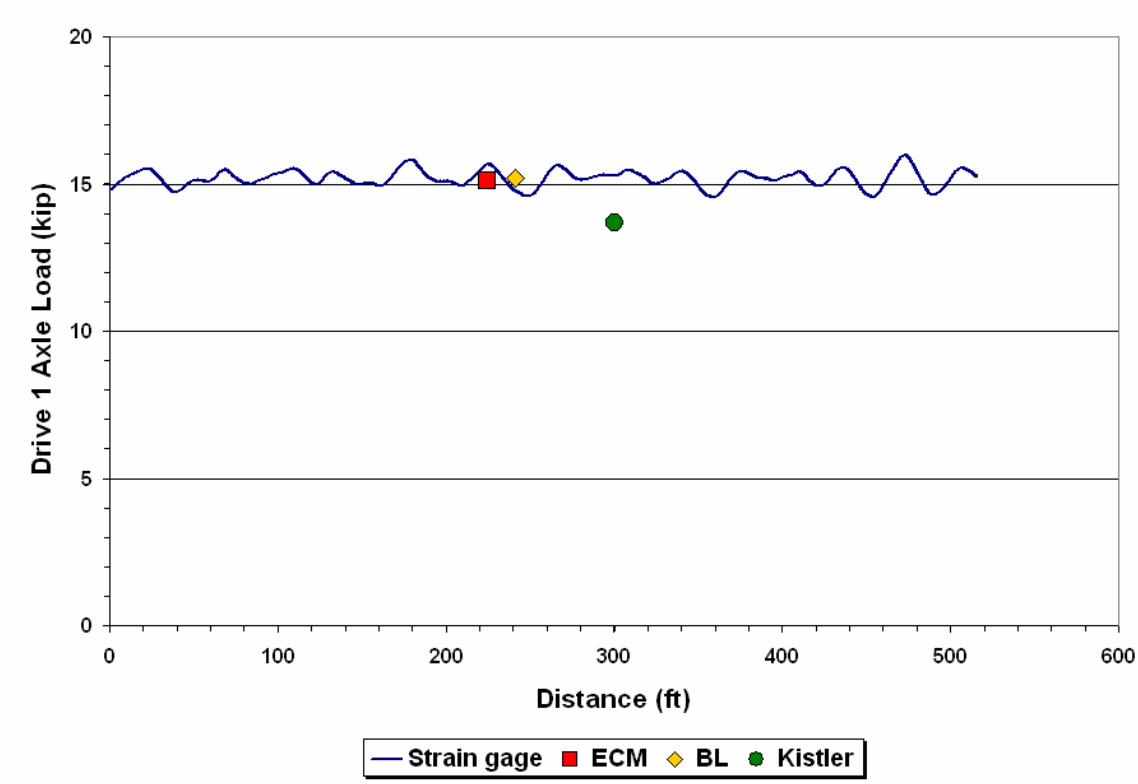

Figure 4.2. Comparison of Dynamic Load Measurements for Drive Axle #1 with WIM Data at a Test Speed of 60 mph.

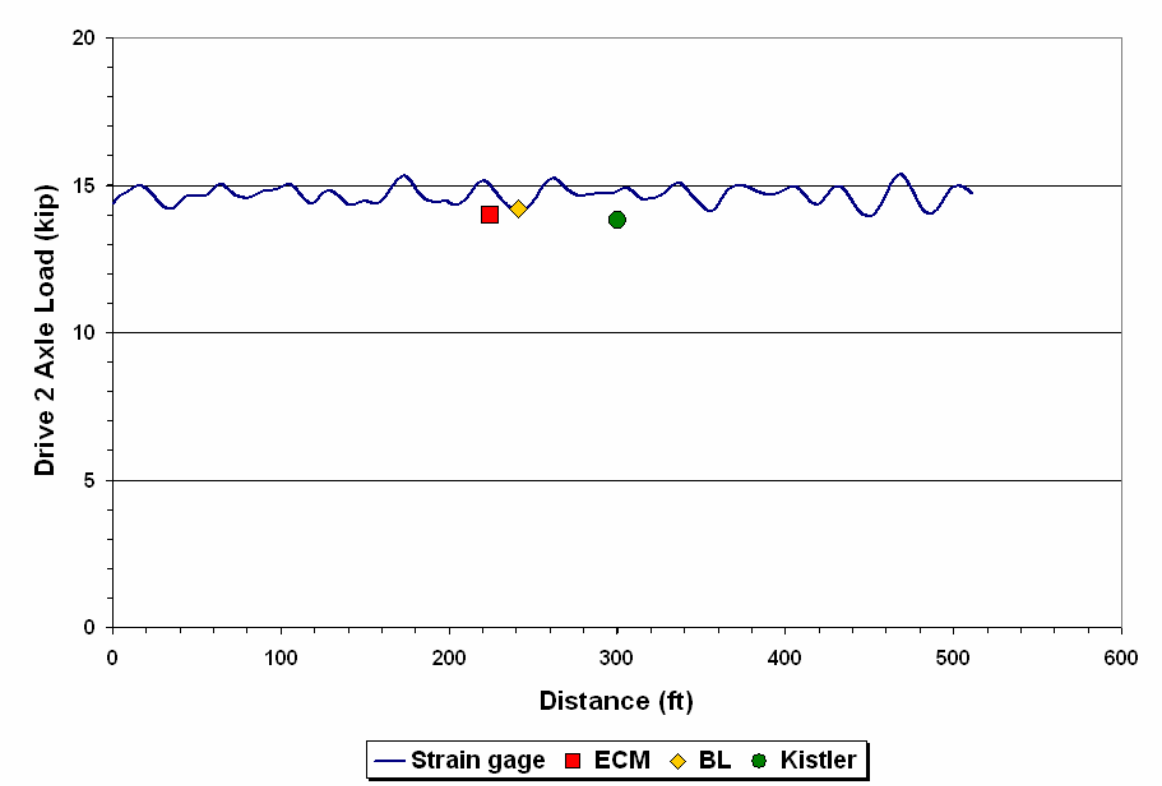

Figure 4.3. Comparison of Dynamic Load Measurements for Drive Axle #2 with WIM Data at a Test Speed of 60 mph.

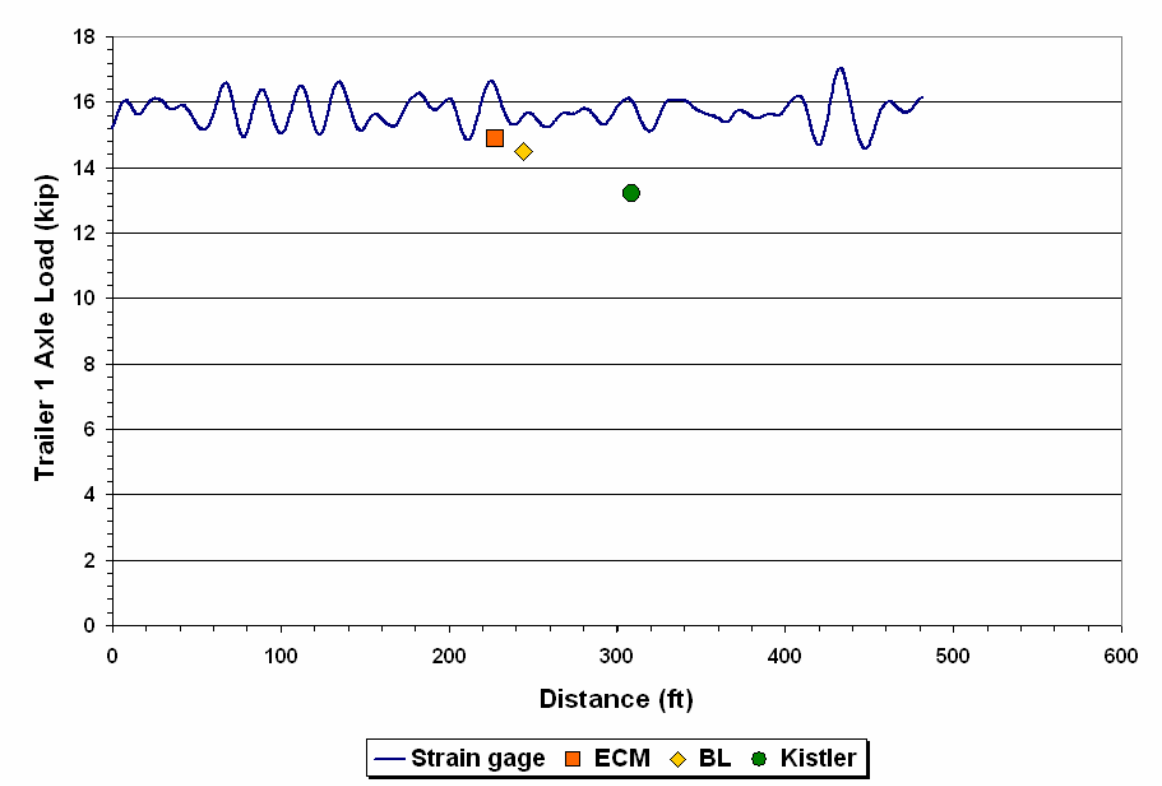

Figure 4.4. Comparison of Dynamic Load Measurements for Trailer Axle #1 with WIM Data at a Test Speed of 60 mph.

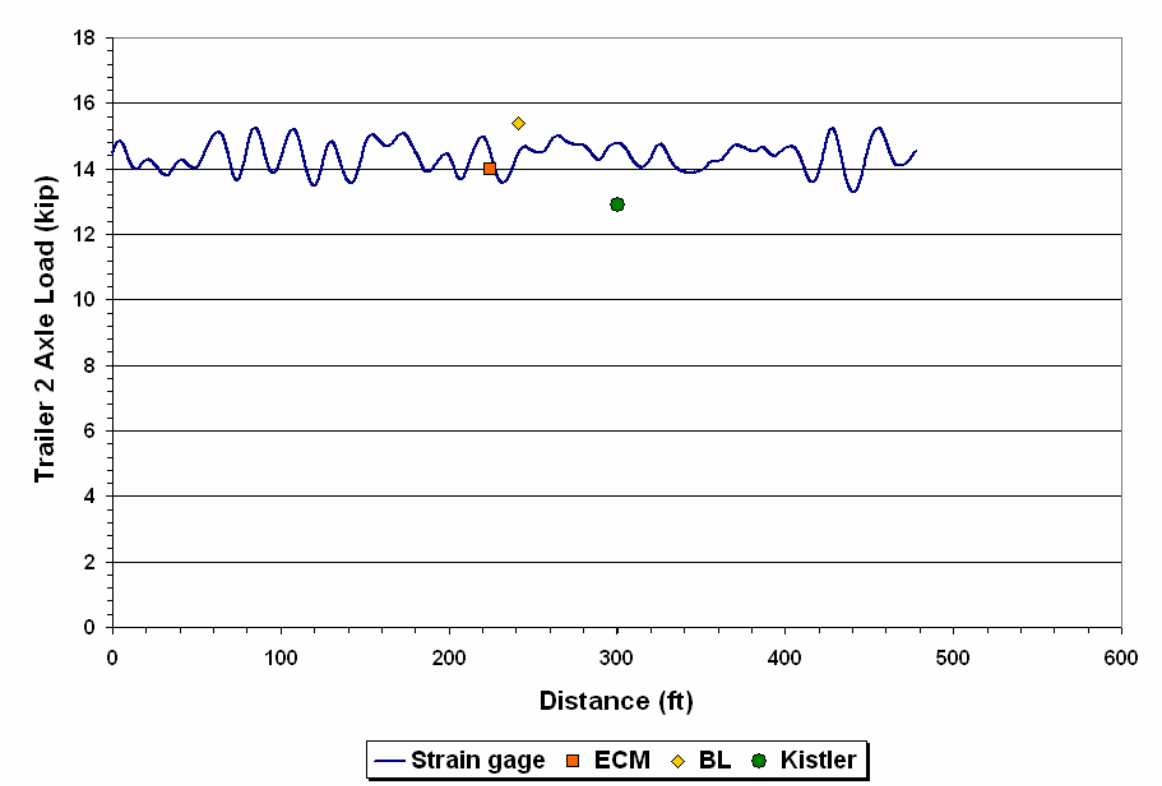

Figure 4.5. Comparison of Dynamic Load Measurements for Trailer Axle #2 with WIM Data at a Test Speed of 60 mph.

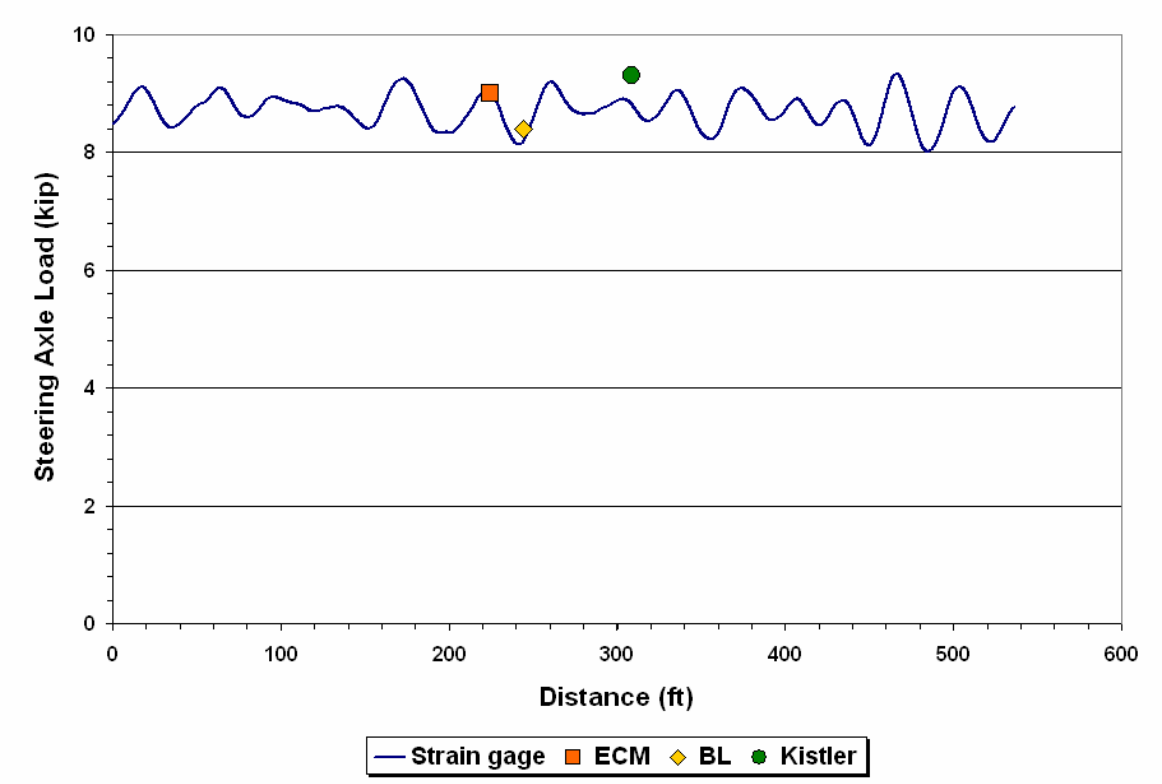

Figure 4.6. Comparison of Dynamic Load Measurements for Steering Axle with WIM Data at a Test Speed of 50 mph.

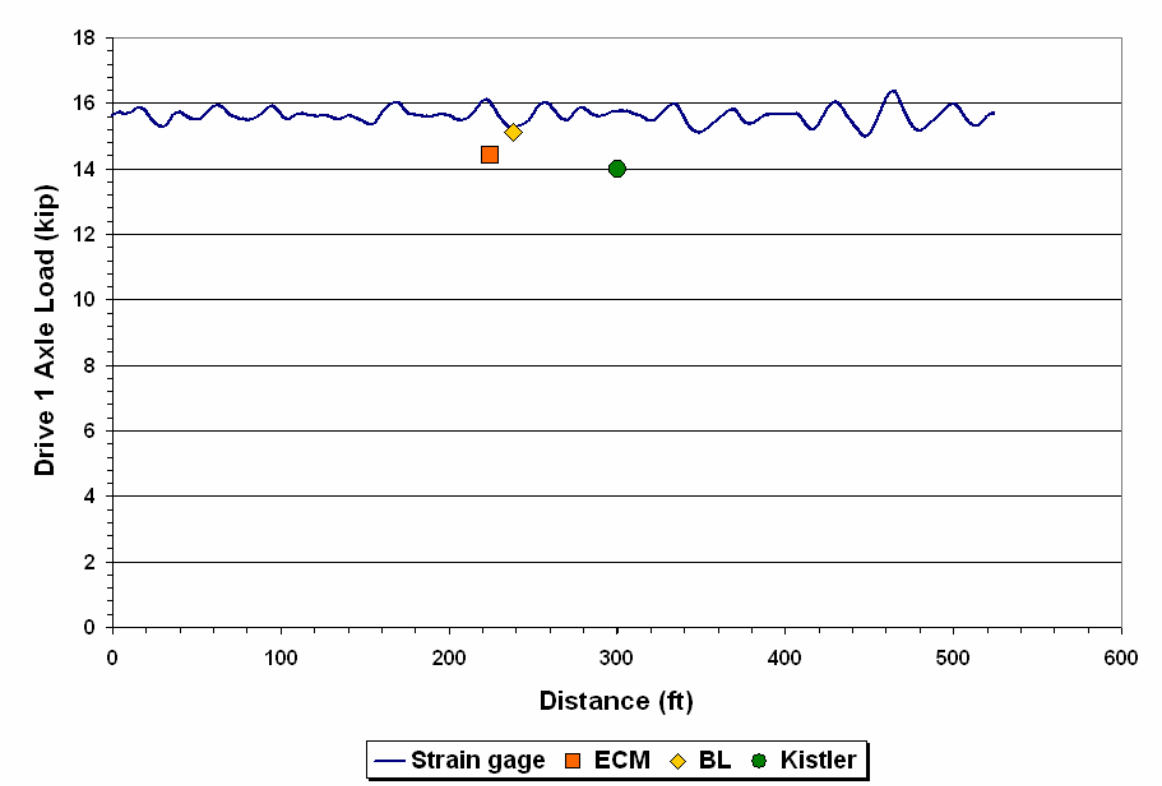

Figure 4.7. Comparison of Dynamic Load Measurements for Drive Axle #1 with WIM Data at a Test Speed of 50 mph.

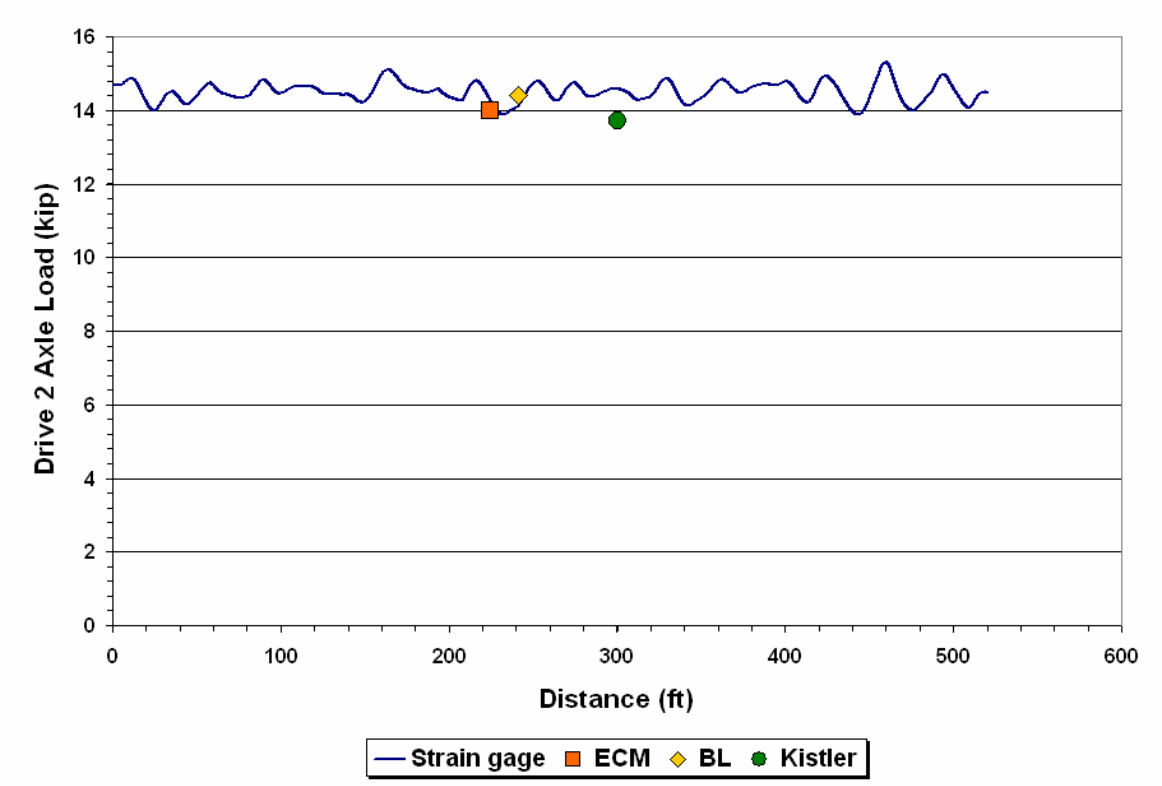

Figure 4.8. Comparison of Dynamic Load Measurements for Drive Axle #2 with WIM Data at a Test Speed of 50 mph.

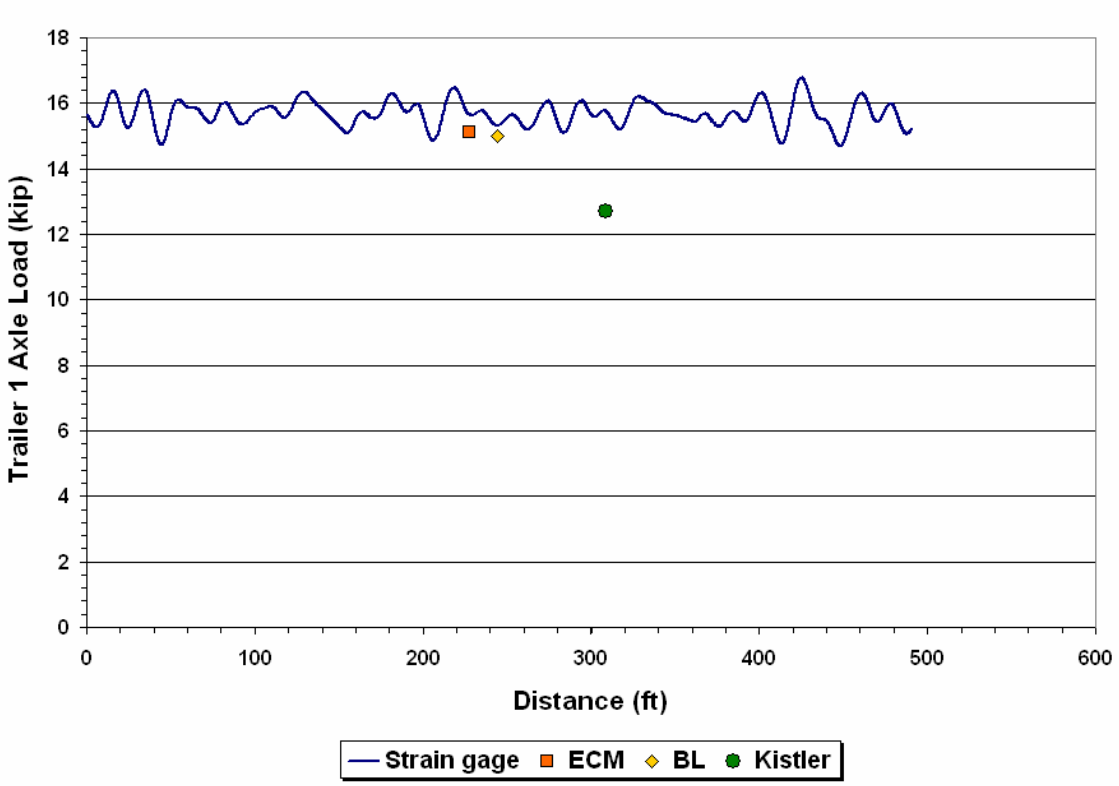

Figure 4.9. Comparison of Dynamic Load Measurements for Trailer Axle #1 with WIM Data at a Test Speed of 50 mph.

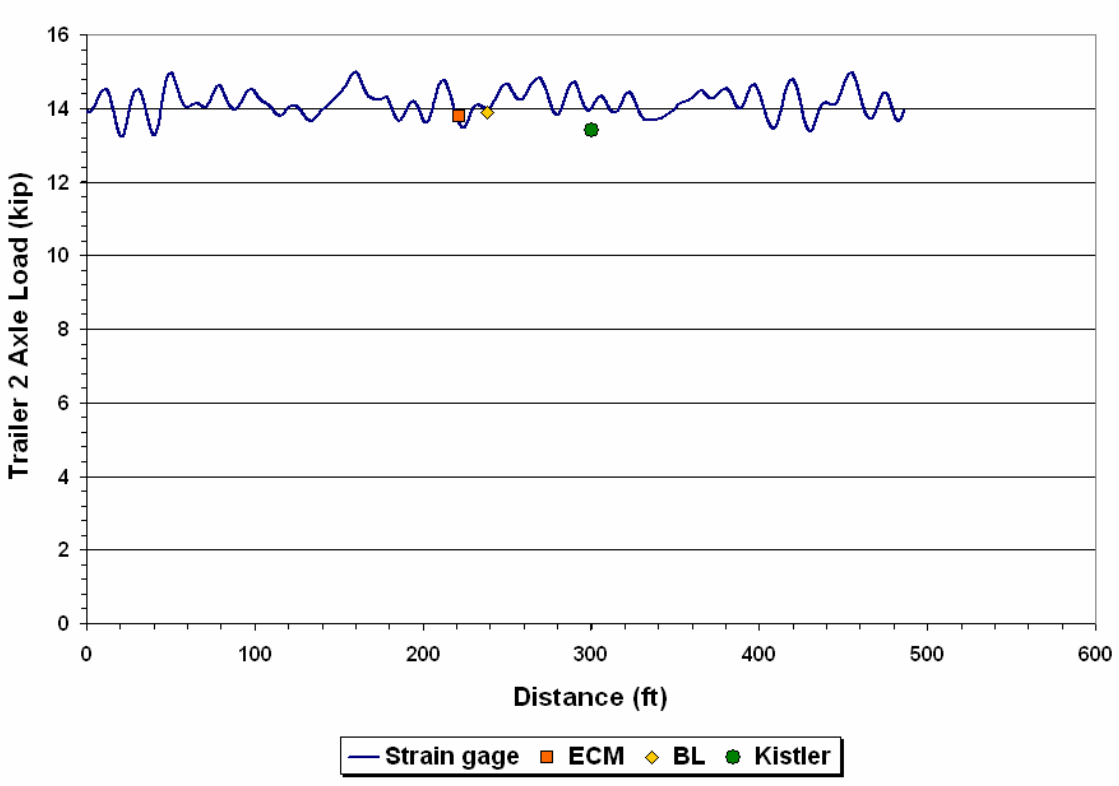

Figure 4.10. Comparison of Dynamic Load Measurements for Trailer Axle #2 with WIM Data at a Test Speed of 50 mph.

ANALYSIS OF TEST DATA FROM INSTRUMENTED TRUCK

The literature review presented in Appendix A found that surface roughness directly affects the variability of dynamic loads applied on the pavement. The greater the roughness, the more pounding the pavement gets from the vehicles that use the road. Sweatman (1983) reported test results from a field experiment conducted in Australia in which dynamic loads were measured for different suspensions, pavement roughness, and vehicle speed. A statistic, called the dynamic load coefficient (DLC), was used to characterize the dynamic loading for each suspension tested in the experiment. Sweatman (1983) defined this statistic as the standard deviation of the measured dynamic loads divided by the mean axle group load. It is thus equivalent to a coefficient of variation. From the test results, the DLCs on smooth pavements varied from close to zero to about 10 percent for the different suspensions included in the experiment. Sweatman also found from his field experiment that the DLCs increase with increase in roughness and vehicle speed according to the relation:

$$DLC = V R^{0.5} \qquad (4.1)$$

where:

V = vehicle speed in km/hr, and

R = surface roughness in counts/km as measured with the Mays Meter.

Fernando (2002) proposed an index for evaluating the acceptability of overlay smoothness that is related to the predicted performance of the overlay based on reflection crack growth. From theoretical considerations, he derived an equation that relates the predicted change in service life with the difference between the as-built surface profile and the design or target profile. The index he proposed is presented as Eq. A1 in Appendix A of this report. It is a function of the coefficients of variation of the predicted dynamic load profiles corresponding to the target and as-built surface profiles. In an earlier project conducted for TxDOT, Fernando (1998) proposed a profile-based smoothness specification based on a target coefficient of variation of 4 percent corresponding to the average predicted dynamic load variability of newly overlaid segments monitored during that project. The damage index is then evaluated based on the difference between this target coefficient of variation and the corresponding statistic determined from the as-built surface profile.

In view of the significant relationships that have been reported between dynamic load variability, surface roughness, and predicted pavement life, researchers examined the variability of the measured dynamic tire loads from the projects tested to evaluate TxDOT's

current ride specification. Specifically, researchers compared the coefficients of variation of measured tire loads with corresponding parameters used for acceptance testing of the ride quality of the finished surface under TxDOT's Item 585 ride specification. These parameters include the IRIs and the defects determined from surface profile measurements on the projects surveyed. The following sections present the findings from this investigation using data from specific projects as examples.

FM1462 Project

Figure 4.11 shows the coefficients of variation (CVs) of the measured dynamic tire loads for the steering axle determined from data collected along the K6 lane of the FM1462 project in Fort Bend County. To detect features in the measured dynamic load profiles that may be associated with localized roughness or with rough 0.1-mile sections, the coefficients of variation of dynamic tire loads were computed at 25-ft intervals along the given test lane. The computed CVs range from about 0.1 to about 6.6 percent.

Figure 4.11 exhibits peaks in the computed coefficients of variation of the measured steering tire loads for the left and right truck wheel paths. The peaks are particularly dominant around the middle of the chart, from about 8500 to 11,000 ft, where groups of peaks are found corresponding to CVs above 4 percent. Researchers examined the IRIs determined from the surface profiles to verify whether the higher dynamic load variability is associated with rough sections within this interval. This examination identified a group of four 0.1-mile contiguous sections where the right wheel path IRIs are all above 95 in/mile. Figure 4.12 illustrates this finding where the wheel path IRIs are plotted with the coefficients of variation of the measured tire loads on the steering axle. It is of interest to note that the left wheel path is a lot smoother than the right wheel path within the interval where the dynamic load variability is observed to be high. Within this interval, the left wheel path IRIs are all below 60 in/mile, while the right wheel path IRIs are all above 95 in/mile.

While this evaluation shows that the current ride specification identified sections of poor ride quality that generate a high level of dynamic load variability, no corrective work on these rough sections will be required from the contractor based on the current ride specification criteria. This situation comes about because of the disparity between the left and right wheel path smoothness that researchers noted previously. Since the left wheel path is significantly smoother than the right wheel path, none of the rough sections classify as deficient (i.e., sections with average IRIs higher than 95 in/mile) to warrant corrective work

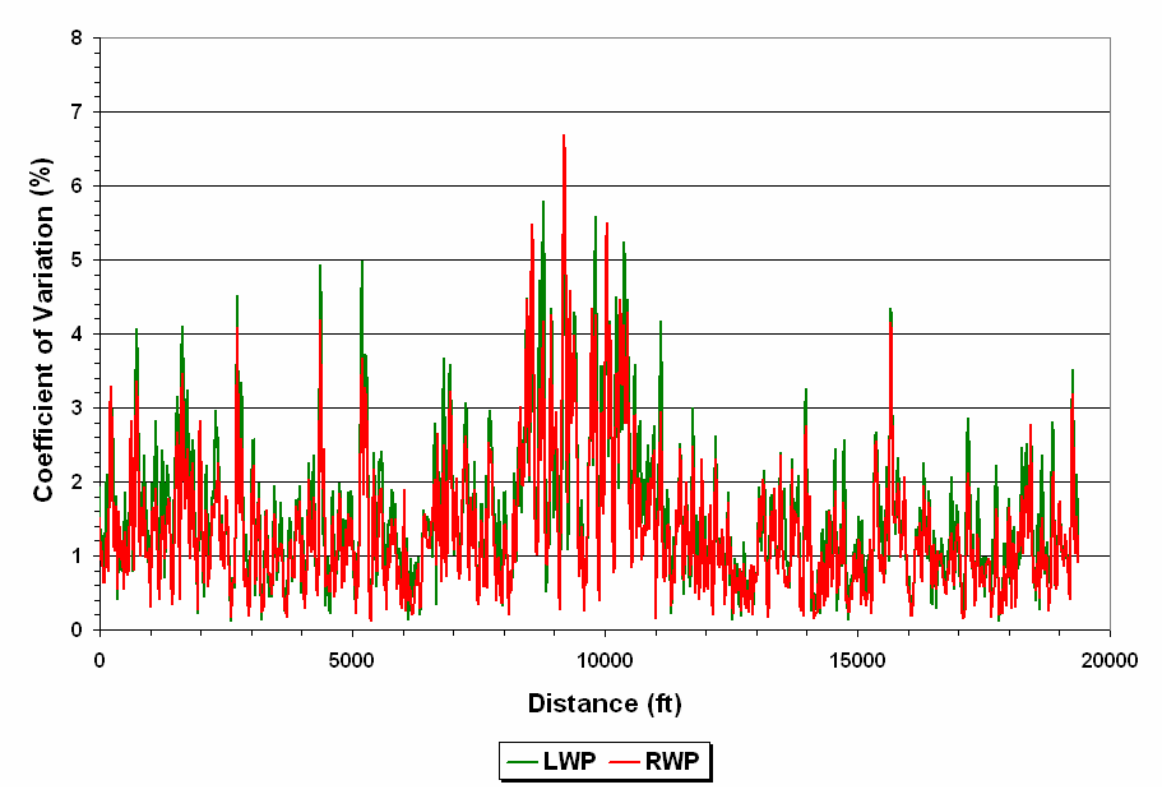

Figure 4.11. Coefficients of Variation of Dynamic Tire Loads for Steering Axle from Tests with Instrumented Vehicle on K6 Lane of FM1462 Project.

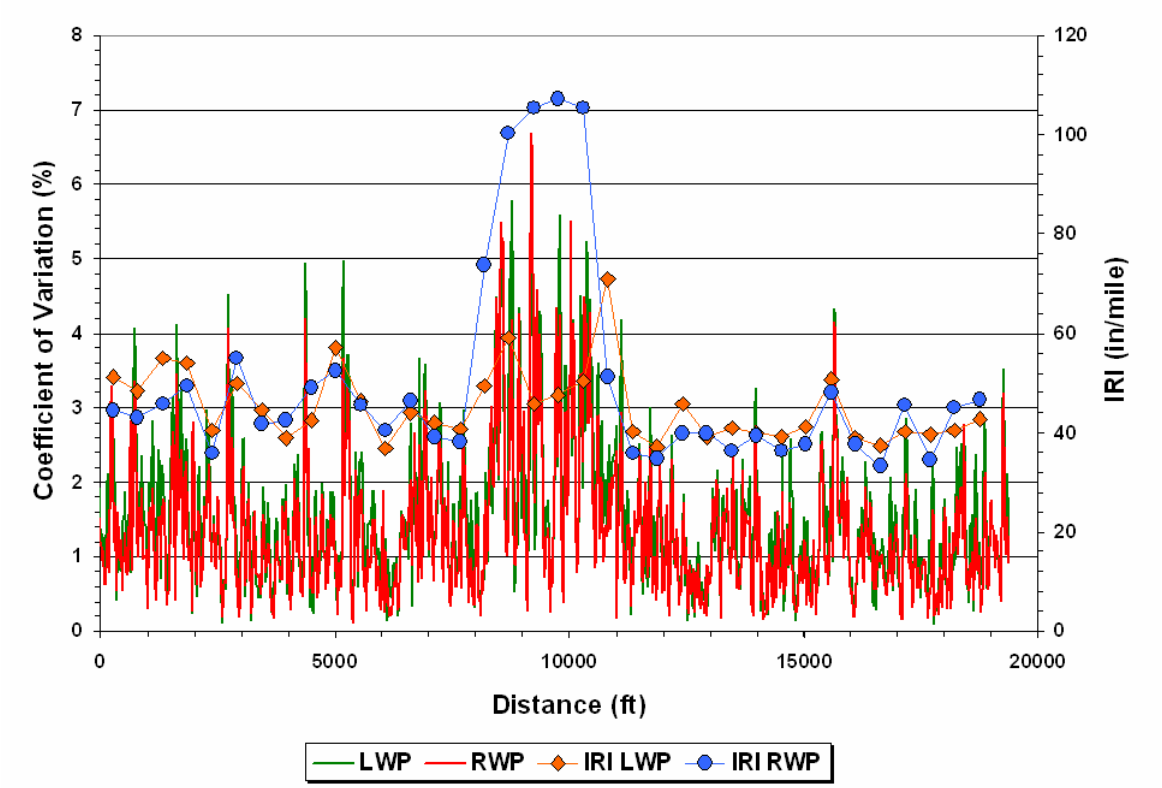

Figure 4.12. Coefficients of Variation of Dynamic Tire Loads for Steering Axle Plotted with IRIs Computed from Profiles Taken along K6 Lane of FM1462 Project.

from the contractor to reduce the roughness on those sections. In addition, because of the disparity between the left and right wheel path smoothness, no defects are detected based on the average profile, as shown in Table 4.31. Thus, there will also be no work required to correct localized roughness with the consequence that the observed dynamic load variability from the tests conducted will not be reduced under the current ride specification.

In view of these results, researchers tried a different approach to the current procedure for detecting localized roughness. Specifically, instead of running the current procedure on the average profile, researchers applied the same procedure on the individual wheel path profiles measured along the FM1462 project. From this analysis, researchers found defects along the individual wheel paths that are summarized in Table 4.32. This table shows more defects along the right wheel path compared to the left wheel path, which is consistent with the trends in the computed IRIs on the left and right wheel paths of the projects tested. Note that no defects were detected using the current method for detecting localized roughness as shown in Table 4.32.

Figures 4.13 to 4.17 plot the defects identified in Table 4.32 with the CVs and IRIs determined from test data collected along the FM1462 project. These figures show that the defects are associated with several occurrences of peaks in the dynamic load variability of the measured tire loads for the different axles. In the researchers' opinion, these results provide justification for using the individual wheel path profiles to determine localized roughness during quality assurance testing of pavement smoothness. An interesting observation from Figures 4.13 to 4.17 is that the peaks in the computed CVs tend to recur at generally the same locations along the project for each axle of the test vehicle. This observation suggests that these locations will likely develop distress earlier than similar locations where the dynamic load variability is less. Thus, it becomes important to properly detect and correct defects to minimize the dynamic load variability. To this end, the discussion presented herein suggests the need to find defects along the individual wheel paths, particularly for cases (such as shown here for the FM1462 project) where there is a significant disparity between the smoothness of the left and right wheel paths. For these cases, evaluating the defects based on the average of the left and right wheel path profiles will tend to mask the defects that exist along the individual wheel paths.

Table 4.32. Defects Located from Profiles Taken along K6 Lane of FM1462 Project in Fort Bend County[1].

LWP Profile			RWP Profile			Average Profile		
Location (feet)	Type	Magnitude (mils)	Location (feet)	Type	Magnitude (mils)	Location (feet)	Type	Magnitude (mils)
			909	Bump	153			
			2729	Bump	153			
			8914	Bump	158			
8924	Dip	-163	8924	Dip	-167			
8933	Bump	155						
			8970	Bump	171			
			9813	Dip	-178			
			9975	Dip	-165			
			10500	Dip	-169			
			10401	Dip	-151			
			10476	Bump	169			
			14643	Dip	-158			
			15751	Bump	248			

[1] Shaded cells indicate no defects found for the given profile.

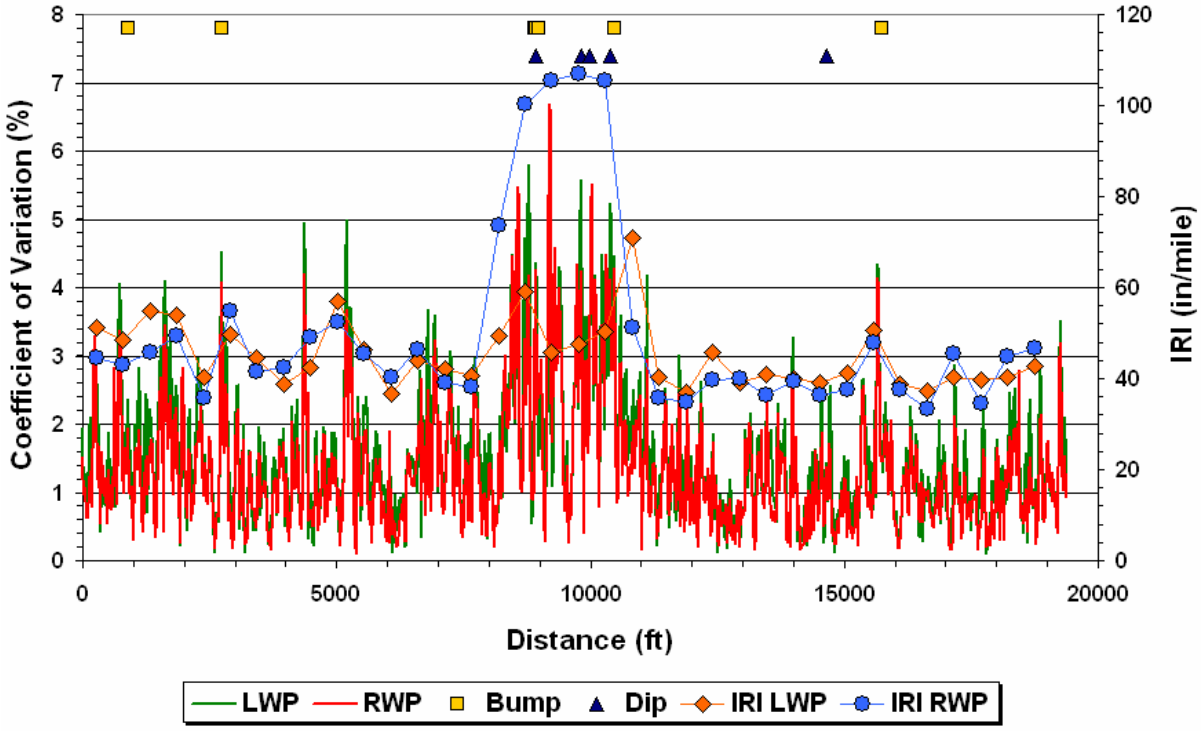

Figure 4.13. Coefficients of Variation of Dynamic Tire Loads for Steering Axle Plotted with IRIs and Defects Computed from K6 Lane Profiles Taken along FM1462 Project.

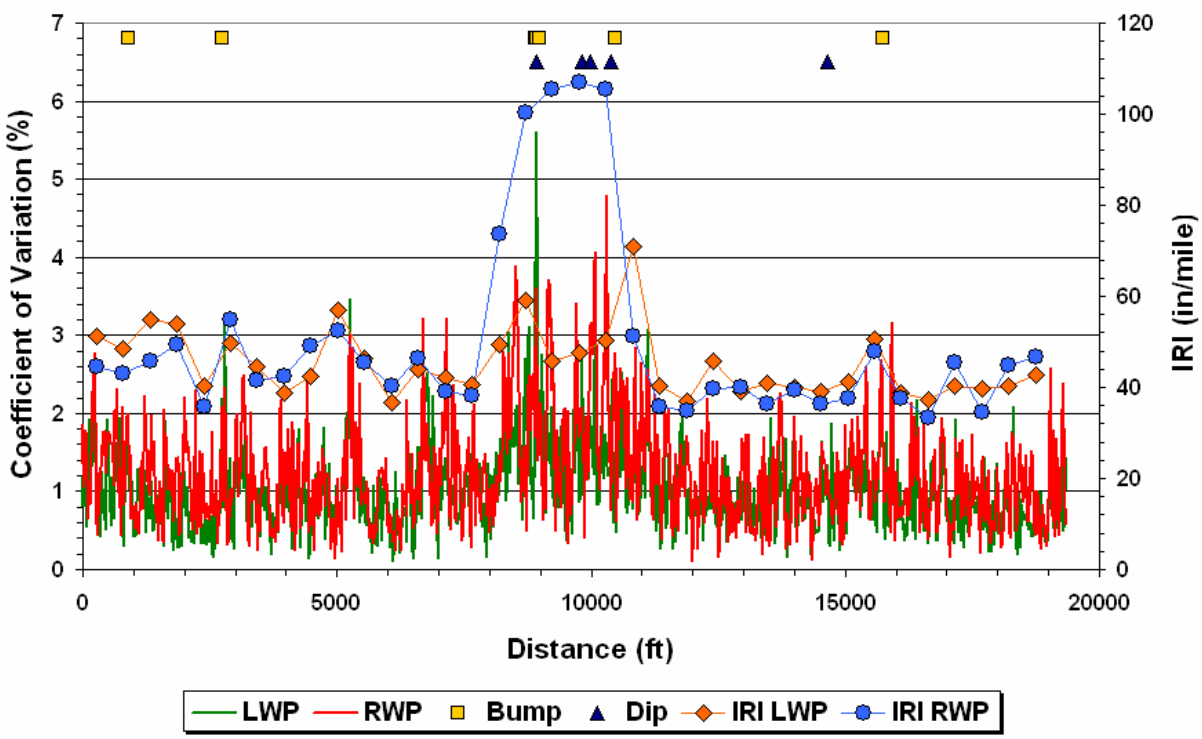

Figure 4.14. Coefficients of Variation of Dynamic Tire Loads for Drive Axle #1 Plotted with IRIs and Defects Computed from K6 Lane Profiles Taken along FM1462 Project.

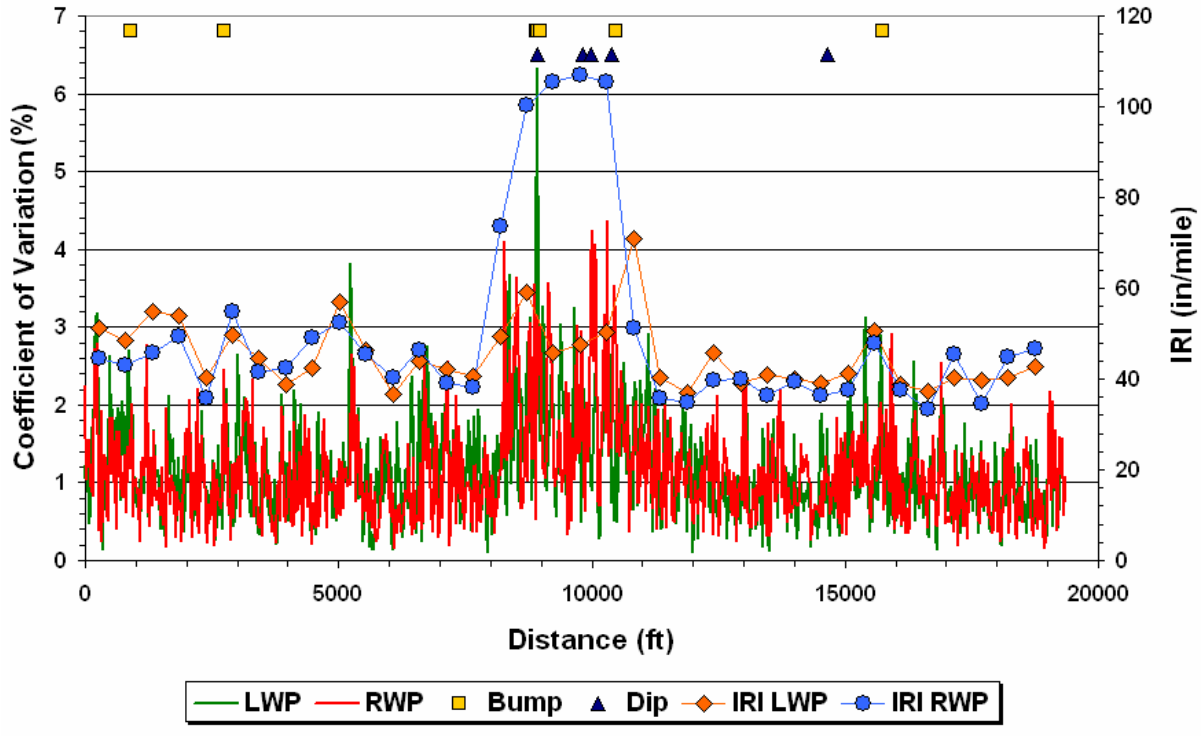

Figure 4.15. Coefficients of Variation of Dynamic Tire Loads for Drive Axle #2 Plotted with IRIs and Defects Computed from K6 Lane Profiles Taken along FM1462 Project.

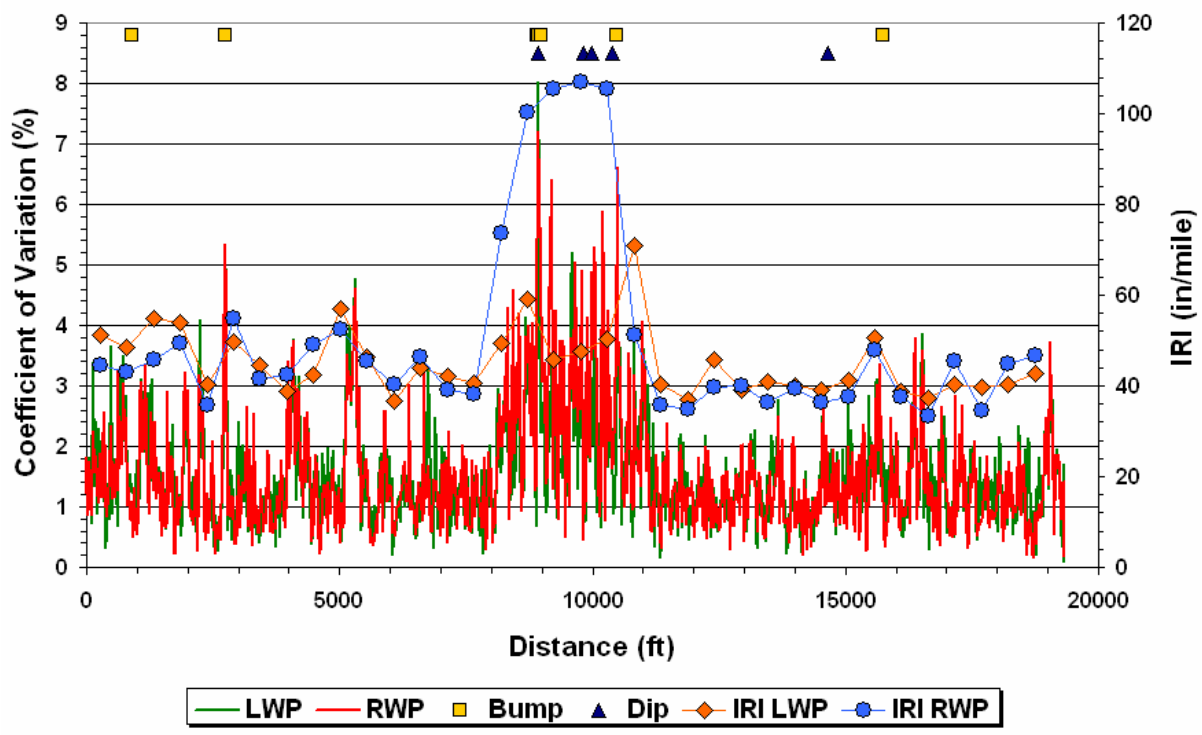

Figure 4.16. Coefficients of Variation of Dynamic Tire Loads for Trailer Axle #1 Plotted with IRIs and Defects Computed from K6 Lane Profiles Taken along FM1462 Project.

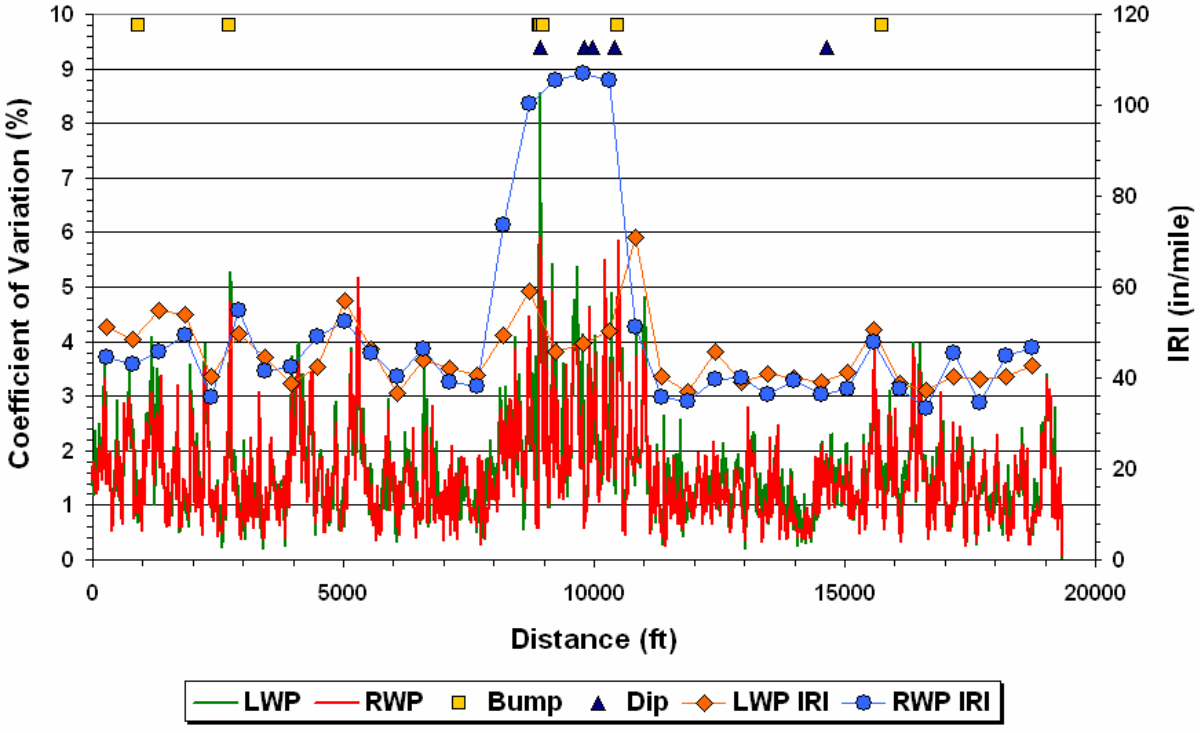

Figure 4.17. Coefficients of Variation of Dynamic Tire Loads for Trailer Axle #2 Plotted with IRIs and Defects Computed from K6 Lane Profiles Taken along FM1462 Project.

FM1994 Project

Figure 4.18 shows the coefficients of variation determined from the dynamic tire loads measured on the steering axle from tests done on the K1 lane of the FM1994 project in Fort Bend County. Also plotted in this figure are IRIs computed from the surface profiles measured along the test lane and the defects determined from these profiles using the current method implemented by TxDOT. From examination of the output from TxDOT's Ride Quality program, the 10th 0.1-mile section on the K1 lane will require corrective work in view of the average IRI of 99 in/mile determined on this section as well as the defects found within the section. This section can be located on Figure 4.18 by counting sequentially from left to right the pairs of IRI points denoting the left and right wheel path IRIs at 0.1-mile intervals along the project tested. The computed CVs on the 10th 0.1-mile section also show a peak around the same area where defects were found based on the average profile.

The left wheel path is also observed to be significantly rough on the seventh 0.1-mile section, with an IRI of about 82 in/mile compared to 52 in/mile for the right wheel path on the same section. In addition, Figure 4.18 shows wheel path IRIs above 60 in/mile for the 11th, 12th, and 13th 0.1-mile sections that follow the deficient 10th 0.1-mile section found on the test lane. The Ride Quality output shows the average IRIs on these sections to be within the penalty range of TxDOT's Item 585 pay adjustment schedules, specifically, schedules 1 and 2. In addition, Figure 4.18 shows peaks in the computed CVs at about the location of the 12th 0.1-mile section. To verify whether this observation might be associated with defects that exist on the individual wheel paths, researchers ran TxDOT's Ride Quality program for each wheel path profile. This task was accomplished by first generating TxDOT formatted files of profile elevations (one file per wheel path). Then, each file was processed using TxDOT's Ride Quality program.

Table 4.33 identifies the defects found along the left and right wheel path profiles of the K1 lane along the FM1994 project. It is observed that additional defects were found within the deficient 0.1-mile section on the test lane that were not detected by the current bump template. Figures 4.19 to 4.23 plot the defects identified in Table 4.33 with the CVs and IRIs determined from test data collected along the FM1994 project. It is observed that the peaks in the computed CVs at about the location of the 12th 0.1-mile section are associated with a couple of bumps detected along the left wheel path at close to 6000 ft from the start of the test lane (see Table 4.33). There are also defects found on the right wheel

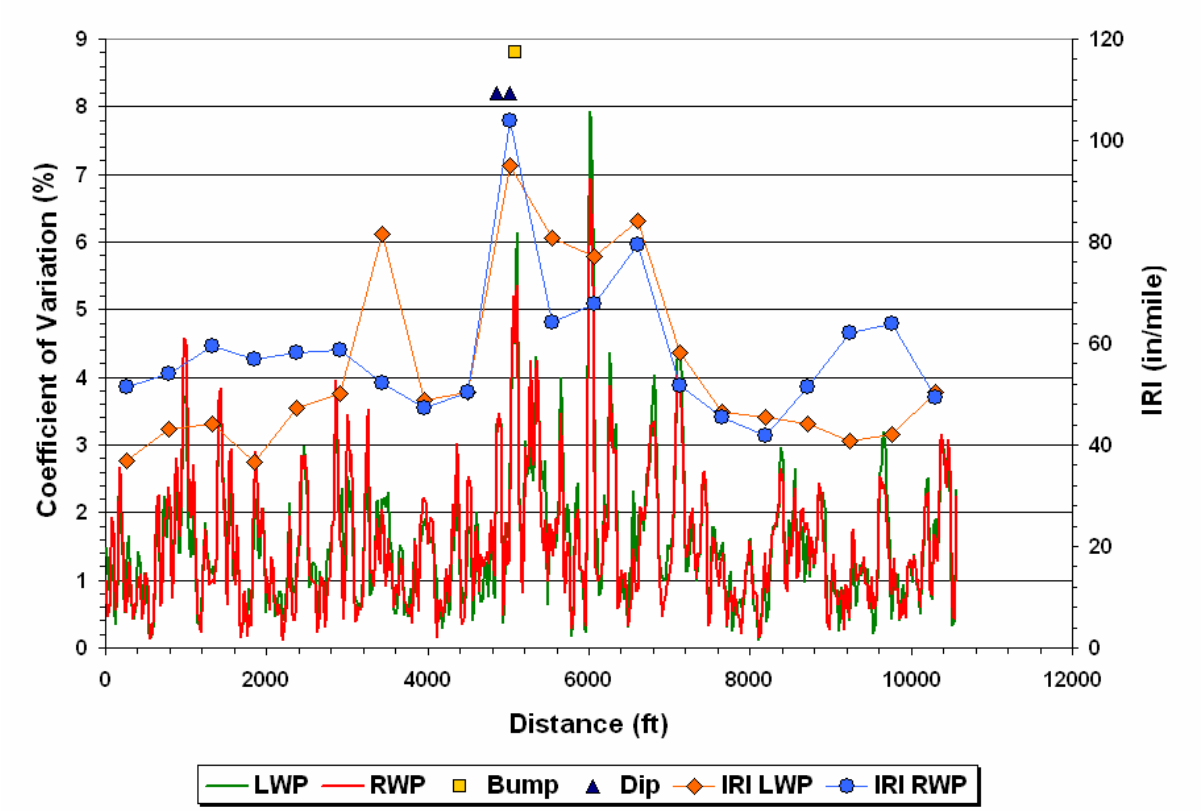

Figure 4.18. Coefficients of Variation of Dynamic Tire Loads for Steering Axle Plotted with IRIs and Defects Determined from TxDOT's Ride Quality Program from Tests on K1 Lane of FM1994 Project.

Table 4.33. Defects Located from Profiles Taken along K1 Lane of FM1994 Project in Fort Bend County[2].

LWP Profile			RWP Profile			Average Profile		
Location (feet)	Type	Magnitude (mils)	Location (feet)	Type	Magnitude (mils)	Location (feet)	Type	Magnitude (mils)
3241	Dip	-166						
4781	Dip	-191						
			4855	Bump	201			
4857	**Dip**	**-190**	**4857**	**Dip**	**-230**	**4857**	**Dip**	**-204**
5018	**Dip**	**-209**				**5018**	**Dip**	**-162**
5074	Dip	-154						
			5083	**Bump**	**285**	**5083**	**Bump**	**206**
5979	Bump	165						
5981	Bump	173						
			6469	Dip	-155			
			6669	Bump	168			
10637	**Bump**	**177**	**10637**	**Bump**	**180**	**10637**	**Bump**	**179**

[2] Shaded cells indicate no defects found for the given profile. Entries in bold indicate defects common to average profile and either or both LWP/RWP profiles.

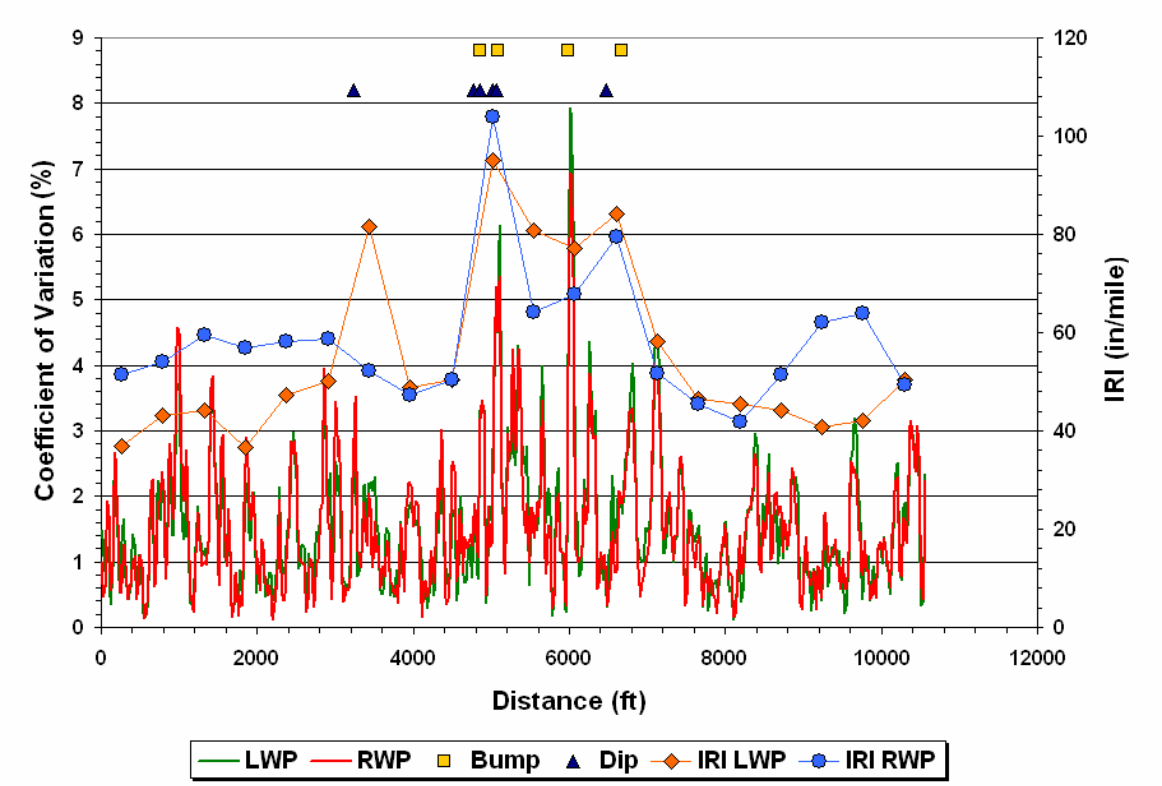

Figure 4.19. Coefficients of Variation of Dynamic Tire Loads for Steering Axle Plotted with IRIs and Defects Computed from K1 Lane Profiles Taken along FM1994 Project.

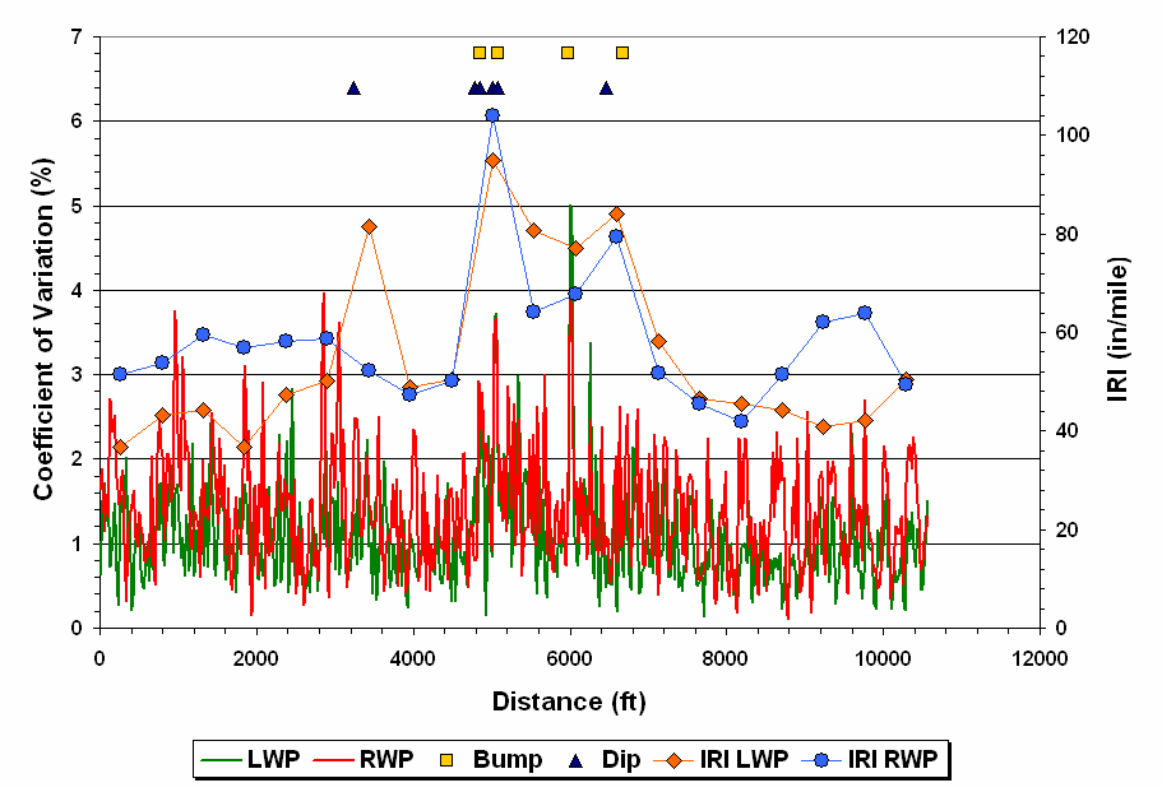

Figure 4.20. Coefficients of Variation of Dynamic Tire Loads for Drive Axle #1 Plotted with IRIs and Defects Computed from K1 Lane Profiles Taken along FM1994 Project.

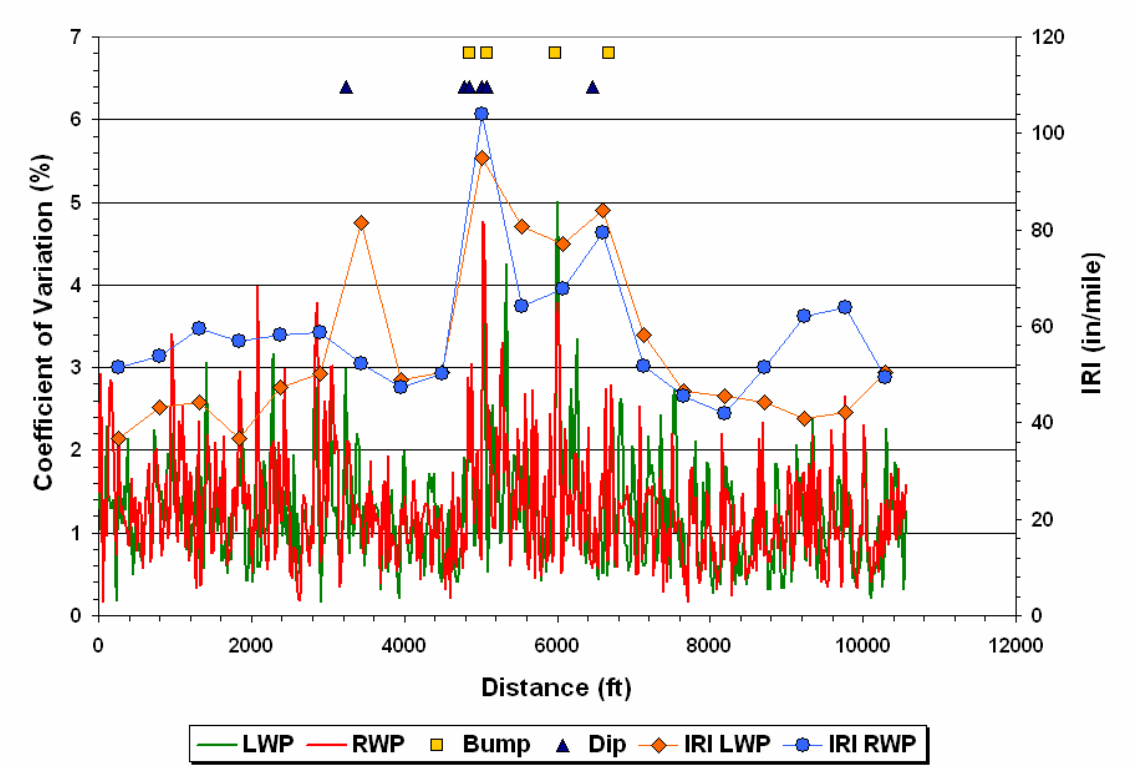

Figure 4.21. Coefficients of Variation of Dynamic Tire Loads for Drive Axle #2 Plotted with IRIs and Defects Computed from K1 Lane Profiles Taken along FM1994 Project.

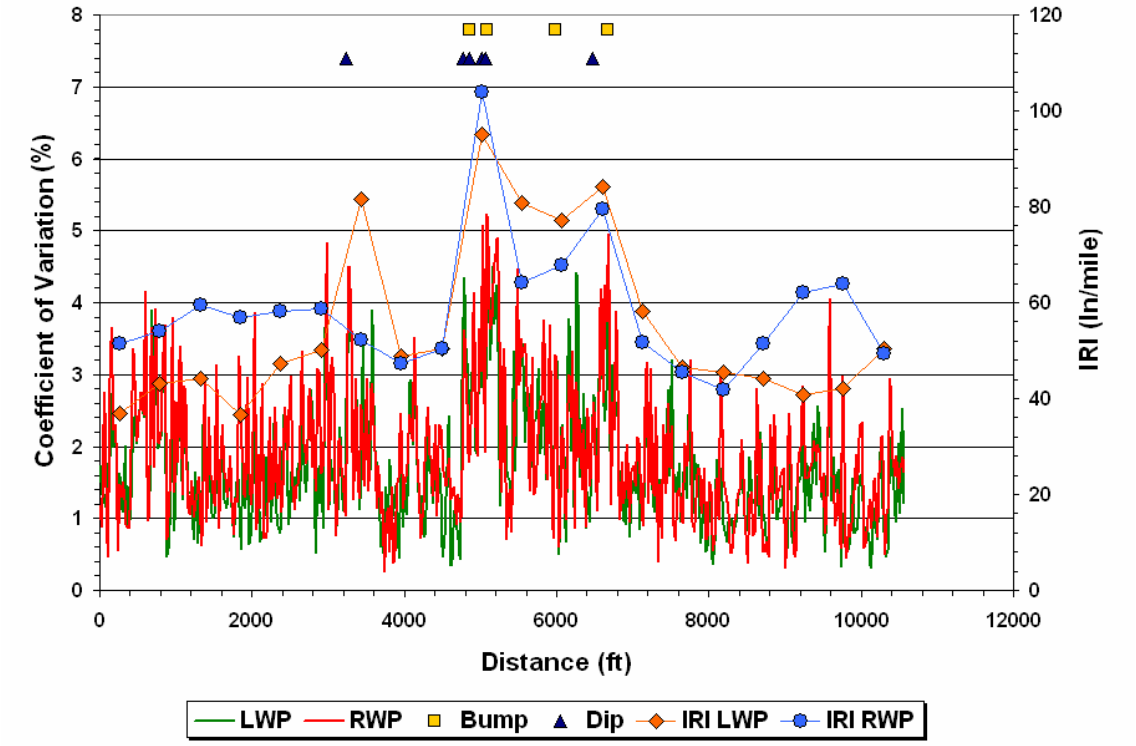

Figure 4.22. Coefficients of Variation of Dynamic Tire Loads for Trailer Axle #1 Plotted with IRIs and Defects Computed from K1 Lane Profiles Taken along FM1994 Project.

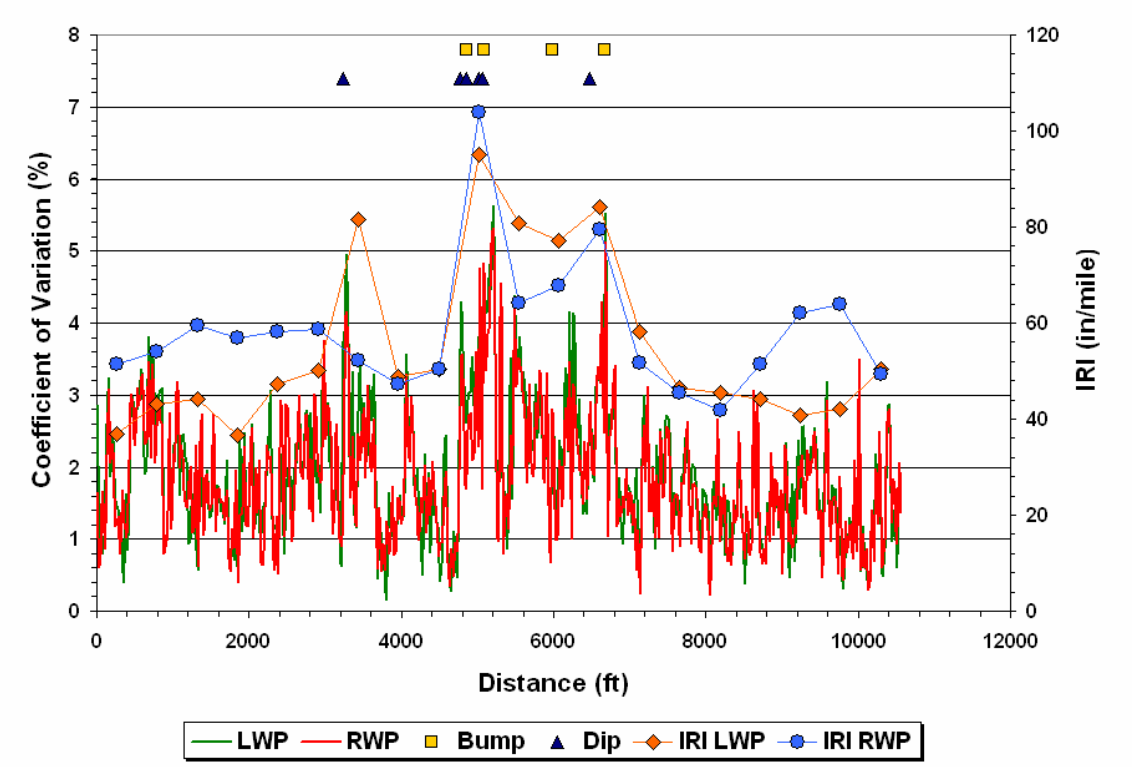

Figure 4.23. Coefficients of Variation of Dynamic Tire Loads for Trailer Axle #2 Plotted with IRIs and Defects Computed from K1 Lane Profiles Taken along FM1994 Project.

path of the 13th 0.1-mile section that show where corrections might be made to reduce the roughness on this section as well as the variability of the measured dynamic tire loads, specifically for the trailer axles, where peaks are observed in the computed CVs within this section as shown in Figures 4.22 and 4.23. Finally, researchers note the defect found along the left wheel path within the seventh 0.1-mile section that is associated with the higher left wheel path IRI computed on this section as well as the peaks in the computed CVs for the trailer axles at the vicinity of the defect.

SH21 Project in Lee County

The SH21 project in Lee County is relatively rougher than the FM1462 and FM1994 projects presented previously. This observation may be inferred from Table 4.31 by comparing the summary indicators of pavement ride quality on these three projects. Figure 4.24 shows the coefficients of variation determined from the dynamic tire loads measured on the steering axle from tests done on the K6 lane of the SH21 project. Also plotted in the figure are IRIs computed from the surface profiles measured along the test lane

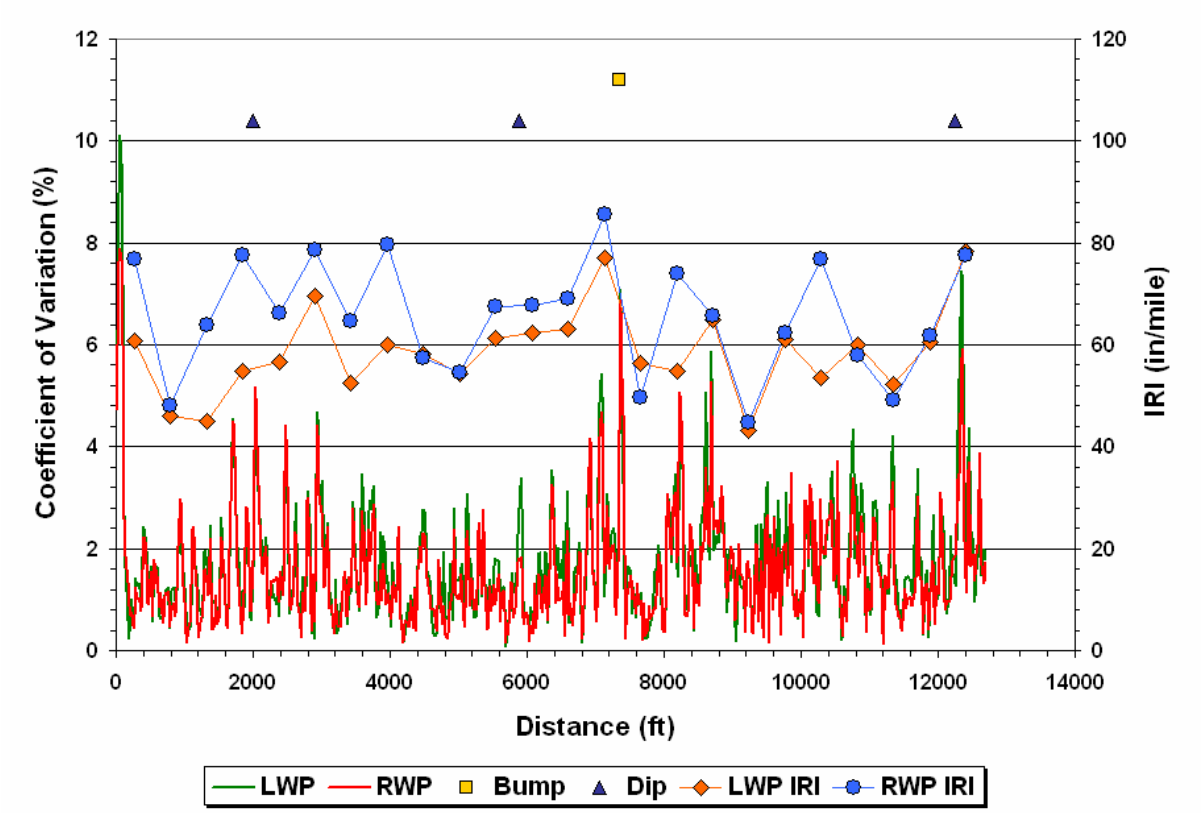

Figure 4.24. Coefficients of Variation of Dynamic Tire Loads for Steering Axle Plotted with IRIs and Defects Determined from TxDOT's Ride Quality Program from Tests on K6 Lane of SH21 Project in Lee County.

and the defects determined from these profiles using the current method implemented by TxDOT.

From examination of the output from TxDOT's Ride Quality program, no deficient sections are reported that require corrective work from the contractor. However, there are six sections where the average IRIs fall within the penalty range of TxDOT's Item 585 specification, specifically, the first, fourth, sixth, eighth, 14th, and 24th tenth of a mile sections. These sections can be located in Figure 4.24 by counting sequentially from left to right the pairs of IRI symbols denoting the left and right wheel path IRIs of the 0.1-mile sections within the lane tested. On all of these sections but the last, Figure 4.24 shows that the right wheel path IRIs are higher than the corresponding left wheel path IRIs, with differences ranging from about 7 in/mile to about 22 in/mile.

Figure 4.24 shows several peaks in the computed CVs that are above 4 percent, with dominant peaks found close to the beginning and end of the K6 lane, and one close to 7400 ft from the start of the lane. Looking at the correspondence between these peaks and the ride

quality indicators used in Item 585 and plotted in Figure 4.24, the following observations are noted:

- The dynamic load variability observed on the steering axle at the beginning of the test lane does not correspond to any of the defects detected using TxDOT's current bump template. While the average IRI of 69 in/mile for the first 0.1-mile section fall within the penalty range of schedule 1 of the Item 585 ride specification, the observation that the steering tire loads exhibit the most variability at the beginning of the run suggests that this behavior is due to roughness on the wheel paths that are found before the start of the run. Researchers note that prior to the start of the test lane, there are rough areas associated with expansive soils that affected the truck dynamics as the truck crossed the beginning of the lane.
- The variability in the steering tire loads at about 7400 ft corresponds to a bump detected close to that location. There are also a couple of areas preceding this location where the coefficients of variation of the steering tire loads are above 4 percent. These peaks in the CVs determined from the tire load measurements fall within the 14th tenth of a mile section, which is the roughest section along the lane tested.
- The dynamic load variability observed close to the end of the run corresponds to a dip in the average profile found at that location using TxDOT's Ride Quality program.

To check for the presence of defects in each wheel path, researchers ran TxDOT's Ride Quality program on each wheel path profile. Table 4.34 shows the results from this analysis. Once more, researchers found additional defects on each wheel path tested. Figures 4.25 to 4.29 plot the defects identified in Table 4.34 with the CVs and IRIs determined from test data collected along the K6 lane of the SH21 project in Lee County. The following observations are noted from these figures:

- Running the bump template on each wheel path profile identified a bump on the right wheel path of the first 0.1-mile section that was not detected using the current procedure based on the average profile. This finding is particularly useful for the engineer and the contractor as it identifies a specific location where grinding can be done to improve the smoothness on the right wheel path, where the IRI is about 77 in/mile.

Table 4.34. Defects Located from Profiles Taken along K6 Lane of SH21 Project in Lee County[2].

LWP Profile			RWP Profile			Average Profile		
Location (feet)	Type	Magnitude (mils)	Location (feet)	Type	Magnitude (mils)	Location (feet)	Type	Magnitude (mils)
			270	Bump	154			
			1656	Dip	-179			
			2008	**Dip**	**-294**	**2008**	**Dip**	**-151**
2770	Bump	184						
5877	**Dip**	**-245**				**5877**	**Dip**	**-162**
			6834	Bump	162			
			7004	Bump	163			
			7321	Bump	152			
			7322	Bump	167			
			7334	Dip	-237			
7349	**Bump**	**167**	**7349**	**Bump**	**174**	**7349**	**Bump**	**167**
			8224	Dip	-168			
			8226	Dip	-154			
			10173	Bump	174			
			10250	Bump	163			
12259	**Dip**	**-193**	**12259**	**Dip**	**-183**	**12259**	**Dip**	**-187**
12261	Dip	-152						

[2] Shaded cells indicate no defects found for the given profile. Entries in bold indicate defects common to average profile and either or both LWP/RWP profiles.

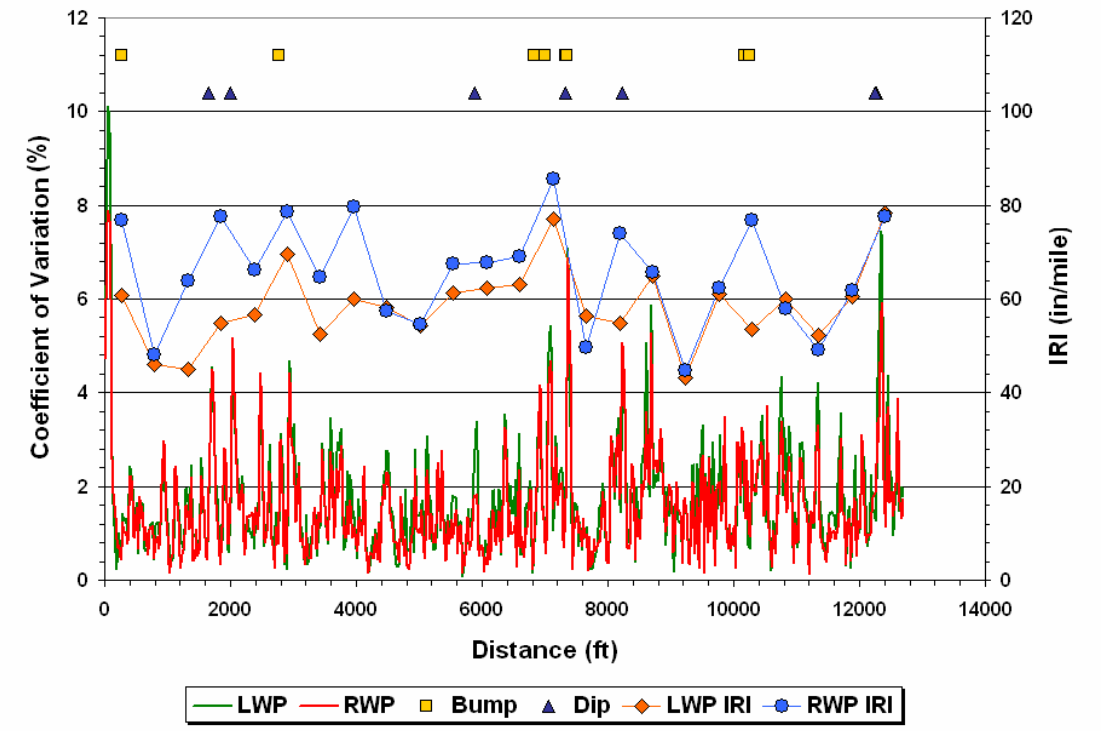

Figure 4.25. Coefficients of Variation of Dynamic Tire Loads for Steering Axle Plotted with IRIs and Defects Computed from K6 Lane Profiles Taken along SH21 Project.

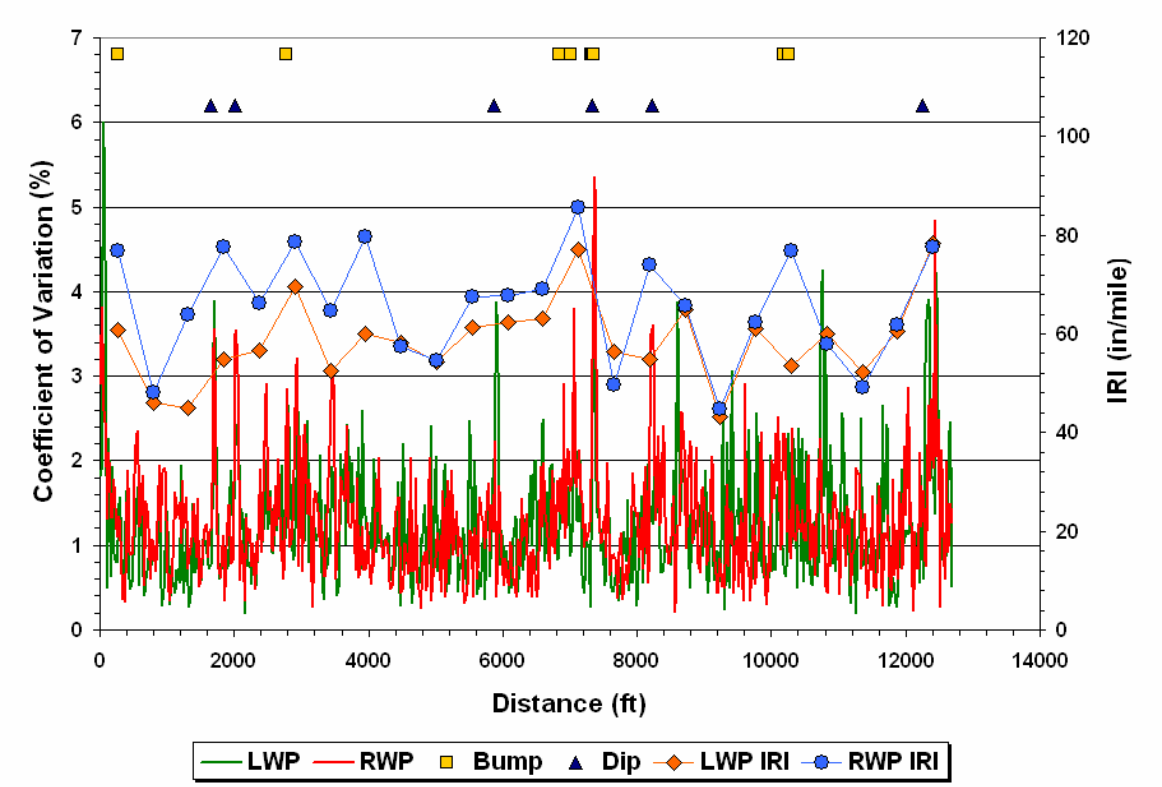

Figure 4.26. Coefficients of Variation of Dynamic Tire Loads for Drive Axle #1 Plotted with IRIs and Defects Computed from K6 Lane Profiles Taken along SH21 Project.

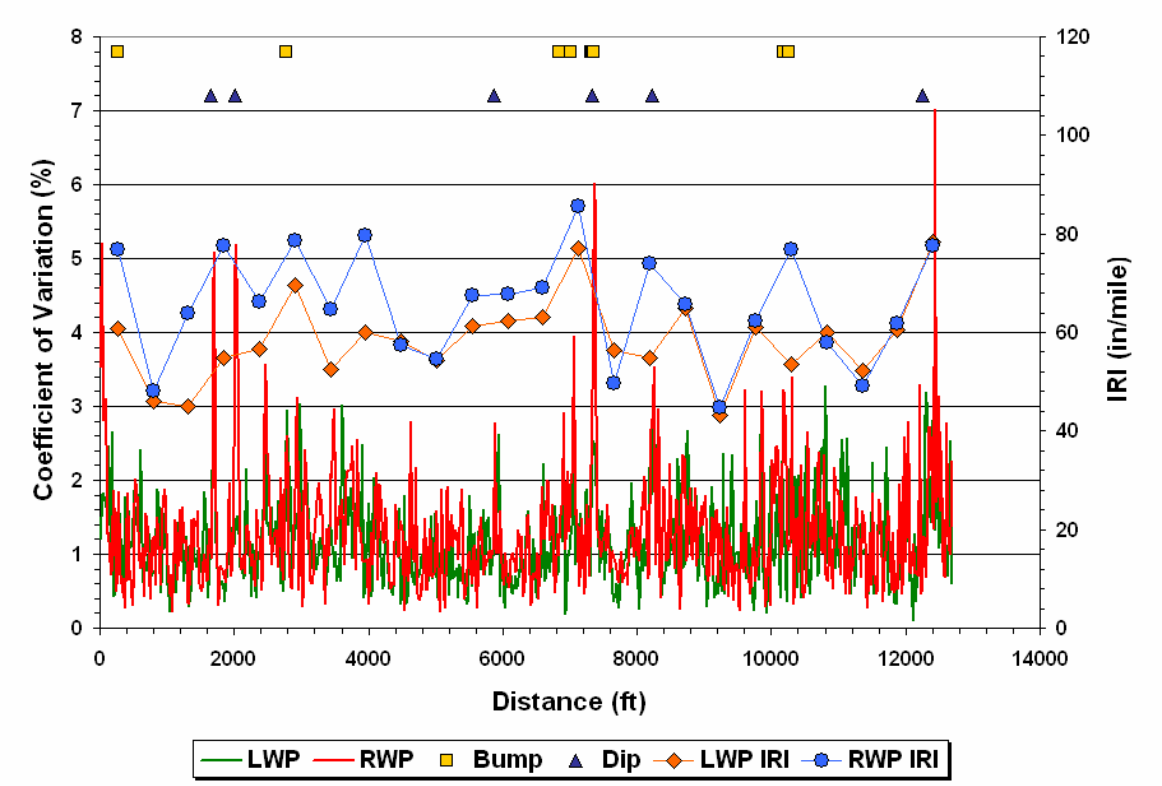

Figure 4.27. Coefficients of Variation of Dynamic Tire Loads for Drive Axle #2 Plotted with IRIs and Defects Computed from K6 Lane Profiles Taken along SH21 Project.

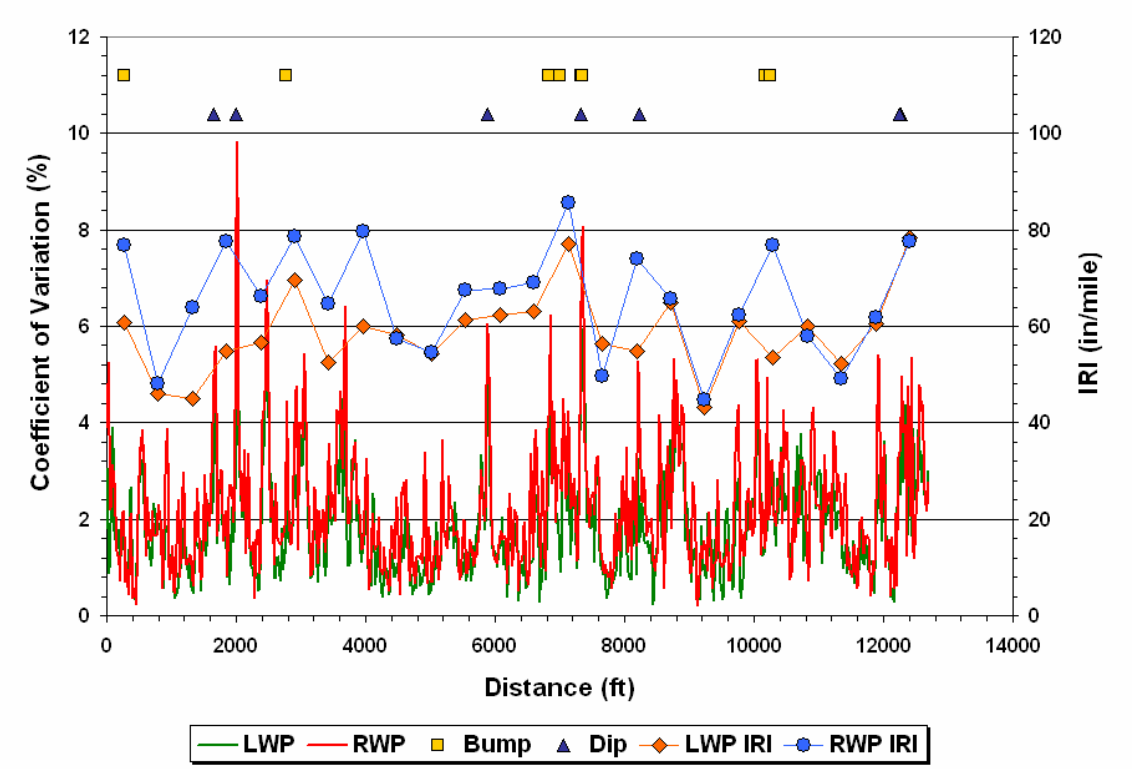

Figure 4.28. Coefficients of Variation of Dynamic Tire Loads for Trailer Axle #1 Plotted with IRIs and Defects Computed from K6 Lane Profiles Taken along SH21 Project.

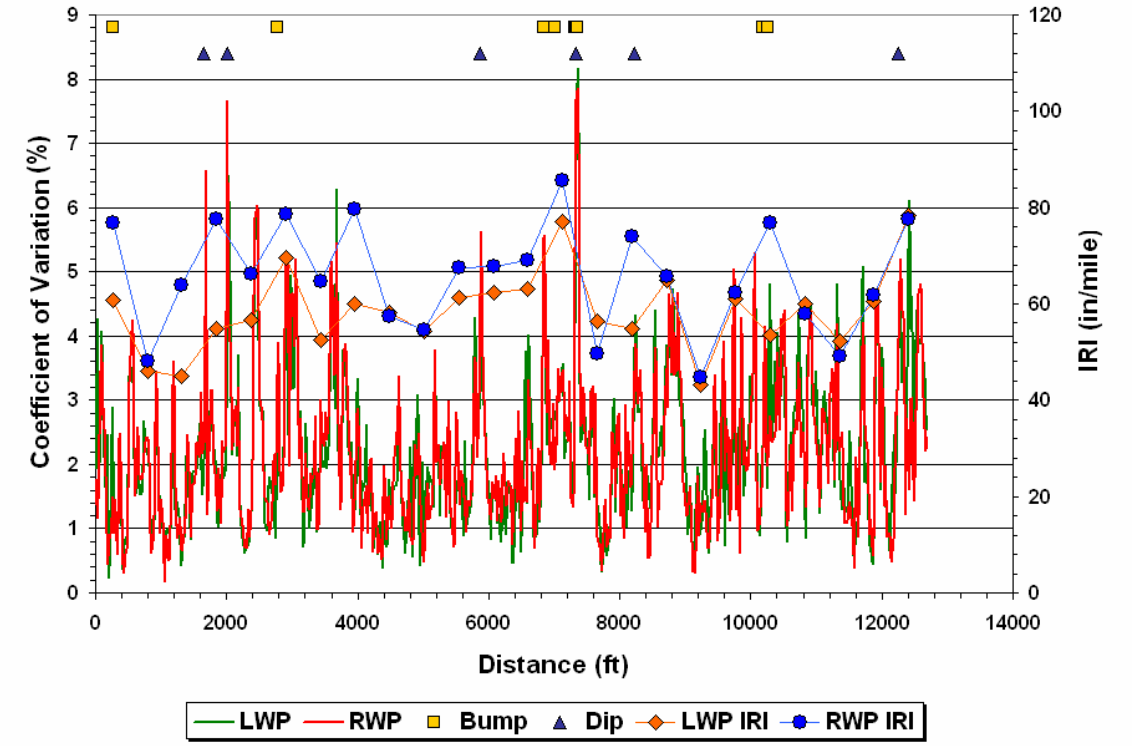

Figure 4.29. Coefficients of Variation of Dynamic Tire Loads for Trailer Axle #2 Plotted with IRIs and Defects Computed from K6 Lane Profiles Taken along SH21 Project.

- There is an additional dip detected on the right wheel path of section 4 at a distance of 1656 ft from the start of the run. This dip and the one that follows it are associated with a couple of peaks in the computed CVs on the fourth 0.1-mile section (see Figures 4.25 to 4.29). The peaks appear on all five charts indicating that the two dips affected the dynamics of the entire vehicle combination. Researchers note that only one of the pair of dips was detected using the current bump template (see Figure 4.24) with the average profile. In the opinion of the authors, this finding demonstrates that a better assessment of corrective actions to improve the ride quality on section 4 can be achieved using the same template on the individual wheel path profiles.
- The analysis of defects on each wheel path identified a bump on the left wheel path of section 6 that was not detected using the average profile. This bump is located at a distance of 2770 ft from the start of the test lane. The engineer can consider having this bump removed to reduce the IRI on the left wheel path of section 6, where the IRI based on the measured profile is about 69 in/mile.
- While the current bump template identified only one bump within section 14 of the lane tested (see Figure 4.24), the analysis of individual wheel paths identified additional defects that explain the peaks in the CVs of the measured tire loads noted previously on this section. Once more, the template analysis of individual wheel paths provided a better assessment of the defects that detract from the ride quality of the given section and produce more severe dynamic load variability.
- The template analysis of individual wheel paths identified other defects not detected using the current method. These additional defects include the dip on the right wheel path of section 16, about 8200 ft from the start of the test lane, and two bumps on the right wheel path of section 20, at distances of 10,173 and 10,250 ft from the start of the lane. Researchers note that on both sections, the right wheel path IRIs are significantly higher than the left wheel path IRIs. The presence of defects along the right wheel path of these sections is consistent with this difference.

SH121 Project

The SH121 project in Denton County is the roughest among the routes that researchers tested in this project. This characteristic is readily inferred from the summary of ride quality indicators shown in Table 4.31 that shows the project as having a lot of defects

and deficient sections that will require corrections from the contractor under the current ride specification. Figure 4.30 illustrates the dynamic load variability associated with the poor ride quality on this project. The data shown are based on the measured tire loads on the steering axle from tests conducted along the R1 lane of the SH121 project (Group A). Note the multiple peaks in the computed CVs, which are higher than those determined on the three projects presented previously. The tire loads exhibit the most variability toward the latter stage of the run, beginning at approximately 8700 ft. Researchers note that the ride inside the instrumented truck was particularly harsh toward the end of the run.

Figure 4.30 also shows the IRIs determined at 0.1-mile intervals as well as the defects detected based on the average profile. There are multiple defects on the test lane that correspond to the peaks observed in the computed CVs of the dynamic tire loads. The defects are particularly dense toward the end of the run that span the last four 0.1-mile sections. These sections have the highest IRIs along the lane tested and exhibit the most variability in the measured dynamic tire loads.

Researchers also ran the existing bump template on each wheel path and identified the defects found from this analysis in Table 4.35. Figures 4.31 to 4.35 plot the defects found with the CVs and IRIs determined from test data collected along the R1 lane of the SH121 project. The results suggest that extensive grinding needs to be carried out on this lane to improve the ride quality and reduce the dynamic load variability.

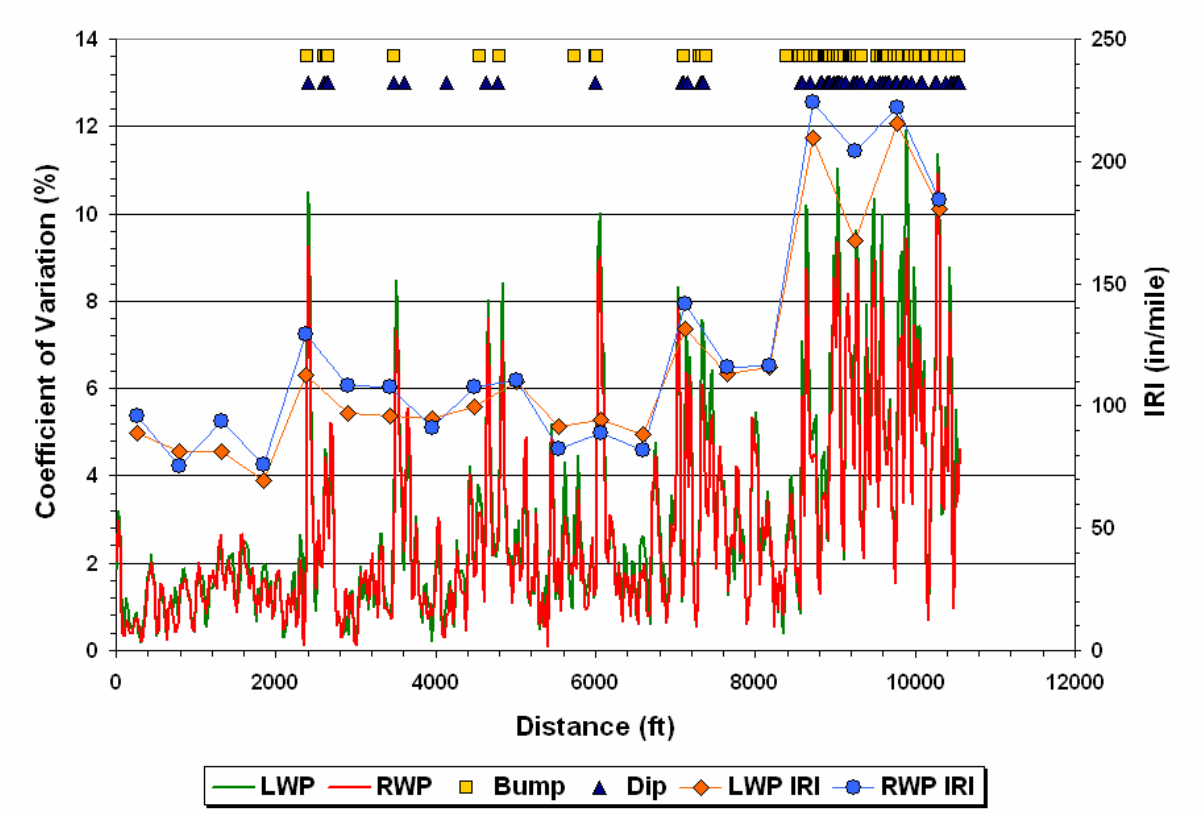

Figure 4.30. Coefficients of Variation of Dynamic Tire Loads for Steering Axle Plotted with IRIs and Defects Determined from TxDOT's Ride Quality Program from Tests on R1 Lane of SH121 (Group A) Project in Denton County.

Table 4.35. Defects Located from Profiles Taken along R1 Lane of SH121 Project in Denton County (Group A)[2].

LWP Profile			RWP Profile			Average Profile		
Location	Type	Magnitude (mils)	Location	Type	Magnitude (mils)	Location	Type	Magnitude (mils)
			2377	Bump	156			
			2378	Bump	164			
2384	**Bump**	**288**	**2384**	**Bump**	**240**	**2384**	**Bump**	**254**
			2391	Bump	214			
			2399	Dip	-164			
2404	**Dip**	**-164**	**2404**	**Dip**	**-254**	**2404**	**Dip**	**-208**
2413	Bump	157						
2414	**Dip**	**-630**	**2414**	**Dip**	**-717**	**2414**	**Dip**	**-656**
2598	**Bump**	**175**	**2598**	**Bump**	**153**	**2598**	**Bump**	**170**
2599	**Bump**	**304**	**2599**	**Bump**	**350**	**2599**	**Bump**	**301**
2606	**Dip**	**-200**	**2606**	**Dip**	**-219**	**2606**	**Dip**	**-208**
2608	**Dip**	**-196**				**2608**	**Dip**	**-176**
2610	**Dip**	**-183**				**2610**	**Dip**	**-161**
2638	**Dip**	**-770**	**2638**	**Dip**	**-742**	**2638**	**Dip**	**-756**
2639	**Bump**	**211**				**2639**	**Bump**	**160**
2640	Bump	154						
			2641	Dip	-154			
2652	**Dip**	**-233**				**2652**	**Dip**	**-174**
2659	**Bump**	**315**	**2659**	**Bump**	**272**	**2659**	**Bump**	**293**
			2669	Dip	-153			
			2670	Dip	-162			
			2671	Dip	-184			
3473	**Bump**	**233**	**3473**	**Bump**	**268**	**3473**	**Bump**	**236**
3481	**Dip**	**-231**	**3481**	**Dip**	**-284**	**3481**	**Dip**	**-256**
			3553	Bump	151			
3616	**Dip**	**-193**	**3616**	**Dip**	**-169**	**3616**	**Dip**	**-175**
			3618	Dip	-158			
4133	**Dip**	**-196**				**4133**	**Dip**	**-157**
4193	Dip	-154						
			4254	Bump	153			
			4543	Dip	-176			
4550	**Bump**	**271**	**4550**	**Bump**	**279**	**4550**	**Bump**	**268**
						4554	Bump	159
			4564	Dip	-169			
4639	**Dip**	**-249**	**4639**	**Dip**	**-198**	**4639**	**Dip**	**-222**
4781	**Dip**	**-176**	**4781**	**Dip**	**-161**	**4781**	**Dip**	**-161**
4783	**Dip**	**-154**				**4783**	**Dip**	**-155**
4799	**Bump**	**204**	**4799**	**Bump**	**209**	**4799**	**Bump**	**206**
5233	Dip	-154						
5666	Dip	-219						

[2] Shaded cells indicate no defects found for the given profile. Entries in bold indicate defects common to average profile and either or both LWP/RWP profiles.

Table 4.35. Defects Located from Profiles Taken along R1 Lane of SH121 Project in Denton County (Group A) (continued).

LWP Profile			RWP Profile			Average Profile		
Location	Type	Magnitude (mils)	Location	Type	Magnitude (mils)	Location	Type	Magnitude (mils)
5741	Bump	161						
5743	Bump	152						
5744	Bump	151	5744	Bump	155			
5745	**Bump**	**151**	**5745**	**Bump**	**154**	**5745**	**Bump**	**153**
5757	Dip	-186						
5999	**Dip**	**-166**	**5999**	**Dip**	**-170**	**5999**	**Dip**	**-153**
6006	**Bump**	**177**	**6006**	**Bump**	**260**	**6006**	**Bump**	**214**
6009	**Bump**	**228**				**6009**	**Bump**	**242**
			6032	Dip	-152			
6639	Bump	167						
6640	Bump	151						
6641	Bump	184						
6642	Bump	194						
6643	Bump	159						
6654	Dip	-178						
			6972	Dip	-157			
			6973	Dip	-165			
			6980	Bump	173			
			6982	Bump	159			
7008	Dip	-151						
7009	Dip	-166						
7088	**Dip**	**-369**	**7088**	**Dip**	**-152**	**7088**	**Dip**	**-255**
7099	**Bump**	**309**	**7099**	**Bump**	**346**	**7099**	**Bump**	**315**
			7106	Bump	214			
7108	**Dip**	**-336**	**7108**	**Dip**	**-364**	**7108**	**Dip**	**-348**
7110	**Dip**	**-370**	**7110**	**Dip**	**-179**	**7110**	**Dip**	**-346**
			7113	Dip	-389			
7154	**Dip**	**-198**	**7154**	**Dip**	**-180**	**7154**	**Dip**	**-182**
7189	Bump	169						
			7310	**Bump**	**188**	**7310**	**Bump**	**157**
7315	**Dip**	**-208**	**7315**	**Dip**	**-214**	**7315**	**Dip**	**-205**
7321	**Dip**	**-360**	**7321**	**Dip**	**-252**	**7321**	**Dip**	**-306**
7341	**Bump**	**289**	**7341**	**Bump**	**162**	**7341**	**Bump**	**214**
7357	**Dip**	**-169**				**7357**	**Dip**	**-152**
			7380	Dip	-153			
7390	**Bump**	**175**	**7390**	**Bump**	**163**	**7390**	**Bump**	**162**
7414	Bump	185						
			7506	Dip	-161			
7568	Bump	179						
8052	Dip	-170						
8054	Dip	-154						

Table 4.35. Defects Located from Profiles Taken along R1 Lane of SH121 Project in Denton County (Group A) (continued).

LWP Profile			RWP Profile			Average Profile		
Location	Type	Magnitude (mils)	Location	Type	Magnitude (mils)	Location	Type	Magnitude (mils)
8102	Dip	-161						
8103	Dip	-167						
			8222	Bump	155			
8342	Bump	158						
			8394	**Bump**	**154**	**8394**	**Bump**	**191**
8593	Bump	183	8393	Bump	202			
8547	**Bump**	**151**	**8547**	**Bump**	**184**	**8547**	**Bump**	**163**
8550	**Bump**	**197**				**8550**	**Bump**	**180**
8565	Dip	-216	8565	Bump	192			
8566	**Dip**	**-154**	**8566**	**Dip**	**-193**	**8566**	**Dip**	**-204**
8584	**Dip**	**-656**	**8584**	**Dip**	**-756**	**8584**	**Dip**	**-566**
8603	**Bump**	**376**	**8603**	**Bump**	**349**	**8603**	**Bump**	**346**
8612	Bump	250						
8636	Bump	159						
8637	Bump	170						
			8640	Bump	203			
8644	Bump	192						
			8659	Bump	203			
			8669	Dip	-156			
			8670	Dip	-169			
			8672	Dip	-154			
			8676	Bump	182			
8685	**Dip**	**-398**	**8685**	**Dip**	**-562**	**8685**	**Dip**	**-350**
8689	**Bump**	**202**	**8689**	**Bump**	**210**	**8689**	**Bump**	**199**
8716	Dip	-157						
8755	**Bump**	**158**	**8755**	**Bump**	**166**	**8755**	**Bump**	**154**
			8760	Dip	-158			
8790	**Bump**	**169**	**8790**	**Bump**	**159**	**8790**	**Bump**	**163**
8792	**Bump**	**158**	**8792**	**Bump**	**157**	**8792**	**Bump**	**152**
8823	**Dip**	**-188**	**8823**	**Dip**	**-167**	**8823**	**Dip**	**-159**
8827	**Dip**	**-161**				**8827**	**Dip**	**-151**
			8855	Dip	-179			
8867	**Bump**	**160**	**8867**	**Bump**	**182**	**8867**	**Bump**	**171**
8889	**Bump**	**235**	**8890**	**Bump**	**259**	**8889**	**Bump**	**246**
8898	**Bump**	**196**				**8898**	**Bump**	**162**
8909	**Dip**	**-244**				**8909**	**Dip**	**-175**
			8913	Bump	226			
8915	**Dip**	**-180**	**8915**	**Dip**	**-520**	**8915**	**Dip**	**-322**
8919	**Dip**	**-195**	**8919**	**Dip**	**-271**	**8919**	**Dip**	**-233**

Table 4.35. Defects Located from Profiles Taken along R1 Lane of SH121 Project in Denton County (Group A) (continued).

LWP Profile			RWP Profile			Average Profile		
Location	Type	Magnitude (mils)	Location	Type	Magnitude (mils)	Location	Type	Magnitude (mils)
8922	**Bump**	**195**	**8922**	**Bump**	**153**	**8922**	**Bump**	**168**
8929	**Dip**	**-160**	**8928**	**Dip**	**-242**	**8929**	**Dip**	**-188**
8932	**Dip**	**-369**	**8932**	**Dip**	**-316**	**8932**	**Dip**	**-333**
8940	**Bump**	**267**	**8940**	**Bump**	**301**	**8940**	**Bump**	**269**
8948	Bump	189						
			8956	Dip	-156			
			8976	**Dip**	**-239**	**8976**	**Dip**	**-157**
8986	**Bump**	**165**	**8986**	**Bump**	**236**	**8986**	**Bump**	**196**
8988	Bump	177						
8990	**Bump**	**182**	**8990**	**Bump**	**226**	**8990**	**Bump**	**202**
8992	Bump	184						
9012	**Dip**	**-207**	**9012**	**Dip**	**-258**	**9012**	**Dip**	**-232**
9024	Dip	-188						
9027	**Dip**	**-151**	**9027**	**Dip**	**-323**	**9027**	**Dip**	**-192**
9030	Bump	203						
			9033	**Bump**	**195**	**9033**	**Bump**	**168**
			9036	**Bump**	**249**	**9036**	**Bump**	**170**
9047	**Dip**	**-223**	**9047**	**Dip**	**-226**	**9047**	**Dip**	**-211**
			9058	**Bump**	**247**	**9058**	**Bump**	**187**
			9077	Dip	-158			
			9079	**Dip**	**-199**	**9079**	**Dip**	**-162**
9110	**Bump**	**163**	**9110**	**Bump**	**157**	**9110**	**Bump**	**153**
9125	**Dip**	**-163**	**9125**	**Dip**	**-197**	**9125**	**Dip**	**-179**
9127	Dip	-163						
			9148	Bump	160			
9169	Dip	-159						
			9189	**Bump**	**187**	**9189**	**Bump**	**154**
9191	**Bump**	**169**	**9191**	**Bump**	**156**	**9191**	**Bump**	**158**
						9192	Bump	151
			9212	Dip	-163			
9216	**Bump**	**244**	**9216**	**Bump**	**296**	**9216**	**Bump**	**266**
						9224	Bump	151
9234	**Dip**	**-162**				**9234**	**Dip**	**-156**
9235	**Dip**	**-252**	9235	Dip	-161	**9235**	**Dip**	**-282**
			9236	Dip	-312			
			9253	**Bump**	**231**	**9254**	**Bump**	**181**
9263	**Dip**	**-197**	**9263**	**Dip**	**-238**	**9263**	**Dip**	**-213**
9275	**Bump**	**152**	**9275**	**Bump**	**210**	**9275**	**Bump**	**180**
9286	**Dip**	**-151**	**9286**	**Dip**	**-172**	**9286**	**Dip**	**-161**

Table 4.35. Defects Located from Profiles Taken along R1 Lane of SH121 Project in Denton County (Group A) (continued).

LWP Profile			RWP Profile			Average Profile		
Location	Type	Magnitude (mils)	Location	Type	Magnitude (mils)	Location	Type	Magnitude (mils)
9325	**Dip**	**-251**	**9325**	**Dip**	**-301**	**9325**	**Dip**	**-269**
			9327	**Bump**	**269**	**9327**	**Bump**	**170**
						9328	Bump	197
9332	Bump	160						
9335	Bump	165						
			9356	Dip	-158			
			9384	Bump	157			
9453	**Dip**	**-160**				**9453**	**Dip**	**-152**
9454	**Dip**	**-203**				**9454**	**Dip**	**-154**
			9455	**Dip**	**-159**	**9455**	**Dip**	**-165**
9531	**Bump**	**165**	**9531**	**Bump**	**217**	**9531**	**Bump**	**152**
9532	**Bump**	**216**				**9532**	**Bump**	**215**
						9534	Bump	160
			9554	Dip	-153			
9555	**Dip**	**-176**	**9555**	**Dip**	**-187**	**9555**	**Dip**	**-179**
9560	Dip	-166						
9581	Bump	155						
			9583	**Bump**	**182**	**9583**	**Bump**	**164**
9594	**Dip**	**-165**	**9594**	**Dip**	**-186**	**9594**	**Dip**	**-171**
9608	**Bump**	**228**				**9608**	**Bump**	**156**
9624	**Bump**	**185**	**9624**	**Bump**	**162**	**9624**	**Bump**	**167**
			9625	Bump	151			
9634	**Dip**	**-475**	**9634**	**Dip**	**-481**	**9634**	**Dip**	**-477**
9641	**Bump**	**360**	**9641**	**Bump**	**286**	**9641**	**Bump**	**310**
9652	**Dip**	**-420**	**9652**	**Dip**	**-429**	**9652**	**Dip**	**-424**
9664	**Bump**	**215**	**9664**	**Bump**	**297**	**9664**	**Bump**	**251**
			9678	**Dip**	**-211**	**9678**	**Dip**	**-170**
			9687	Bump	169			
			9689	Bump	160			
			9691	Bump	205			
			9696	Dip	-163			
9738	**Bump**	**301**	**9738**	**Bump**	**268**	**9738**	**Bump**	**271**
9750	**Dip**	**-243**	**9750**	**Dip**	**-238**	**9750**	**Dip**	**-241**
9767	**Dip**	**-233**	**9767**	**Dip**	**-255**	**9767**	**Dip**	**-238**
9771	Dip	-154						
			9774	Dip	-176			
9788	**Bump**	**199**	**9788**	**Bump**	**169**	**9788**	**Bump**	**182**
9793	**Bump**	**214**	**9793**	**Bump**	**199**	**9793**	**Bump**	**202**
9838	Bump	151						
9843	**Bump**	**229**	**9843**	**Bump**	**270**	**9843**	**Bump**	**228**

Table 4.35. Defects Located from Profiles Taken along R1 Lane of SH121 Project in Denton County (Group A) (continued).

LWP Profile			RWP Profile			Average Profile		
Location	Type	Magnitude (mils)	Location	Type	Magnitude (mils)	Location	Type	Magnitude (mils)
9855	**Dip**	**-236**	**9855**	**Dip**	**-208**	**9855**	**Dip**	**-218**
			9860	Dip	-164			
9870	Dip	-179						
9872	**Dip**	**-162**	**9872**	**Dip**	**-151**	**9872**	**Dip**	**-154**
9884	**Dip**	**-169**	**9884**	**Dip**	**-161**	**9884**	**Dip**	**-161**
9898	Bump	158	9898	Bump	151			
9916	**Bump**	**183**				**9916**	**Bump**	**163**
9919	Bump	155						
9933	**Bump**	**281**	**9933**	**Bump**	**246**	**9933**	**Bump**	**263**
9948	Dip	-397						
			9950	**Dip**	**-335**	**9950**	**Dip**	**-366**
9953	**Dip**	**-222**	**9953**	**Dip**	**-223**	**9953**	**Dip**	**-219**
			9990	Dip	-165			
10008	**Bump**	**284**	**10008**	**Bump**	**288**	**10008**	**Bump**	**272**
10013	Bump	155						
10014	Bump	178						
			10051	**Bump**	**174**	**10051**	**Bump**	**162**
10052	**Bump**	**157**	**10052**	**Bump**	**169**	**10052**	**Bump**	**158**
10079	**Dip**	**-154**	**10079**	**Dip**	**-154**	**10079**	**Dip**	**-152**
10080	**Dip**	**-190**	**10080**	**Dip**	**-166**	**10080**	**Dip**	**-175**
			10136	Bump	153			
10138	**Bump**	**205**	**10138**	**Bump**	**221**	**10138**	**Bump**	**209**
			10146	Dip	-167			
			10156	**Bump**	**208**	**10156**	**Bump**	**171**
			10158	Bump	157			
			10160	Bump	177			
10180	Dip	-168						
			10247	Bump	151			
10251	**Bump**	**161**	**10251**	**Bump**	**214**	**10251**	**Bump**	**186**
10256	**Dip**	**-212**	**10256**	**Dip**	**-151**	**10256**	**Dip**	**-176**
			10257	Dip	-247			
						10260	Dip	-152
10263	**Dip**	**-255**	**10263**	**Dip**	**-520**	**10263**	**Dip**	**-387**
10264	**Bump**	**306**	**10264**	**Bump**	**162**	**10264**	**Bump**	**232**
			10265	Bump	172			
10273	Dip	-190						
10282	Dip	-200						
10287	Dip	-179						
10348	Bump	171						
10371	**Bump**	**303**	**10371**	**Bump**	**240**	**10371**	**Bump**	**266**

Table 4.35. Defects Located from Profiles Taken along R1 Lane of SH121 Project in Denton County (Group A) (continued).

LWP Profile			RWP Profile			Average Profile		
Location	Type	Magnitude (mils)	Location	Type	Magnitude (mils)	Location	Type	Magnitude (mils)
			10377	Bump	151			
10384	Dip	-153						
10386	**Dip**	**-189**	**10386**	**Dip**	**-184**	**10386**	**Dip**	**-186**
10458	**Dip**	**-188**	**10458**	**Dip**	**-281**	**10458**	**Dip**	**-233**
10466	**Bump**	**187**	**10466**	**Bump**	**267**	**10466**	**Bump**	**247**
10467	Bump	227						
10478	**Dip**	**-180**	**10478**	**Dip**	**-286**	**10478**	**Dip**	**-226**
			10513	Dip	-165			
			10519	**Dip**	**-184**	**10519**	**Dip**	**-159**
			10527	Bump	201			
10532	Bump	151						
			10541	**Dip**	**-839**	**10541**	**Dip**	**-479**
10543	**Dip**	**-748**				**10543**	**Dip**	**-365**
			10545	Bump	224			
10547	**Bump**	**267**				**10547**	**Bump**	**209**
10558	Dip	-161						

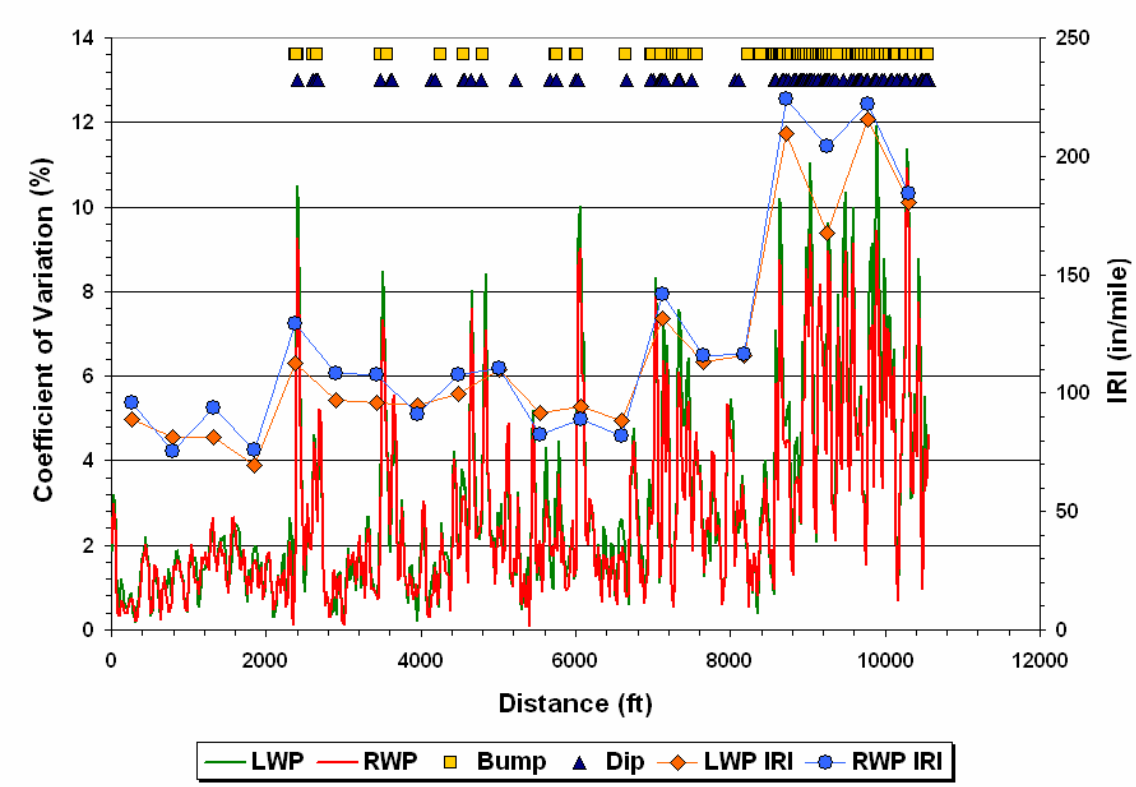

Figure 4.31. Coefficients of Variation of Dynamic Tire Loads for Steering Axle Plotted with IRIs and Defects Computed from R1 Lane Profiles Taken along SH121 Project.

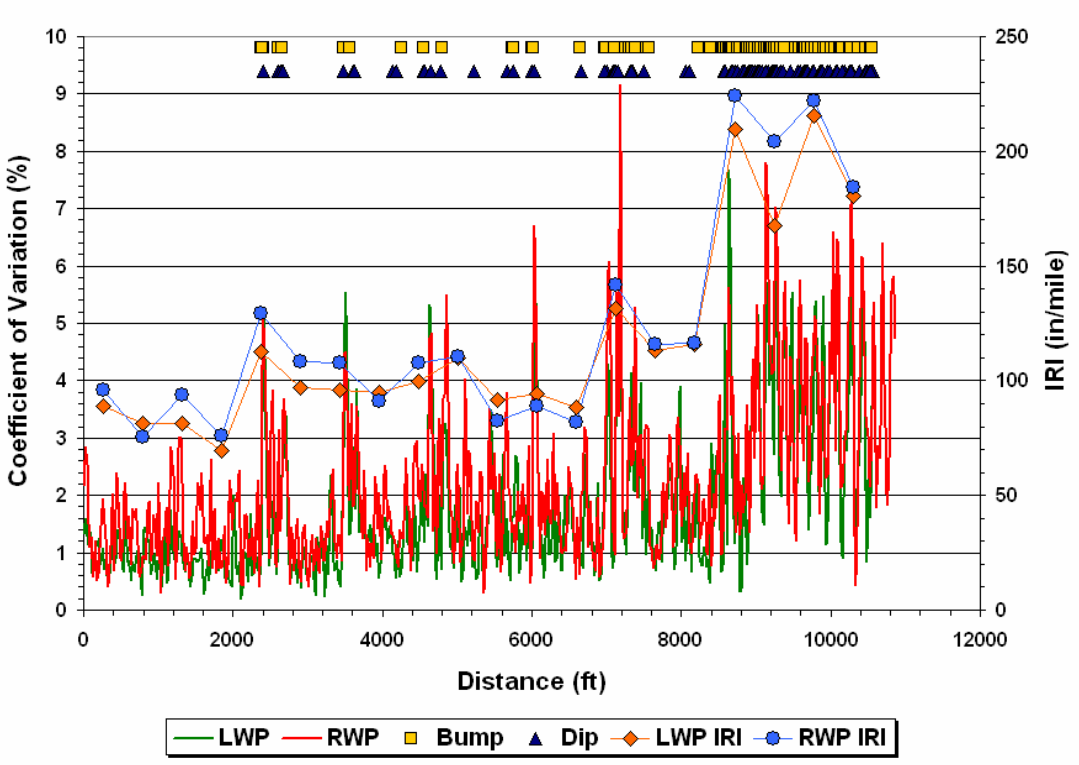

Figure 4.32. Coefficients of Variation of Dynamic Tire Loads for Drive Axle #1 Plotted with IRIs and Defects Computed from R1 Lane Profiles Taken along SH121 Project.

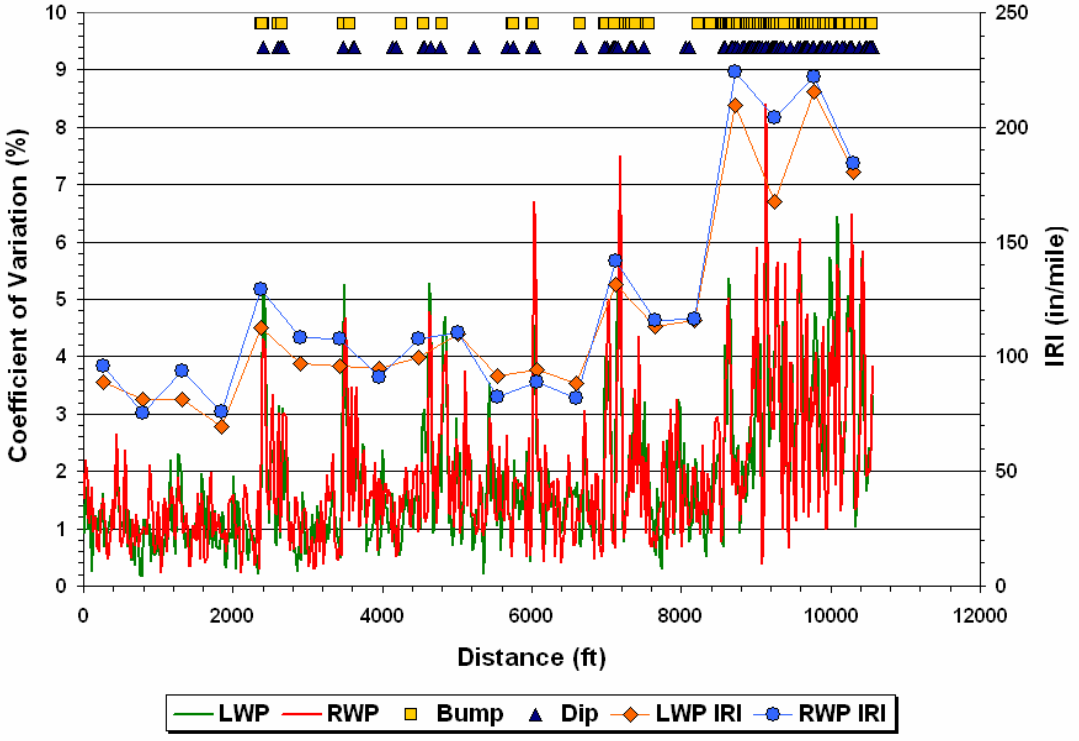

Figure 4.33. Coefficients of Variation of Dynamic Tire Loads for Drive Axle #2 Plotted with IRIs and Defects Computed from R1 Lane Profiles Taken along SH121 Project.

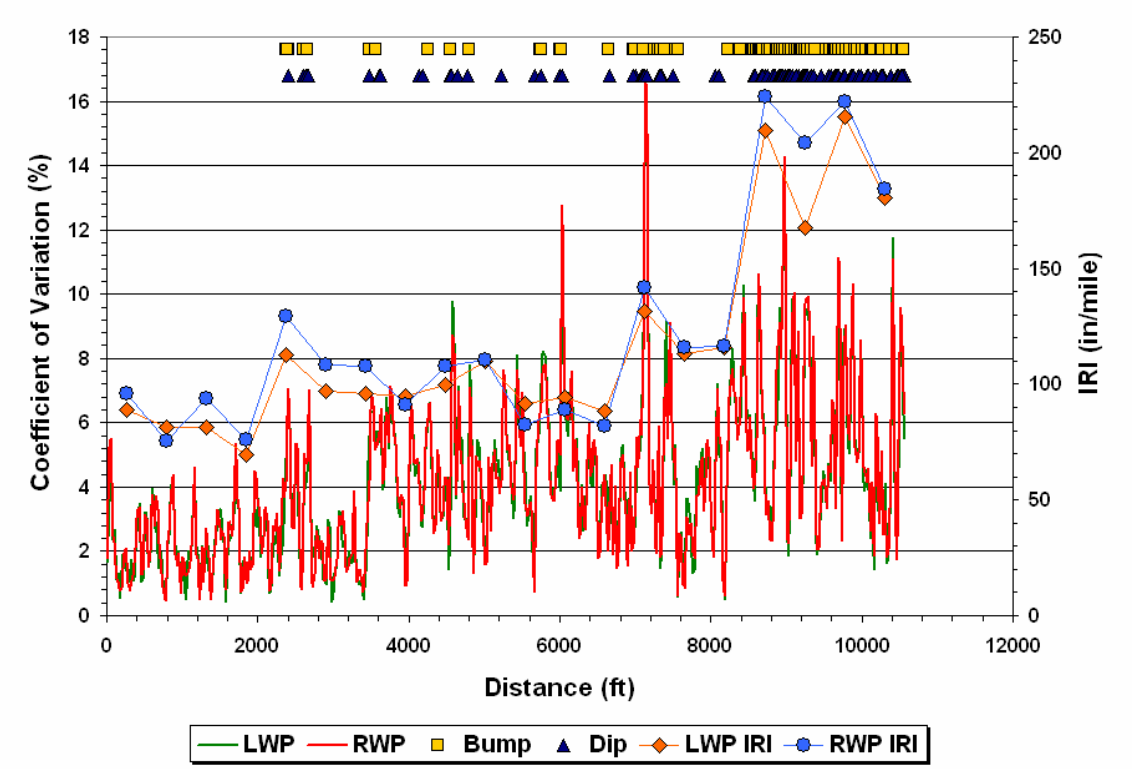

Figure 4.34. Coefficients of Variation of Dynamic Tire Loads for Trailer Axle #1 Plotted with IRIs and Defects Computed from R1 Lane Profiles Taken along SH121 Project.

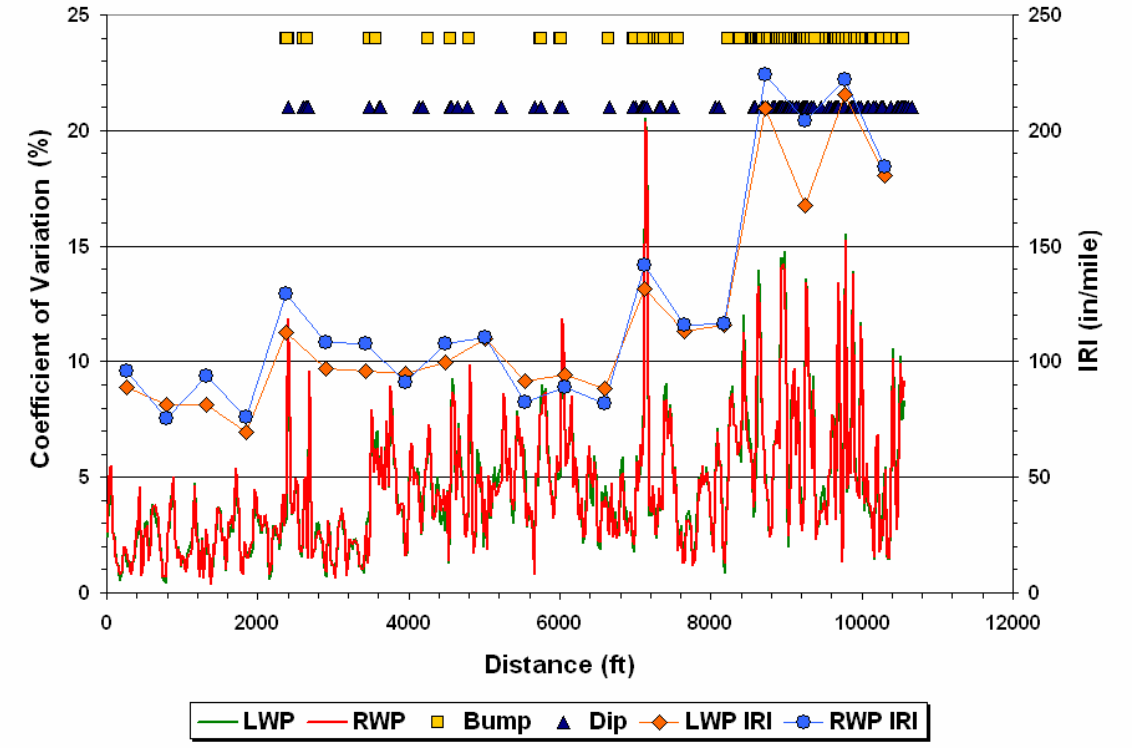

Figure 4.35. Coefficients of Variation of Dynamic Tire Loads for Trailer Axle #2 Plotted with IRIs and Defects Computed from R1 Lane Profiles Taken along SH121 Project.

CHAPTER V. SUMMARY OF FINDINGS AND RECOMMENDATIONS

This research report documented the efforts conducted in this project to provide an instrumented tractor-semitrailer combination for measurement of dynamic loads and a high-speed inertial profiler for measurement of surface profiles. Researchers conducted these tasks for the purpose of collecting data to verify TxDOT's current ride specification. Based on the experience with the instrumentation efforts and the analyses of test data collected during the project, the authors note the following findings:

- The application of strain gages for load measurement was successfully demonstrated in a laboratory setting with a shear beam load cell experiment wherein a steel bar, instrumented with shear strain gages in a full bridge configuration, was used to measure the total weight of a known set of circular disks. The shear beam load cell gave a measurement within 0.33 percent of the known total weight of the circular disks.
- Small-scale testing with an instrumented trailer verified the method for positioning, mounting, wiring, and calibrating the strain gages on the test vehicle. From the results of trailer calibration, researchers observed a strong linear relationship between tire load and strain over the range of loads at which the calibration was conducted. In addition, results of tests on a weigh-in-motion site showed that:
  - the dynamic tire loads determined from the strain gages vary closely about the measured static tire load of 700 lb on the trailer;
  - the dynamic tire loads determined around the vicinity of the WIM sensor are in reasonable agreement with the corresponding WIM measurement on each repeat run; and
  - the load measurements exhibit similar patterns between repeat runs.

  In view of the positive results, researchers proceeded with instrumenting and calibrating a tractor-semitrailer combination following the same approach used for the small-scale trailer tests.
- The calibration curves from full-scale laboratory tests of the instrumented tractor-semitrailer exhibit a strong linear relationship between tire load and shear strain. The shear strains measured between the left and right sides of a given axle also show a difference in signs as expected from theory.

- Researchers also verified the instrumented tractor-semitrailer combination by running the test vehicle on a weigh-in-motion site. Comparisons of the tire loads measured from the strain gages with the loads from the WIM sensors showed reasonable agreement between both sets of readings for each axle of the test vehicle and for the test speeds of 50 and 60 mph at which tests were conducted.
- Researchers also instrumented a test vehicle with an inertial profiling system and verified its performance based on TxDOT Test Method Tex-1001S. The results obtained show that the profiler meets the certification requirements specified in the test method.
- Test data collected on TxDOT paving projects with the instrumented vehicle showed that load variability, as measured with the coefficient of variation of the dynamic tire loads, goes up with increase in pavement roughness. In addition, examination of the patterns in the dynamic load variability revealed that the peaks in the computed CVs tend to recur at generally the same locations along the project for each axle of the test vehicle. This observation suggests that these locations will receive the most pounding from the trucks that use the road and will likely develop distress earlier than other similar locations where the dynamic load variability is less.
- Analyses of the measurements with the instrumented vehicle also showed that the occurrences of high dynamic load variability are associated with defects found on the pavement surface from the measured elevation profiles along the given project. This work showed that the current bump template based on the individual wheel path profiles gave a better assessment of the locations of defects where peaks in the computed CVs of the dynamic tire loads were observed. Researchers found that evaluating the defects based on the average of the left and right wheel path profiles tends to mask the defects that exist along the individual wheel paths, particularly for pavement sections where there is a significant difference in the wheel path IRIs. Researchers also found that using the individual wheel path elevation profiles gives the correct magnitudes (heights or depths) of the defects found on the pavement surface compared to the magnitudes obtained based on the average profile.

Based on the findings from tests made with the instrumented truck on this project, researchers recommend that in lieu of locating defects based on the average profile, TxDOT should use the actual measured profile on each wheel path to evaluate localized roughness

using the existing bump template. Researchers note that the average profile is a calculated profile, whereas the individual wheel path profiles are the measured data from the inertial profiler. Thus, using the current bump template with the individual wheel path profiles should give a better assessment of the localized roughness that exists on a given project, in terms of where the defects are, and the magnitudes of these defects. Having the correct information is necessary to determine the proper corrections that need to be applied on a given project to remove features that detract from ride quality and increase the dynamic load variability.

To have the least impact on the existing pay adjustments that are made, TxDOT should continue using the existing 5-ft bump penalty gap in Item 585 with the gap applied on the test lane width (at least in the interim) instead of the length of each individual wheel path profile. Applying the bump penalty gap on the test lane width means that no more than one penalty will be assessed for all occurrences of defects found on both wheel paths over the 5-ft longitudinal distance of the test lane. In this way, no change will be required in the current language of the ride specification to implement the change recommended by researchers in this project. However, Section 7 of TxDOT Test Method Tex-1001S will have to be modified. In connection with this change, researchers prepared a draft of a revised section on localized roughness (see Figure 5.1) to replace the existing section found in the test method. Researchers recommend that TxDOT modify its Ride Quality program to permit the evaluation of localized roughness by wheel path according to the revised language given in Figure 5.1.

Researchers also recommend that TxDOT monitor the performance of the projects discussed in Chapter IV of this report. This monitoring effort should include measurements of surface profile, rut depths, and visual distress over the limits of the projects tested. Researchers recommend that surface profiles and rut depths be taken at 6-month intervals with an inertial profiler equipped with a rut bar of sensors for measuring longitudinal and transverse profiles. Visual surveys can be taken annually, but consideration should be made to conducting the surveys twice each year, particularly if the longitudinal or transverse profiles begin to show more roughness or rutting developing within a given project. This monitoring effort would provide TxDOT with data to compare the performance over time of initially smooth and initially rough pavement sections to establish the benefit of building smooth pavements.

Section 7

Detecting Localized Roughness

Using Department software, identify areas of localized roughness with the same measured profiles required for QA tests.

The Department software will:

- apply a 25-ft. moving average filter to each wheel path profile
- determine the difference between the wheel path and the 25-ft moving average filtered profiles for every profile point in each wheel path and
- identify deviations greater than 0.150 inches as a detected area of localized roughness. (Positive deviations are "bumps" and negative deviations are "dips.")
- determine locations where corrective work is necessary to correct localized roughness and calculate pay adjustments according to the specified schedule.

The following reference illustrates the methodology: "Application of Profile Data to Detect Localized Roughness" by Emmanuel Fernando and Carl Bertrand, Transportation Research Record 1813, Transportation Research Board, Washington, D.C., 2002, pp 55-61.

Figure 5.1. Proposed Revised Section on Localized Roughness in TxDOT Test Method Tex-1001S to Implement Recommendation on Determining Defects by Wheel Path.

REFERENCES

Addis, R.R., A.R. Halliday, and C.G.B. Mitchell. Dynamic Loading of Road Pavements by Heavy Goods Vehicles. Congress on Engineering Design, Seminar 4A-03, Birmingham, Institution of Mechanical Engineers, United Kingdom, 1986.

Chatti, K., and D. Lee. Development of New Profile-Based Truck Dynamic Load Index. Transportation Research Record 1806, Transportation Research Board, Washington, D.C., 2002, pp. 149-159.

Dally, J.W., and W.F. Riley. Experimental Stress Analysis. 2nd edition, McGraw-Hill, Inc., New York, 1978.

Fernando, E.G. Index for Evaluating Initial Overlay Smoothness with Measured Profiles. Transportation Research Record 1806, Transportation Research Board, Washington, D.C., 2002, pp. 121-130.

Fernando, E.G., and C. Bertrand. Application of Profile Data to Detect Localized Roughness. Transportation Research Record 1813, Transportation Research Board, Washington, D.C., 2002, pp. 55-61.

Fernando, E.G. Development of a Profile-Based Smoothness Specification for Asphalt Concrete Overlays. Research Report 1378-S, Texas Transportation Institute, Texas A&M University, College Station, Texas, 1998.

Gyenes, L., and C.G.B. Mitchell. Measuring Dynamic Loads for Heavy Vehicle Suspensions Using a Road Simulator. International Journal of Heavy Vehicle Systems, Vol. 3, Inderscience Publishers, Switzerland, 1996.

Hassan, R.A., and K. McManus. Assessment of Interaction Between Road Roughness and Heavy Vehicles. Transportation Research Record 1819, Transportation Research Board, Washington, D.C., 2003, pp. 236-243.

Huhtala, M., V. Laitinen, and P. Halonen. Roughness Measurement Devices and Dynamic Truck Index. International Conference on the Bearing Capacity of Roads and Airfields, Minneapolis, Minnesota, 1994, pp. 1517-1531.

Jacob, B., and V. Dolcemascolo. Dynamic Interactions Between Instrumented Vehicles and Pavements. International Symposium on Heavy Vehicle Weights and Dimensions, Queensland, Australia, 1998, pp. 142-160.

Merril, D.B., D. Blackman, and V. Ramdas. The Implications of Dynamic Loading and Tire Type on the UK Road Network. International Conference on Asphalt Pavements, Copenhagen, Denmark, 2002.

Middleton, J., and A.H. Rhodes. The Effect of Dynamic Loading on Road Pavement Wear: A Study of the Relationship Between Road Profiles and Pavement Wear on an Instrumented Test Road. Proceedings of the Institution of Civil Engineers, Vol. 105, London, United Kingdom, 1994.

Papagiannakis, T., and B. Raveendran. International Standards Organization – Compatible Index for Pavement Roughness. Transportation Research Record 1643, Transportation Research Board, Washington, D.C., 1998, pp. 110-115.

Roberts, F.L., J.T. Tielking, D. Middleton, R.L. Lytton, and K. Tseng. Effects of Tire Pressures on Flexible Pavements. Research Report 372-1F, Texas Transportation Institute, Texas A&M University, College Station, Texas, 1986.

Steven, B., and J. de Pont. Dynamic Loading Effects on Pavement Performance – The OECD Divine Test at CAPTIF. ARRB Transport Research Conference, Christchurch, New Zealand, 1998, pp. 93-107.

Sweatman, P.F. A Study of Dynamic Wheel Forces in Axle Group Suspensions of Heavy Vehicles. Special Report No. 27, Australian Road Research Board, Vermont, South Victoria, Australia, 1983.

University of Michigan Transportation Research Institute (UMTRI). RoadRuf User Reference Manual, The University of Michigan, Ann Arbor, Michigan, 1997.

Walker, R.S. Real-Time Data Acquisition for Surface Measurement/Implementation of Intelligent Bus Systems for Distress Measurements. Research Report 19987-F, The University of Texas at Arlington, Arlington, Texas, 1997.

Wang, F., and R.B. Machemehl. Current Status and Variability of In-Service Truck Tire Pressures in Texas. Transportation Research Record 1853, Transportation Research Board, Washington, D.C., 2003, pp. 157-164.

Wang, F., R.F. Inman, R.B. Machemehl, Z. Zhang, and C.M. Walton. Study of Current Truck Configurations. CTR Report 0-1862-1, Center for Transportation Research, The University of Texas at Austin, Austin, Texas, 2000.

APPENDIX A

LITERATURE REVIEW

APPENDIX A. LITERATURE REVIEW

Researchers conducted a literature review to gather information considered useful for accomplishing the objectives of this project. The review covered the following areas:

- measurement of vehicle dynamic loads,
- surveys of truck use that identified configurations commonly used by carriers to transport goods and commodities,
- profile statistics for characterizing pavement smoothness based on truck damage criteria,
- vehicle transfer functions relating pavement roughness to dynamic tire loading, and
- compilations of data on truck properties for simulating the response of trucks to pavement roughness.

The findings from the literature review are presented in this appendix.

TRUCK TESTS TO INVESTIGATE RELATIONSHIPS BETWEEN PAVEMENT ROUGHNESS, VEHICLE CHARACTERISTICS, AND DYNAMIC TIRE LOADS

In a 1996 report, Gyenes and Mitchell detail research conducted at Transport Research Laboratories (TRL) in the United Kingdom (UK), in which the Volvo test facility in Gothenburg was utilized to develop a simulated test to rate suspensions in terms of their potential for causing road wear. This goal was accomplished by comparing simulated wheel load measurements published by TRL in 1993 to actual dynamic behavior of heavy goods vehicle suspensions over the TRL test track. The first test series in 1991 involved a computer-controlled Volvo rig made up of six hydraulic actuators capable of exercising a fully laden vehicle. The TRL test track profiles were run through the actuators, and a comparison was made between the Volvo instrumentation, which measured the dynamic loads under the tire patch using load cells built into the actuators, and the TRL instrumentation, which uses strain gages and accelerometers. In addition, researchers compared rig generated wheel load histories against real road-based load histories from the TRL test track program.

A second test series was conducted in 1993 to obtain the unsprung masses by the process of dynamic calibration, followed by systematic runs at simulated test speeds of 20,

30, 40, 50, and 60 mph using the smooth and medium-smooth wheel track profiles of the TRL test track as inputs. The suspensions for the two-axle semitrailer bogies used for testing included a tandem axle air suspension; a tandem axle, single-leaf steel suspension; and a rubber mounted walking beam suspension. The vehicles were fully loaded to the UK gross vehicle weight limit of 32.5 tons with tandem axle weights of about 18 tons on each semitrailer bogie.

Wheel loads on the road simulator were measured using load cells built into the actuators close to the wheel platforms. The load on each wheel of the replaceable sub-chassis unit was determined by measuring the bending of the axle between the spring mount and the wheel hub using strain gages, and the vertical inertia of the wheel mass using an accelerometer mounted on the hub back plate. Strain gages fitted to the bogie with the rubber-mounted walking beam suspension measured the shear force on the axle tube, a technique that provided higher accuracy in dynamic load measurement compared to bending gages.

Accelerometers were fitted to the semitrailer platform to measure body bounce, pitch, and roll accelerations. Displacement transducers were also fitted to each semitrailer wheel to measure vertical displacement between the axle center and the trailer platform. The accelerometers and strain gages were calibrated before each test series, and the signals from the actuator sensors and body-mounted sensors were recorded on the same data logger. The steel, air, and rubber-suspended tandem axles were sinusoidally excited over a range of frequencies from 0.5 Hz to 20 Hz in bounce, pitch, roll, and twist modes. The results of the constant speed excitation in bounce for the nearside rear wheel of all three suspension types indicate that there are two dominant modes – the body bounce at low frequency and the wheel hop at high frequency. As the excitation frequency is increased, the effect of the unsprung mass on wheel loads becomes significant. The results of the constant speed excitation in pitch for the nearside rear wheel of all three suspension types indicate that there is one dominant mode, which is at high frequency. The results of the constant speed excitation in roll for the nearside rear wheel of all three suspension types are evident at around 1 Hz. The results of the constant speed excitation in twist for the nearside rear wheel of all three suspension types indicate that there is no distinct mode in the range of excitation frequencies.

The results of these tests showed that the dynamic wheel load can be measured within 1 to 2 percent accuracy when using an improved technique, which involves the use of shear gages and a dynamic calibration procedure that corrects for the angular and vertical accelerations of the wheel components outboard of the strain gages. According to the researchers, this method is an improvement over other methods, which use bending gages that are subject to anomalous readings of the roll component of wheel load.

Middleton and Rhodes' 1994 report detail their research, which was based on previous work conducted by Addis, Halliday, and Mitchell in 1986. In the research performed by Addis et al., a two-axle, semitrailer was instrumented, and results were obtained from one vehicle operating over one instrumented pavement. Middleton and Rhodes decided to further this research and constructed a test laboratory with a more comprehensive system of strain gages that could be used to monitor the structural effects of the passage of any vehicle passing over the test section at various speeds. Each strain gage was calibrated using dynamic wheel loads data from an instrumented two-axle heavy goods vehicle, which allowed the monitoring of instantaneous dynamic wheel loads of any vehicle at any point along the test section. The test facility was instrumented with strain gages with 120 ohm resistance-foil located at the bottom of the roadbed to measure the transient horizontal radial strain at 0.5 m centers under each wheel path. There were a total of 126 strain gages.

The test vehicle used in the study was a Volvo instrumented at TRL. It was instrumented to permit measurements of all wheel loads simultaneously, using strain gages that measured the bending of the axles between the suspension and the hub. Accelerometers were also used to correct the vertical inertial loads due to the unsprung mass outboard of the strain gages.

The instrumented test vehicle was used to calibrate the strain gages. This was done to establish the relationship between vehicle speed, transient strain, and the respective dynamic wheel loads. The calibration data were used so that the instantaneous wheel loads of any vehicle traveling along the wheel paths could be monitored.

The longitudinal profiles of the two wheel-tracks were monitored regularly using the TRL high speed road monitor. During testing, a record was kept for temperature, wind speed, and rainfall in order to ensure that strain measurements were taken under similar conditions. Wheel paths were surveyed regularly for rutting and cracking. Twelve sets of

dynamic wheel load data were collected under a combination of variables, which included number of axles, speed, and number of wheel paths. A minimum of two sets of pavement strain data were collected for each strain gage, and thermocouples were used to measure the pavement temperatures at the surface, at 20 mm depth, and at 250 mm depth at the beginning, middle, and end of the test section.

The results of this research provided several conclusions. One conclusion was that the wheels of the test vehicles applied dynamic loading, which oscillated between 3 Hz and appeared to be independent of speed, load, tire type, and suspension system. Also, the researchers concluded that each axle of the test vehicles applied maximum and minimum dynamic loads at common points for a specific speed and that the ratio of mean dynamic axle load and static axle load increased with speed.

Jacob and Dolcemascolo's 1998 report details their investigation into dynamic loads on pavements and their spatial repeatability to assess the sensitivity to pavement profile, road roughness, vehicle characteristics, and traveling conditions. The investigation also looked into the effects of dynamic loads on vehicles and the infrastructure and focused on the response of two instrumented vehicles traveling at the same speeds on different road profiles, whose evenness were considered excellent, good, and poor. The IRI values in m/km of each road section were found to be 0.8 for the road in excellent condition, 1.73 for the road in good condition, and 3.57 for the road in poor condition.

The two vehicles were instrumented with strain gages mounted on the axles and accelerometers on the bodies, which provide the data to calculate dynamic wheel impact forces at high frequency. The wheel load instrumentation was made up of two strain gage bridges and two accelerometers per axle, which were configured as full bridge circuits that were sensitive to shear force. These instrumented vehicles could measure dynamic wheel loads with a sampling frequency of 500 Hz.

An instrumented vehicle was also used in this research, which consisted of a two-axle tractor with a single-axle instrumented trailer that could be equipped with two suspension types, which were either air or steel leaf spring. This instrumented vehicle could measure dynamic wheel loads with a sampling frequency of 200 Hz.

For each of the three test sites, the power spectral density (PSD) of the pavement profile was calculated and plotted versus the wavelength λ. The PSD may be plotted as a function of frequency f or wavelength because both are linked to the vehicle velocity V

according to the relation $V = f \lambda$. When plotting the PSD of the pavement profile, the larger the area under the PSD curve, the greater the roughness.

Two PSDs were calculated for the impact forces of the trailer corresponding to each combination of the test variables, i.e., test site, suspension, load, and speed. One PSD was for the axle impact force, which is the sum of both wheel loads and is considered to be representative of the bounce and axle hop motions. The other PSD was for the difference between the left and right wheel loads, which is representative of the roll motion. The main findings were that the body bounce of the steel suspension gives the highest peaks, which generally increased with pavement roughness. The body bounce peak amplitude is between 10 to 20 times lower with the air suspension than with the steel suspension.

PSDs were also calculated for each wheel and axle load of the instrumented vehicle. It was found that the shapes of the PSDs for wheel and axle loads are similar for each speed with the same approximate peaks. The roll effect is more important for wheels, while the axle hop is higher for axles. The body motions were dominant for the heaviest load, while the axle hops became the main effect at lower loads with a slight shift in the frequency. Other significant findings of this research were the importance of wheel imbalance to the wheel and axle dynamic impact factors, especially at low speed and on smooth road profiles where the body bounce and axle hop motions are low, the significant reduction in dynamic load increments from the air suspensions, and the great influence of pavement roughness on dynamic loads.

INDICES CHARACTERIZING TRUCK DYNAMIC LOADING

The effect of surface profile on vehicle dynamic loads is illustrated in Figures A1 to A3 (Fernando, 2002). Shown in these figures are the predicted vehicle responses to measured surface profiles as determined using a vehicle simulation model. Figure A1 shows the predicted variation in dynamic axle loads on a smooth pavement having a serviceability index (SI) of 4.5. The plot shown is referred to in this proposal as the dynamic load profile, analogous to a surface or road profile, which shows the variation in elevation with distance along a given segment. Figure A2 illustrates the predicted dynamic load profile for a medium-smooth pavement (SI of 3.4), while Figure A3 shows the load profile for a rough pavement (SI of 2.5). It is observed from Figures A1 to A3 that the variability in predicted dynamic axle loads increases with an increase in surface roughness.

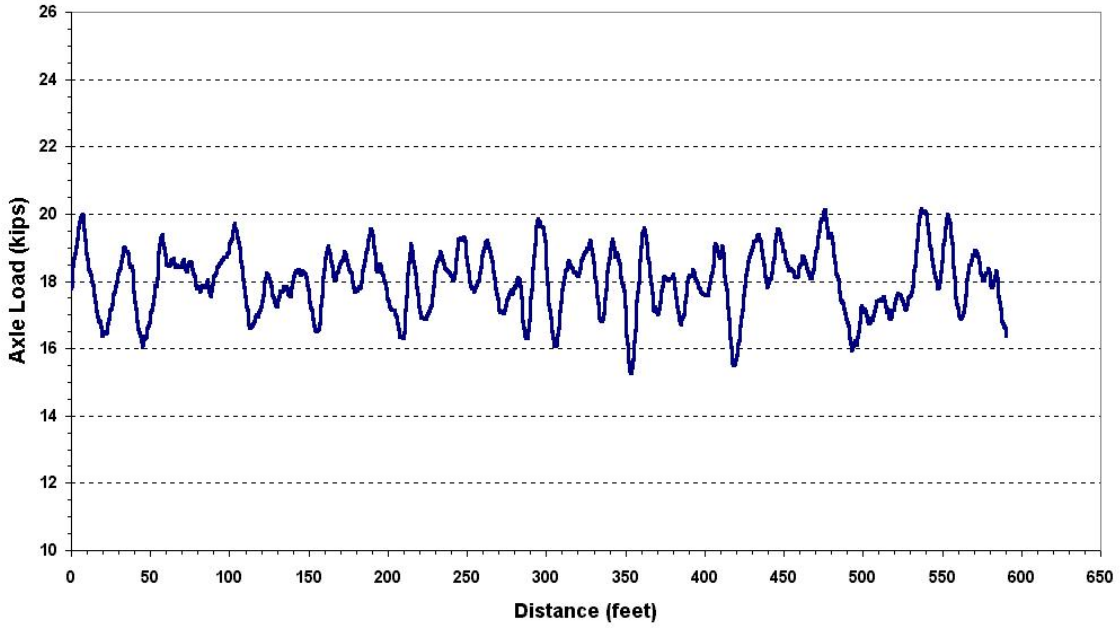

Figure A1. Predicted Dynamic Loads on a Smooth Pavement (SI = 4.5).

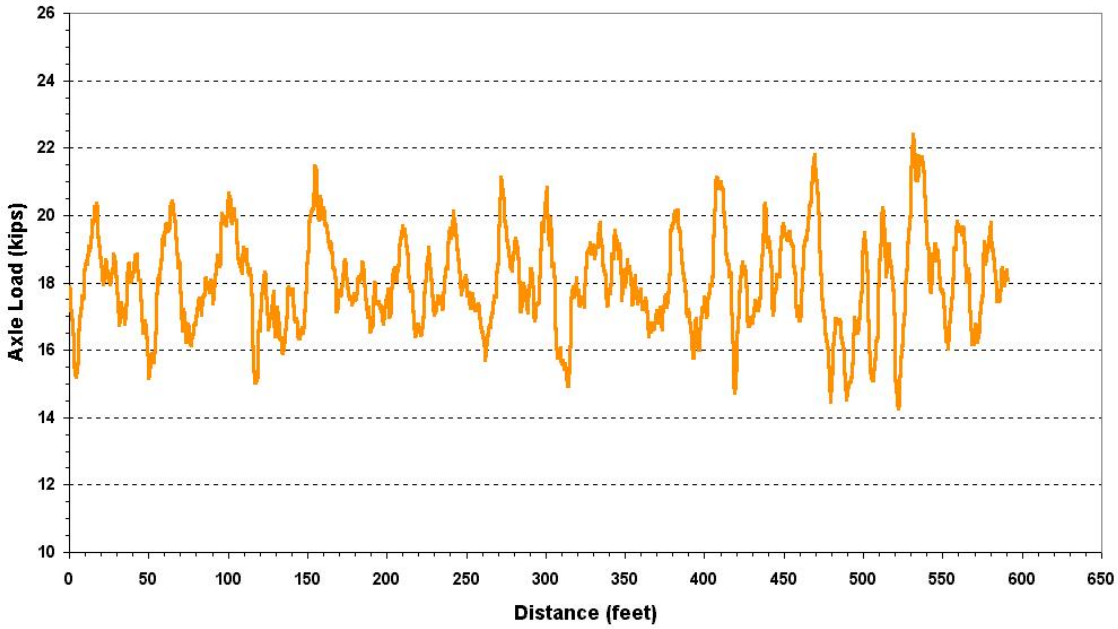

Figure A2. Predicted Dynamic Loads on a Medium-Smooth Pavement (SI = 3.4).

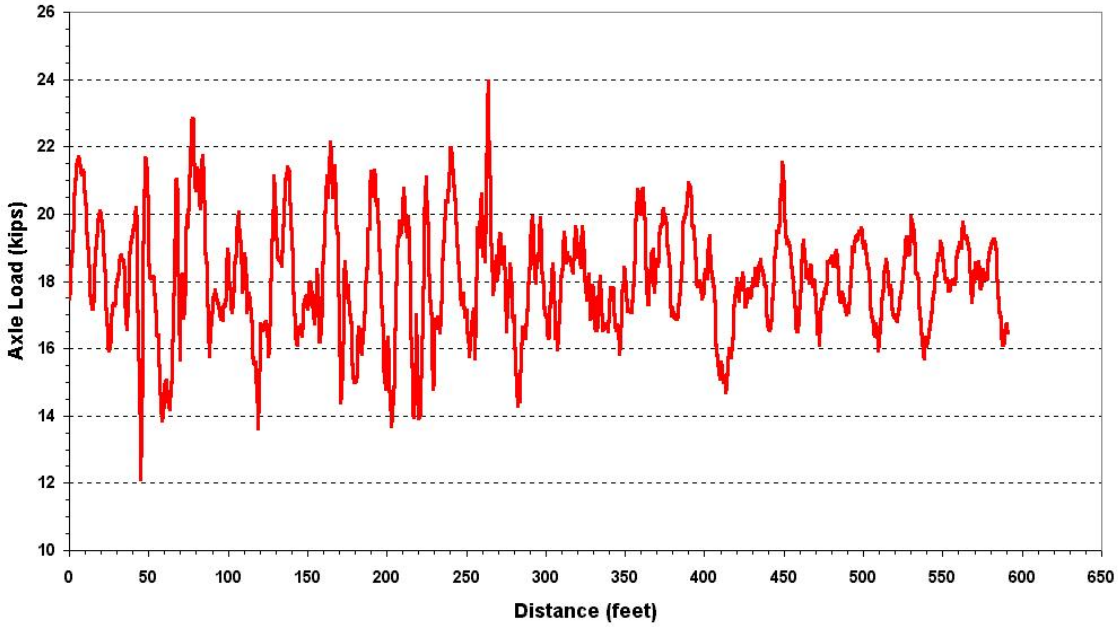

Figure A3. Predicted Dynamic Loads on a Rough Pavement (SI = 2.5).

The dynamic axle loads fluctuate about the static axle load, which corresponds to the mean of the predicted dynamic loadings. In the figures given, the static axle load is 18 kips corresponding to the standard single axle used in pavement designs currently implemented within state highway agencies. In the limit, if the surface profile is perfectly flat, the predicted dynamic loads would be a constant, equal to the static axle load, and the load profile would plot as a horizontal line. In this case, there will be no variability in the predicted axle loads. Because pavement response is directly tied to axle load magnitudes, it is logical to expect that dynamic axle load variations will lead to differences in predicted pavement performance.

Fernando (2002) proposed an index for evaluating the acceptability of overlay smoothness that is related to the predicted performance of the overlay based on reflection crack growth. To illustrate the concept underlying the development of this index, consider the two pavements shown in Figure A4. In the first case, a smooth overlay is built over the existing pavement, while in the second case, a rough overlay is constructed. Note that the underlying pavement is the same for both scenarios as would be true for a given resurfacing project. Only the effect of differences in surface profile is considered. From theoretical considerations, Fernando (1998) developed an index for predicting the change in overlay life

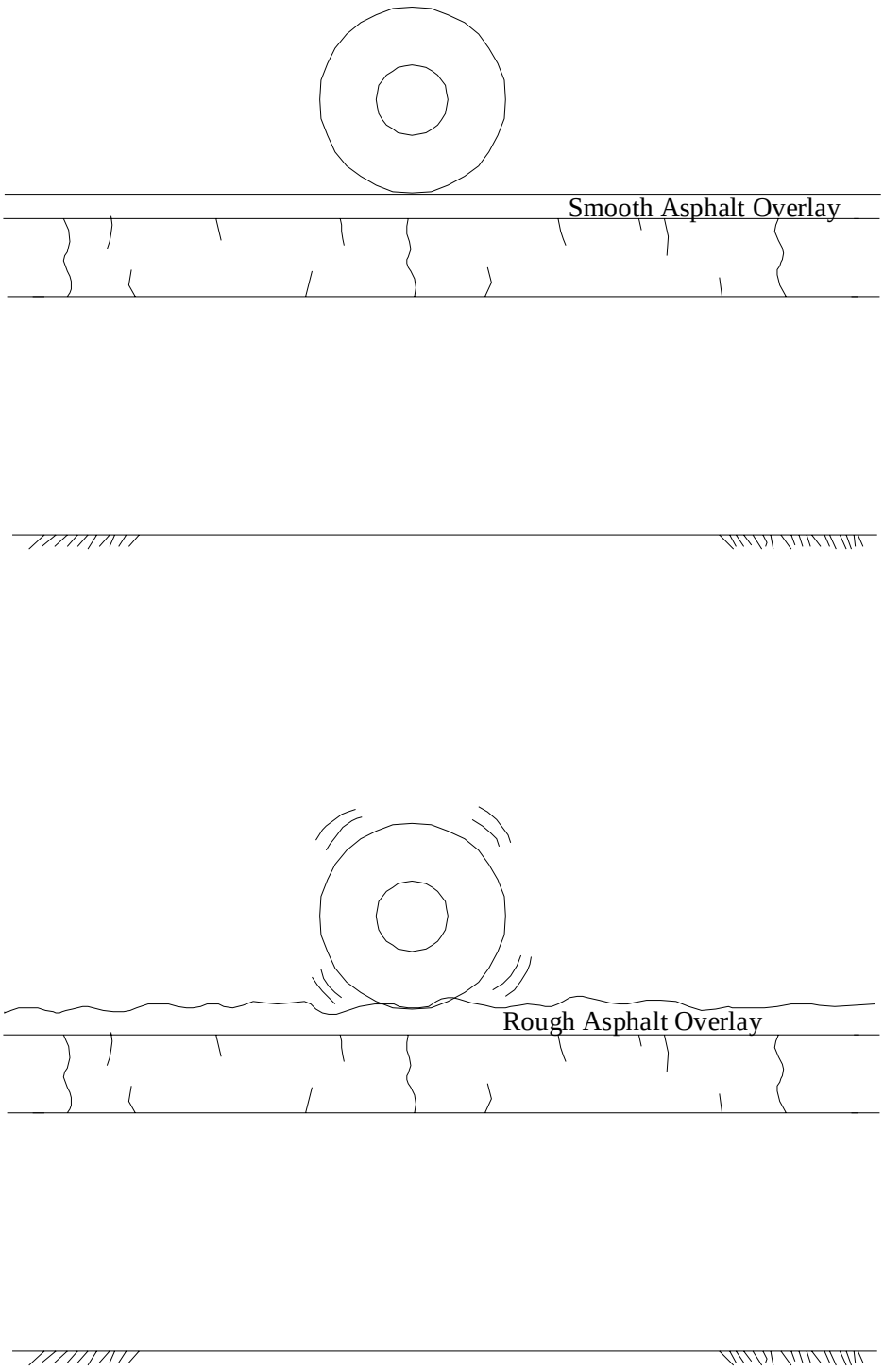

Figure A4. Illustration of Approach Used to Evaluate Initial Overlay Smoothness.

due to differences between the target and as-built surface profiles. It is given by the equation:

$$\Delta = \left[\frac{1+z\,CV_0}{1+z\,CV_1}\right]^n - 1 \qquad \text{(A1)}$$

where,

CV_0 = coefficient of variation of the applied dynamic wheel loads associated with the target profile from design,

CV_1 = coefficient of variation of the applied dynamic wheel loads associated with the as-built profile,

z = the number of standard deviations corresponding to a given percentile of the predicted dynamic load distribution, and

n = the exponent of the Paris-Erdogan crack growth law that affects the rate of crack propagation through the overlay.

The reader is referred to the report by Fernando (1998) for the derivation of Eq. A1. This equation provides a rational method for evaluating the quality of the finished surface on the basis of predicted performance. In practice, the coefficient of variation in Eq. A1 is determined by vehicle simulation using the measured profile. Note that Δ is related not only to the surface profile but to vehicle suspension and geometric characteristics, which all affect the variability in the applied dynamic wheel loads. The benefit of reducing this variability on predicted pavement life is readily apparent from Eq. A1. If $CV_1 < CV_0$, the predicted index is positive, indicating a predicted increase in pavement life with a smoother surface. Note that the reduction in wheel load variability is achieved not only by building smoother pavements but also by designing, manufacturing, and encouraging the use of trucks with improved dynamic performance. If the as-built and target profiles are the same, $CV_0 = CV_1$ and the predicted Δ is zero, indicating that the as-built surface meets the predicted service life associated with the target smoothness. Finally, if the as-built surface is rougher than the target, i.e., $CV_1 > CV_0$, Δ is negative indicating a reduction in predicted pavement life because of the expected higher impact loading.

Huhtala et al. (1994) reported on the international roughness index developed by the World Bank in 1982 to classify road surface evenness. The IRI is determined from the longitudinal profile of the road, which is measured through a variety of methods. The IRI

value of the measured profile is determined using the reference quarter car simulation model, which has standard tire, suspension, and damper properties, and moves at a constant speed along the measured profile. The relative vertical displacement between the sprung and unsprung masses is calculated from the movements of the axle and body. The IRI statistic is then computed as the average of the computed relative displacements over a specified interval.

The road surface monitoring vehicle (PTM) and Roadman were used to measure pavement profiles. The PTM was developed to meet the demand for fast and reliable measurement of road surface characteristics, permitting data collection at speeds of 40 to 90 kph (25 to 56 mph) with a daily measuring capacity of 100 to 400 km (62 to 249 miles). The test vehicle is fitted with beam-mounted ultrasonic distance sensors to measure the transverse profile at 2 m intervals. From the transverse profile, the depth of the rut, the height of the ridge between them, and the cross area of the rutting can be determined. A laser detector and accelerometer measure the longitudinal profile, which is then processed through the IRI quarter car simulator. Road geometry, which includes cross-fall, gradient, and curvature, is measured by gyroscopes and inclinometers. A visual inspection of surface distresses is conducted and entered manually in the computer.

The Roadman device measures the IRI values and also evaluates surface conditions. This device can be mounted in any passenger vehicle and consists of an accelerometer, pulse detector, and a central unit. The longitudinal profile is measured using an accelerometer, which is mounted on the axle beside the right wheel of the car.

A reported finding from this research is that the axle load of a heavy vehicle is not steady, but varies because the road is uneven. The dynamic axle load can be measured with an instrumented vehicle, simulated with computers, or measured locally by weigh-in-motion devices. The instrumented vehicle used for this study has three axles. The front axle has a leaf spring with dampers, and the tandem axle has a leaf suspension without dampers. The load is measured with strain gages at the ends of the axles, and the inertia effects are corrected with accelerometer measurements. With this configuration, the body pitch or bounce mode is much more important on the front axle, and axle hop mode is more important on the drive axle of the tandem axle.

Out of this research, it was determined that a new index was needed in addition to the IRI to describe how the dynamic axle loads due to unevenness of the road affect the life of a

pavement. Therefore, the dynamic roughness index (DRI) was developed. For this purpose, the quarter car model was used. Its parameters are the sprung mass, unsprung mass, suspension spring rate, tire spring rate, and the damping rate of the shock absorber. Four approaches were used to select a model to determine the DRI:

- spectral analysis of the road profile,
- maxima of dynamic axle loads,
- standard deviation of the axle loads, and
- application of the fourth power law.

Researchers found the fourth power law to be the most realistic and useful for determining the DRI. Researchers computed the IRIs and DRIs from 140 profiles and found the correlation coefficient between these statistics to be 0.67. At an IRI value of 1.5 m/km, the DRI is between 100 and 140. At an IRI value of 3 m/km, the DRI is between 120 and 160. The researchers were of the opinion that useful information can be obtained from this index.

Chatti and Lee (2002) developed a new roughness index called the dynamic load index (DLI) in order to identify pavement profiles that were likely to generate high dynamic truck-axle loads. Previously, Chatti had developed relationships between dynamic axle loads and road roughness to confirm the existence of a critical roughness level that leads to the accelerated pavement damage. However, this development was based only on passenger car response to pavement roughness as measured by the ride quality index (RQI). Researchers realized that the majority of pavement damage is caused by heavy truck axle loads and that an accurate prediction of roughness level that would excite trucks required the evaluation of dynamic truck-axle loads likely to be generated by the profile characteristics of individual pavements. The new DLI negates the need for running a truck simulation program to determine whether a pavement profile is in need of smoothing based on truck dynamic loads.

Because a large portion of heavy vehicles have similar geometric and dynamic characteristics and tend to travel at similar highway speeds, spatial repeatability of dynamic loads is expected in normal traffic conditions. To investigate the spatial repeatability of the dynamic axle loads for all truck axles, the correlations between the different axles were studied. Because axle load variation is a function of the given pavement profile and truck characteristics, the coefficient of correlation between two axles for a given set of profiles is a

good measure of spatial repeatability, which has been shown to be indicated by a correlation coefficient of 0.707.

The spatial repeatability of dynamic truck-axle load was analyzed using three different truck types – a two-axle single unit truck, a three-axle single unit truck, and a five-axle tractor semitrailer. Researchers used the TruckSim program to predict the dynamic axle loads generated by these trucks for 68 pavement profiles. All three truck types were equipped with standard flat lead suspensions, and default parameters in the TruckSim program were assumed. Researchers found that the best correlations between profiles for each axle load and those for the reference axle load were among the drive axles for all three trucks. The worst correlation was with the rear axle of the tractor semi-trailer, which indicates that the trailer was out of phase with the tractor. In these findings, it was determined that the second axle load in a five-axle semitrailer was representative of the three truck types. This reference axle was used to develop relationships between the RQI, DLI, and dynamic load.

The RQI was developed by the Michigan Department of Transportation in the early 1970s. Through a series of mathematical and statistical steps, the PSD was found to have a 90 percent correlation with subjective opinions of ride quality. From this finding, the method developed for computing RQI splits the profile into three wavelength bands. The index is then determined from these three wavelength bands using the equation:

$$RQI = 3\ln(Var1) + 6\ln(Var\ 2) + 9\ln(Var3) \qquad (A2)$$

where:

Var1 = the variance for 7.6 to 15.2 m wavelengths,

Var2 = the variance for 1.5 to 7.6 m wavelengths, and

Var3 = the variance for 0.6 to 1.5 m wavelengths.

An RQI value from 0 to 30 indicates excellent ride quality. RQI values from 31 to 54 indicate good ride quality. Values from 55 to 70 indicate fair ride quality, and values above 70 indicate poor ride quality.

However, researchers determined that a profile-based index focused on wavelengths in the 6.7 to 17.9 m range and the 1.8 to 3.3 m range would have a better correlation with truck dynamic axle loads than car response-based pavement roughness indices, such as the RQI and IRI. By examining the PSDs of dynamic axle loads on two rigid pavements with

the same RQI but different dynamic loading coefficients, researchers confirmed that the dynamic truck axle load is related to profile elevations having wavelengths from 6.7 to 17.9 m, which excites the truck body bounce, and from 1.8 to 3.3 m, which excites the axle bounce.

The new profile index was found according to linear random vibration theory, in which the PSD of the truck response was obtained by multiplying the square of the truck response function by the PSD of the surface profile. The variance of the truck response was then found by considering only the frequency ranges of 1.5 to 4.0 and 8.0 to 15.0 Hz, which correspond to the truck and axle bounces, respectively. The variance V_y is determined from the following equation:

$$V_y = |G(w_1)|^2 V_1 + |G(w_2)|^2 V_2 \quad \text{(A3)}$$

where:

$G(w_1)$ = peak value of truck response function in the frequency range of 1.5 to 4.0 Hz,

$G(w_2)$ = peak value of truck response function in the frequency range of 8.0 to 15.0 Hz,

V_1 = variance of the elevation in the frequency range of 1.5 to 4.0 Hz, and

V_2 = variance of the elevation in the frequency range of 8.0 to 15.0 Hz.

Based on the standard deviation of the truck response and Eq. A3, the new roughness index, DLI, is determined from the following equation:

$$DLI = \sqrt{a_1 V_1 + a_2 V_2} \quad \text{(A4)}$$

where:

V_1 = variance of the profile elevation in the wavelength range of 6.7 to 17.9 m corresponding to a frequency range of 1.5 to 4.0 Hz for a truck traveling at 96 kph,

V_2 = variance of the profile in the wavelength range of 1.8 to 3.3 m corresponding to a frequency range of 8.0 to 15.0 Hz for a truck traveling at 96 kph, and

a_1, a_2= weighting factors.

For convenience, researchers set a_1 equal to one and a_2 equal to 14, the value that gave the highest correlation between DLI and dynamic loads. Therefore, the final equation for computing DLI is:

$$DLI = \sqrt{V_1 + 14 V_2} \quad \text{(A5)}$$

According to the researchers, the use of DLI is beneficial in the following ways:

- DLI can differentiate between profiles that generate high dynamic loads and those having the same RQI but generating low dynamic loads.
- DLI can be used to decide the need for smoothing or correcting the profile of a given section without running a truck simulation program.

Papagiannakis and Raveendran (1998) developed the roughness index for driving expenditure (RIDE), which is compatible to the International Standards Organization (ISO) standard on "exposure to whole-body vibration." The two main requirements for the development of the index were that it be related to the riding comfort of passenger cars and heavy trucks and that it reflect the pavement roughness aspects that relate to the dynamic axle loads generated by heavy trucks. Papagiannakis demonstrated in previous research that the main contributor to the dynamic axle loads of heavy trucks is the vertical acceleration of the sprung mass with no dependence on suspension type. This work was done with instrumentation that measured both dynamic axle loads and sprung mass acceleration. Based on this research, it became evident that a pavement roughness index based on sprung mass acceleration would be preferable to one based on relative axle displacement, such as the IRI. It was also determined from previous research that the calculation of an index based on sprung mass acceleration is more efficient in the frequency domain than in the time domain, and that a frequency domain transfer function with a resonant frequency of about 3 Hz and corresponding amplitude of about 400 m/sec^2/m is representative of the sprung mass response exhibited by both heavy trucks and passenger cars.

The transfer function that was selected to be used as a reference in calculating RIDE was determined from data obtained from an instrumented five-axle semitrailer truck on a pavement of medium roughness at 80 kph. This selection was made in order to provide a comparison to IRI, which is also calculated based on a speed of 80 kph. The power spectral density of the sprung mass acceleration response was found by multiplying the PSD of the pavement profile by the square of the reference frequency domain transfer function. The new index, RIDE, was then found by integrating the PSD of the pavement profile over the frequency range from 0 to 50 Hz. This gives the sum of the squares of the sprung mass acceleration response of the reference vehicle. The square root of this integral divided by the length of the pavement traveled results in a root-mean-square (RMS) of the acceleration response per unit length, which is compatible with ISO 2631.

Hassan and McManus (2003) developed a new pavement roughness index that represents the heavy-vehicle driver's perception of pavement rideability using existing profile data measured along the wheel paths of a passenger car. This was done by conducting an assessment survey to gather truck drivers' ratings of the ride quality of a number of road sections with various roughness levels along a highway in rural Victoria, Australia, on which there is a high percentage of heavy vehicle traffic. The data were then analyzed by correlating the mean panel rating (MPR) to roughness content in different wavebands of each road section. The roughness content that resulted in the highest correlation was then used in developing the new index referred to as the profile index for trucks (PI_t).

Researchers performed PSD analyses on the road surface profile data using the RoadRuf software developed by the University of Michigan Transportation Research Institute (1997). Profile data were converted into slope values by subtracting adjacent elevation readings and dividing by the sample interval. RMS values of profile slope in one-third octave bands were then determined. The MPR was correlated with roughness contents in different wavebands to identify wavelengths that influence ride perception. This analysis showed that the waveband between 4.88 and 19.51 m gave the highest correlation with the MPR. Thus, researchers used the roughness content in this band to establish the new index given below:

$$PI_t = \sqrt{\frac{(PI_{OWP})^2 + (PI_{IWP})^2}{2}} \qquad \text{(A6)}$$

where:

PI_{OWP} = the average of the RMS values of the profile slope for the outer wheel path, and

PI_{IWP} = the average of the RMS values of the profile slope for the inner wheel path.

An exponential transform was also used to develop a truck ride number (TRN) to predict pavement ride quality, as perceived by heavy-vehicle occupants, from existing road surface profile data. This index is given by the following equation:

$$TRN = 5e^{-140(PI_t)^{0.84}} \qquad \text{(A7)}$$

Equation A7 gave the highest correlation coefficient between predicted TRN values and actual MPR values. Another TRN equation was developed using IRI as the predictor of

MPR. This alternative equation was also found to be a good predictor of MPR, but not as good as Eq. A7. The TRN equation based on IRI is given by:

$$TRN_{IRI} = 5e^{-118.70(IRI)^{0.9}} \quad \text{(A8)}$$

TRUCK TESTS ON INSTRUMENTED PAVEMENT SECTIONS

Steven and de Pont (1998) conducted research at the Canterbury Accelerated Pavement Testing Indoor Facility (CAPTIF) to investigate the relationship between the dynamic loadings produced by different suspensions and the resultant pavement performance. This research was done by comparing two different suspensions, whose performance characteristics were at opposite ends of the spectrum, with the simulated loading and vehicle emulator (SLAVE). The two SLAVE vehicles use standard heavy-vehicle suspension components, which are equipped with half-axle assemblies that can carry either single or dual tires. The SLAVE was fitted with suspensions similar to actual heavy-vehicle components with one vehicle having an air spring suspension with hydraulic shock absorbers and the other having a multi-leaf steel spring.

After construction of a test pavement, 600 loading cycles of the SLAVE were applied to condition it before any testing was done. Transverse profiles were taken at each station, and longitudinal profiles were also measured with the Dipstick. The IRI values of the profiles were calculated from the longitudinal profiles and were found to be 4.8 m/km and 4.1 m/km for the inner and outer wheel paths, respectively. Tire deflections and imprints were measured at different applied load increments. Suspension stiffness was measured by recording displacements as load increments were applied to characterize the natural frequency and damping characteristics of the suspension.

The pavement started to show signs of deterioration at 60,000 loading cycles. The rate of deterioration slowed down after 105 loading cycles. After completion of 2.5×10^5 cycles, all of the H-bar gages in the asphalt pavement had failed because strains measured in the asphalt exceeded the capacity of the gages.

Researchers found that the pavement response was relatively constant during the experiment. The IRI values varied only slightly throughout the test, and the dynamic load coefficient (DLC) of the steel spring suspension is significantly higher than the air bag suspension. It was concluded that the effect of the steel spring suspension was an increase in the rate of pavement deterioration when compared to the air bag suspension.

Merrill, Blackman, and Ramdas (2002) conducted an international study to assess the significance of vehicle dynamic loading on the performance and maintenance costs of road pavements and bridges. This research arose from the results of a project, the Dynamic Interaction between Vehicle and Infrastructure Experiment (DIVINE), sponsored by the Organization for Economic Cooperation and Development, which was based on the limited testing of a few pavements and bridges. Also considered in this research were the results of the European Commission's Cooperation in Science and Technology (EC COST) Action 334, in which the effects of wide-single and dual tires on pavement wear were examined.

EC COST Action 334 considered the effects of wide-base single and dual tire assemblies on pavement damage, vehicle operating costs, vehicle safety and comfort, and the environment, especially noise. Particular attention was paid to the effects of single tires, wide-base single tires, and dual tires on pavement wear with respect to tire type and inflation pressure. The study conducted by Merrill et al. included the measurement of pavement response under dynamic loading, the measurement of contact stress distributions, and the assessment of pavement wear through trafficking. It was conducted at TRL's Pavement Test Facility (PTF). Equipment at this facility can traffic pavements with loads up to 100 kN (22.5 kip) at a maximum speed of 20 kph (12 mph) along a linear path.

Testing was conducted on a thin asphalt pavement, with a 100 mm layer of high density macadam (HDM) road base, and on a medium pavement, with 100 mm of HDM road base, 50 mm of dense bitumen macadam base course, and 50 mm of hot rolled asphalt surfacing. Both sections were constructed on 225 mm of unbound granular sub-base. Six tires were used in the study, which included four dual tires and two types of single tires. The tires used were:

- 495/45R22.5 Michelin Energy XDA wide-base single,
- 385/65R22.5 Michelin X XZA wide-base single,
- 295/60R22.5 Michelin X XDA dual pair,
- 295/80R22.5 Michelin X Pilote XDA dual pair,
- 315/70R22.5 Michelin X XDA dual pair, and
- 315/80R22.5 Michelin X Pilote XDA dual pair.

To measure the effects that different tire types, inflation pressures, and wheel loads have on the pavement structures, the subgrade was instrumented with soil strain gages placed

150 mm below the surface of the subgrade prior to laying the sub-base. These gages were oriented to measure the transient vertical compressive component of strain for all six tire types for a variety of loads and inflation pressures. The wheel of the heavy vehicle was also moved laterally to measure the strain in relation to the position of the load. Measurements were also taken at varying tire pressures, which ranged between 5 and 10 bars for each tire. The Tekscan Industrial Sensing (I-Scan) system was used to measure the load distribution for the different tire types at different loads and inflation pressures with a low resolution mat.

It was found that subgrade strains under the single tires diminish more rapidly as the tire moved away from the central position when compared to the dual tire assemblies. The difference was attributed to the differing contact areas in regard to the different tire types, but the difference diminished with an increase in pavement thickness. Inflation pressure had a negligible effect on subgrade strain, even with differentially inflated dual tires. Subgrade strain was measured with a change in load, and it varied linearly with both pavement thicknesses. However, the magnitude of the strain was higher for single tires than for dual tires. Also, the gradient of change was higher for the single tires than for the dual tires. In general, the pressure increased in the center of the contact areas for all tires with a negligible change at the edges of the tires. It was determined that the 385/65R22.5 Michelin X XZA wide-base single tire had a concentration of pressure in the center of the distribution, but the highest pressures are scattered. This difference was probably due to tread effects. The 495/45R22.5 Michelin Energy XDA wide-base single tire had three areas of high pressure, with a constant area of high pressure in the center and two areas closer to the edge of the tire. Also evaluated in this experiment was pavement wear under accelerated trafficking using the heavy-vehicle simulator at TRL and the two single tires. The following criteria were considered in this evaluation: rutting, deformation, subgrade stain, and cracking. The tires used for testing were loaded to 44 kN and to the manufacturers' recommended inflation pressures. Over 110,000 passes were applied to each pavement with the thinner pavement failing at 57,000 passes.

Deformation was measured at intervals during breaks in the trafficking using an optical level and measuring staff, which behaved as expected. Inferences were made from the deformation profiles in that there were fewer formations of small shoulders in the thin pavements on either side of the rut than for the thicker pavements. This observation indicated a punching action as opposed to a layer deformation. The ratio for the 385 to the

495 single tires on each pavement thickness showed that there was a much smaller difference between the two tire types on the thin pavement than on the thicker pavements. This was attributed to the failure of the thin pavement.

Rut depths were measured using straightedge and wedge, which differ from the optical levels because the reference point is not fixed and is a line that joins the two highest points over a 2-meter distance. Again, the rate of rutting was compared for the 385 and 495 single tires. The depth ratio reached 1.8 for the 100 mm pavement and reduced to 1.2 at the point of failure. The ratio for the 200 mm pavement reached 2.5 before reducing to 1.7 beyond 110,000 passes. The 200 mm pavement experienced about 40 percent less rutting with the 495 single tire than with the 385 single tire. Since no dual tires were tested in this part of the study, an attempt was made to estimate the likely outcomes for the accelerated testing with all tires.

Subgrade strain measurements were taken at the end of the trafficking and were compared to the measurements made at 2000 passes. The 100 mm pavement failed rapidly, and the strain increased by 5 times after 57,000 passes. The subgrade strain only doubled for the 200 mm pavement at 300,000 passes; however, there was significant difference between the two types of single tires.

Pavements were also monitored for signs of distress, such as cracking. The thin pavement for both tire types showed signs of distress after 15,000 passes, and the full length and width of the thin pavement was distressed after 30,000 passes. No visual signs of distress were observed for the 200 mm pavement.

Another part of this project accepted the detailed information available in regard to dynamic loading behavior with respect to the behavior of the vehicle. This study sought to link the contribution of dynamic loading by commercial vehicles to pavement wear, to quantify the relationship between profile unevenness and the deterioration caused by dynamic loading effects, and to assess any significant repeat loadings on the development of localized deterioration. This objective was accomplished by examining the loading effects of actual commercial traffic on 10 in-service flexible and flexible composite pavements with a range of profile unevenness, commercial traffic, and structural strengths. Pavement deterioration was assessed from changes in longitudinal profile and rutting, and the dynamic loading was measured using an instrumented heavy goods vehicle.

The 10 sites were surveyed using a variety of equipment. These included an instrumented five-axle articulated lorry, TRL's high-speed survey vehicle (HSV), and the falling weight deflectometer (FWD). The instrumented lorry was used to measure the spatial repeatability and amplitudes of dynamic loading. The HSV uses laser sensors and a specially programmed computer to measure profile amplitude and wheel track rut depth, and the FWD was used to collect pavement deflection data. The results of this survey indicated a small but significant link between dynamic loading and change in road roughness.

The results of this research study show significant differences between tire types, but the thin pavements tested had some bearing on these results. The subgrade strain is significantly reduced with pavement thickness, so it was concluded that the effect of tire type on subgrade strain is negligible. The results of the accelerated trafficking tests showed that the 385/65R22.5 Michelin X XZA wide-base single tire consistently produced more wear than the 495/45R22.5 Michelin Energy XDA wide-base single tire under the same conditions. The rutting behavior was the most significantly affected by differences in tire types. Based on these results, it was determined that the single tires would have produced 1.5 to 2.5 times the deformation potential of the dual tires.

TRUCK SURVEYS

Wang and Machemehl (2003) conducted a survey to characterize in-service truck configurations on Texas highways. More specifically, they sought to characterize the in-service truck tire pressures on trucks and to identify factors that might be related to differences in tire pressure. To conduct this study, a three-factor factorial experiment was designed in which the state was broken up into six geographic regions. These regions were: Lubbock-Midland, Dallas, Houston, San Antonio-Austin, Corpus Christi, and the border areas. Also considered were two highway classes and two highway directions. A total of 623 trucks, classified according to the FHWA Truck Size and Weight Codes, were selected for the truck configuration survey and were tested for tire inflation pressure, tire temperature, tire size, and tire manufacturer.

Laboratory experiments and linear regressions were conducted on the data collected to establish the relationship between tire inflation pressure and tire temperature. The relationship determined by researchers is given by the following equation:

$$P_2 = P_1 + 0.22\,(T_2 - T_1) \quad \text{(A9)}$$

where P_1 and P_2 are tire inflation pressures in psi corresponding, respectively, to tire temperatures T_1 and T_2 in °F.

This study sought to characterize truck tire pressures across Texas and to verify if tire pressures were related to factors like geographic area, highway class, and highway direction. However, since tire temperature is directly affected by air and pavement temperatures, it was necessary to correct the tire pressure data to a standard temperature of 60 °C (140 °F) in order to characterize the relationship between tire pressure and tire temperature. In order to do this, researchers used the following equations:

$$P_2 = P_1 + \alpha \Delta T \quad \text{(A10)}$$

$$\alpha = \frac{P_1}{T_1} = \frac{n R}{V} \quad \text{(A11)}$$

where:

R = ideal gas constant,

P_1 = gas pressure in atmospheres,

T_1 = absolute gas temperature in °K,

V = gas volume in liters,

N = number of gas molecules in moles, and

α = coefficient of the relationship between pressure and temperature.

To obtain values for α, inflated truck tires were tested at different temperatures in the laboratory, and a linear regression was run using the temperature and pressure data. The average α was found to be 2.73 kPa/°C.

A *t*-test was conducted to check whether there is a significant difference in tire inflation pressures between loaded and empty trucks. Table A1 shows the results of this test. The results indicate a significant difference in tire inflation pressures between loaded and empty trucks.

A *t*-test was also conducted on the effect of highway direction versus truck tire pressure. No significant differences were found. The effect of geographic region was found to match with the 1986 survey conducted by Roberts et al. Geographic regions were ranked in ascending order as follows: Border, San Antonio-Austin, Houston, Dallas, Corpus Christi, and Lubbock-Midland.

Table A1. Summary of *t*-test on Difference in Truck Tire Inflation Pressures between Loaded and Empty Trucks (Wang and Machemehl, 2000).

Test Group	Sample Size	Mean (kPa)	Standard Dev. (kPa)	Test Statistics	
435 loaded trucks	435 trucks	756.9	60.2	t=6.90	$Z_{95\%}$=1.96
169 empty trucks	169 trucks	718.2	69.1		

A one-way analysis of variance (ANOVA) was conducted for the comparison of border and non-border areas with respect to truck tire inflation pressure. The results of this test (Table A2) show a significant difference in tire inflation pressures between border and non-border areas, as indicated from the very small *p*-value given in the table. The low tire pressures in the border areas could be attributed to the North American Free Trade Agreement, which prohibits Mexican trucks from operating in the United States. More than 50 percent of the trucks selected in the border areas were empty.

A two-way ANOVA test was conducted to evaluate the effect of geographic area and highway class on truck tire inflation pressures. The results (Table A3) show the effects of geographic area and highway class to be significant, indicating that trucks in different geographical areas had different tire inflation pressures, and similarly for trucks in different highway classes.

A comparison was also made among the five axles of 500 3-S2 trucks selected using a one-way ANOVA. All tires of the same axle were pooled and averaged to represent the axle tire inflation pressure. The test results given in Table A4 show a significant difference among the five axles of the 3-S2s. The most significant of these results is that the first axle, which is the steering, possessed a much higher axle tire inflation pressure than the other four. Also, axles 2 and 3, which are the drive axles, possessed almost the same mean and variance values. Axles 4 and 5, which are the trailer axles, were different, but many of the trailers surveyed had a different license plate number than the tractor and were poorly maintained.

The study concluded that factors such as axle weight, tire temperature, geographic area, highway class, and axle type are related to tire inflation pressure. The results also suggest that trucks operating with high axle weights over long-haul distances traveling interstate highways with high operating temperatures will have higher tire inflation pressures in particular geographic areas. Lastly, it was determined that the steering axles have the highest tire inflation pressures of all the truck axles.

Table A2. One-Way ANOVA Results from Test of Difference in Tire Inflation Pressures between Border and Non-Border Areas (Wang and Machemehl, 2000).

Factor	Sample Size	Mean (kPa)	Standard Dev. (kPa)	Test Statistics	
Non-border areas	483 trucks	759.9	52.4	$F = 126.35$	$p = 0.000$
Border areas	140 trucks	695.9	78.7		

Table A3. Two-Way ANOVA Results for Geographic Area and Highway Class (Wang and Machemehl, 2000).

Factor	Test Statistics	
Geographic Area	$F = 11.58$	$p = 0.000$
Highway Class	$F = 14.74$	$p = 0.000$
Area × Highway Class	$F = 6.77$	$p = 0.000$

Table A4. One-way ANOVA Results for Different Truck Axles (Wang and Machemehl, 2000).

Axle	Sample Size	Mean (kPa)	Standard Dev. (kPa)	Test Statistics	
1	499 axles	785.7	71.7	$F = 23.54$	$p = 0.000$
2	500 axles	751.3	73.5		
3	498 axles	750.4	72.4		
4	491 axles	752.9	78.9		
5	491 axles	743.6	83.4		

APPENDIX B

LONGITUDINAL SURFACE PROFILES OF HIGHWAY LANES TESTED WITH INERTIAL PROFILER

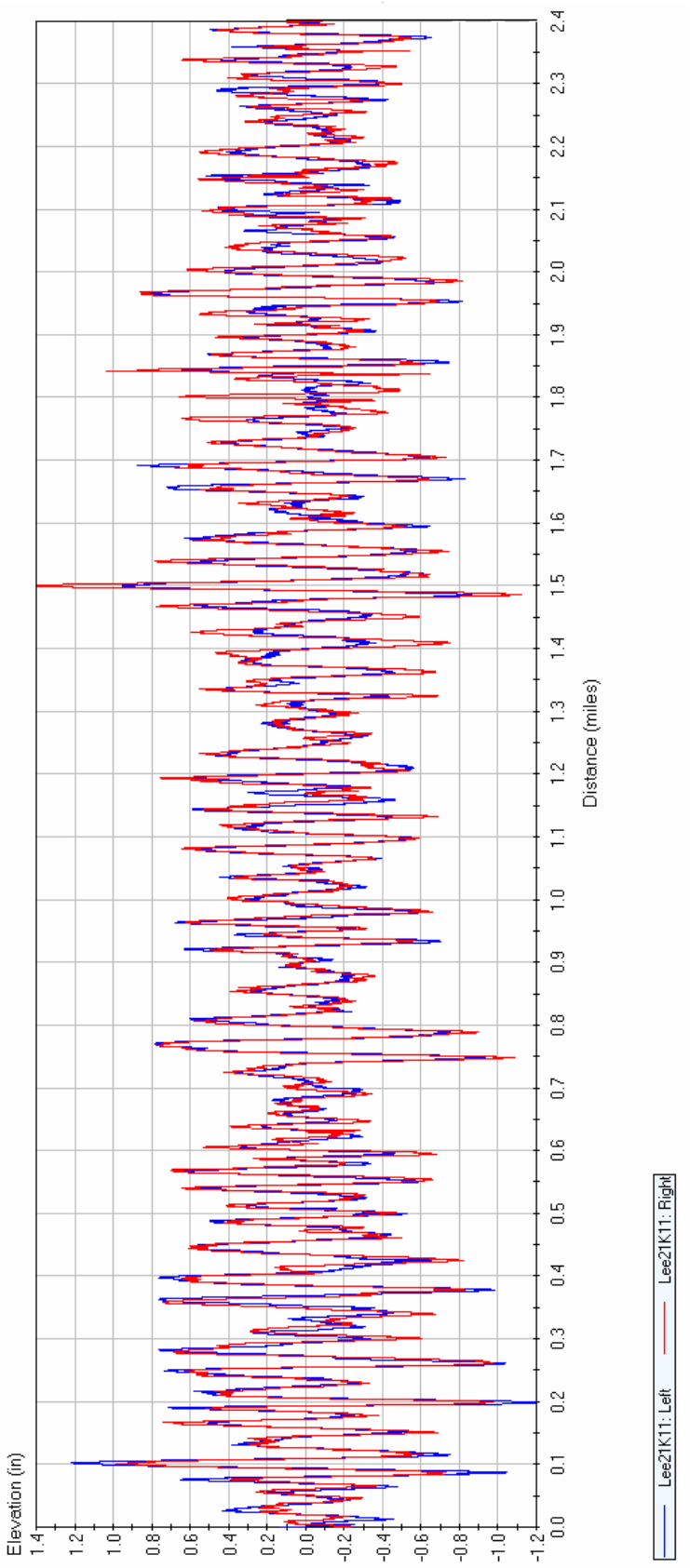

Figure B1. Measured Profiles on K1 Lane of SH21 Project in Lee County.

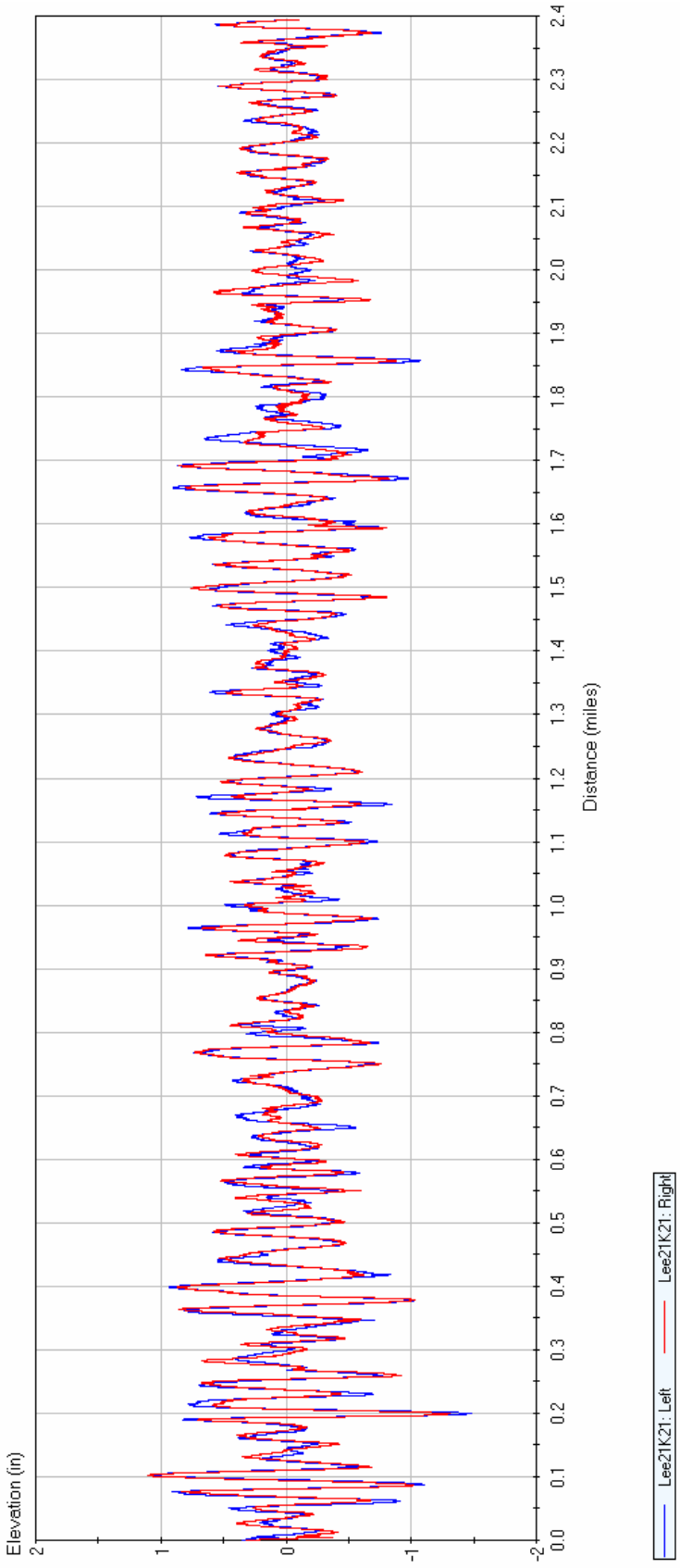

Figure B2. Measured Profiles on K2 Lane of SH21 Project in Lee County.

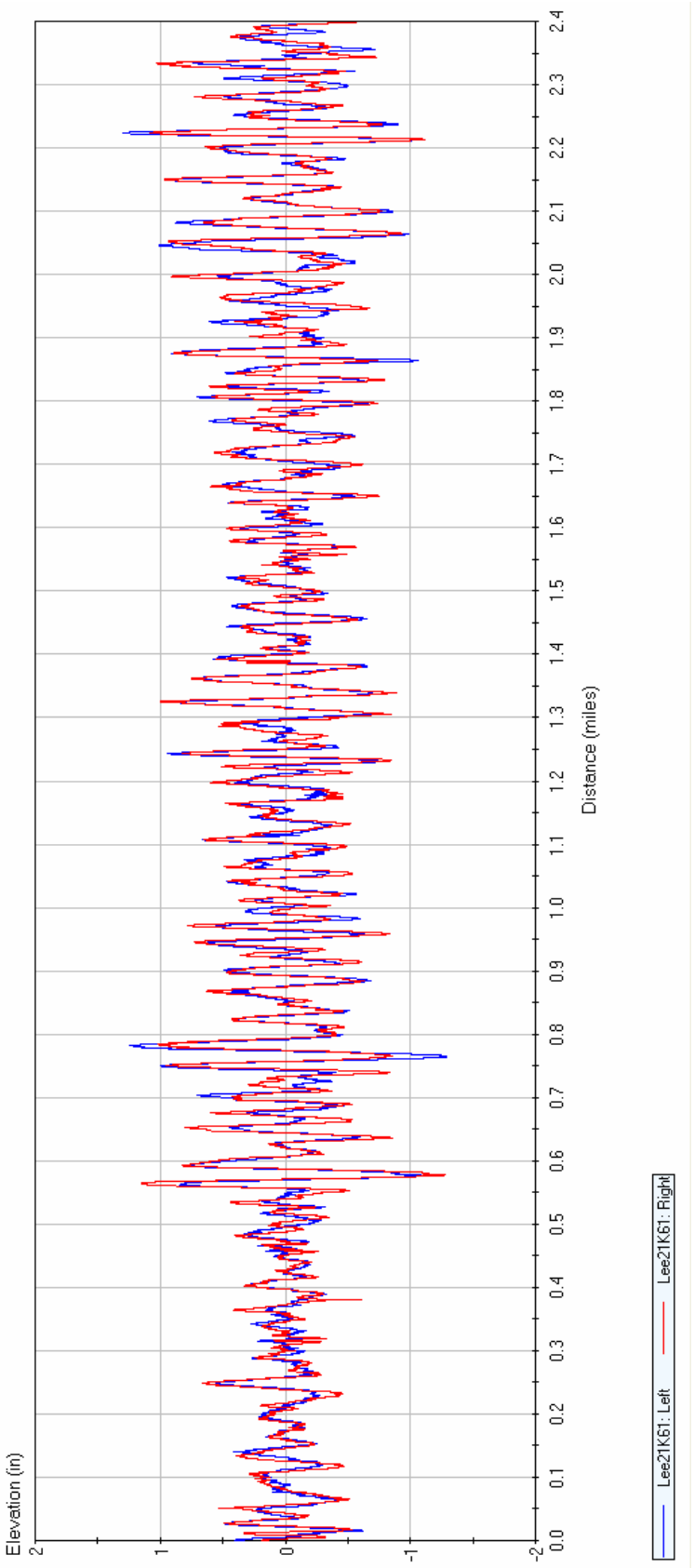

Figure B3. Measured Profiles on K6 Lane of SH21 Project in Lee County.

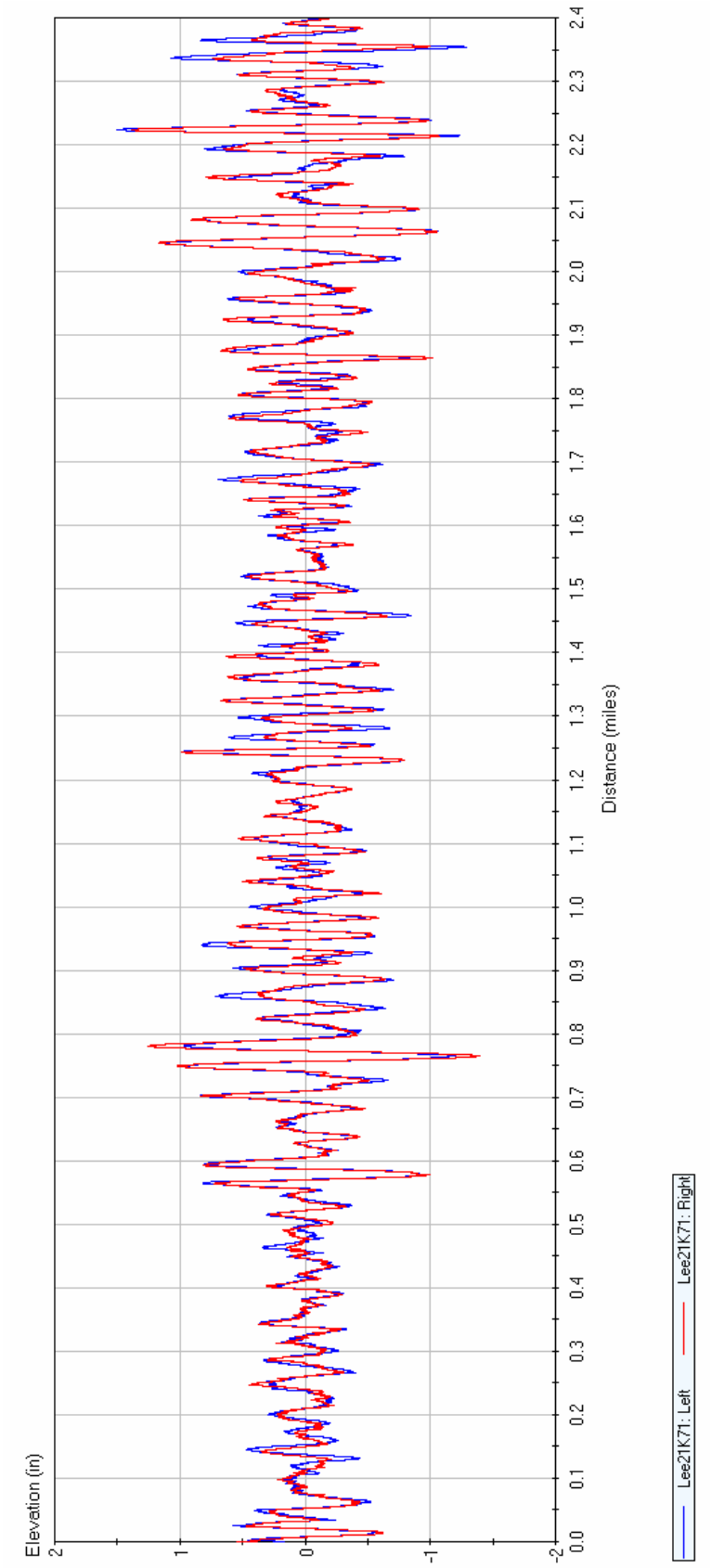

Figure B4. Measured Profiles on K7 Lane of SH21 Project in Lee County.

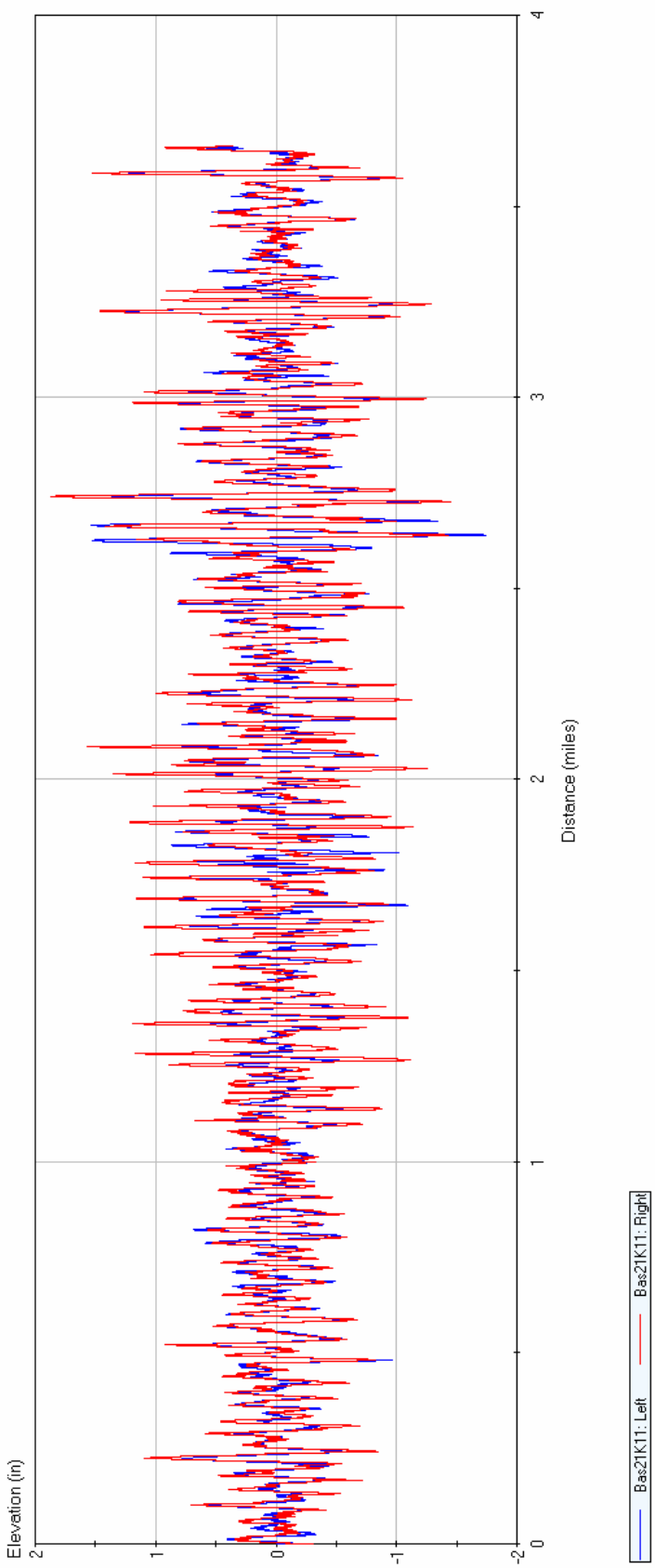

Figure B5. Measured Profiles on K1 Lane of SH21 Project in Bastrop County.

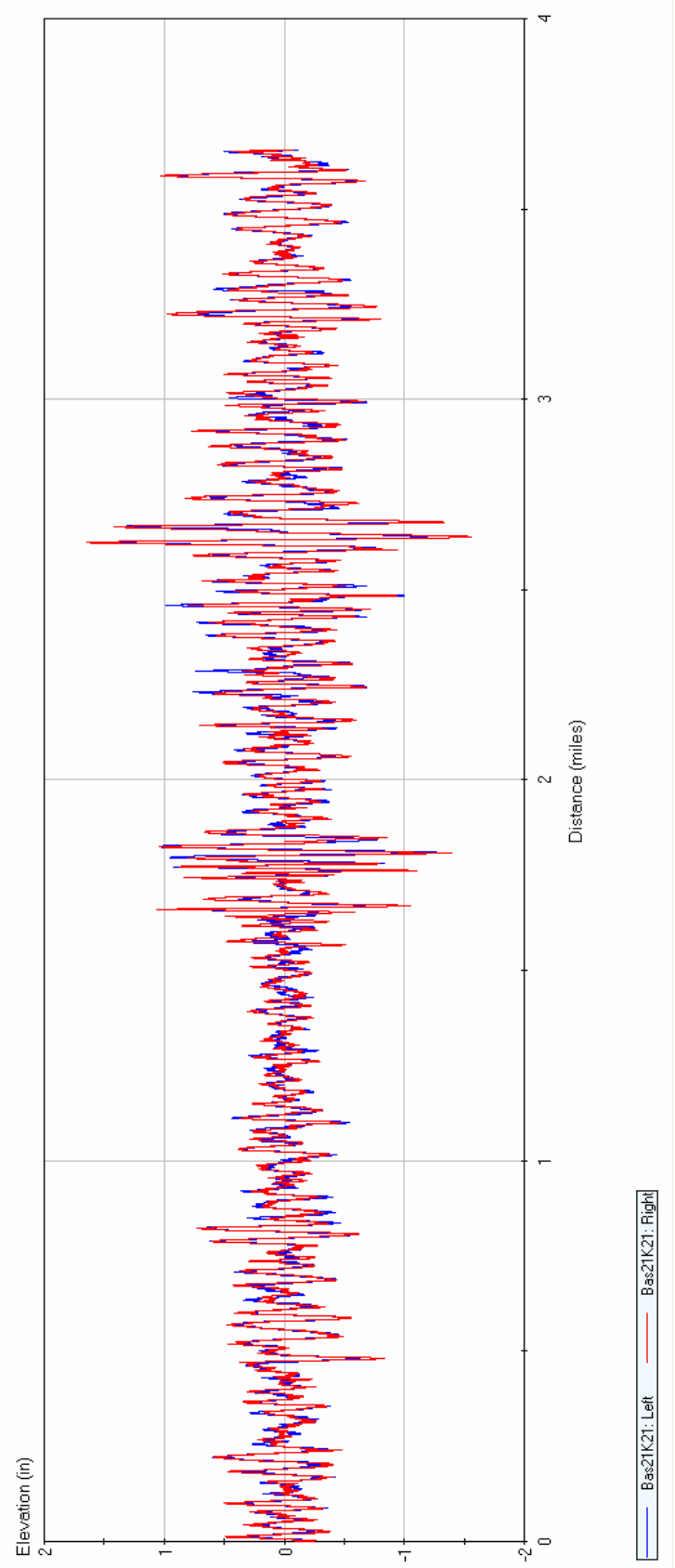

Figure B6. Measured Profiles on K2 Lane of SH21 Project in Bastrop County.

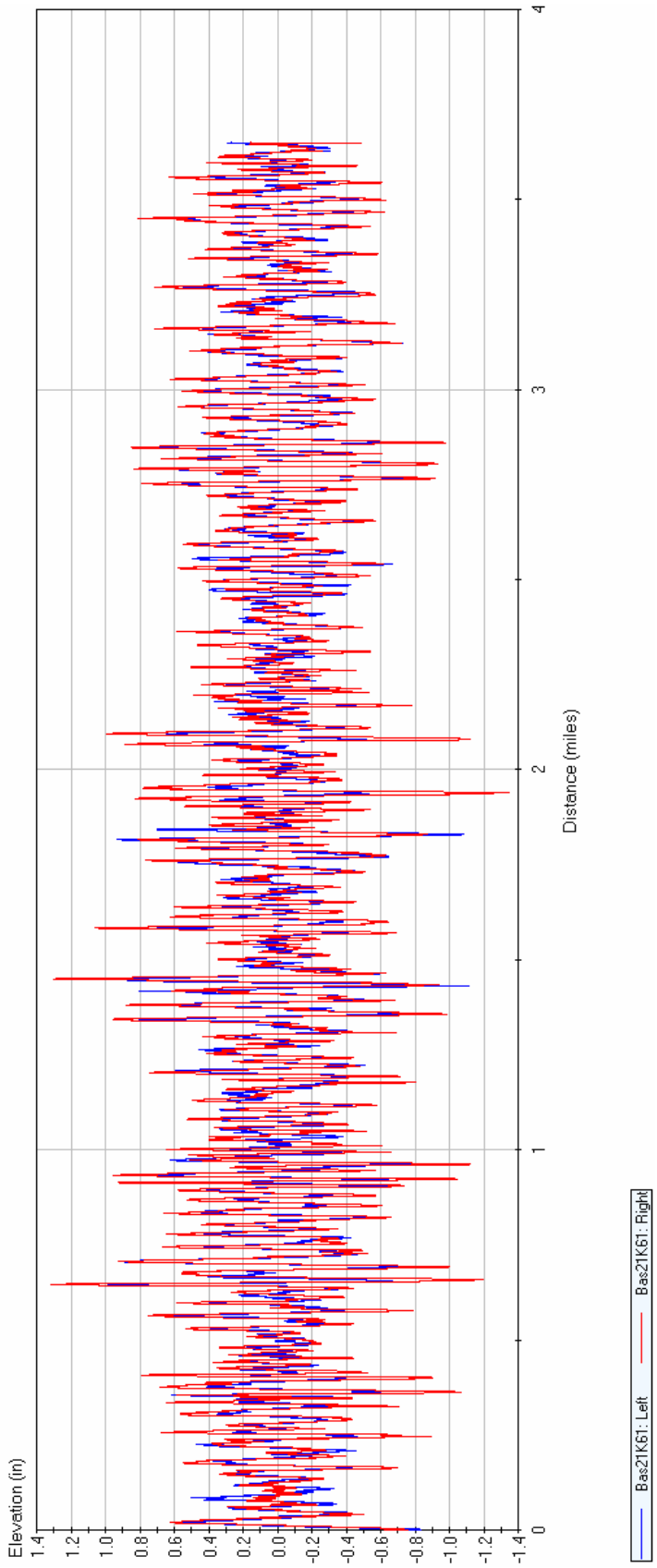

Figure B7. Measured Profiles on K6 Lane of SH21 Project in Bastrop County.

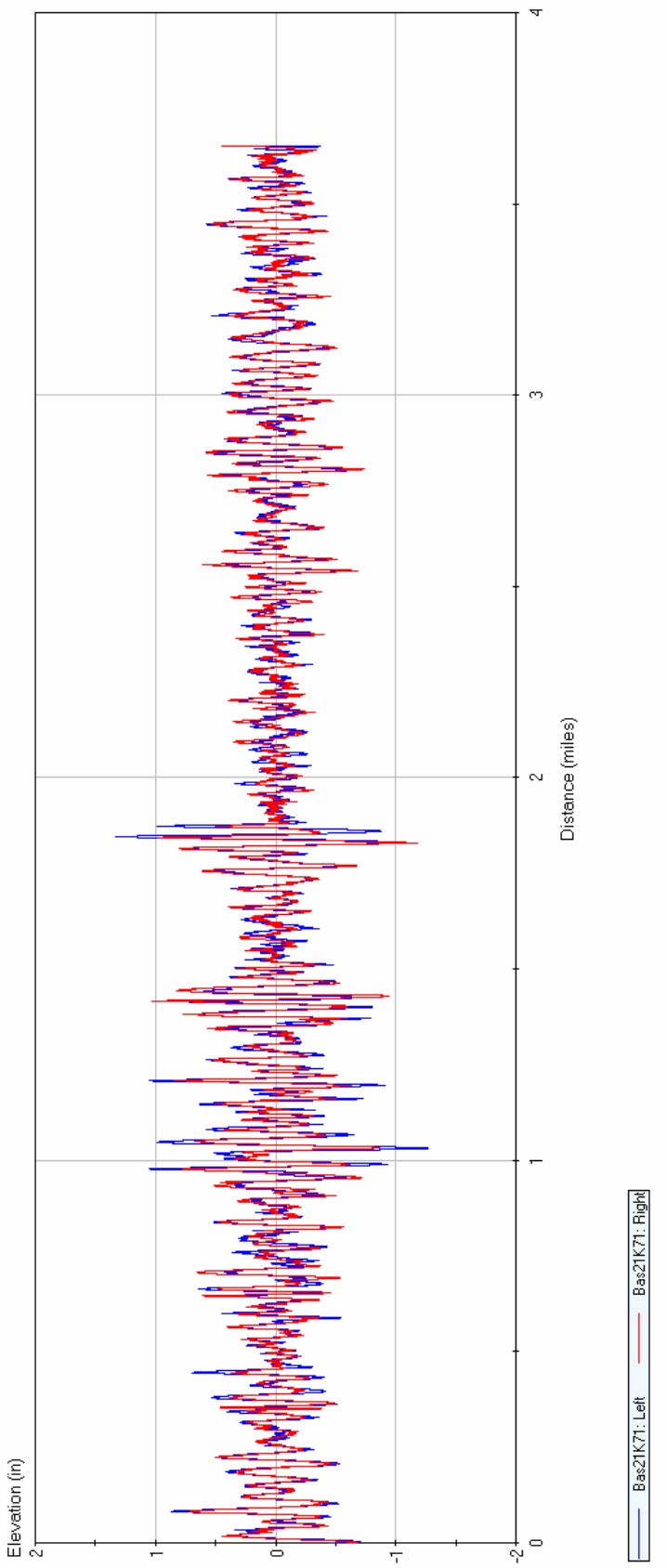

Figure B8. Measured Profiles on K7 Lane of SH21 Project in Bastrop County.

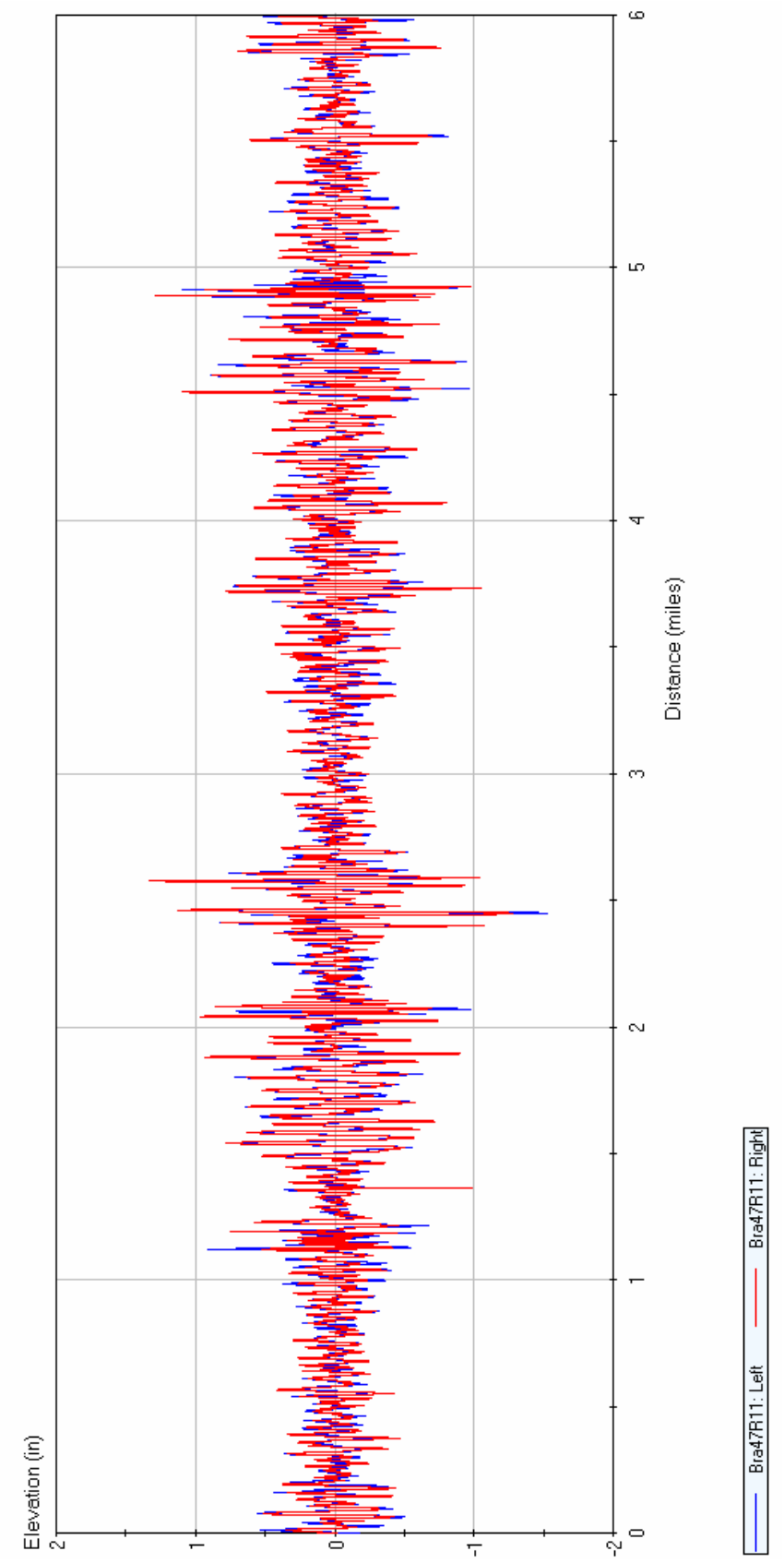

Figure B9. Measured Profiles on R1 Lane of SH47 in Brazos County.

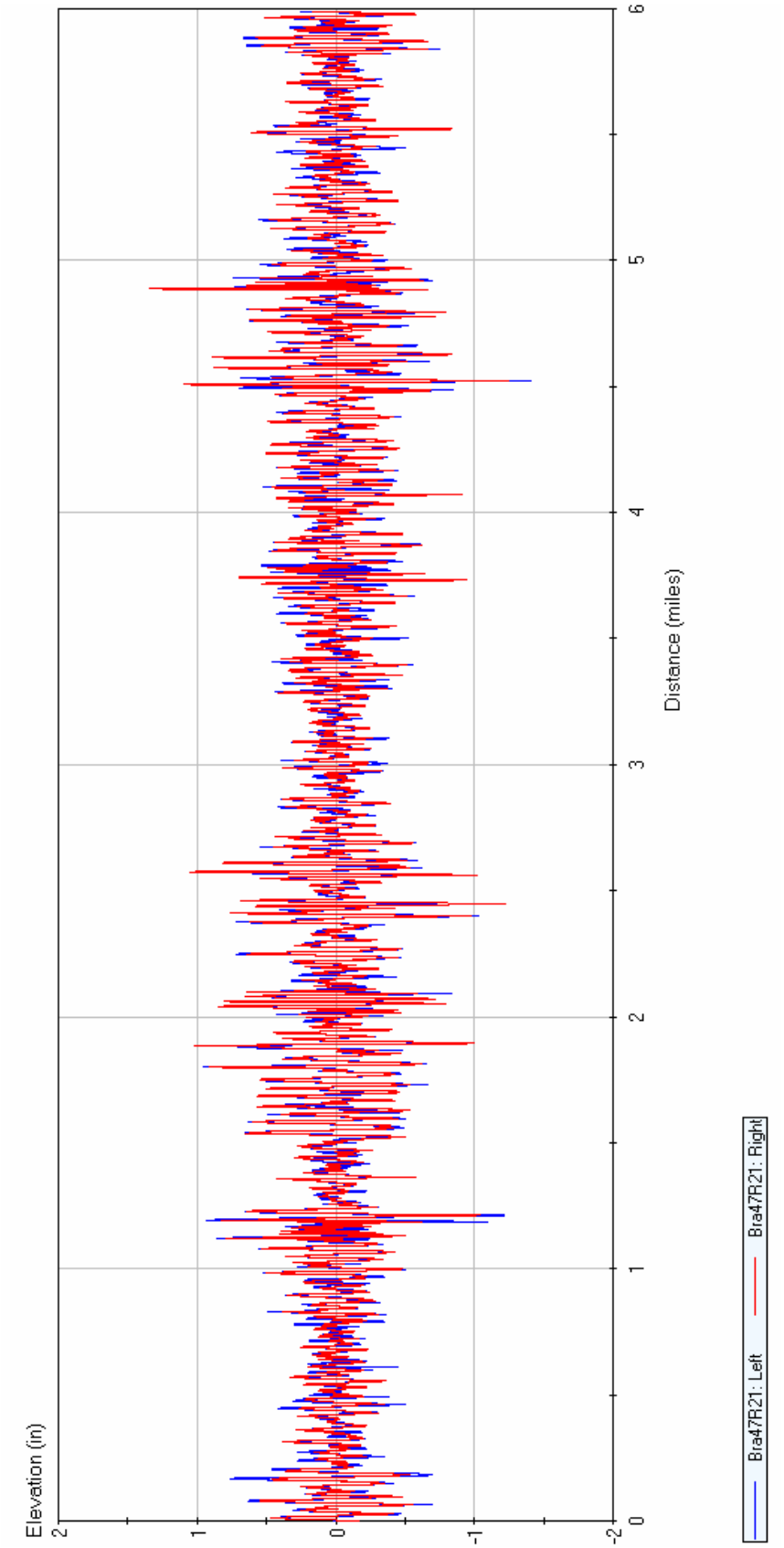

Figure B10. Measured Profiles on R2 Lane of SH47 in Brazos County.

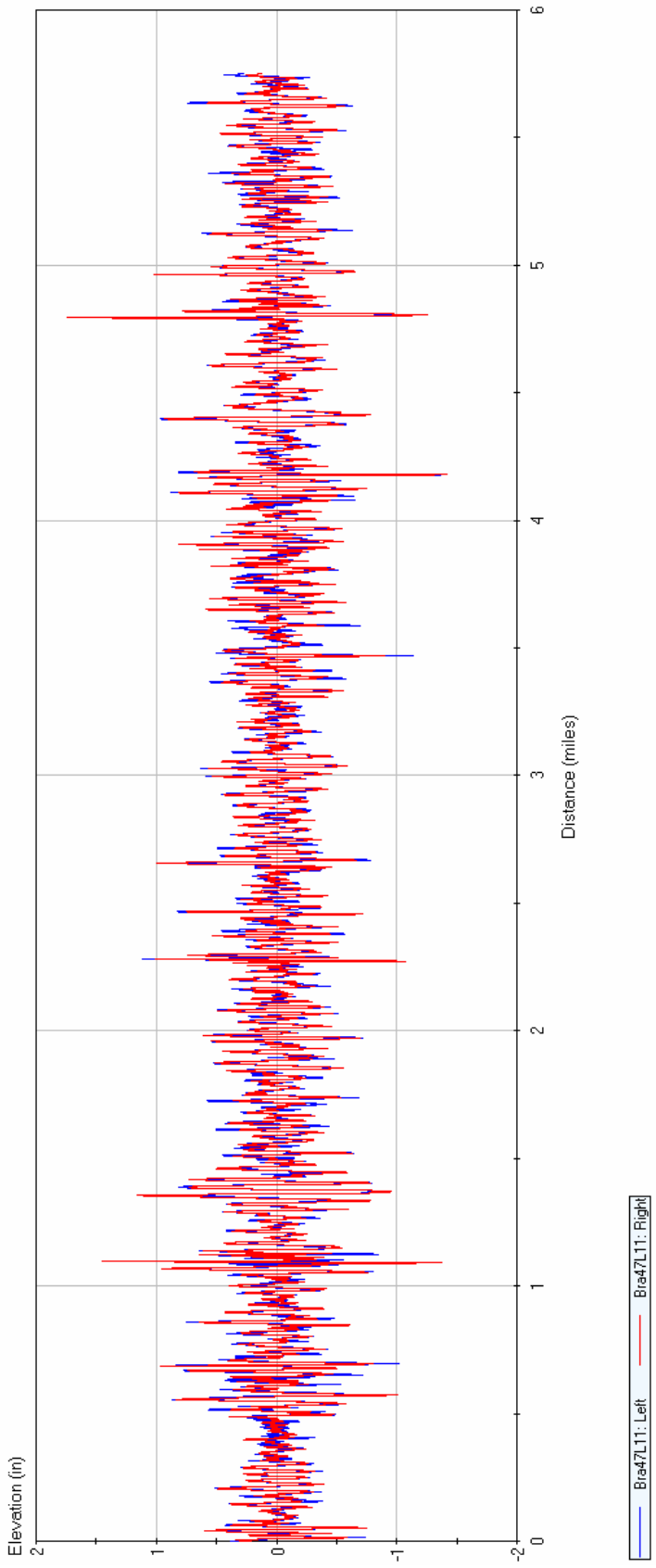

Figure B11. Measured Profiles on L1 Lane of SH47 in Brazos County.

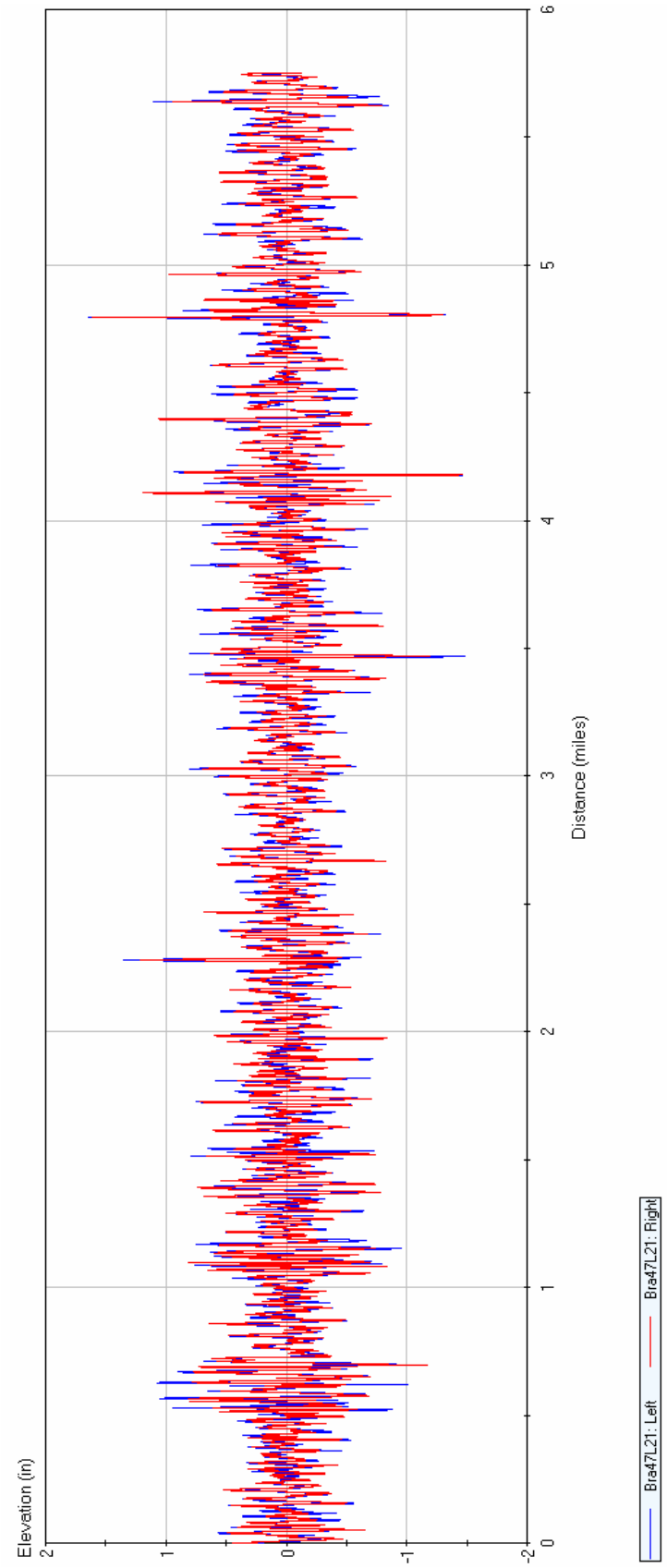

Figure B12. Measured Profiles on L2 Lane of SH47 in Brazos County.

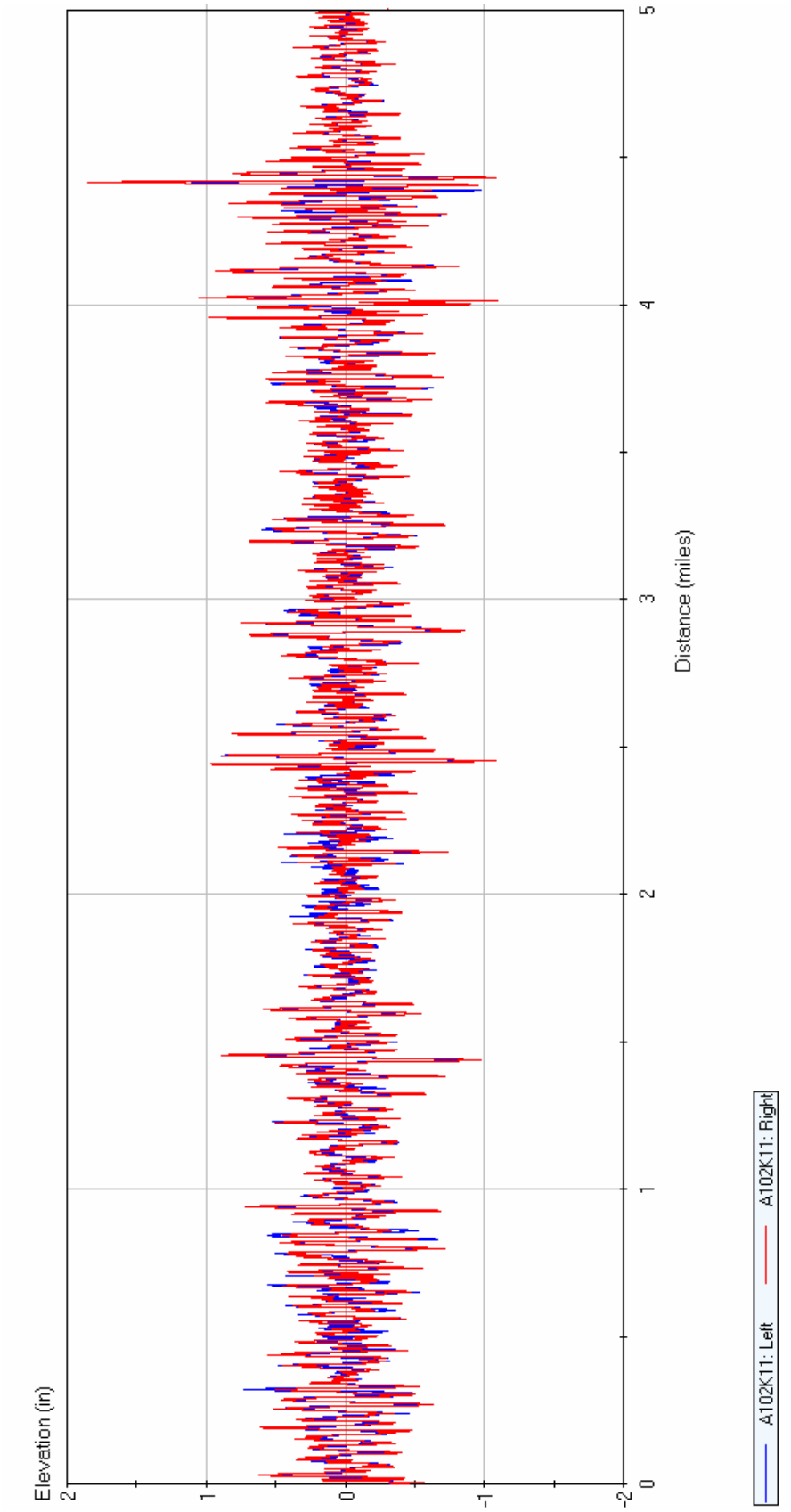

Figure B13. K1 Lane Profiles along FM102 Project in Wharton County (Group A).

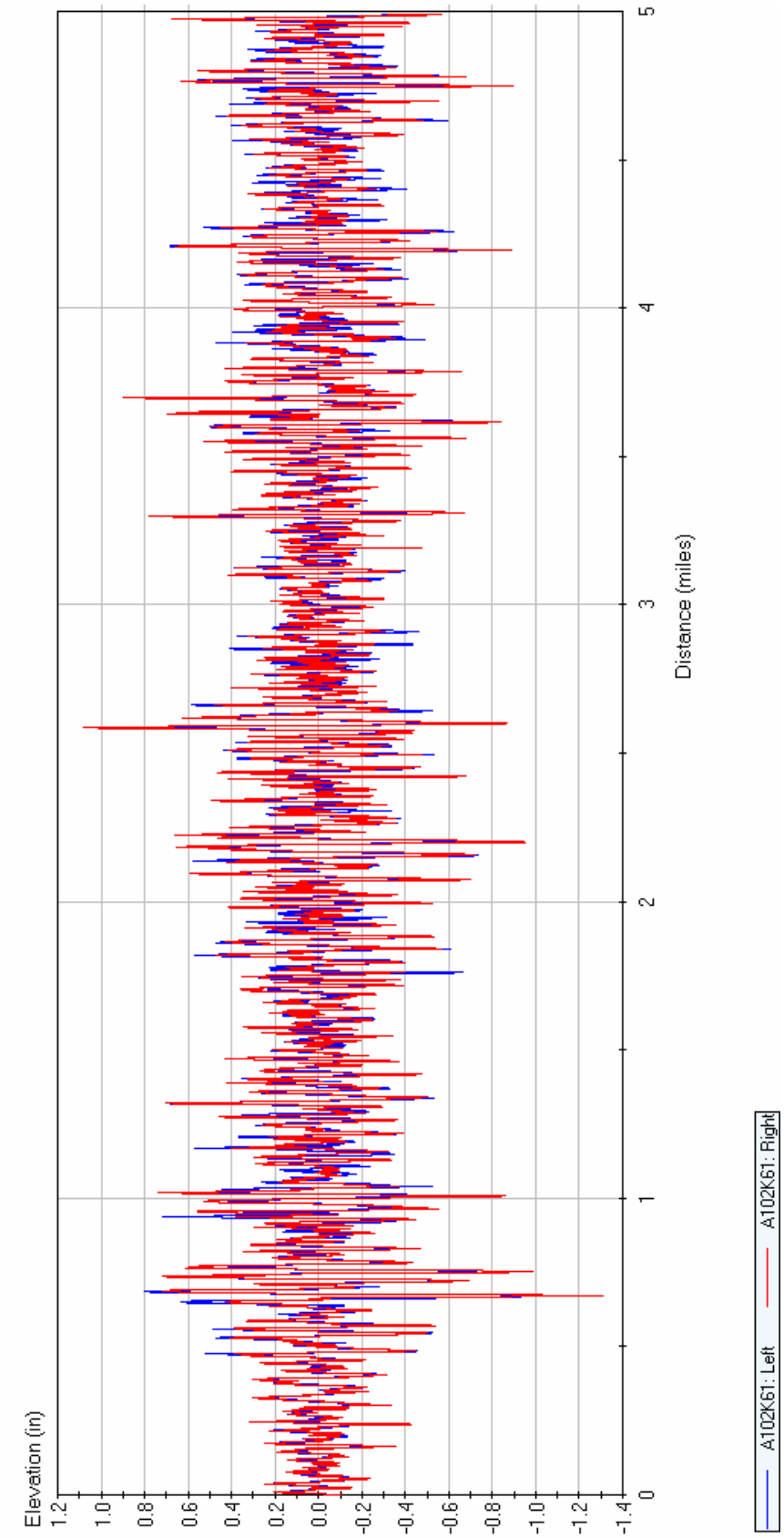

Figure B14. K6 Lane Profiles along FM102 Project in Wharton County (Group A).

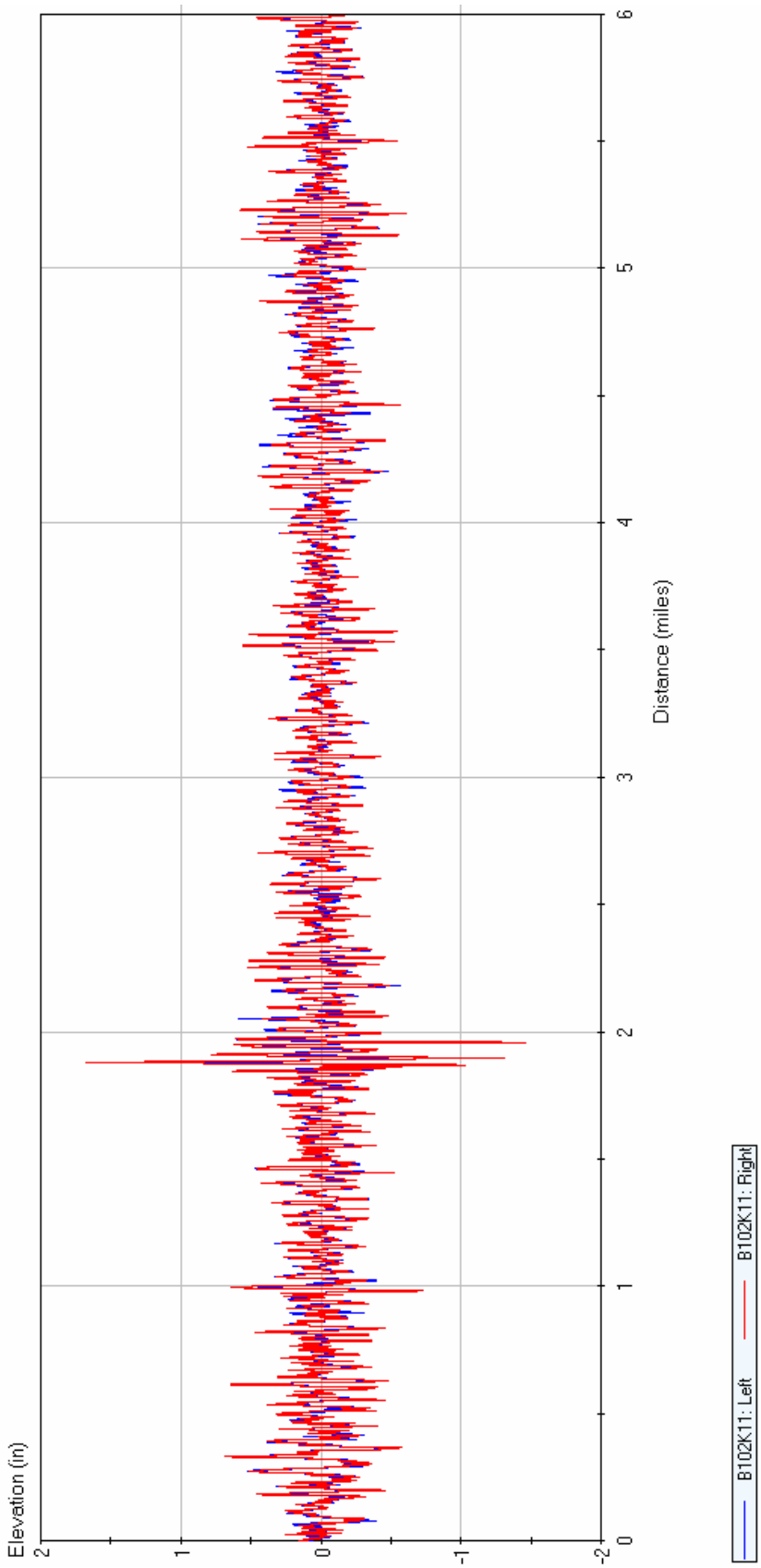

Figure B15. K1 Lane Profiles along FM102 Project in Wharton County (Group B).

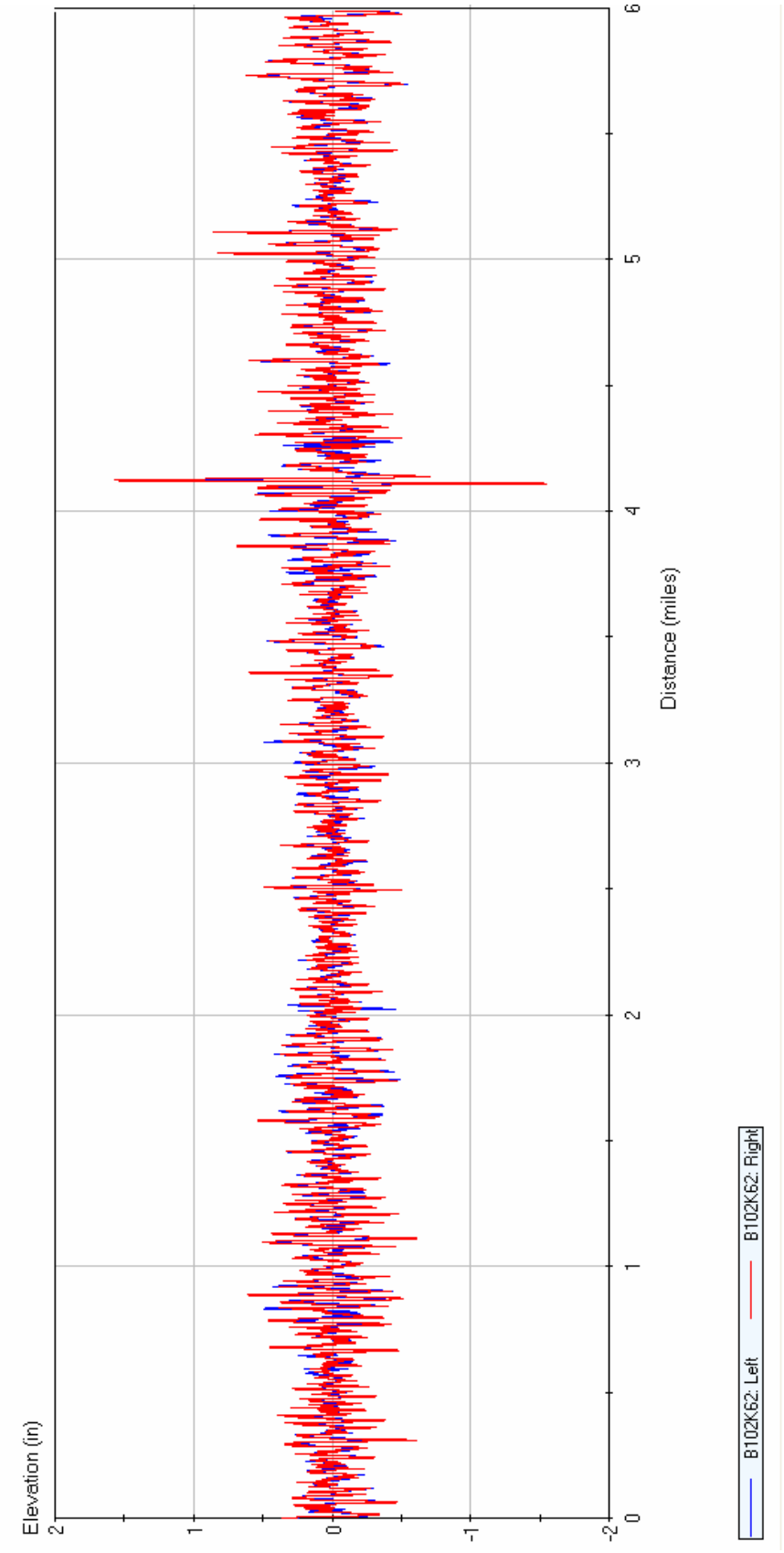

Figure B16. K6 Lane Profiles along FM102 Project in Wharton County (Group B).

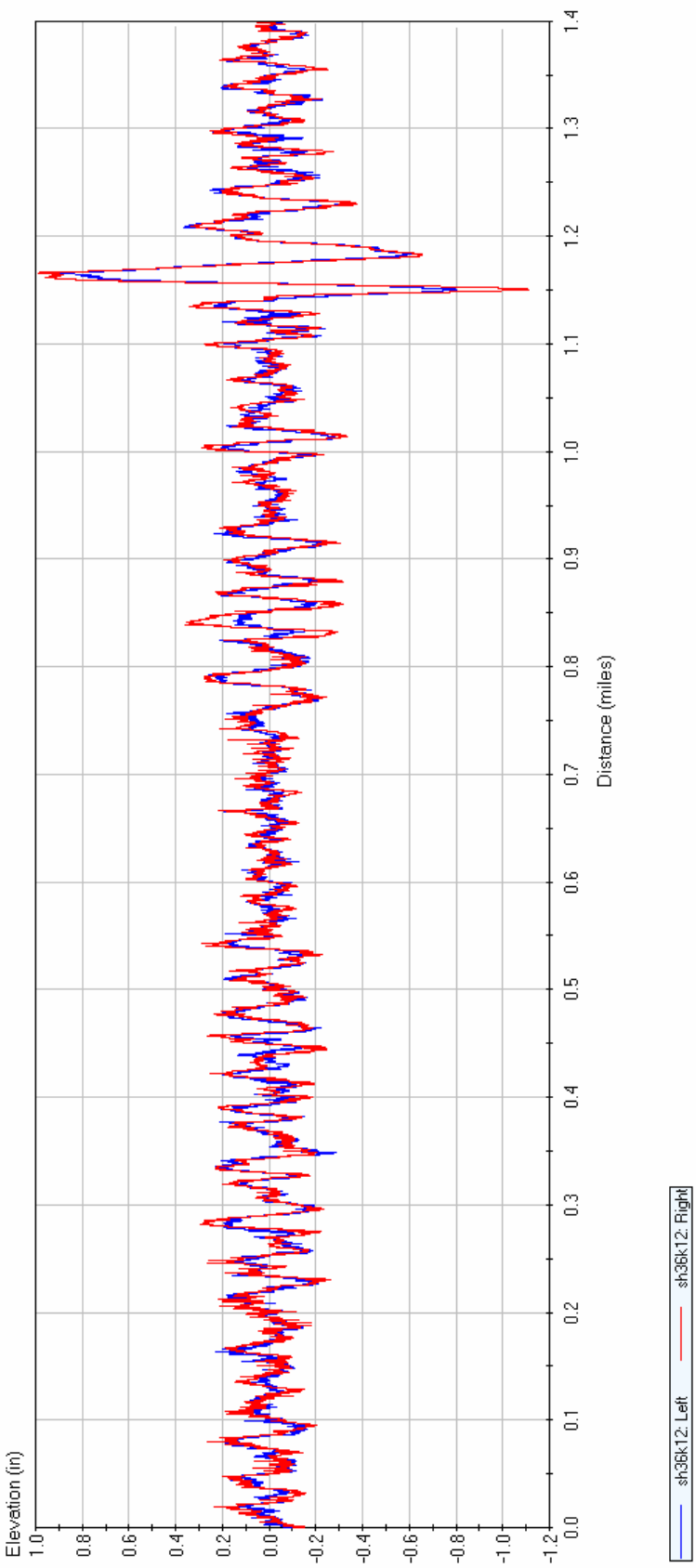

Figure B17. Measured Profiles along K1 Lane of SH36 Project in Fort Bend County.

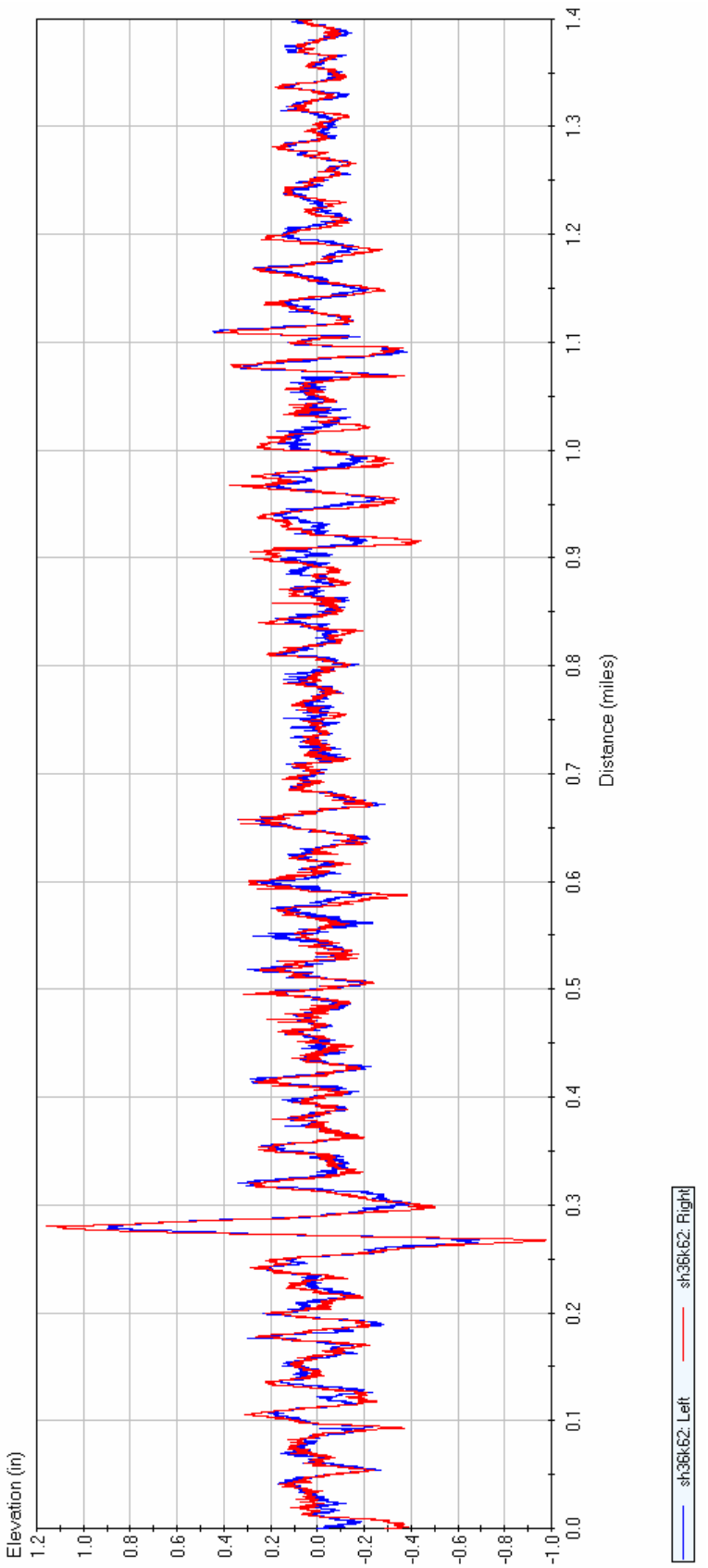

Figure B18. Measured Profiles along K2 Lane of SH36 Project in Fort Bend County.

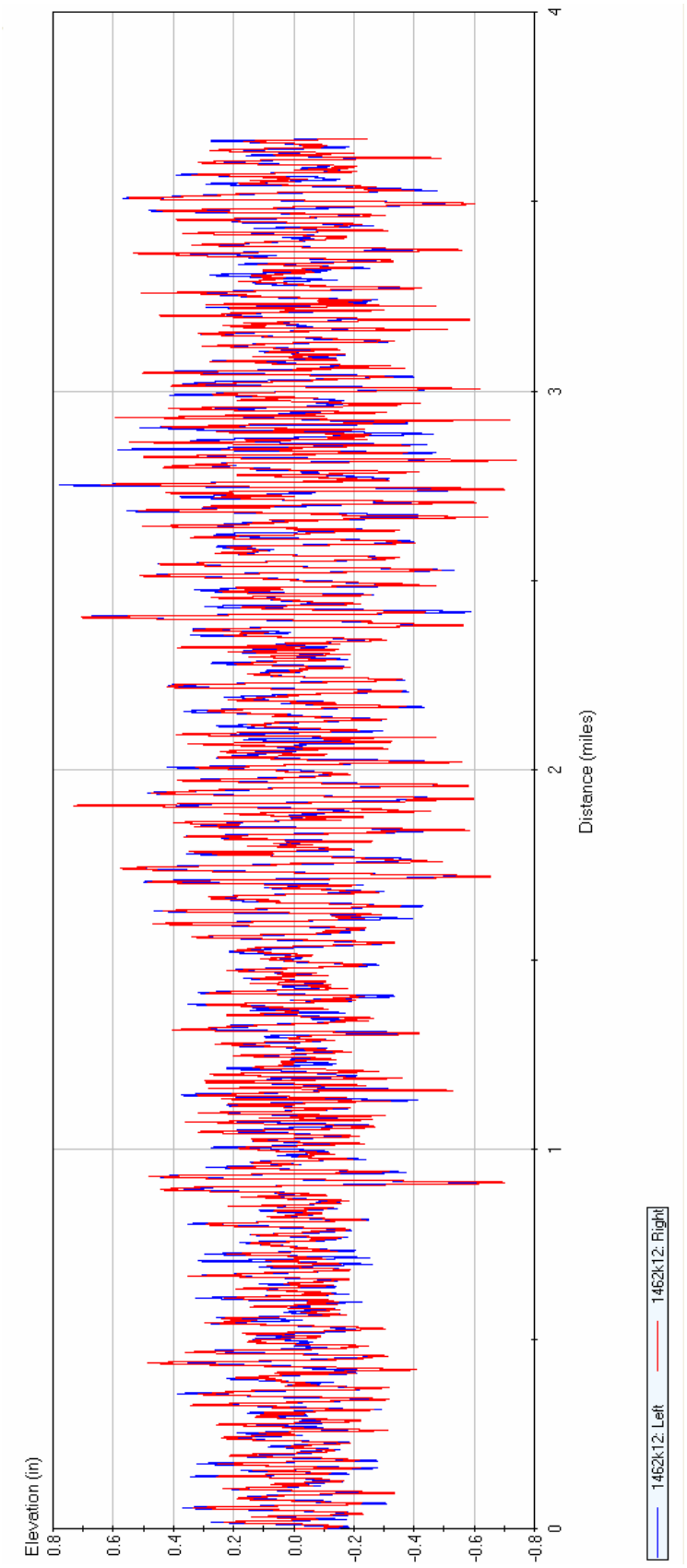

Figure B19. Measured Profiles along K1 Lane of FM1462 Project in Fort Bend County.

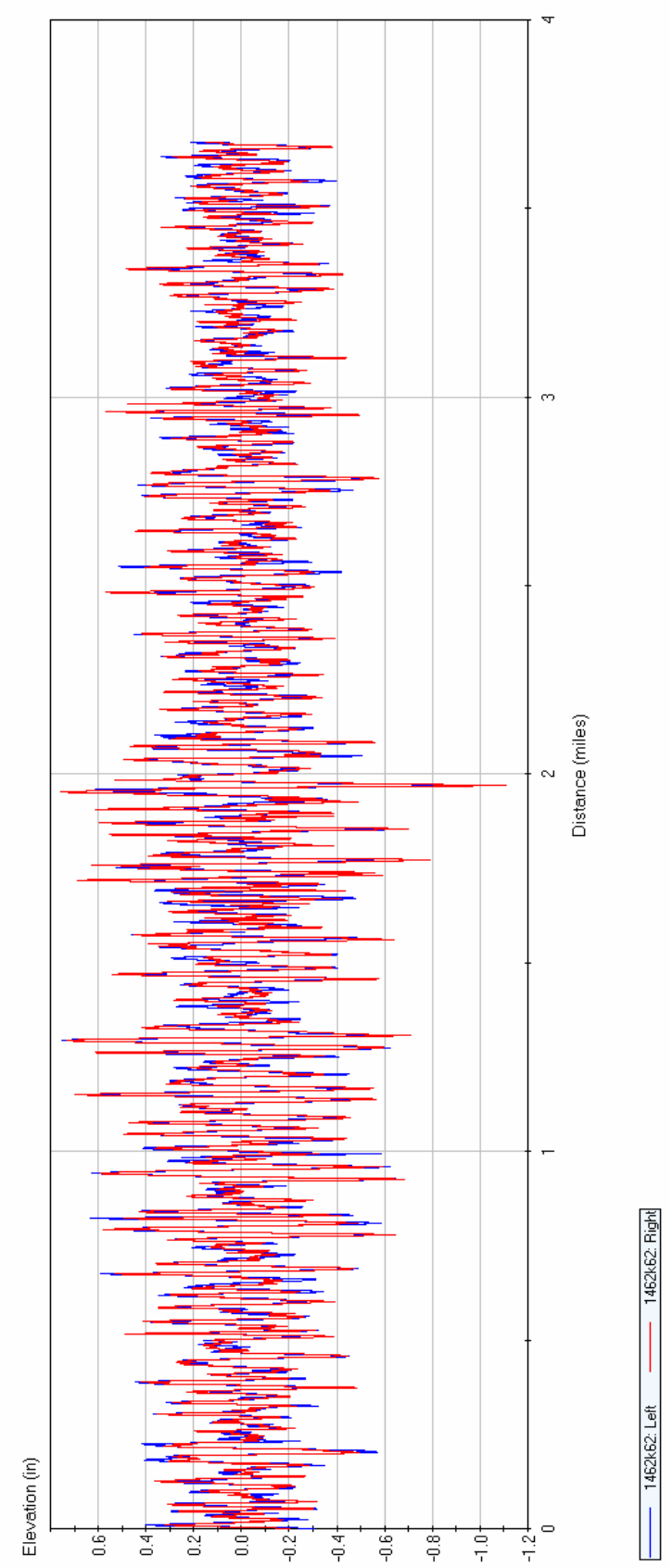

Figure B20. Measured Profiles along K6 Lane of FM1462 Project in Fort Bend County.

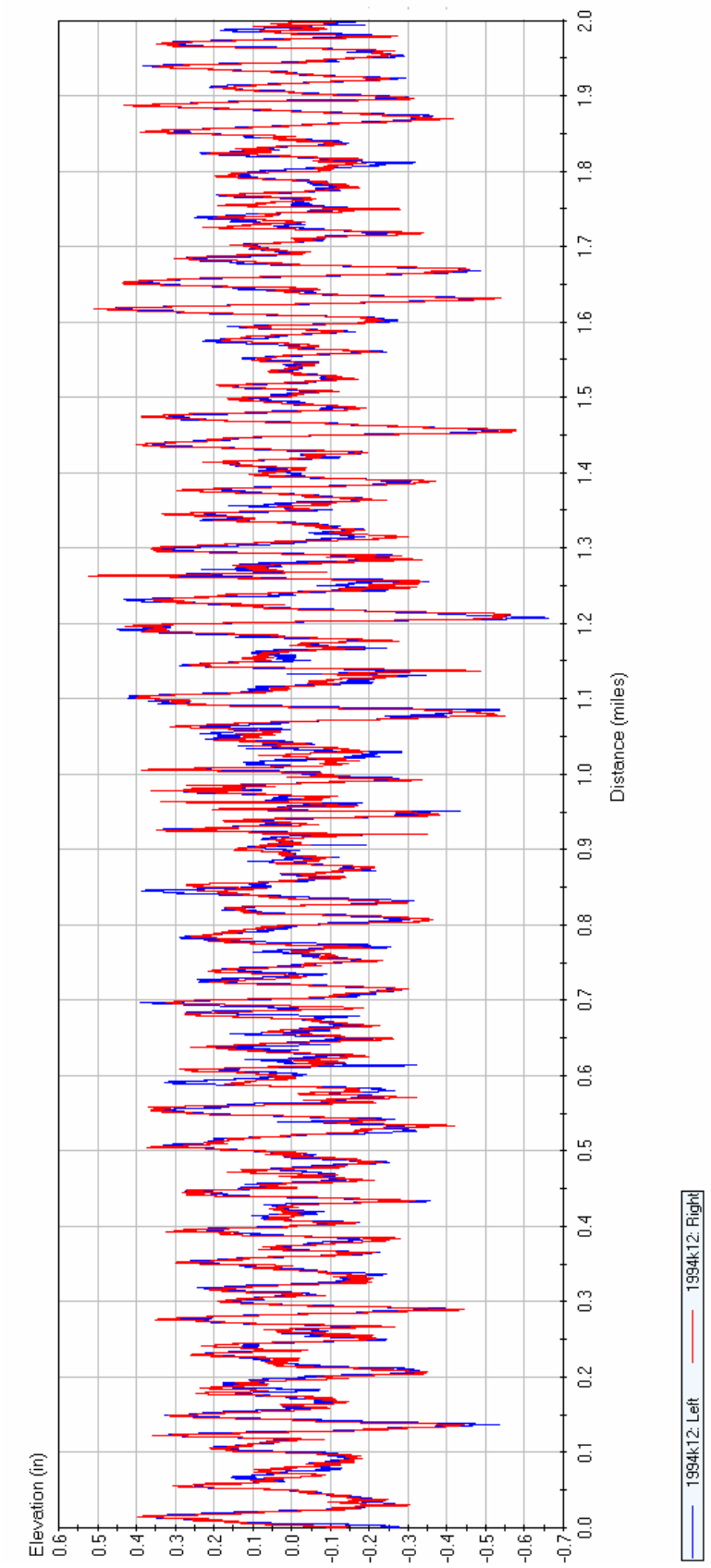

Figure B21. Measured Profiles along K1 Lane of FM1994 Project in Fort Bend County.

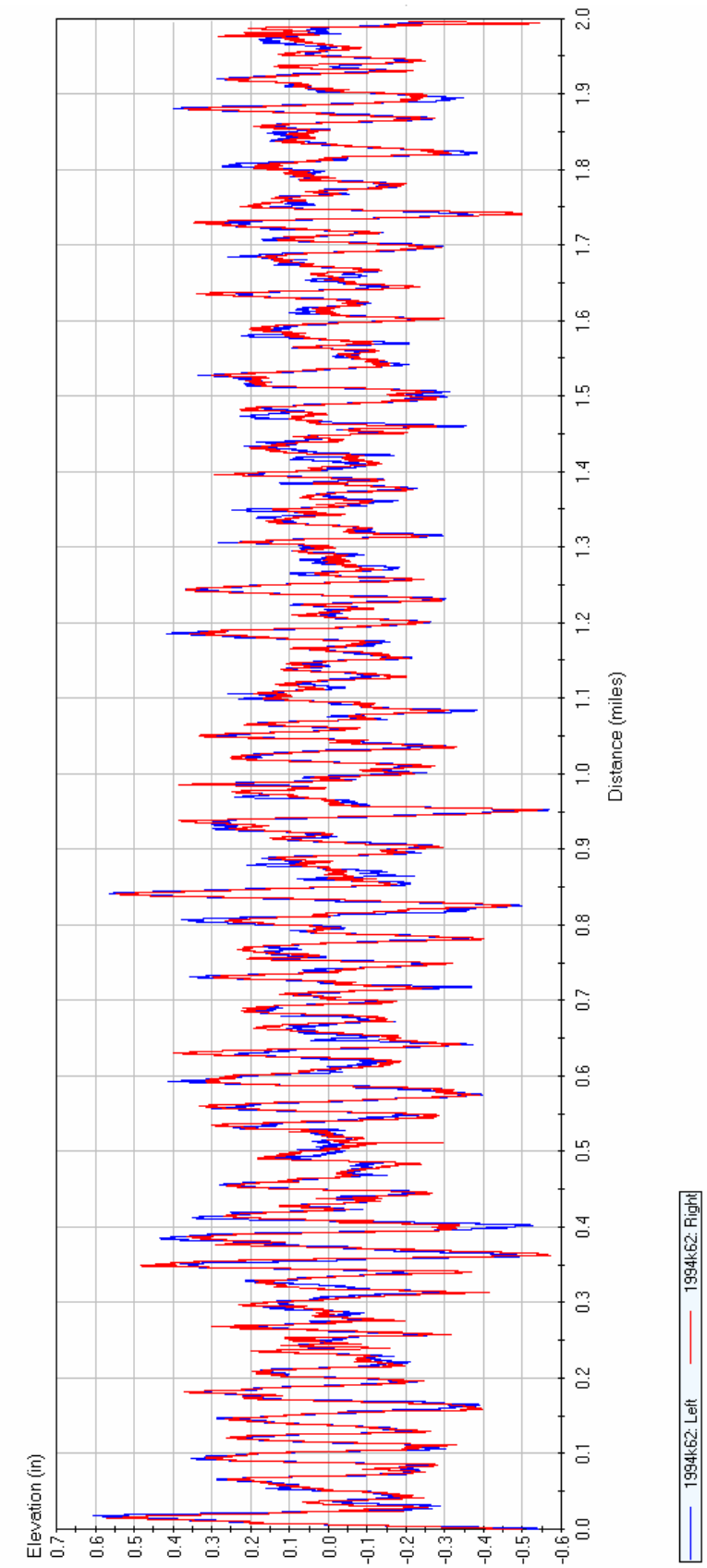

Figure B22. Measured Profiles along K6 Lane of FM1994 Project in Fort Bend County.

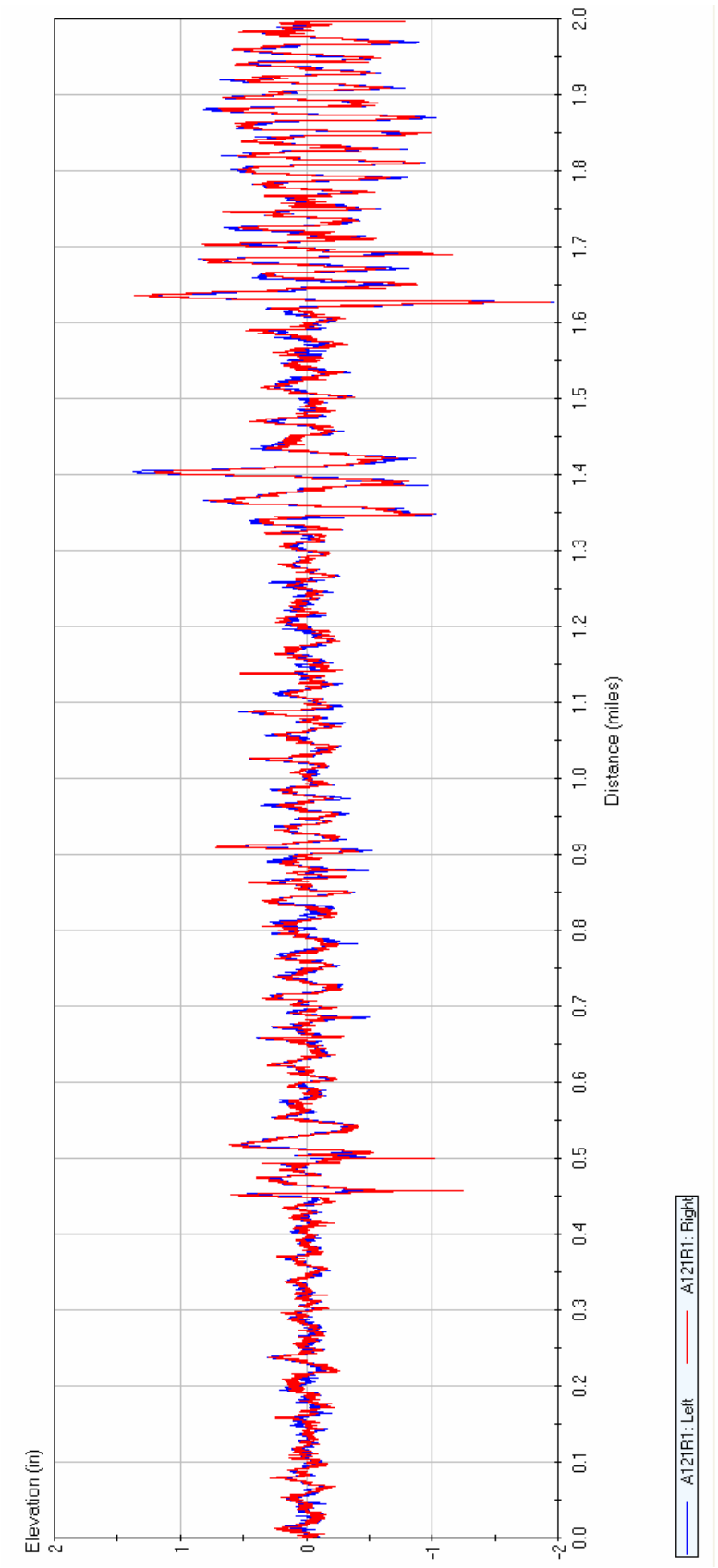

Figure B23. R1 Lane Profiles along SH121 Project in Denton County (Group A).

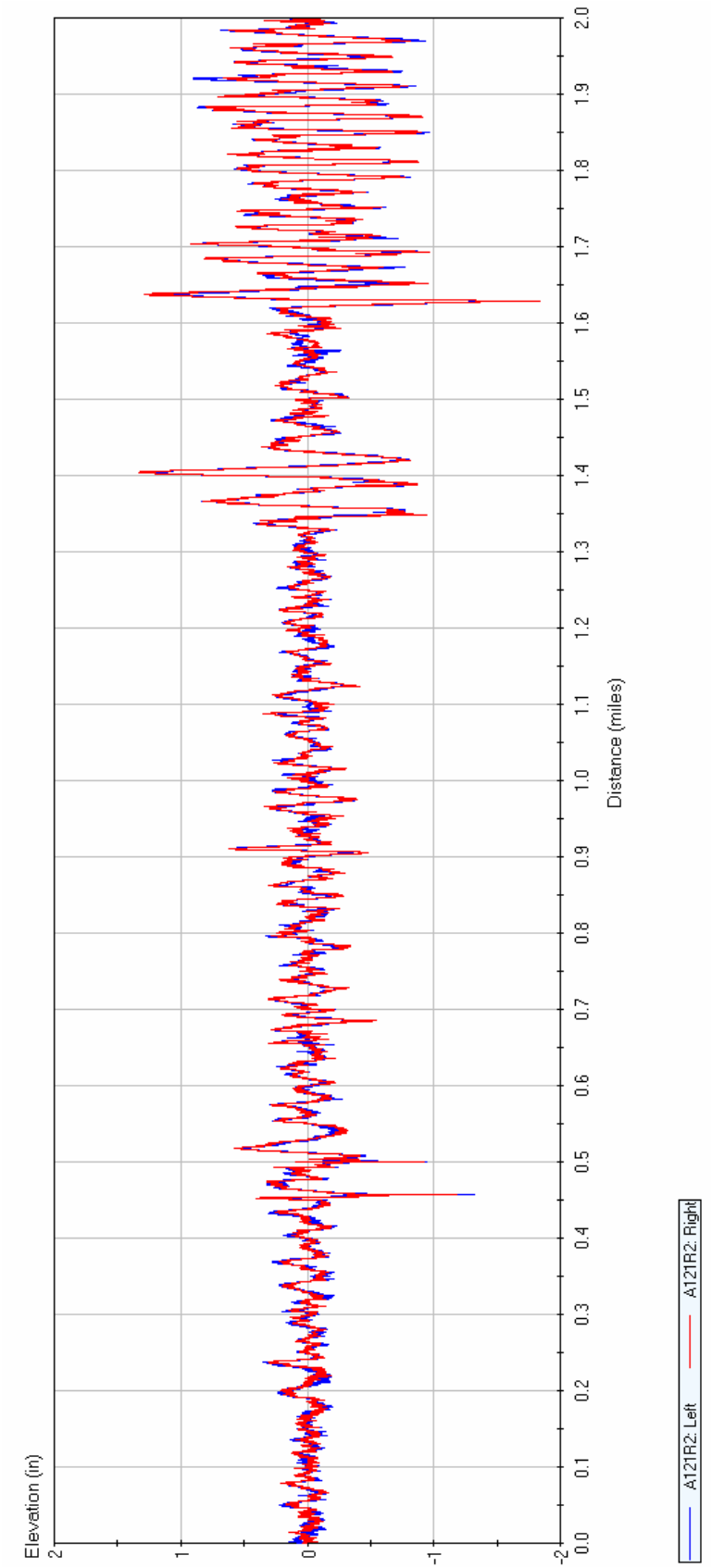

Figure B24. R2 Lane Profiles along SH121 Project in Denton County (Group A).

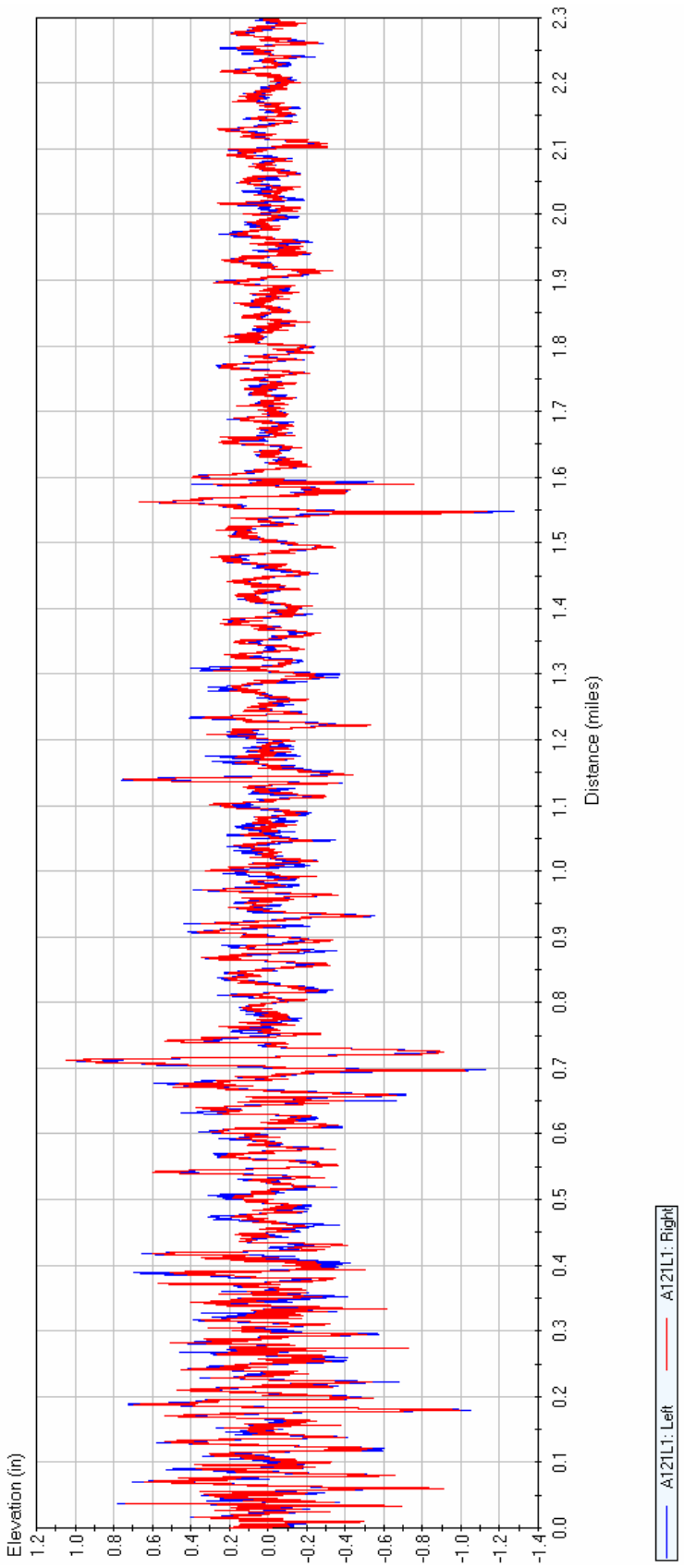

Figure B25. L1 Lane Profiles along SH121 Project in Denton County (Group B).

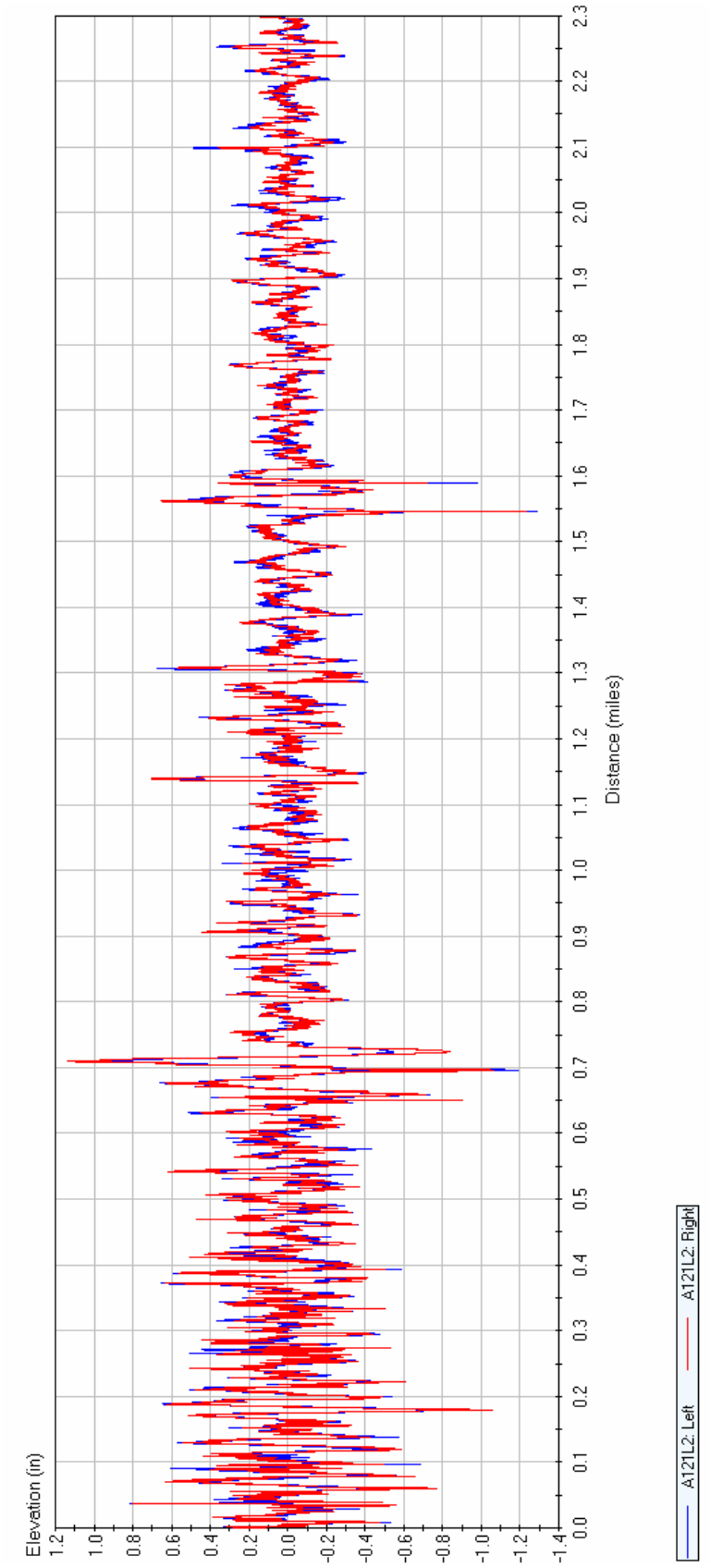

Figure B26. L2 Lane Profiles along SH121 Project in Denton County (Group B).

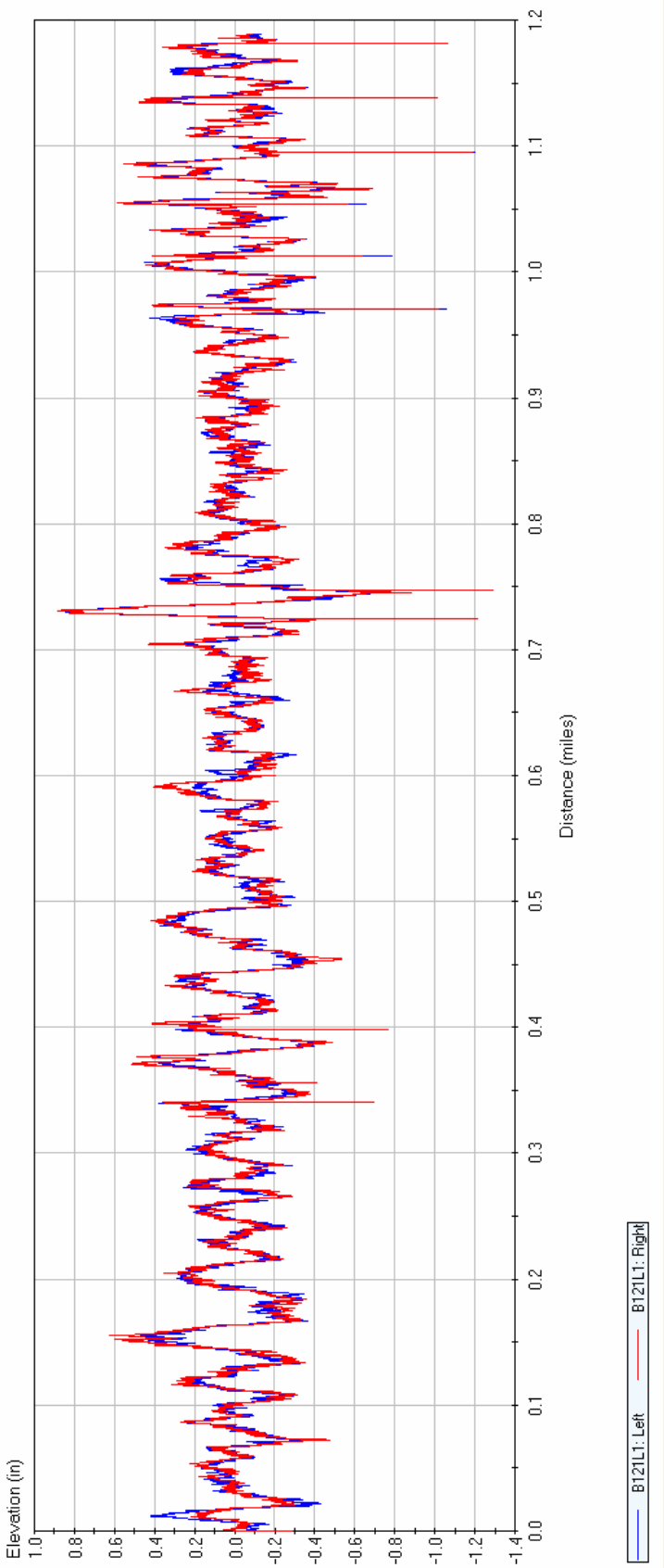

Figure B27. L1 Lane Profiles along SH121 Project in Denton County (Group C).

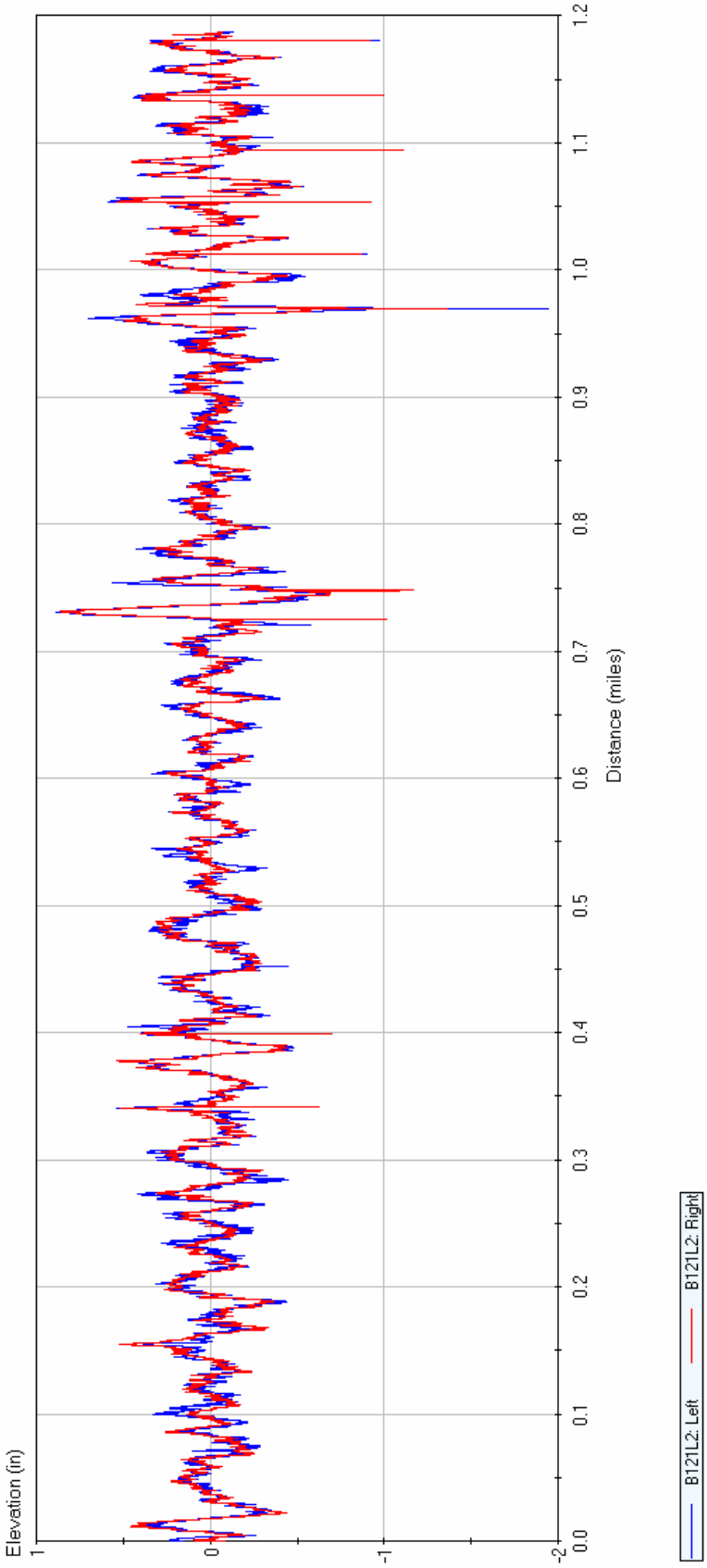

Figure B28. L2 Lane Profiles along SH121 Project in Denton County (Group C).

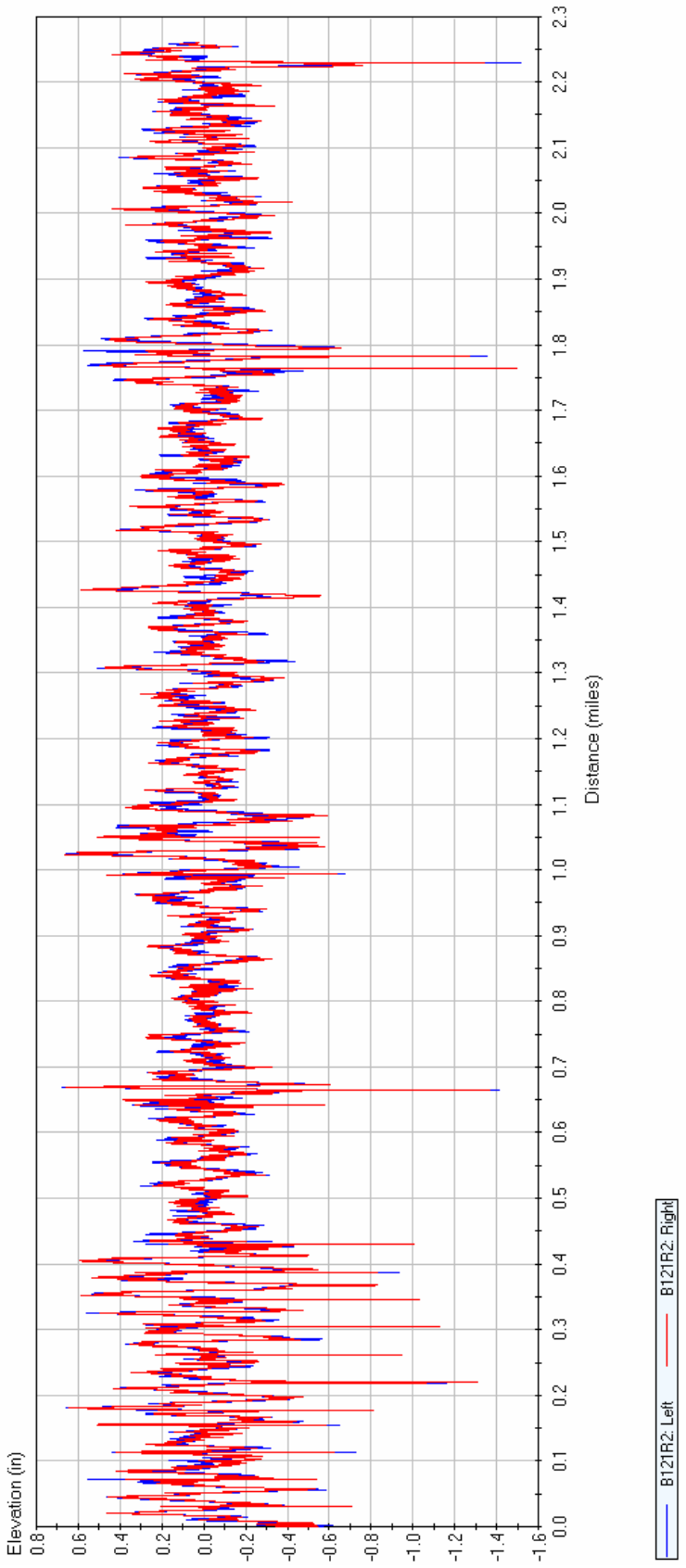

Figure B29. R2 Lane Profiles along SH121 Project in Denton County (Group D).

APPENDIX C

TRANSFER FUNCTIONS OF VEHICLE DYNAMIC TIRE LOADING

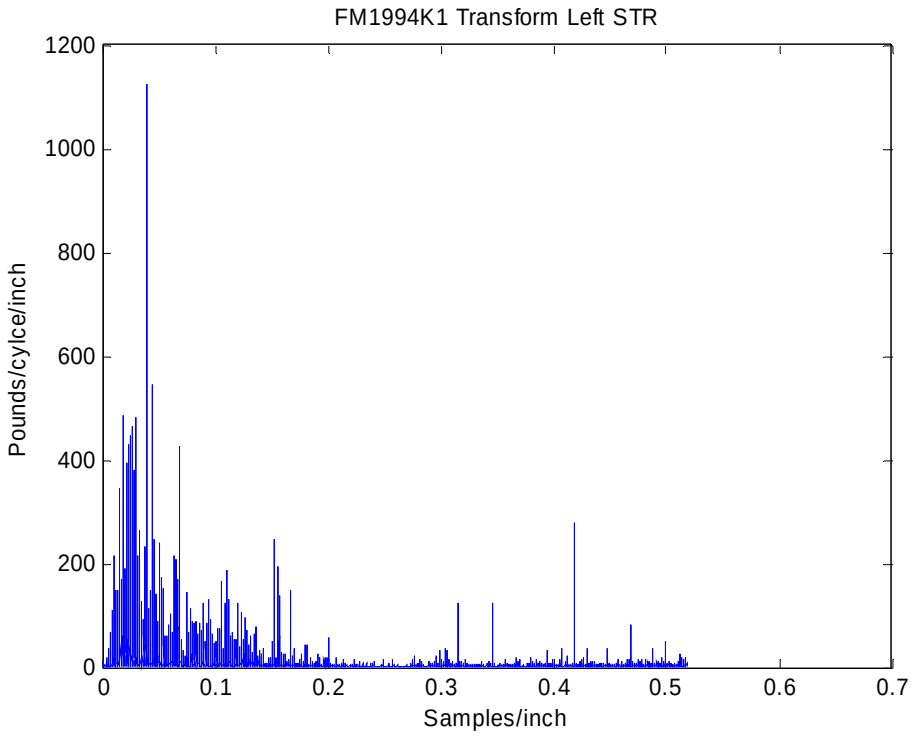

Figure C1. Transfer Function Chart for Dynamic Tire Loading on Left Wheel Path of Steering Axle from Tests on K1 Lane of FM1994 Project.

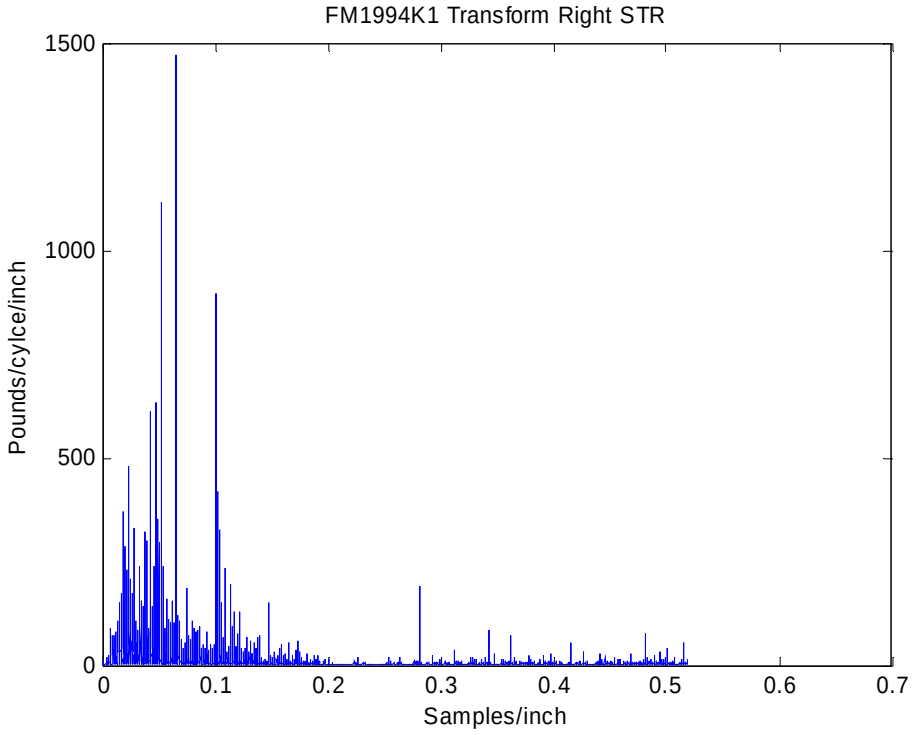

Figure C2. Transfer Function Chart for Dynamic Tire Loading on Right Wheel Path of Steering Axle from Tests on K1 Lane of FM1994 Project.

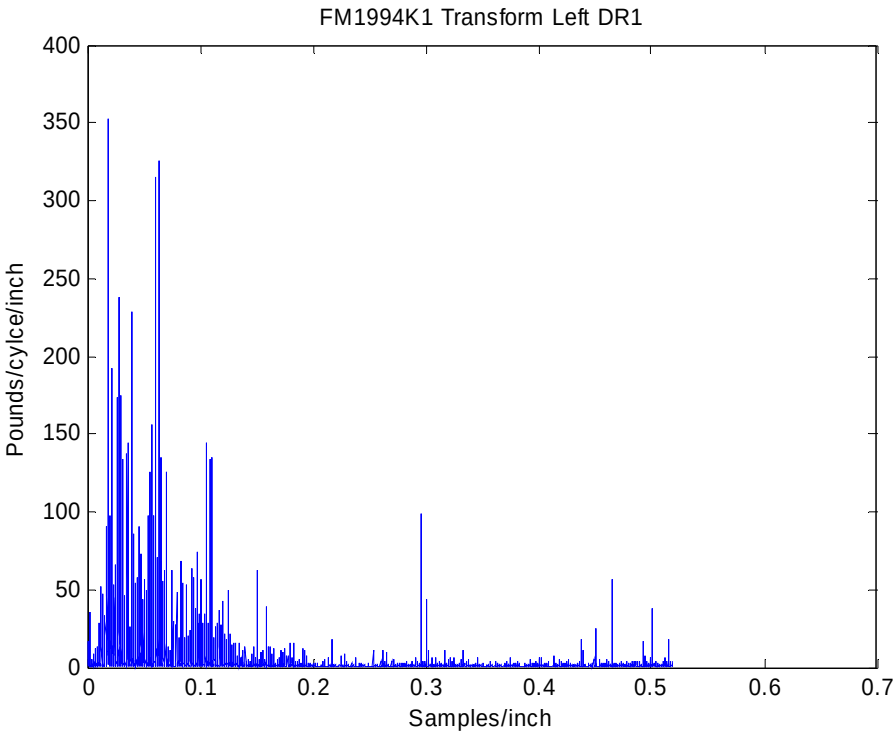

Figure C3. Transfer Function Chart for Dynamic Tire Loading on Left Wheel Path of Drive Axle from Tests on K1 Lane of FM1994 Project.

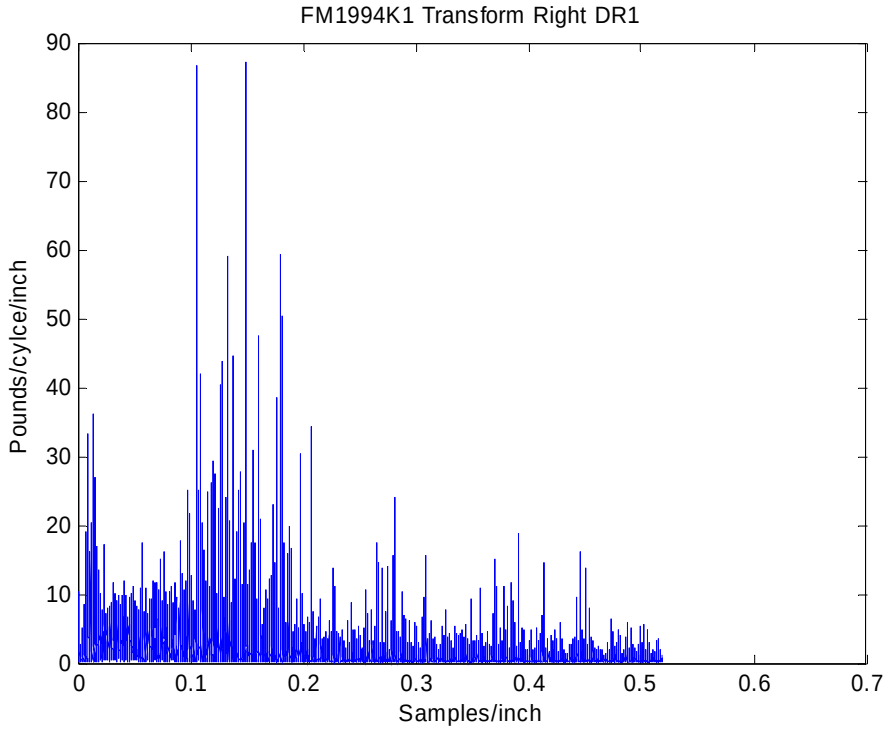

Figure C4. Transfer Function Chart for Dynamic Tire Loading on Right Wheel Path of Drive Axle from Tests on K1 Lane of FM1994 Project.

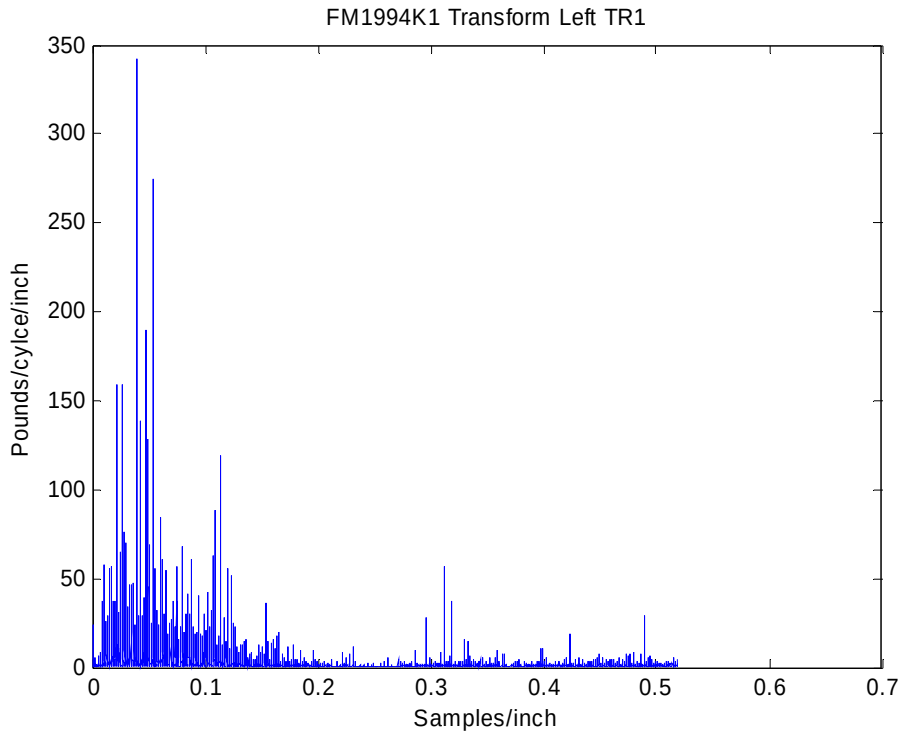

Figure C5. Transfer Function Chart for Dynamic Tire Loading on Left Wheel Path of Trailer Axle from Tests on K1 Lane of FM1994 Project.

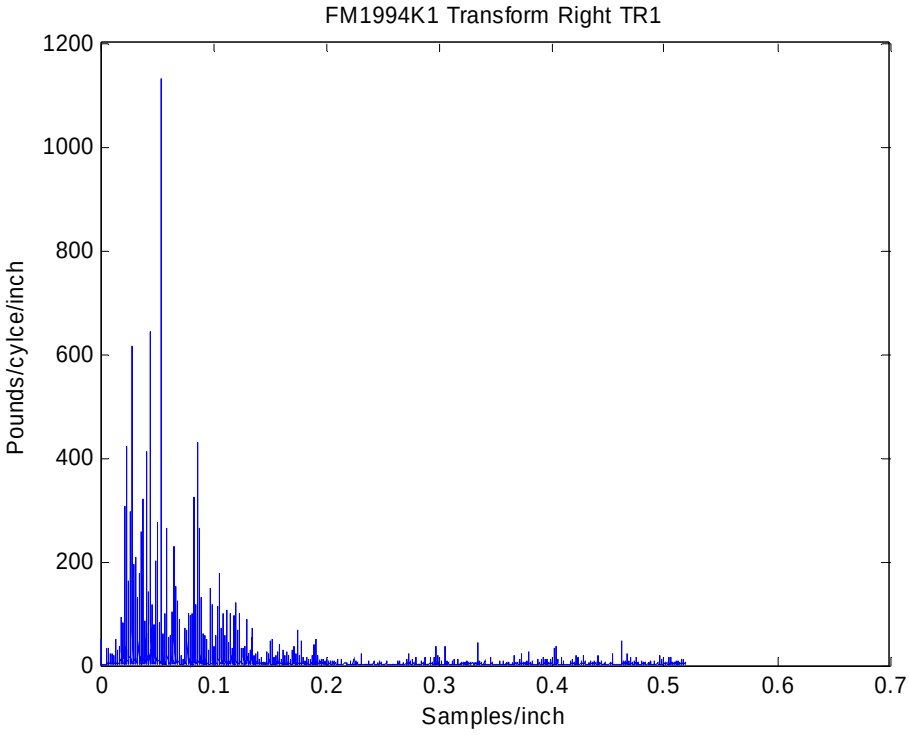

Figure C6. Transfer Function Chart for Dynamic Tire Loading on Right Wheel Path of Trailer Axle from Tests on K1 Lane of FM1994 Project.

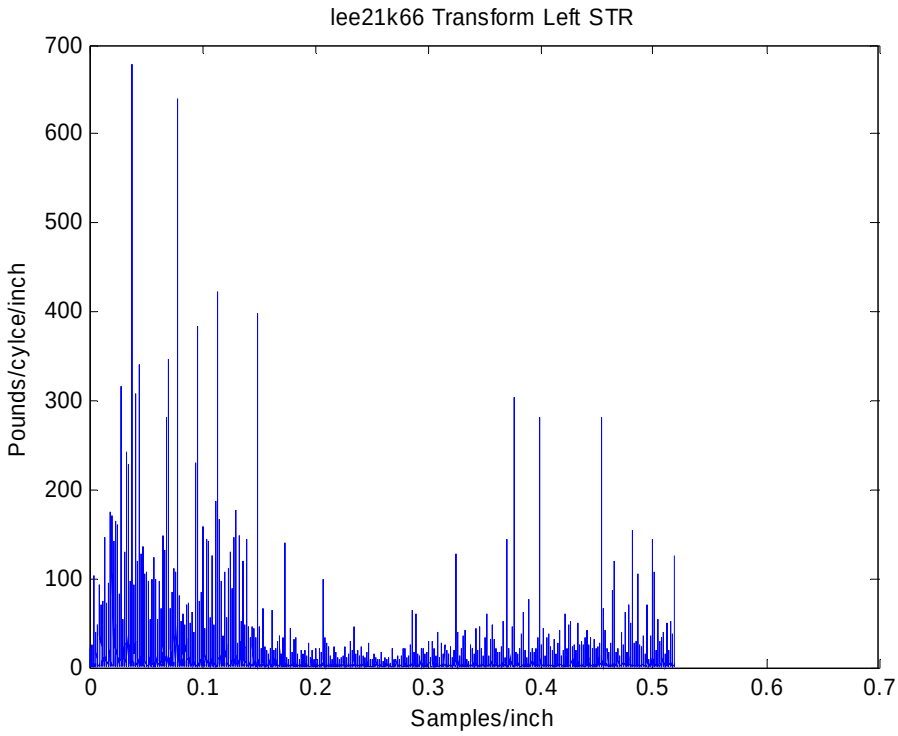

Figure C7. Transfer Function Chart for Dynamic Tire Loading on Left Wheel Path of Steering Axle from Tests on K6 Lane of SH21 Project in Lee County.

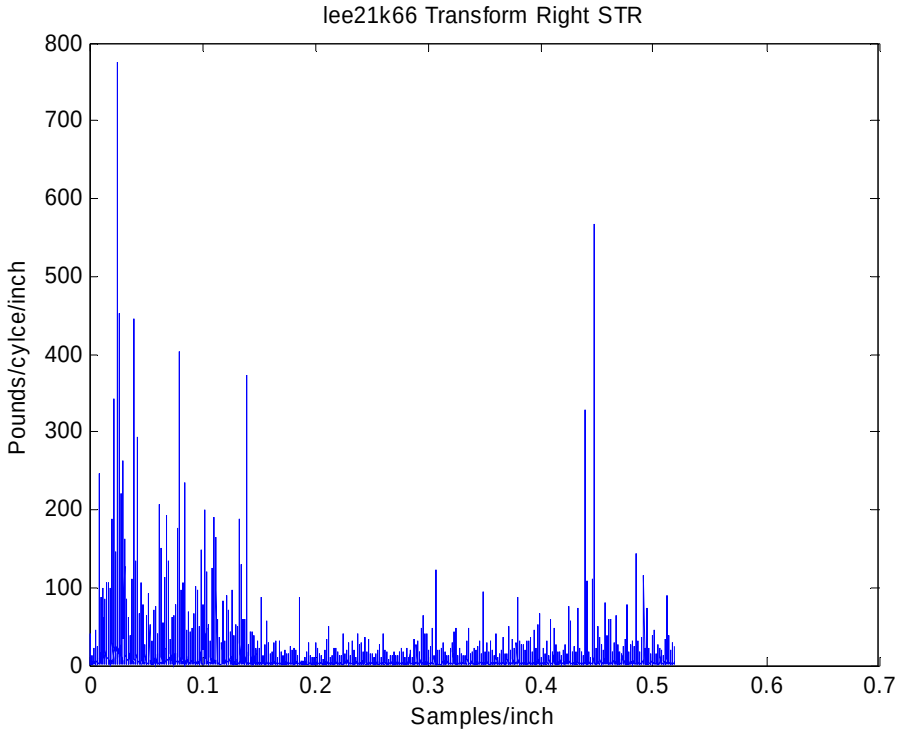

Figure C8. Transfer Function Chart for Dynamic Tire Loading on Right Wheel Path of Steering Axle from Tests on K6 Lane of SH21 Project in Lee County.

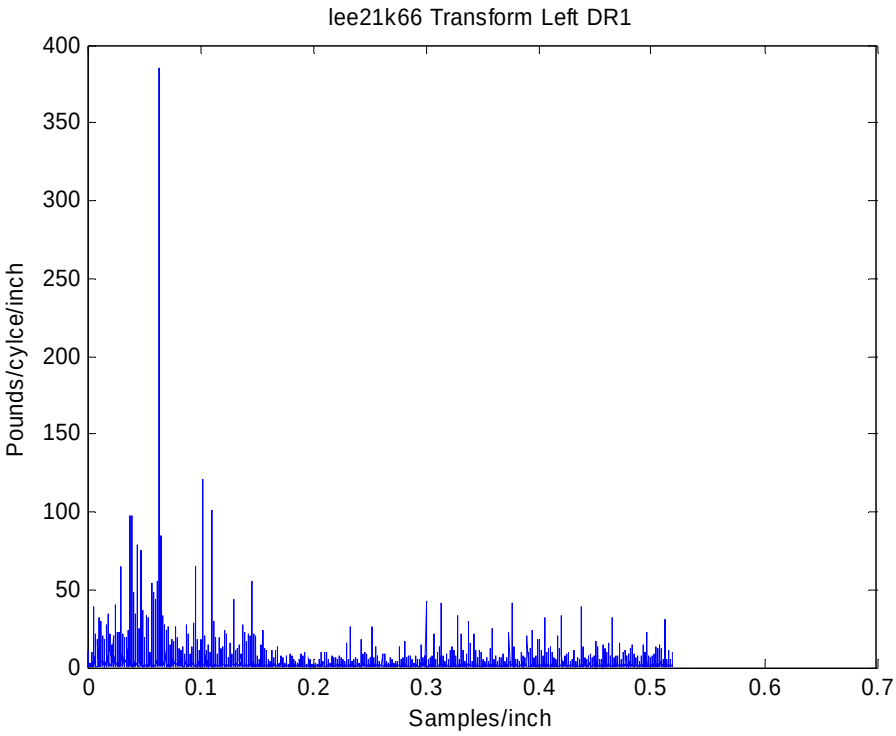

Figure C9. Transfer Function Chart for Dynamic Tire Loading on Left Wheel Path of Drive Axle from Tests on K6 Lane of SH21 Project in Lee County.

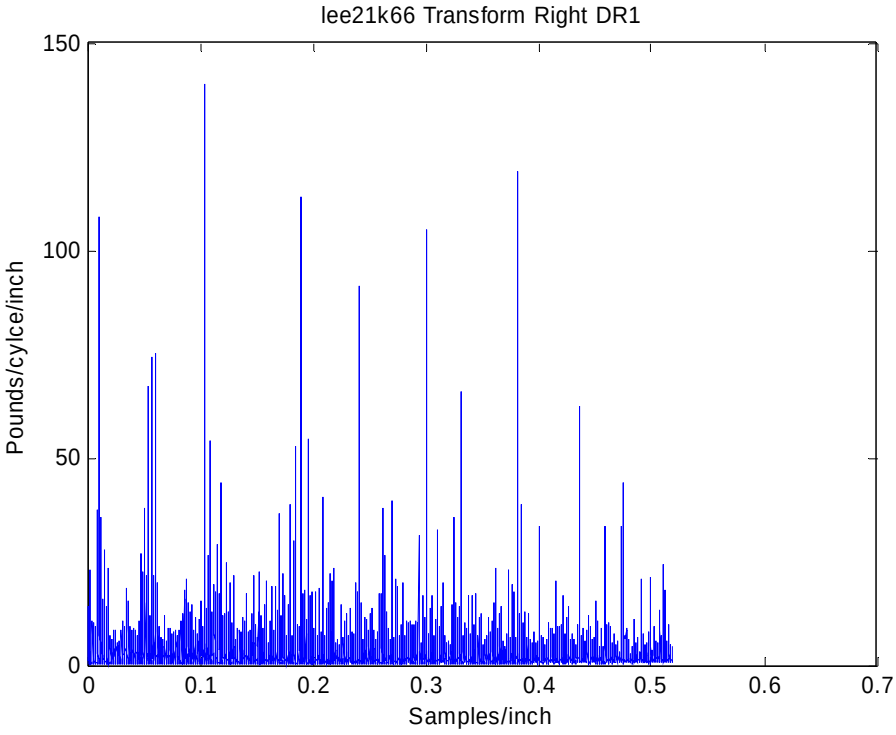

Figure C10. Transfer Function Chart for Dynamic Tire Loading on Right Wheel Path of Drive Axle from Tests on K6 Lane of SH21 Project in Lee County.

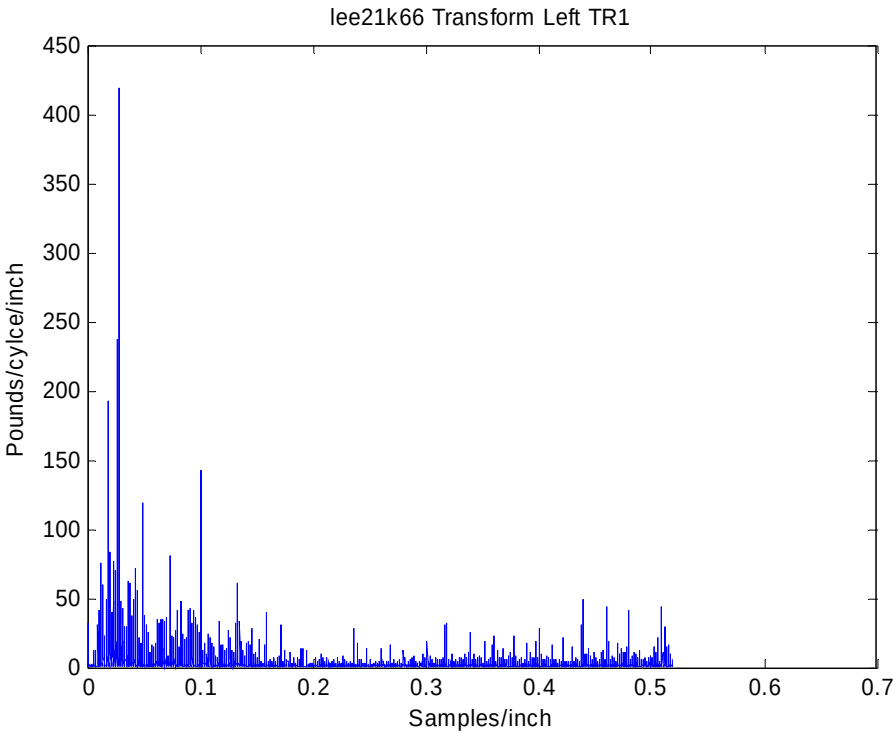

Figure C11. Transfer Function Chart for Dynamic Tire Loading on Left Wheel Path of Trailer Axle from Tests on K6 Lane of SH21 Project in Lee County.

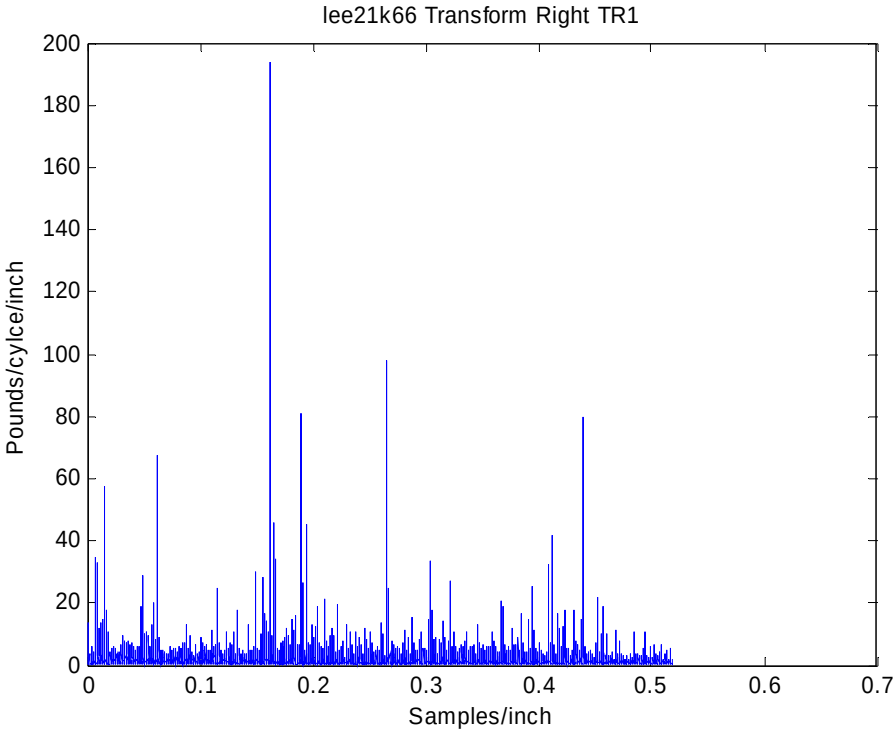

Figure C12. Transfer Function Chart for Dynamic Tire Loading on Right Wheel Path of Trailer Axle from Tests on K6 Lane of SH21 Project in Lee County.

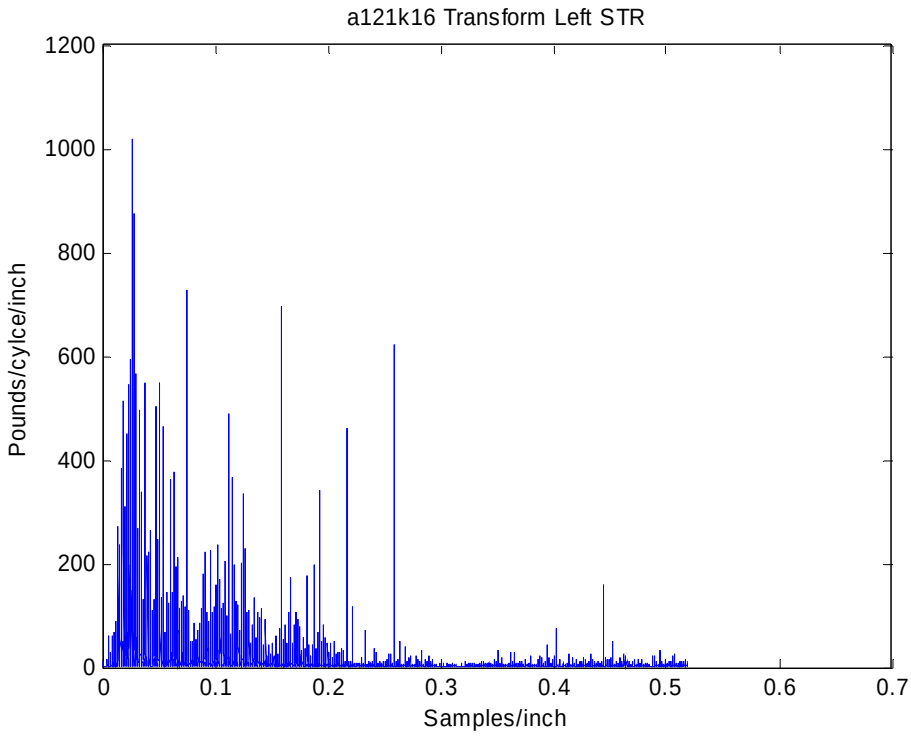

Figure C13. Transfer Function Chart for Dynamic Tire Loading on Left Wheel Path of Steering Axle from Tests on R1 Lane of SH121 Project.

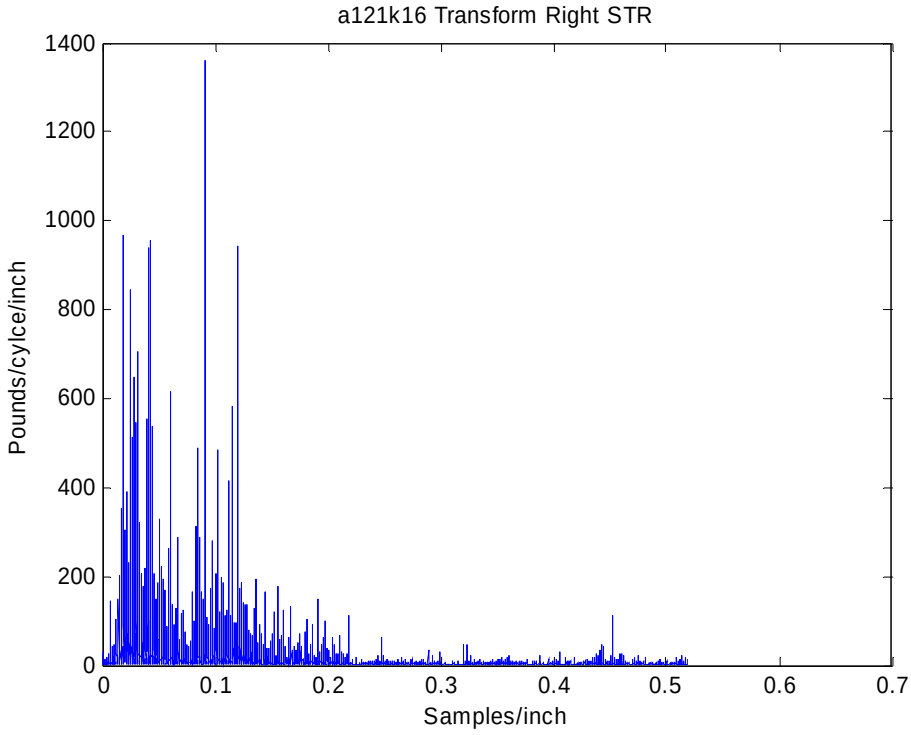

Figure C14. Transfer Function Chart for Dynamic Tire Loading on Right Wheel Path of Steering Axle from Tests on R1 Lane of SH121 Project.

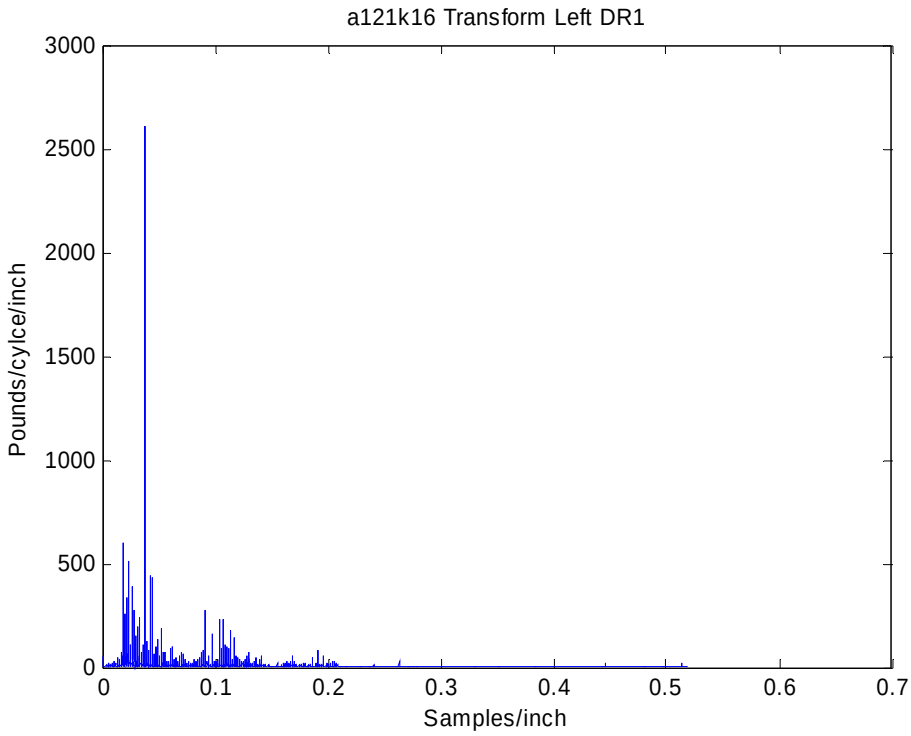

Figure C15. Transfer Function Chart for Dynamic Tire Loading on Left Wheel Path of Drive Axle from Tests on R1 Lane of SH121 Project.

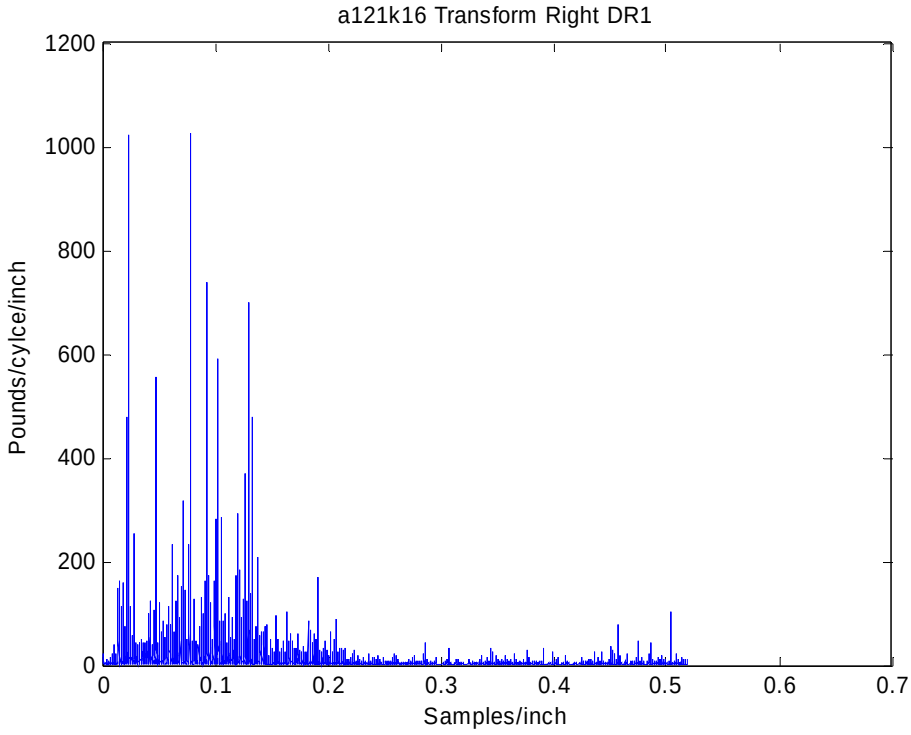

Figure C16. Transfer Function Chart for Dynamic Tire Loading on Right Wheel Path of Drive Axle from Tests on R1 Lane of SH121 Project.

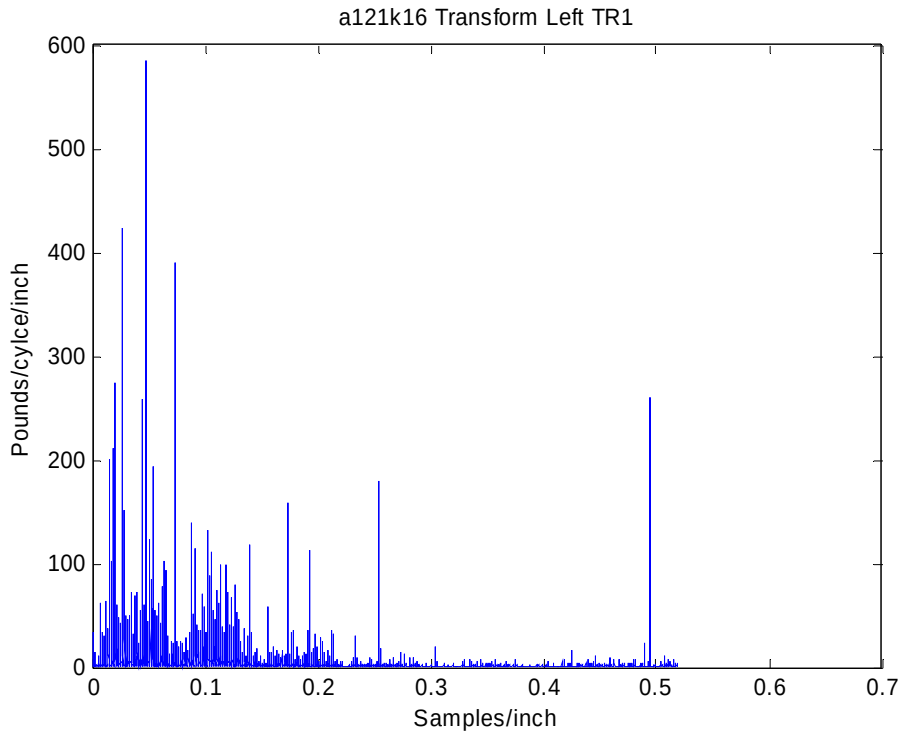

Figure C17. Transfer Function Chart for Dynamic Tire Loading on Left Wheel Path of Trailer Axle from Tests on R1 Lane of SH121 Project.

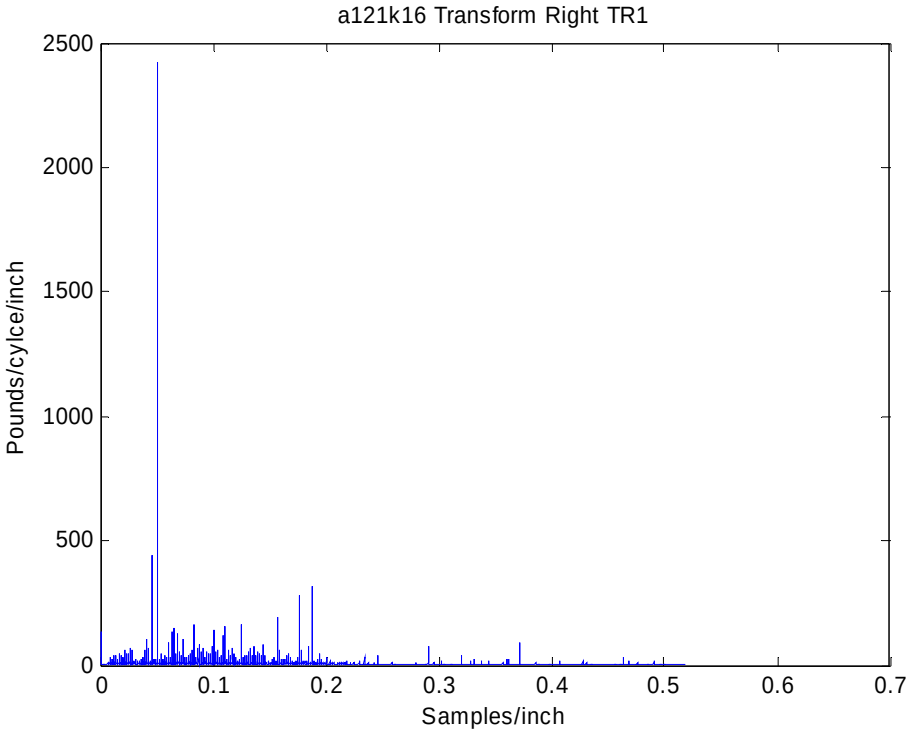

Figure C18. Transfer Function Chart for Dynamic Tire Loading on Right Wheel Path of Trailer Axle from Tests on R1 Lane of SH121 Project.

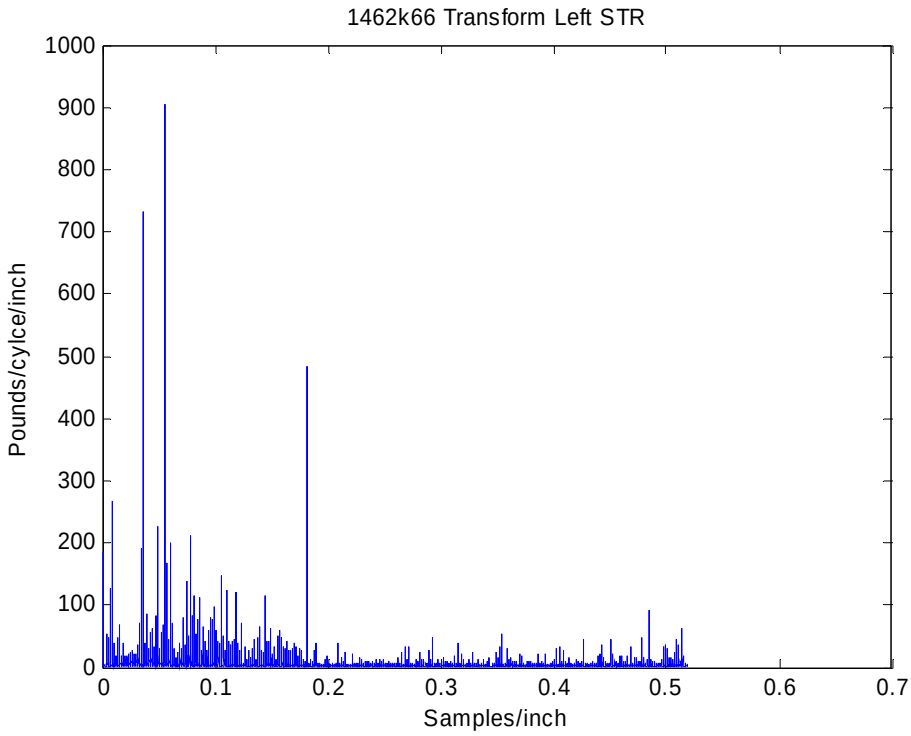

Figure C19. Transfer Function Chart for Dynamic Tire Loading on Left Wheel Path of Steering Axle from Tests on K6 Lane of FM1462 Project.

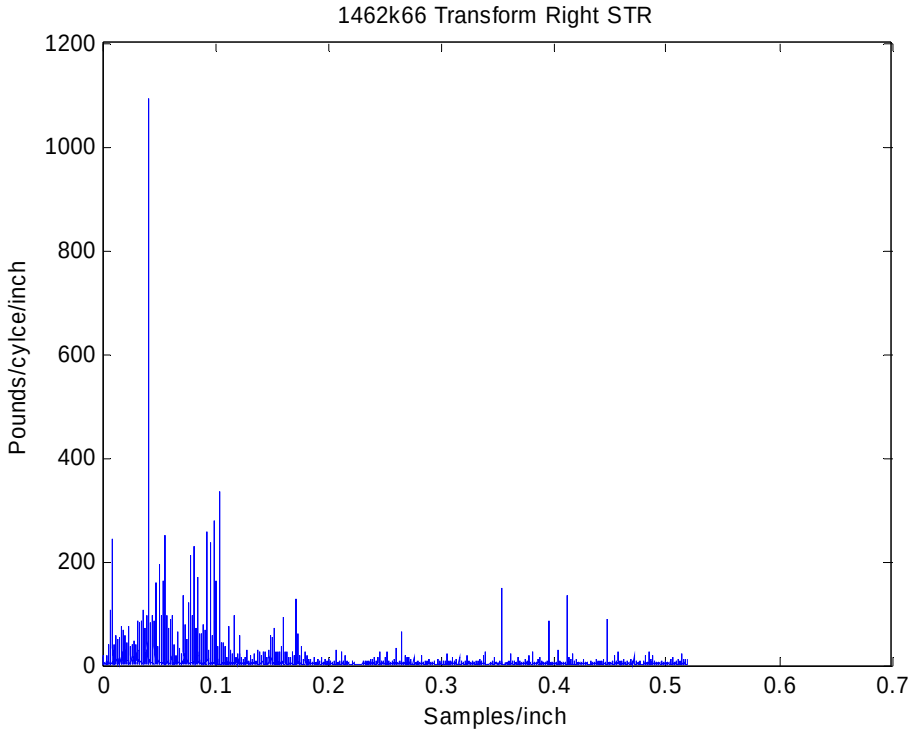

Figure C20. Transfer Function Chart for Dynamic Tire Loading on Right Wheel Path of Steering Axle from Tests on K6 Lane of FM1462 Project.

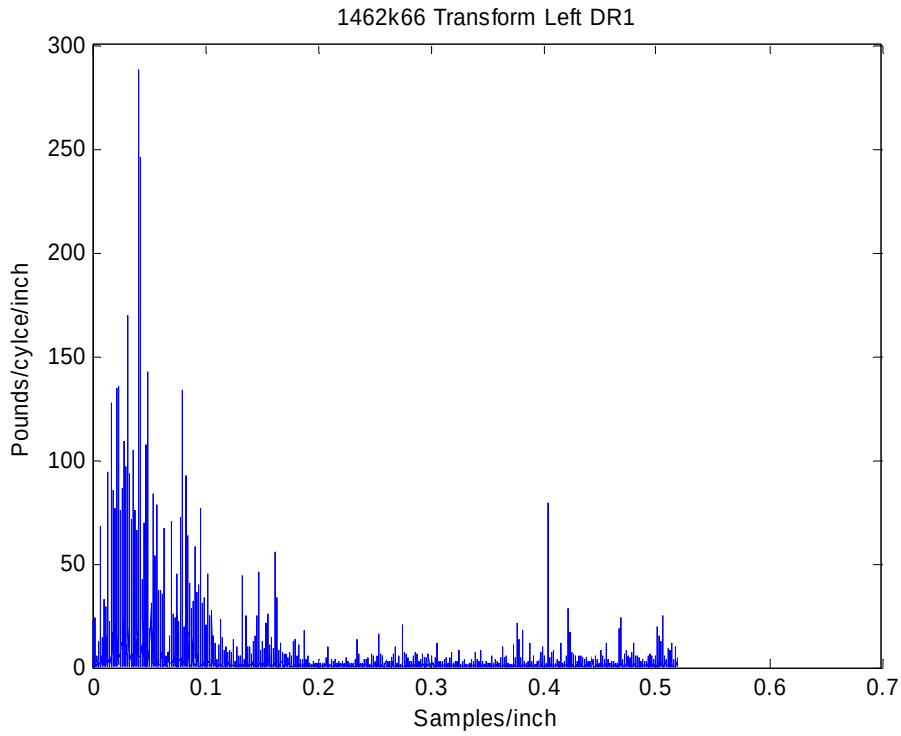

Figure C21. Transfer Function Chart for Dynamic Tire Loading on Left Wheel Path of Drive Axle from Tests on K6 Lane of FM1462 Project.

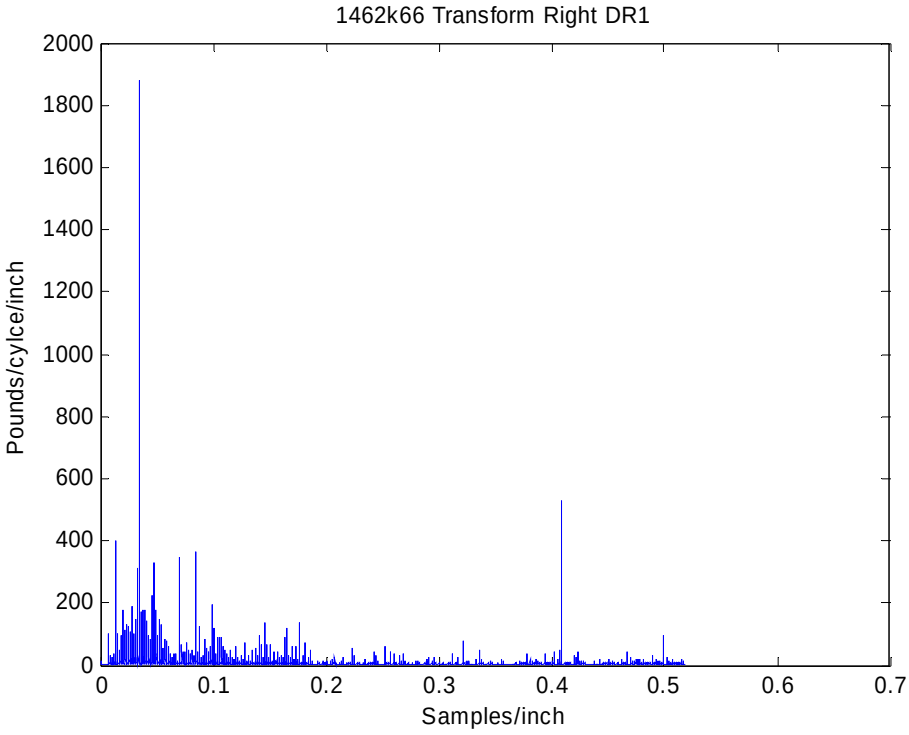

Figure C22. Transfer Function Chart for Dynamic Tire Loading on Right Wheel Path of Drive Axle from Tests on K6 Lane of FM1462 Project.

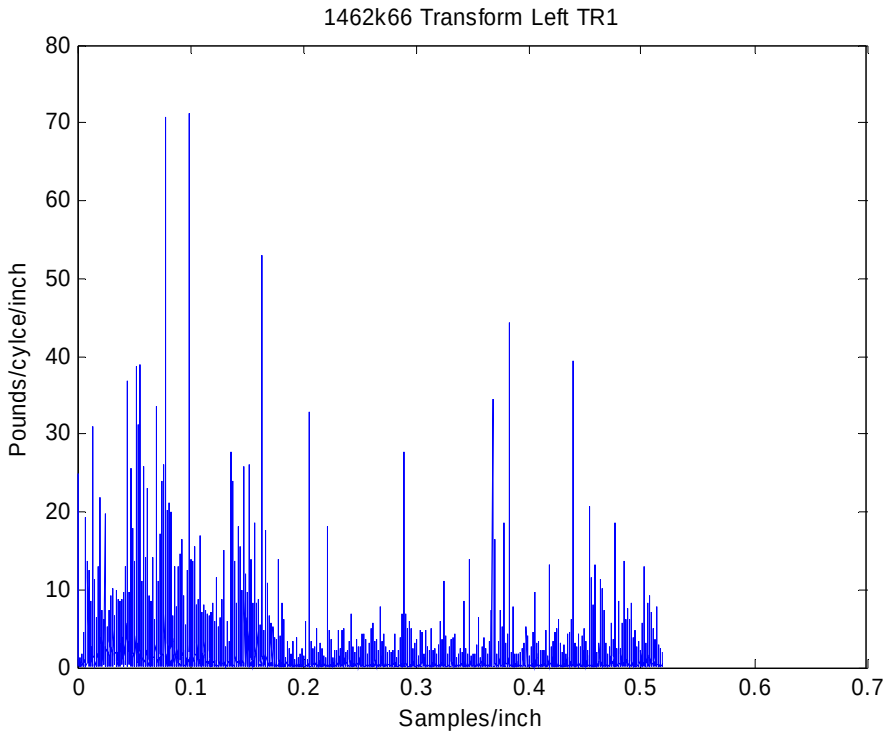

Figure C23. Transfer Function Chart for Dynamic Tire Loading on Left Wheel Path of Trailer Axle from Tests on K6 Lane of FM1462 Project.

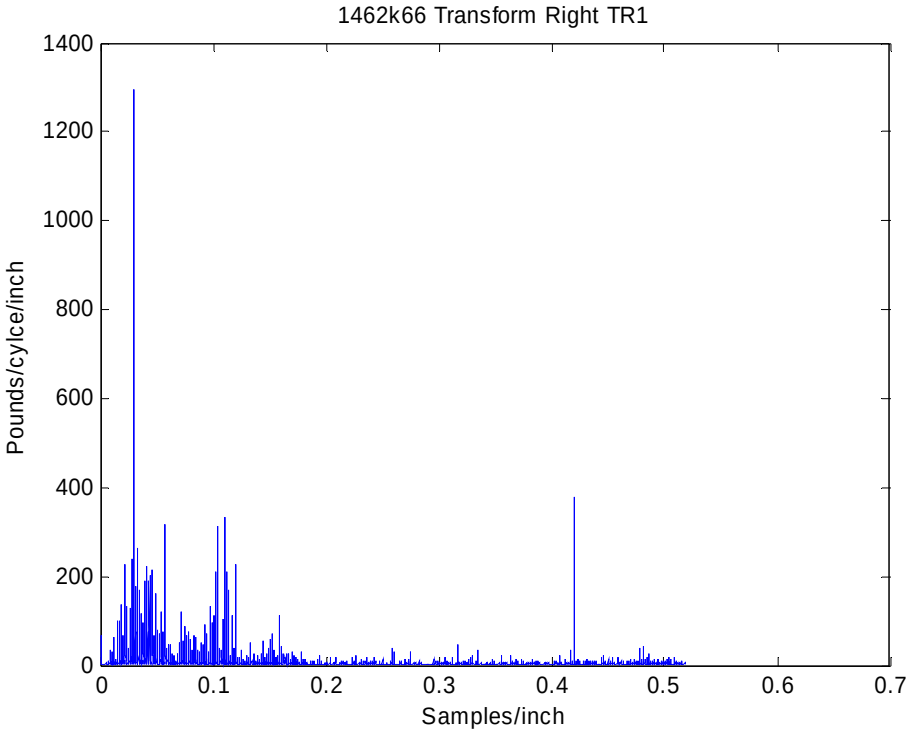

Figure C24. Transfer Function Chart for Dynamic Tire Loading on Right Wheel Path of Trailer Axle from Tests on K6 Lane of FM1462 Project.